RADIOGENIC ISOTOPE GEOCHEMISTRY

A Guide for Industry Professionals

What is a model age, and why do we need to know it? How can we test whether ore-forming fluids carry a mantle signature? What is the difference between a SHRIMP and a LA-ICPMS U–Pb age and is it significant?

Isotopes provide important information on many geological processes, with key relevance to the mining and petroleum industries, yet the techniques to obtain, process and interpret the data can be complex to master. This accessible book provides broad coverage of radiogenic isotopes in geochronology and geochemistry, explaining the basic principles and state-of-the-art techniques used to study them, with an emphasis on industry applications.

The major isotopic systems are fully summarised with relation to real-world applications, enabling readers to decide which technique is most relevant for the problem they want to solve, and then to rigorously evaluate existing data, or recalculate and reassess data sets to avoid duplication of effort. Written at a level appropriate for advanced undergraduate students, the book also includes detail which allows more experienced practitioners to maximise the potential value of isotopic data sets.

BRUCE F. SCHAEFER is a Senior Lecturer in isotope geochemistry at Macquarie University, Australia. His work uses isotopes to solve a broad range of geological problems, by identifying and subsequently applying, or on occasion developing, an appropriate isotopic tracer to solve the issue. His research interests include planetary differentiation, mantle plumes, Precambrian geodynamics and magmatic processes. Dr. Schaefer was awarded the Tate Memorial Medal for original research from Adelaide University, where he graduated. Subsequently he has held positions at the Open University, UK, and Monash University, Australia, before moving to Macquarie. His publications include work on magmatism, Precambrian tectonics, mineralised systems, groundwater, weathering rates, geophysics and meteorites.

RADIOGENIC ISOTOPE GEOCHEMISTRY

A Guide for Industry Professionals

BRUCE F. SCHAEFER
Macquarie University, Sydney, Australia

CAMBRIDGE
UNIVERSITY PRESS

CAMBRIDGE
UNIVERSITY PRESS

University Printing House, Cambridge CB2 8BS, United Kingdom

Cambridge University Press is part of the University of Cambridge.

It furthers the University's mission by disseminating knowledge in the pursuit of education, learning, and research at the highest international levels of excellence.

www.cambridge.org
Information on this title: www.cambridge.org/9781107039582

First published 2016

Printed in the United Kingdom by TJ International Ltd. Padstow Cornwall

A catalogue record for this publication is available from the British Library.

Library of Congress Cataloguing in Publication Data
Schaefer, Bruce F., 1972–
Radiogenic isotope geochemistry : a guide for industry professionals / Bruce F. Schaefer, Macquarie University, Sydney, Australia.
Cambridge : Cambridge University Press, 2016. | Includes bibliographical references and index.
LCCN 2015048524 | ISBN 9781107039582
LCSH: Isotope geology. | Geochemistry. | Isotopes.
LCC QE501.4.N9 S33 2016 | DDC 551.9–dc23
LC record available at http://lccn.loc.gov/2015048524

ISBN 978-1-107-03958-2 Hardback

For Nazy
Thank you for your unwavering love, support and belief

Contents

Preface

The vast majority of geoscience graduates proceed to careers in the extractive minerals industry. This includes the coal and petroleum industries, all of which require an understanding of how, why and when the commodity of interest accumulated. The 'where' is the focus of the exploration industry, and every year immense amounts of money are spent globally on locating the next 'world class' ore deposit.

In all of these endeavours, naturally occurring isotopes play a pivotal role in deciphering aspects of the resource industry. Specifically, naturally occurring radioactive isotopes can be applied as chronometers to date 'when' various aspects of the mineralising process took place, and the complementary stable isotopes offer mechanisms for tracking the sources of metals and reactive ligands necessary to form an economic accumulation of a resource.

Despite this, graduate geologists often have only a limited exposure to isotope geochemistry, and over time this knowledge, if not used regularly, becomes forgotten. This book is aimed to help refresh the memory of those who encounter isotopes in the course of their work – either in the minerals industry or in research fields. It is structured as a reference guide which assumes some understanding of geochemistry; however, it is hoped that it also contains enough depth for the interested reader to comprehend isotopic systems and processes they may not have previously encountered. Hence it is not designed as a conventional textbook, although it could be tackled in a sequential manner for learning, but I anticipate its utility will come for those time-poor individuals who need to 'dip in' to a certain section to clarify a concept, gain an understanding or recalculate a data set in order to solve a particular problem.

The world of radiogenic isotope geochemistry is one of often arcane concepts and obscure terminology, so it is also hoped that this will go some way to demystifying aspects of it while maintaining a level of rigour that allows a professional to obtain the maximum value from an (often costly) data set.

Significantly, I have resisted the urge to populate the book with specific case studies and worked examples, and focus instead on general processes. Such a broad base from first principles ultimately allows a broader range of applications and prevents a ‘one size fits all’ approach to using isotopic data. My hope is to aid the newcomer in comprehension and deepen the understanding (if possible) of the more experienced user. Time will tell if I have had any success in these measures!

Acknowledgements

This work has been a long time in the making. The genesis for the idea came in the days of the pmd*CRC during the mid 2000s, when I was interacting regularly with colleagues, many of whom I had gone through undergraduate study with, who were now working in the minerals industry. Consistently the message was that, while they liked using the interpretations from isotopic data, many of them didn't have the time to assess, or had forgotten how to manipulate, the very data they had paid large amounts of money to acquire. Given that such people are by definition time-poor and often have drivers other than simply understanding a piece of geology, I found myself often helping out in the course of an hour or so, (re-) interpreting the latest geochronology that had been acquired. I realised that all of these people knew enough to do this themselves if only they had some ready reference guides on hand to encourage them that they were doing the right thing and that they were on the right path. So, to all of you people, I hope this is another tool which helps you get to where you need to be, and thank you for identifying the need for it.

The numerous colleagues I have discussed aspects of isotope geochemistry with over the years I must thank, as you have all contributed in some way, knowingly or otherwise. Specifically here at Macquarie I must thank Simon Turner for being a great sounding board (about many things beyond this book!), Ron Vernon for encouraging me to stick with it and Norm Pearson for discussions about all aspects of plasma mass spectrometry and lasers. Of course, all errors or omissions are my own and cannot be laid at the feet of these people.

The team at Cambridge University Press have been fantastic – very patient with an academic trying to do too many things at once, and so a big thank-you to Zoë Pruce in particular.

Finally, I must thank my wife, Nazy, for her unquestioning support and belief that I would finish it, even if I wasn't so sure! Thank you from the bottom of my heart!

Abbreviations and symbols

AFC	assimilation–fractionation–crystallisation. A dynamic process of modification of the composition of magma through interaction with its wallrocks during ascent and crystallisation.
amu	atomic mass unit, generally defined such that $^{12}C = 12.000000$ amu
C	'common' mantle component determined by the convergence of the global MORB Pb isotope arrays. Almost identical to FOZO.
CDT	Canyon Diablo troilite. A standard reference material for $\delta^{34}S$, derived from metal obtained from the meteorite responsible for Meteor Crater, Arizona.
CF	continuous flow (IMRS)
CFB	continental flood basalt
CHUR	chondritic uniform reservoir. The purported homogeneous isotopic reservoir present in the early solar system from which the earth condensed and subsequently differentiated. Based upon the composition of chondritic meteorites. Used as a comparison isotopic reservoir, particularly for Nd isotopes, to describe relative enrichment or depletion in isotopic signature in terms of ε notation.
cps	counts per second
DL	detection limit (level)
DMM	depleted MORB mantle. The chemically depleted upper convecting mantle. Conceptually this reservoir can be thought of as the residue after continental crust extraction, and is depleted in lithophile elements.
EMI	enriched mantle type 1. OIB mantle component interpreted to represent recycled SCLM.

EMII	enriched mantle type 2. OIB mantle component interpreted to represent recycled continental crust, possibly in the form of terrigenous sediment.
ESA	electrostatic analyser
FOZO	focal zone. Theoretical ubiquitous mantle component defined by the intersection of MORB and OIB arrays, particularly in Pb–Nd–Sr isotope space. Differs only in detail from PHEM, PREMA and C.
GC	gas chromatographic
GS	gas source
HFSE	high field strength elements = Zr, Nb, Hf, Ta
HIMU (‘high μ’)	OIB with high time integrated U–Pb ratios resulting in very high $^{206}Pb/^{204}Pb$ ratios. Such fractionation of U from Pb and Th is thought to take place in subducted oceanic crust.
HREE	heavy REE: Er, Tm, Yb ± Lu
IC	ion counter (also sometimes used for isotope composition, which is the measured ratio of two isotopes)
ICP(-MS)	inductively coupled plasma (mass spectrometry)
ID	isotope dilution
ID-ICP-MS	isotope dilution inductively coupled plasma mass spectrometry
ID-TIMS	isotope dilution thermal ionisation mass spectrometry
INAA	instrumental neutron activation analysis
IR	infrared
IRMS	isotope ratio mass spectrometry
KDE	kernel density estimator
LA	laser ablation
LIEF	laser induced elemental fractionation
LILE	large ion lithophile elements. Elements with a large ionic radius and small ionic charge; includes K, Rb, Sr, Cs and Ba.
LOI	loss on ignition
LREE	light REE: La, Ce, Pr, Nd
max dep	maximum deposition age of a sediment, usually constrained by the age of the youngest detrital zircon population within a sample.
MC	multi-collector
MIF	mass independent fractionation. Isotopic fractionation whereby the degree of isotopic separation does not scale as a proportion of the mass difference between the isotopes.
MORB	mid ocean ridge basalt

Part One

‘How’

Isotopes and how they are measured

1

Isotopes and geochemistry

1.1 Introduction

Economic geology is, at heart, the most fundamental form of applied geochemistry. In essence, the industry professional is focused on understanding where accumulations of geochemical anomalies (i.e. the mineralisation) occur. Whether that be in an exploration setting or a resource evaluation context, all geologists involved in this task are trying to pinpoint where a certain element (or elements) are located. In this task a large number of tools are applied: understanding the relationship of mineralogy to structure, fluid pathways, relative timing and often the association of economic commodities with other, more common, chemical proxies.

In essence, isotopes are simply the most distinctive chemical proxy a geologist can have in the toolkit – they are (trace) elements with labels on them. These labels, when interrogated, allow us to varying degrees to investigate when and how the elements got to where they are today. However, often the information isotopes contain is not utilised effectively – the reasons for this are many, including geological and educational. Often, even the specialist needs to refer back to a source of information or reference when understanding a system they have not used for some time or may not have encountered previously, and the same is certainly true of isotopes. Sometimes perceived complexity can obscure fundamental simple understanding, and the converse can be true as well.

This contribution attempts to make the sometimes arcane world of isotopes more accessible and tractable for those who have had little or no formal background in isotope geochemistry, while maintaining a level of sophistication and detail that allows those more familiar with the issues to maximise the benefits of isotopic data sets. To this end, there is some basic background regarding nomenclature and shorthand that the reader should familiarise themselves with, but at heart it is worth remembering that although we are dealing with isotopes and often ‘nuclear’ processes, the way these are distributed in the earth is often

controlled by more familiar *chemical* processes. From this basis, a linking of chemistry with the nucleus allows us to interrogate the geological record and apply that understanding in a huge range of situations in the minerals industry. Thus, the isotopic toolkit primarily contains methods of determining when events took place (geochronology) and fingerprinting where elements have come from (geotracing). However, there are many applications which involve the 'how'; and hence at every level the processes involved in the system of interest are intrinsically embedded within understanding. An upshot of this is that a single tool does not enjoy universal application – just because Re–Os molybdenite geochronology might date sulphide mineralisation in one setting does not mean that all molybdenites globally will date their associated sulphide assemblages. At heart, isotopes are only as good as the geological understanding of the situation in which they are being applied, and therefore the geologist needs to consider all possible interpretations. Hopefully this contribution will aid professionals who are time-poor in achieving a fuller understanding of their particular problem, and in some cases possibly encourage them to try new techniques or ideas for situations that were previously ambiguous.

How to use this book

This book is not intended to be a textbook in the instructional sense, although one could use it as such if one wished. Rather, this book is intended to serve as a reference guide for persons with some appreciation of geochemistry and in all likelihood previous exposure to isotopes. Therefore, the user is encouraged instead to dip into the book at the section of interest, which should generally be 'stand-alone' in terms of concepts and applications. This inevitably results in repetition within the book between sections – for example, the introduction to the radioactive decay schemes in Part I is re-emphasised and elaborated further in Part II; however, it is not necessary to have read the section in Part I on the isotope system of interest in order to follow the arguments in Part II.

I also have not shied away from including relevant equations where appropriate. While the equations may appear daunting to those who are not mathematically inclined, I have generally included only those that require no knowledge of calculus, and hence readers with a basic understanding of algebra should be able to use these with ease. The purpose of this is to allow the reader to actually manipulate and recalculate the data they obtain, and form their own interpretations. I have also attempted to include currently accepted values for decay constants and geochemical reservoirs in order to allow the reader to conduct their own modelling and to act as a ready reference. Again, some of the reservoir values are a matter of preference; however, the ability to choose and (re)calculate model ages etc. may greatly aid the explorationist in targeting

prospective lithologies. Other equations are included purely by means of explanation – some of the logic chains for the reasoning behind the principles described can be summarised succinctly in the language of mathematics, and the more numerate may prefer to view things from this perspective.

Finally, although not the focus of this book, it is inevitable that stable isotopes form a significant portion of the geochemist's repertoire. Therefore I have included a holistic introduction to nomenclature and processes in Part I which forms a basis for understanding both stable and radiogenic isotopes. From this holistic basis it is hoped that the reader can gain an appreciation of the processes responsible for fractionation in all settings, rather than dealing with radiogenic decay in isolation. Chapter 4 therefore attempts to give a flavour for the nature of stable isotope geochemistry in order to allow the reader to navigate the extensive literature available, but is by no means intended to be comprehensive or exhaustive! However, an integrated approach is necessary for a complete understanding of *any* system, and the burgeoning field of transition metal stable isotope geochemistry offers one of the great growth areas in the geosciences.

1.2 Elements and isotopes

Economic geology deals with chemical processes, usually centred upon the behaviour of a single key chemical element, say Pb, Au or Cu. However, many elements contain isotopes, which are in essence chemically identical with each other, but have a different mass due to their nuclear structure. This difference in nuclear configuration permits two fundamental types of behaviour that geochemists can use – namely *fractionation* of masses (isotopes) of the same element, and *radioactive decay* from one element to another. In order to understand these, we need first to clarify what they are and distinguish between some important terms when describing atomic structure.

1.2.1 Atoms, ions and isotopes

An atom is the smallest component of a chemical element that retains the chemical properties of that element. Atoms contain three fundamental particles: **protons** and **neutrons**, which occur in the nucleus and are hence termed **nucleons**; and **electrons**, which orbit the dense nucleus. Protons and neutrons have approximately the same mass, whereas the electron is ~2000 times lighter than the nucleons. For the purposes of geological nuclear chemistry it is usually regarded as having negligible mass. Protons and neutrons weigh ~1 atomic mass unit (amu). An atom is electrically neutral, since the number of orbiting negatively charged electrons balances the number of positively charged protons in the nucleus. Neutrons have no electrical charge.

The number of protons defines the **atomic number (*Z*)**, and therefore which element it is. In other words, each element has a unique atomic number (e.g. Cu = 29; Au = 79), which governs the corresponding number of electrons and hence the chemical properties of the element. The **atomic mass number (*A*)** of an element is the total number of nucleons it contains, i.e. the sum of the protons (Z) and the neutrons (N). Therefore $A = N + Z$.

An **ion** is an electrically charged atom; this charge can occur by loss or gain of electrons. This ability to change charge controls the chemical behaviour of the element, which is governed by ions attempting to become electrically stable. A hydrogen atom (H) can *lose* an electron to become *positively* charged since it has one proton more than it has electrons, and hence becomes a hydrogen ion, H^+. Conversely, a chlorine atom can gain an electron to form a chloride ion, Cl^-. These can combine to form an electrically neutral molecule, HCl; i.e.:

$$H^+ + Cl^- \rightarrow HCl.$$

A **cation** is a positively charged ion (i.e. one which has fewer electrons than protons) and an **anion** is negatively charged (containing an excess of electrons). In the above example, H^+ is the cation and Cl^- the anion. Generally, metals produce cationic species and non-metals anionic; however, there are very significant exceptions to these generalisations (particularly among the non-metals, such as S, As and Te).

A **molecule** is therefore the smallest freely existing part of a substance that retains the chemical properties of that substance. They can be multielemental (most common, e.g. HCl, H_2O), monoelemental (e.g. O_2, N_2) and even monoatomic (rare, e.g. Ar gas, Au metal). In geology, we are primarily dealing with molecular materials which are crystalline (e.g. silicates and sulphides) or less frequently ionic species which are dissolved in fluids (e.g. ligands and dissolved metals).

1.2.2 Isotopes

All atoms of a given element have the same number of protons (i.e. they have the same Z); however, they do not necessarily have the same number of neutrons (i.e. they can have different A). These are said to be **isotopes** of the element. Isotopes have (essentially) identical chemical properties, since these are determined by the number of electrons, which is in turn controlled by the number of protons in the nucleus.

The neutrons are necessary to provide a mechanism by which the nuclear force is able to bind protons together – otherwise the positive electromagnetic repulsion drives protons apart and no elements heavier than H would be able to form. The number of neutrons (N) required to prevent the positively charged protons

from repelling each other is generally greater than or equal to the number of protons (the only stable exceptions to this in nature are ^{1}H (simply one proton) and ^{3}He (two protons and one neutron).

Hence the atomic structure for an element *E* can be written in shorthand notation as:

$$^{A}_{Z}E$$

Note that *chemical* formulae, whether expressing the charge on an ion, or the number of atoms in a molecule, always use super- and subscripts on the right-hand side of the elemental symbol. By contrast, *nuclear* and hence isotopic properties, such as atomic number (*Z*) and atomic mass (*A*) are always expressed using super- and subscripts on the left-hand side of the elemental symbol.

Thus, **isotopes** of a given element are nucleii which have varying *A* for a constant *Z*; i.e. variable numbers of neutrons for a given number of protons. E.g. in nature, hydrogen has three isotopes, ^{1}H, ^{2}H (aka deuterium) and ^{3}H (aka tritium) containing zero, one and two neutrons, respectively. However, they all contain only one proton ($Z = 1$). Thus for a given element (i.e. constant *Z*) there may be a number of different values of *A* which result in a stable nucleus. Other configurations, such as tritium, may result in either overly light or excessively heavy nucleii which are unstable, and will ultimately fall apart through nuclear (radioactive) decay.

A perhaps more pertinent example to solid earth geochemistry is illustrated in Figure 1.1. The element Sr ($Z = 38$) comprises four naturally occurring isotopes;

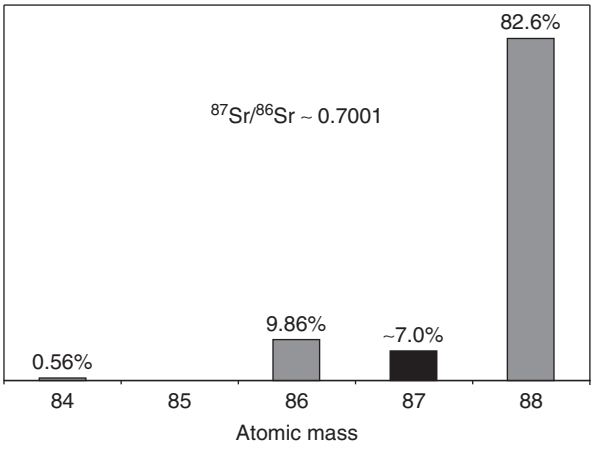

Figure 1.1 An example of an element (Sr) containing isotopes in different relative proportions. Note that ^{87}Sr is continually accumulating due to the decay of ^{87}Rb, and hence the relative proportion of ^{87}Sr with respect to the other isotopes of Sr increases over time.

the most common of these is ^{88}Sr. Significantly, each of these isotopes is stable. Therefore the ratio of $^{86}Sr/^{88}Sr$ will not be modified by radioactivity. In contrast, ^{87}Sr, despite being stable, is constantly being formed due to the radioactive decay of an isotope of Rb, namely ^{87}Rb. Therefore the relative proportion of ^{87}Sr with respect to ^{86}Sr will change over time. Such changes in the abundances of certain isotopes form the basis of one of the most powerful tools in geochemistry and is at the heart of geochronology. This will be investigated further in Chapter 5, but it is useful to note at this point that the approach of measuring relative ratios of the isotopes, rather than their absolute abundances (i.e. reporting the $^{87}Sr/^{86}Sr$ ratio rather than the actual number of ^{87}Sr and ^{88}Sr atoms present) is central to both the measurement of isotopes and their interpretation. The reasons for this are both instrumental and mathematical.

2

Processes

At this point, with an appreciation of what an isotope actually is with respect to a chemical element and/or an ion, it is useful to investigate the processes that can cause variations in the relative proportions of the isotopes of an element. At heart, this is the key to the isotope geochemistry, as it is the *changes* in isotopic ratios that inform geoscientists of rates and process.

2.1 Fractionation: chemical vs isotopic

In essence, isotope geochemistry is an understanding of fractionation, a term that is used in a range of applications and situations. Fractionation is used in several confusing contexts in geochemistry, and it is important to distinguish between *chemical* fractionation and *isotopic* fractionation.

Although it is often clear from the context, chemical fractionation is the process by which a mixture is separated into smaller quantities of differing compositions. That is, changing the chemical composition through successive operations (e.g. crystallisation, boiling, precipitation), each of which removes one or other of the constituents. Such a process is driven by a gradient, generally thermal or chemical, but it can also be physical. Hence chemical fractionation drives differentiation of magmas (e.g. fractional crystallisation), or can occur during boiling and/or phase separation of hydrothermal fluids. Significantly, however, all chemical fractionation processes generally refer to changing chemical proportions or phases.

A commonly observed example of chemical fractionation in the earth sciences is the presence of the Eu anomaly in magmas crystallising plagioclase (Figure 2.1). Unlike the other rare earth elements (REE), Eu is unique in that it can form Eu^{2+} ions which are small enough to sit happily in the crystal lattice instead of the Ca^{2+} ions which make up the bulk of the crystal. In this case the Eu is said to substitute for Ca, and is extracted from the magma preferentially with respect to the other REE, which are otherwise chemically very similar to Eu. This has the result that the remaining liquid

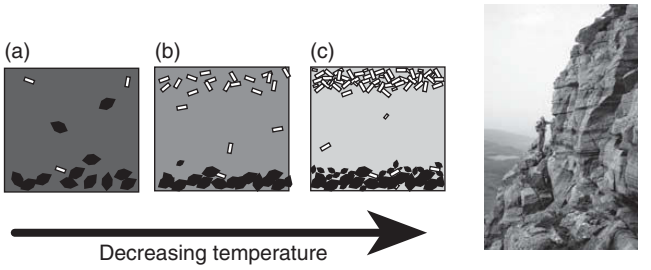

Figure 2.1 A schematic example of chemical fractionation as observed in a hypothetical crystallising magma chamber. A mafic magma may crystallise olivine (a), which is dense and accumulates in the bottom of the chamber. Due to the change in composition of the magma, plagioclase crystallisation is promoted (b), which is less dense and accumulates at the top of the chamber. Crystallisation continues until either the magma has frozen solid or the fractionated liquid in panel (c) is extracted, leaving cumulates of alternating light and dark bands, as observed in the layered ultramafic complex on the Isle of Rum, Scotland.

will not have as much Eu as expected, since it is locked up (fractionated) in the plagioclase. If the magma subsequently separates from the plagioclase and crystallises elsewhere, when we analyse it and observe the presence of the negative Eu anomaly we can infer the role of plagioclase fractionation. Thus chemical fractionation occurs in almost every geological process, and in essence ore deposits are the end product of the most impressive chemical fractionation processes operating in the crust.

2.2 Isotopic fractionation

Chemical fractionation may itself impart an isotopic fractionation between the starting material and the product(s). However, it is useful to think of isotopic fractionation as *any* process which is able to change the *ratio* of two isotopes of the *same chemical element*, and this can occur via four fundamental processes:

(1) equilibrium fractionation
(2) kinetic fractionation
(3) transient kinetic fractionation
(4) mass independent fractionation.

A fifth process, radioactive decay, also changes the isotopic ratios of an element, but the process is distinctly different (i.e. is nuclear, not physicochemical) and is worth considering independently (see Chapter 5). Of these four processes, the first two are of great importance in understanding mineralised systems. The third, transient kinetic fractionation, undoubtedly takes place; however, the geological record does not preserve its effects due to the time scales involved. Mass

independent fractionation is only now being routinely measured in some isotope systems and is likely to become of greater significance in ore deposit studies in the future.

2.2.1 Equilibrium fractionation

This is the partial separation of isotopes between two or more substances which are in chemical equilibrium: i.e. the forward and backward reaction rates between the reactants are identical. Light isotopes remain in the higher-energy state as the heavier isotopes energetically favour the low-energy state. Most equilibrium fractionations are considered to take place from the reduction in vibrational energy within a molecule when a heavier isotope is substituted for a lighter one.

Significantly, each reactant molecule is identical to a product molecule except for the change in distribution of isotopes. In chemistry such molecules are described as isotopologues.

For example, the equilibrium exchange between quartz and haematite:

$$2Si^{16}O_2 + Fe_3{}^{18}O_4 \Leftrightarrow 2Si^{18}O_2 + Fe_3{}^{16}O_4.$$

In this example, the Si–O bond is stronger than the Fe–O and so the reduction in vibrational energy is greater when a heavier O isotope (either ^{17}O or ^{18}O) is substituted for ^{16}O.

Similarly, phase-change reactions, such as evaporation of water or melting of ice, are equilibrium processes (when in a closed system) and are therefore able to fractionate isotopes. The heavy isotopes are invariably concentrated in the denser phase, e.g.:

$$H_2{}^{16}O_{(l)} + H_2{}^{18}O_{(g)} \Leftrightarrow H_2{}^{18}O_{(l)} + H_2{}^{16}O_{(g)}$$

and

$$H_2{}^{16}O_{(s)} + H_2{}^{18}O_{(l)} \Leftrightarrow H_2{}^{18}O_{(s)} + H_2{}^{16}O_{(l)}.$$

Equilibrium processes are quite common, and can be quite temperature sensitive. Such fractionations form the basis of many of the commonly applied palaeothermometers (O and H isotopes in ice cores, speleothems). The effects are strongest at low temperatures, and in general the isotopes of lighter elements are more susceptible to the effects since the relative difference in mass between the isotopes is greater. For example, ^{2}H is twice as heavy as ^{1}H, and ^{18}O is 12.5 per cent heavier than ^{16}O.

Such behaviour can be described in terms of the **fractionation factor**, α:

$$\alpha = \frac{({}^{h}X/{}^{l}X)_{AX}}{({}^{h}X/{}^{l}X)_{BX}}, \qquad \text{(Eq 2.1)}$$

where h and l refer to the heavy and light isotopes of element X in compounds AX and BX. For $\alpha = 1$, the isotopes are distributed evenly between the reactant and product, and hence no isotopic fractionation takes place. $\alpha > 1$ indicates that the heavy isotope is preferentially distributed into substance AX, whereas $\alpha < 1$ indicates that the heavy isotope is concentrated into BX. Using the quartz–haematite example above:

$$\alpha = \frac{({}^{18}\mathrm{O}/{}^{16}\mathrm{O})_{\mathrm{qtz}}}{({}^{18}\mathrm{O}/{}^{16}\mathrm{O})_{\mathrm{hem}}}. \qquad \text{(Eq 2.2)}$$

Note that convention dictates that isotopes are generally expressed in ratios of heavy over light (${}^{h}X/{}^{l}X$), so you will often see ${}^{18}\mathrm{O}/{}^{16}\mathrm{O}$, ${}^{2}\mathrm{H}/{}^{1}\mathrm{H}$, etc. Exceptions do exist, so it is important to always pay attention to the system in question (see Section 4.1).

Equilibrium fractionation is a type of **mass dependent** fractionation, as the masses of the isotopes involved are controlling or playing a role in their subsequent distribution. Such fractionations are intuitively more readily grasped than **mass independent fractionation** (see Section 2.2.4).

2.2.2 Kinetic fractionation

Kinetic fractionation occurs when the forward and backward reaction rates are not the same, and hence there is a preferred 'direction' in the reaction. It is useful to think of kinetic effects as being associated with chemical reactions in which chemical bonds are being broken and new ones being formed. Hence the reaction rates, and therefore relative proportions of isotopes available to be incorporated in the products, can be thought to be a function of the vibrational energy of the bond in question. Since the vibrational energy is itself a consequence of the relative masses of the isotopes at either end, then different isotopes of an element occupying the same chemical bond will react at different rates. Since heavier isotopes will react more slowly than lighter ones, residual reactants will become enriched in heavy isotopes and products enriched in light ones.

Such examples are well illustrated in organic systems, specifically by the relative behaviours of the C–H bond. Substituting a ${}^{1}\mathrm{H}$ with ${}^{2}\mathrm{H}$ represents a change in mass of 100 per cent, whereas substituting a ${}^{12}\mathrm{C}$ with ${}^{13}\mathrm{C}$ represents only an 8 per cent mass increase. Significantly, reactions involving a ${}^{12}\mathrm{C}$–${}^{1}\mathrm{H}$ bond are typically

approximately eight times faster than those involving a $^{12}C–^{2}H$ bond, whereas a $^{12}C–^{1}H$ is only 1.04 times faster than a $^{13}C–^{1}H$ bond, even though in both cases there is only 1 amu difference. This distribution of mass produces a measurable effect on the reaction rate, with lighter isotopes generally favoured for participation within the reaction.

Hence the **isotopic kinetic effect** can be represented as:

$$\alpha_{KE} = \frac{k_l}{k_h}, \qquad \text{(Eq 2.3)}$$

where k_l is the reaction rate constant for the light isotope and k_h represents the reaction rate constant for the heavy. The reaction rate (k) is itself a function of temperature and the relative concentrations of the reactants and products.

Note that this differs from the equilibrium situation (Equation 2.1), where the fractionation was described simply by the relative isotopic ratios of the reactants and products. In this case the degree of fractionation depends on the rate of the reaction – hence the term kinetic.

2.2.2.1 Rayleigh fractionation

The Rayleigh equation and derivative forms refer to the kinetic partitioning of isotopes between two reservoirs as one reservoir decreases in size during the reaction. Hence they can be used to describe a system that contains a mixture of molecules of two or more isotopic species (often, say, water containing ^{18}O and ^{16}O) in which:

(1) material is continuously removed or transferred to a site in which it is no longer in equilibrium with the reaction(s); and
(2) isotopic fractionation associated with the removal of material can be described by a constant (unchanging) fractionation factor, α.

In such scenarios:

$$\left(\frac{R}{R_o}\right) = \left(\frac{X_l}{X_{l_o}}\right)^{\alpha-1}, \qquad \text{(Eq 2.4)}$$

where R is the isotopic ratio (e.g. $^{18}O/^{16}O$) of the remaining reactants, and R_o is original isotopic ratio; X_l is the concentration of the light isotope and X_{lo} is the original concentration of that isotope.

What is useful about this description is that we can consider it in terms of the fraction of material remaining (i.e. that is available to be reacted), f.

Hence if $f = X_l/X_{lo}$, then:

$$R = R_o f^{(\alpha-1)}. \quad \text{(Eq 2.5)}$$

Therefore Rayleigh fractionation deals with a situation in which the isotopic composition of the reactant is itself constantly changing due to the reaction that is taking place. Such situations are very common in the geosciences, and include crystal settling in a magma chamber or wind-blown evaporation. Indeed, the term f is commonly used in equations describing chemical fractionation of trace elements in magmatic systems.

2.2.3 Transient kinetic isotopic fractionation

When the chemical reactions producing isotopic fractionation cannot be described using simple kinetic criteria, such as the Rayleigh equation, transient kinetic fractionation effects can be described. These are significant in biological processes, particularly in reactions which involve catalysts and/or enzymes. The descriptions of these processes are related to the rates of the reactions and act on time scales which are generally shorter than those of interest to economic isotope geochemists. Indeed, the specialised formulations of these equations were developed in terms of biochemical processes explicitly related to biomass and the effectiveness of biological substrates, and have applications in the soil sciences in particular.

It is mathematically possible to substitute the forms of the General Equations for Biochemical Isotope Kinetics (GEBIK) and General Equations for Biochemical Isotopic Fraction (GEBIF) to geological equivalents; however, the emphasis in such formulations is on describing the instantaneous isotopic ratio within reaction systems that are of short time duration, and are implicitly assumed to continue to completion. Such situations, particularly when the masses of reactants and catalysts are not appreciably changing with time, can generally be approximated by Rayleigh-type processes for geological applications. Additional factors, such as quasi-steady state assumptions, can also be considered; however, to date their application within the geosciences has been limited to an understanding of organic isotope geochemical processes.

2.2.4 Mass independent fractionation

Mass independent fractionation (MIF) refers to isotopic separation where the degree of separation does not scale as a proportion of the difference in masses. This is in stark contrast with the three examples described above, where isotopic fractionation is described mathematically and systematically due to the differences

in isotopic mass controlling atomic/molecular velocities, diffusivity, bond strengths and vibrational frequency.

Although far less common in nature, MIF processes are generally associated with photochemical reactions and the so-called 'forbidden transition' reactions. In quantum physics and chemistry this term does not mean that such reactions are impossible, rather that a specific subset of reaction types (the electric-dipole transitions) are forbidden. The reaction (transition) can still occur, albeit at a lower rate than the 'allowed' transitions. Significantly, MIF processes are determined by nuclear volume and nuclear spin effects. These relate to the distribution of the neutrons and protons *within* the nucleus. This distribution actually affects the chemical behaviour of isotopes via (1) the distribution of electrons within their orbitals (nuclear field shift) and (2) the electrons' magnetic field interactions with the nucleus (nuclear spin effect).

MIF was first observed in O isotopes in highly refractory inclusions in meteorites. The significance was that in such inclusions both $^{18}O/^{16}O$ and $^{17}O/^{16}O$ vary by the same amount, even though the mass difference between ^{18}O and ^{16}O is almost twice as much as the mass difference between ^{17}O and ^{16}O. Since kinetic or equilibrium effects would predict that the fractionation would be greater for isotopes that have a greater mass difference, clearly another factor is at play. Initially attributed to incomplete mixing of different reservoirs of differing compositions in the early solar system, subsequent investigations of the solar wind and a greater understanding of MIF suggests that photochemical dissociation of CO in the solar nebula may be responsible.

A more significant example for the minerals industry relates to MIF of S isotopes on the early Earth. The presence of an oxygen-rich atmosphere would effectively prevent, or severely retard, MIF of S due to photodissociation by ultraviolet (UV) radiation. The observation that sediments older than 2.45 Ga actually contain MIF S isotopic signatures points to a highly reducing atmosphere prior to this time. Further, such signatures highlight the key role of sulphate-reducing bacteria prior to oxidation of the atmosphere.

Unfortunately the theoretical underpinning of MIF is not at the same state as for equilibrium and kinetic fractionations – for the latter we are able to calculate the fractionation factor (α) from quantum mechanics (although we did not do so here!). Our approach to date for MIF has been more empirical, and in the absence of any general forms of governing equations, the interested reader is referred to the review article by Thiemens *et al.* (2012).

For readers interested in the application of analytical techniques to the development of 'non-traditional' metal isotopes, an excellent summary can be found in Epov *et al.* (2011), although rapid advances in the field mean such summaries tend to date rapidly. Of interest to the industry at the current time is

that appreciable natural MIF has been observed in some metals, most notably Hg, and, with smaller magnitudes Sn, Cd and Te. U also displays redox-sensitive isotopic fractionations which may be due to nuclear field shift effects and hence mass independent. Future applications as tracers in both exploration and environmental settings are foreseeable as the technology improves; however, at the time of writing there are no 'routine' metal isotope protocols. The potential is, however, enormous in tracking potential sources of metals in both economic geology and particularly the environmental sciences, where photo-dissociation may play a role.

3

Mass spectrometry

Mass spectrometry comprises a range of different sample introduction and ionisation techniques, but all (TIMS, PIMS, N-TIMS, ICP-MS, etc.) effectively analyse the sample in the same way. Many applications of mass spectrometry are oriented towards measurement of isotopic ratios, but mass spectrometric methods also offer some of the highest precision concentration determinations for a wide range of elements. Therefore this section will review what a mass spectrometer is and how it works, before touching upon quantitative analysis of elemental abundances in addition to precise isotopic analysis.

3.1 Principles of mass spectrometry

Gas source mass spectrometers are generally used for lighter-mass stable isotope studies and Ar isotope geochronology, whereas **solid** and **plasma** source mass spectrometry are used for other isotopic and trace element analysis.

Regardless of sample preparation, introduction and ionisation (see below), the actual measurement procedure of all mass spectrometers revolves around the same basic method. In essence, this comprises ionisation of the sample, and then accelerating the ions to a known velocity in a high vacuum. The ions are then deflected by virtue of their mass through a strong magnetic field. Hence ions of a single atomic mass will form a beam which can be measured in terms of its intensity – the more ions present, the more intense the beam of a given atomic mass. The only variation on the magnetic mass discrimination just described involves the use of a quadrupole; however, 'magnetic sector' instruments still provide the greatest mass resolution and hence precision on isotopic ratios. Both methods are able to measure the amount of a given element present and also the relative amounts (ratios) of isotopes present.

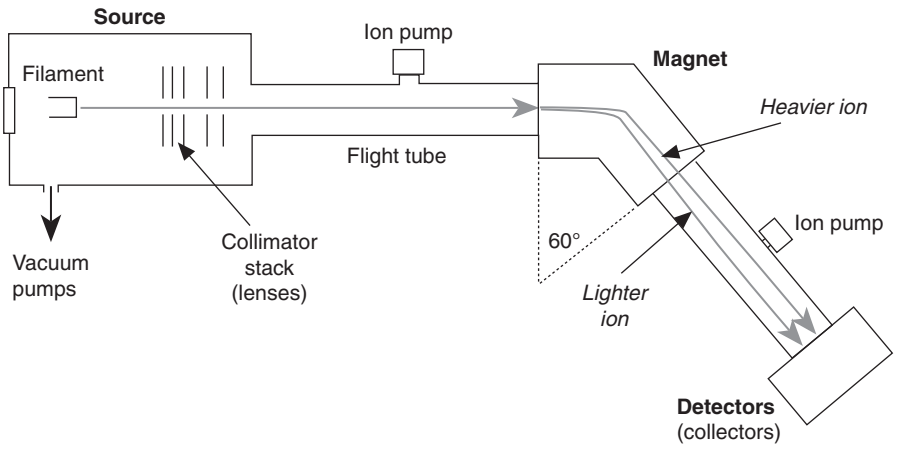

Figure 3.1 Schematic summary of a thermal ionisation mass spectrometer (TIMS) with a magnetic sector analyser. Ions are accelerated through the collimator stack to produce an ion beam in which all ions are travelling at the same velocity. These ions then pass through a strong magnetic field. Ions are deflected in the presence of a magnetic field by an amount that is proportional to their mass and velocity – therefore heavier ions are not deflected as much as light ions. The resulting stream of ions ('beam') of constant mass is then focused into a detector (see Section 3.1), where the intensity of the beam is directly proportional to the number of ions present of that mass.

3.1.1 Ion extraction

Regardless of how the sample is ionised (see below), ion extraction measurement systems are typically at very high vacuums (3×10^{-7} to 8×10^{-8} mbar). Acceleration of the cloud of ions is achieved by a series of plates (the source collimator stack). The first (extractor) plate is held at very high potential – usually 10 000 V (10 kV). The potential on the plates progressively decreases, until the last is at 0 V, resulting in a beam of ions which are all travelling at exactly the same velocity. Slightly altering the voltages on the subsequent plates allows the ion beam to be focused. The beam of ions then passes through into the flight tube (Figure 3.1), and on to the magnet for mass discrimination.

3.1.2 Magnetic sector analysis (MSA)

The most common form of mass spectrometer for precise isotopic ratio measurement discriminates on the basis of passing the beam of ions through a magnetic field (Figure 3.1). The magnet is a large electromagnet, which is capable of changing the intensity of the magnetic field in order to select the required mass. As the ions are electrically charged particles, they are deflected

by the intense magnetic field generated by the magnet. Lighter ions are deflected further than heavy ions by their interaction with any given magnetic field intensity. This deflection takes the form of a circular path, the radius (r) of which is

$$r = \frac{mv}{qB}, \qquad \text{(Eq 3.1)}$$

where v is the velocity of the ion, q is the charge of the ion, m is the mass of the ion and B is the strength of the magnetic field. Since we have accelerated all of the ions to a constant velocity, and the ionisation procedure (see below) produces singly charged cations (such as Nd^+ or Sr^+), the two variables controlling the amount of deflection of ions are their mass (m) and the strength of the magnetic field. By carefully adjusting the magnetic field intensity, the spectrometer is able to target ions of specific mass into the collector.

3.1.3 Quadrupole analysis

Alternatively, ions can be sorted into the masses by use of a quadrupole, or 'quad'. In principle the quad is relatively simple, but in reality it is a highly sophisticated instrument. It consists of four parallel circular rods, each about 30 cm long and 1 cm in diameter (more advanced versions have hyperbolic sections rather than circular) arranged in a square (Figure 3.2). Pairs of opposing rods are connected to a radio frequency (RF; typically about 1 MHz) and DC electrical supply, respectively. Ions of different mass (m) to charge (q) ratio (m/q) resonate in the RF, and by changing the ratio between the DC and the RF, only those ions of a particular m/q resonate on a harmonic which allows them to pass through the quad to the collector.

3.1.3.1 Electrostatic analysis

Whereas a TIMS machine will change mass by changing the magnetic field, on many ICPs and even GC IRMS the magnet will be held stationary for small mass ranges (<10 amu) and the different masses will be directed into the detector by small variations in the *electrostatic analyser* (ESA). The ESA is a pair of curved plates held at high voltage to impart an electrostatic field on the ion beam. Thus the radius of curvature of an ion beam can be further modified (or focused) after it has passed through the magnet, allowing rapid scanning through adjacent masses simply by varying the potential on the ESA. This is because scanning through masses by changing the magnetic field takes slightly longer, and the magnet needs time to settle ('dead time') between each mass. The ESA, on the other hand, simply changes the potential across the electrostatic field, allowing quick changes between

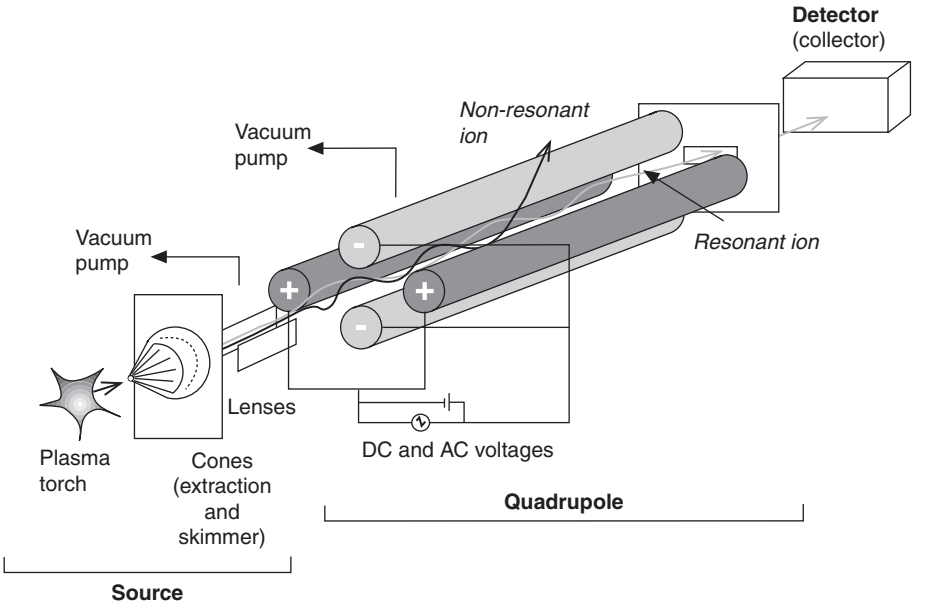

Figure 3.2 Schematic summary of a quadrupole mass analyser. The ion beam is subjected to combined electric fields which impose resonance on the ions, the wavelength of which is a function of their mass.

closely spaced mass units. Hence the ESA is seldom used as the sole means of mass discrimination, but is often placed in conjunction with a quadrupole or magnet. If the ESA is after the magnet/quad, the mass spectrometer is said to have a 'normal' geometry; if it is placed before, the mass spectrometer has a reverse geometry. The nuances and advantages of these configurations are beyond the scope of this introduction, but the terminology does come up in everyday use – SHRIMP RG, for example, stands for SHRIMP reverse geometry.

3.1.4 Collectors/detectors

The simplest type of collector in common use is the Faraday cup, which is also the collector used for most data collection. The stream of ions arriving at the detector is effectively carrying an electric current, and hence the intensity of the signal is measured in millivolts (mV); i.e. the more ions arriving, the greater the current across the Faraday cup. However, some elements have isotopes that are only present at abundances below the detection limit for a Faraday cup. In these instances, more sensitive detectors are used, such as a secondary electron multiplier (SEM). These detectors are up to 1000 times more sensitive than the Faraday cup, and can be referred to as ion counters (ICs). Effectively, these detectors 'count' the

arrival of each individual ion in the detector, and hence the intensity of the signal is recorded in counts per second (cps = the number of ions arriving at the detector per second). Each arriving ion strikes the surface of the detector, causing the emission of 'secondary' electrons, which in turn strike a second surface, causing emission of more electrons and so on, until a significant cascade of electrons is developed, allowing measurement of signal strength through the current generated. Other ion counters are also used, although increasingly rarely, including the Daly doorknob (a post-acceleration detector with a photomultiplier).

The background noise on an SEM is typically of the order of 0.5–1 cps, resulting in a detection limit for ion counters of 2–3 cps.

3.1.5 Detection limit and sensitivity

For elements of low abundance, the peak intensity seen by a detector may be very close to the background level of 'noise' produced by the machine. As elements of low abundance approach the background, they become close to their detection limit. The detection limit is usually taken to be the mean value of the background, plus three standard deviations. There is therefore a 99.87 per cent probability (see Section 6.2.2) that any signal greater than background + 3σ is a true signal and not a random fluctuation in the background. When a signal is below this limit, it is said to be below detection (often written as b.d.).

Sensitivity is a measure of the ability of a detector to record a signal. Given a constant level of background noise, and hence detection limit for a given element, then a detector with high sensitivity will record signals above the detection limit at lower concentrations than a detector with low sensitivity (Figure 3.3).

3.1.6 Data collection

Regardless of ion source or means of mass discrimination, data are collected by altering the (magnetic or electric) field to alternately collect ions of different mass. Individual masses are targeted at the collector for a few seconds each. The ratios between the total voltages recorded at each mass are then used to give isotope ratios. This is called dynamic collection, which takes place on *single collector* machines. Modern machines have up to 15 collectors (some of which are moveable), enabling isotopes of different masses of the same element to be collected simultaneously. This is called static collection and takes place on *multi-collector* (MC) mass spectrometers. Multi-collection is by far the most efficient form of analysis as measurements of high precision require far less time to make. This optimises the amount of data collected on ion beams of small intensity or short duration, a feature particularly important for *in situ* analytical techniques.

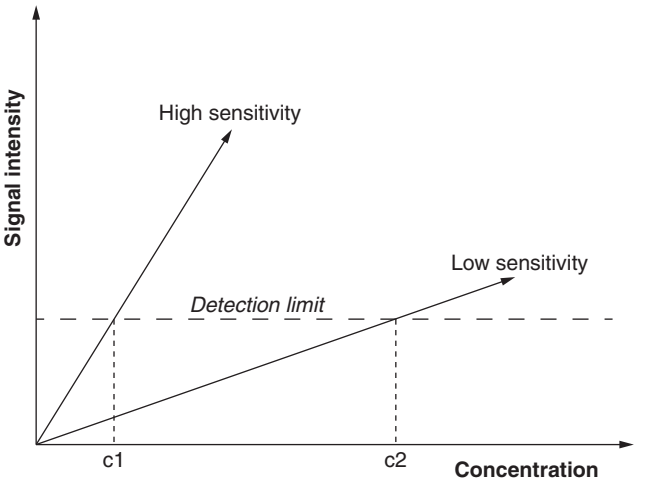

Figure 3.3 Relationship between the sensitivity of a detector (or different elements in the same detector) and the detection limit. Detectors (or elements) with higher sensitivities will produce signals above the detection limit at lower concentrations (c1) than those with low sensitivity (c2).

Aside: the separation between peaks of adjacent masses is referred to as the mass resolution. It is defined as the ratio between the distance by which the centres of two adjacent peaks are separated, and the width of the peak at 10 per cent of its intensity. Although not critically important for trace element analysis, mass resolution can be the limiting factor for the sensitivity of a mass spectrometer (before you get into quantum effects). In the quest for ever-increasing mass resolution, the latest generation of mass spectrometers have magnets which weigh several tonnes and flight tubes ~15 m long (cf. the more typical 1–2 m, Figure 3.1), which result in widely spread adjacent mass peaks by the time the ions reach the collectors. Magnetic sector analysis (Figure 3.1) generally offers better mass resolution than quadrupole analysis (Figure 3.2); however, increasingly machines are being designed which combine both with ESAs. The pros and cons of different configurations of mass discrimination techniques fill many volumes of turgid scientific literature. For our purposes, it is sufficient to appreciate the conceptual difference between them.

3.2 TIMS vs ICP-MS (PIMS) vs GS IRMS

Thermal ionisation mass spectrometry vs inductively coupled plasma mass spectrometry (or, more generally, plasma ionisation mass spectrometry) vs gas source isotope ratio mass spectrometry.

The preceding discussion has centred wholly upon actually measuring the sample in a mass spectrometer once it has been ionised. There are three methods of ionising geological samples for mass spectrometric analysis:

(1) thermally,
(2) by plasma,
(3) by combustion (for gas source mass spectrometers; see below).

Because of the quite pronounced differences between the sample preparation and introduction techniques, many people regard TIMS, ICP-MS and IRMS as fundamentally different. However, as we have seen from the preceding description, they are all fundamentally the same in the middle (mass discrimination) and at the detection end.

3.2.1 Thermal ionisation mass spectrometry

Thermal ionisation mass spectrometry (TIMS) involves an extended chemical extraction procedure to produce a highly purified salt of the element of interest. This purified salt (such as $OsBr_2$ or $NdCl_2$, or a nitrate, depending on the element of interest) is carefully loaded onto a filament which is made of a high melting point metal, such as Ta, Re, Ni, W or Pt (obviously Re filaments aren't used for Re–Os analysis as they would interfere with the analysis). These loaded filaments are placed in the mass spectrometer, which is then pumped down to ultra-high vacuum. A current is run through the filament – depending on the composition of the filament, anywhere between 0.9 A (~850 °C in a Pt filament) and up to 6 A (>2000 °C in an Re filament). The process is analogous to an incandescent light bulb; at these temperatures ions of the purified sample loaded on the filament are formed. These ions are extracted into the mass spectrometer and analysed as described above.

3.2.1.1 N-TIMS and analysis of oxides

Just about all mass spectrometers produce beams of positively charged ions such as Sr^+, Nd^+, Pb^+, etc. However, some elements (such as Re, Os, W and Ir) are very reluctant to form such positively charged species, and it was discovered that instead they ionise readily as oxides to form negatively charged ionic species (e.g. Os forms OsO_3^-, Re forms ReO_4^-, etc.). Thus, by reversing the polarity of the magnet and changing the accelerating voltage in the collimator stack, it is possible to convert many mass spectrometers to measure negative ions. This has resulted in remarkable increases in *ionisation efficiency*, going from ~0.2 per cent as metallic positive ions (i.e. Os^+ and Re^+) to 15 and 30 per cent for OsO_3^- and ReO_4^-, respectively. This negative ionisation technique is referred to as N-TIMS. Other

elements can also be more efficiently measured as oxides as well, but these elements may form oxides which are positively charged. NdO^+ is one example where increased sensitivity in a standard (positive ion) mass spectrometer can be achieved by ionising in the presence of oxygen in the source to form ionised oxide complexes.

3.2.2 PIMS/ICP-MS

In contrast to the long and labour-intensive chemical sample preparation conducted for TIMS, sample preparation for most PIMS techniques involves simply dissolving the (silicate) sample to produce an aqueous solution. Generally, sample dissolution is conducted using an $HF–HNO_3$ mixture, and is commonly done in high-temperature, high-pressure Teflon 'bombs' (typically overnight at ~240 °C) to ensure complete dissolution of resistant accessory phases, such as zircon.

Once in aqueous solution, the user has the choice of proceeding with more elaborate chemical purification procedures (and even spiking for isotope dilution (ID) measurement, see below), or simply analysing everything in a PIMS. The sample is diluted in acid (typically nitric), and passed as an aerosol from a nebuliser into an Ar plasma. The plasma is formed by inductive heating of a stream of Ar atoms from a high RF coil (hence the 'inductively coupled' portion of the abbreviation). The plasma torch is ignited by a high-frequency spark. The plasma is typically of the order of 8000 K (~7700 °C), which effectively dissociates most chemical bonds and produces ionised species. These ions are then extracted from the plasma torch and introduced into the mass spectrometer. This effectively results in 100 per cent ionisation of the sample solution, but typically only 1 per cent of the ions are extracted into the mass spectrometer.

3.2.3 Gas source isotope ratio mass spectrometry: GS IRMS

Gas source mass spectrometers generally introduce the sample as a gas, either previously collected or reacted at the time of the analysis (e.g. by combustion of carbonates to produce CO_2), where it is then introduced into the ion source. Ionisation generally takes place in the presence of a hot filament positively ionising the species, which then enters the lens stack. An electron trap absorbs the excess electrons liberated during ionisation in order to avoid charge build up. GS IRMS has long been the workhorse of light element stable isotope geochemistry, with considerable effort being invested in sample preparation and introduction. Many variations exist in terms of equipment configuration and operation, including the development of gas chromatographic (GC) introduction techniques.

At heart, GS IRMS requires measurement relative to a standard gas of known composition which is analysed during the same analytical run. This standardisation can occur either via a dual-inlet system, whereby the standard gas and the unknown are alternately measured repeatedly during the session, or via a continuous flow (CF) IRMS system, whereby the standard gas is analysed before and/or after the sample (or even a series of samples). Such continuous flow instruments allow a greater sample throughput but generally produce data of lower precision than dual-inlet systems due to shorter analysis times and a smaller number of standard analyses.

GC IRMS analyses are therefore heavily dependent on measuring the variation in the isotopic signature of an unknown with respect to the standard – it does not matter as much what values the sample and standard actually return, more how different they are from each other. TIMS and ICPMS instead measure the actual ratios and compare the values obtained with external measurements of standards in order to assess accuracy.

3.3 *In situ* mass spectrometry

3.3.1 Secondary ionisation mass spectrometry

Effectively identical to other mass spectrometers in terms of mass discrimination, secondary ionisation mass spectrometry (SIMS) instruments (of which the SHRIMP has achieved a high profile through applications in U–Pb zircon geochronology) differ by virtue of how the material is sampled and subsequently ionised. In essence a SIMS instrument operates by analysing the material ejected from the surface of a sample by bombarding, or sputtering, it with a beam of heavy ions, such as O^- or Cs^+. The secondary ions liberated from the sample are collected and analysed, generally with a magnetic sector mass spectrometer, often in combination with a quadrupole. Such *in situ* analysis allows isotopes to be measured from within individual grains. The small sample volume analysed, coupled with the excellent spatial control, makes SIMS analysis a very powerful tool for both stable and radiogenic isotopic analysis.

3.3.2 Laser ablation ICP-MS: LA-(MC)-ICP-MS

In a manner analogous to SIMS, a laser can be focused onto the surface of a sample, generally a polished thin section or block, ablating the material. In this case, though, the sample is not ionised at the site, but rather carried by an inert gas, such as Ar or an He–Ar mix, to a plasma where it is ionised and analysed within

a standard geometry (MC)-ICP-MS. Again, the small sample size and good spatial resolution make this technique a powerful tool for isotopic analysis.

3.4 Noble gas mass spectrometry and irradiation for Ar analysis

The noble gases (He, Ne, Ar, Kr and Xe ± Rn) possess a very unique range of geochemical applications due to their highly unreactive and volatile nature. This enables applications in tracer studies through the solid earth which is relatively unaffected by chemical processing. More significantly, the decay of ^{39}K to produce ^{40}Ar has produced a broad range of geochronological applications due to the high abundance of K in the earth, and the unreactive nature of the daughter product. However, such a dichotomy in geochemical behaviour has also been one of the greatest limitations to precise analysis since historically both of these isotopes were measured in radically different ways. Hence considerable effort has been expended on effective ways to analyse Ar in particular.

However, in general, noble gas mass spectrometry can be considered to be a type of GS-IRMS, whereby the sample is introduced to the mass spectrometer and ionised in the presence of a hot filament (see Section 3.2.3). Given that the noble gases are chemically inert, ionisation is relatively inefficient, and in order to maximise the amount of ions produced, the sample is typically all introduced simultaneously with no further supply, unlike conventional IRMS. This is so-called static mass spectrometry.

The truly unique aspect of Ar–Ar geochronology is the development of a protocol to supersede K–Ar measurements. Since K–Ar requires two radically different approaches to analyse the K and the Ar, the two were historically analysed on separate aliquots of the same sample, thus limiting the ultimate precision of the ages obtained. Instead, Ar–Ar involves taking a single aliquot (or mineral separate or grains) and subjecting it to neutron irradiation, thereby converting some ^{39}K to radioactive ^{39}Ar. Since ^{39}Ar has a half life of 269 years, it does not exist in nature and therefore all ^{39}Ar measured, which can be collected simultaneously with the daughter product, ^{40}Ar, must have come from the ^{39}K. Assuming that ^{40}K and ^{39}K exist in constant proportions in nature, it is then relatively simple to calculate the amount of the parent isotope, ^{40}K, based on the amount of ^{39}Ar measured.

Therefore, by converting another, adjacent element into a noble gas, it is possible to measure precisely the relative abundances and ratios of both elements in a single analytical step. While this has been applied primarily for geochronology in the case of Ar (see Chapter 9), such an approach can also be used to determine the ratios of the halogens (particularly, Cl, Br and I), which can be of central importance to ore deposit genesis. In all cases, however, from

a mass spectrometry perspective the noble gases are analysed using a specialised type of magnetic sector GS-IRMS.

3.5 Measurement of concentrations by mass spectrometry: isotope dilution

3.5.1 Principle

Mass spectrometers are only capable of measuring isotope ratios. The relative proportions of isotopes of a given element are not much use to us if we want to know elemental concentrations. This becomes particularly important in many geochronological applications, particularly those involving isochrons (Section 7.1). In order to precisely measure the concentration of an element, we can 'spike' it with an accurately known amount of an artificially enriched isotope. The spike is a known mass of the element to be analysed, and is ideally a mass that does not occur naturally (Figure 3.4) or in significant abundance (Figure 3.5).

Hence the *concentration* of an element having more than one isotope can be determined to high precision on a mass spectrometer by a method known as isotope dilution (ID). This involves measuring the isotopic ratio of a mixture of an accurately weighed amount of sample (with an unknown abundance of an element) and an accurately weighed amount of 'spike' whose concentration and isotope ratio of the element of interest are known. The procedure relies on the spike being

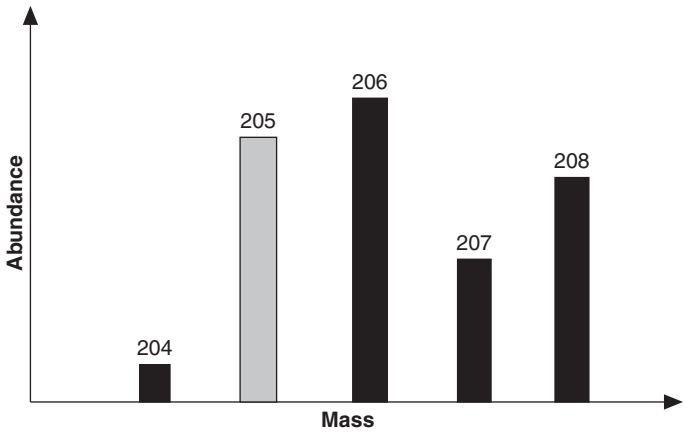

Figure 3.4 Isotope dilution analysis of Pb. ^{204}Pb, ^{206}Pb, ^{207}Pb and ^{208}Pb are all naturally occurring isotopes; ^{205}Pb is an artificial spike. Since we know precisely how much ^{205}Pb we have added to the amount of sample we have analysed, and we know that ^{205}Pb does not occur in nature, the ratio of ^{205}Pb to ^{204}Pb allows us to calculate the total concentration of Pb in the sample.

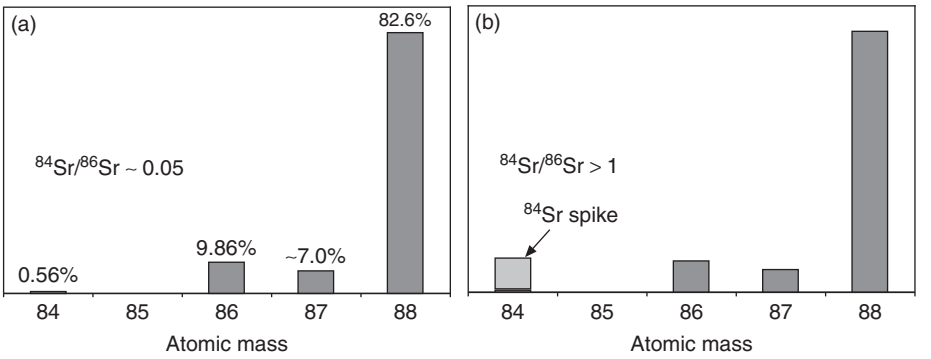

Figure 3.5 Comparison of a spiked and unspiked mass Sr isotope spectrum. In natural samples, ^{84}Sr comprises <1 per cent of all Sr. In isotope dilution (ID), addition of a precisely known quantity of artificially enriched ^{84}Sr allows calculation of the amount of Sr in the sample from measurement of the spiked $^{84}Sr/^{86}Sr$ ratio. This can be analysed in the same session as the radiogenic $^{87}Sr/^{86}Sr$, allowing the maximum amount of data to be obtained from a single sample.

enriched in one of the isotopes of the element. For the general case, the concentration of an element A in a rock or solution is given by:

$$A_m = \left[\frac{^{l}A_s - {}^{h}A_s R_m}{{}^{h}A_n R_m - {}^{l}A_n}\right]\left[\frac{W_n}{W_s}\right]\left[\frac{(\text{weight}_{spike})(\text{conc}_{spike})}{\text{weight}_{sample}}\right], \qquad \text{(Eq 3.2)}$$

where R_m is the measured isotope ratio of the spike–sample mixture (e.g. $^{205}Pb/^{204}Pb$) and ^{h}A and ^{l}A are masses of the two isotopes of element A and the subscripts s and n refer to the isotope abundance in the spike and natural materials (i.e. the sample), respectively. All weights are in grams. W_n and W_s are the atomic weights of the naturally occurring element and the spike, respectively.

More commonly, we will know the spike concentration in moles per gram, in which case the equation reduces to the more usable form:

$$\text{Conc}_{sample} = \left[\frac{R_s - R_m}{R_m - R_n} \times R_n\right]\left[\frac{1 - A_s}{W_n}\right]\left[\frac{(\text{weight}_{spike})(\text{conc}_{spike})}{\text{weight}_{sample}}\right], \qquad \text{(Eq 3.3)}$$

where A_s is the atomic abundance of the spike isotope in nature. This is because generally we are required to spike with artificially enriched naturally occurring isotopes, hence the sample will inevitably contain some of the isotope of interest and hence we must account for it.

However, this equation is particularly useful as we know our sample weight, spike weight and spike concentration; we know the isotopic abundances and

ratios and atomic weight (A_s, R_n and W_n) of natural materials. In addition, we know the isotopic ratio of the spike (R_s), and hence the only unknown in the equation is the isotopic ratio of the mixture, R_m, which is measured on the mass spectrometer.

The concentration is therefore readily calculated. However, care must be taken with units; if all inputs are in grams and moles/gram, then the concentration will be expressed as grams/gram. Given that most trace elements will be present in parts per million or even per billion levels, this will need to be multiplied by 10^6 (to convert to μg/g, or ppm) or 10^9 (to convert to ng/g, or ppb).

Aside: units, and ppm vs μg/g etc. Geochemists and geologists generally think in terms of concentrations in ppm, ppb, etc. and consider these as quite literally so many parts per million or billion of the material in question. These units are actually pseudo-SI units, but are quite useful as long as the user is aware of what is being expressed. As long as it is a truly dimensionless ratio of like-to-like quantities (i.e. mass to mass or volume to volume) they can be useful and instructive. However, when mass to volume conversions, or mole to mass type descriptions, get employed, the potential for confusion escalates. Hence it is generally better (where practical) to use ng/g (ng g^{-1}) or μg/g (μg g^{-1}) than ppb or ppm as this makes it quite clear that the user is intending a mass per mass ratio, and not potentially a volume per volume (as in gas concentrations, say). However, non-standard designations are common throughout the industry, perhaps the most common being g/t for ore grades. Since specialists (and indeed lay-persons through reporting to the stock exchange) are generally familiar with such notation, it has enjoyed widespread use; however, it is potentially an ambiguous term, depending on which ton(ne) is being referred to and the specific commodities in question (which may themselves have a significantly different density and hence atomic proportion per unit volume vs unit mass) with respect to the host material. However, since the tonne = 1000 kg, this is easy to convert to the terms expressed in Table 3.1.

$$
\begin{aligned}
1\ \text{g/tonne} &= 1\ \text{g}/1\,000\,000\ \text{g} && \text{(since there are a million grams in a tonne)}\\
&= 10^{-6}\ \text{g/g} && \text{(dividing both sides by a million)}\\
&= 1\ \mu\text{g/g}, && \text{which is equivalent to ppm (see Table 3.1).}
\end{aligned}
$$

Therefore, 1 g/tonne = 1 ppm.

Although not particularly relevant for isotope work, but in the interests of thoroughness, the other commonly used unit in geochemistry is wt% oxides. Conversion between wt% and ppm (and hence any other g/g unit) of an element is covered in Appendix 1.

Table 3.1 *Equivalence of commonly used concentration units in geochemistry.*

SI prefix	Relative concentration	Concentration per SI unit	Order of magnitude
—	Pure	1 g/g	1
Deci-	%	0.01 g/g	10^{-2}
Milli-	pp thousand*	1 mg/g (0.001 g/g)	10^{-3}
Micro-	ppm	1 μg/g (0.001 mg/g)	10^{-6}
Nano-	ppb	1 ng/g (0.001μg/g)	10^{-9}
Pico-	ppt	1 pg/g (0.001 ng/g)	10^{-12}
Femto-	ppq	1 fg/g (0.001 pg/g)	10^{-15}
Atto-		1 ag/g (0.001 fg/g)	10^{-18}

* Parts per thousand is also sometimes referred to as ppt; however, ppt is more generally used for parts per trillion (pg/g). As long as each abbreviation is clearly defined, either usage is fine. Occasionally parts per thousand can be referred to as per mil (‰), but this is more commonly reserved for parts per thousand variations in isotopic ratios.

3.5.2 Precision of ID analyses

ID offers a highly precise method of determining elemental abundances, and is limited only by how accurately we know both the concentration and isotopic composition of the spike, and how accurately we can weigh out our sample and spike. Unlike other techniques, the precision of the actual measurements made on the machine is one of the smaller sources of error on a concentration determination. Typical detection limits will be of the order of <1 ppb, and for some elements (e.g. Re and Os) can be sub-ppt. Precision depends on how well the spike concentration is known, and can range from as high as 1 per cent relative standard deviation (RSD) in the case of Re to less than 0.25 per cent RSD for elements such as Sm and Nd.

3.5.2.1 Elements able to be analysed

In theory, any element can be measured by ID as long as an artificially enriched spike isotope can be obtained. In reality, because ID techniques are quite time consuming, spikes expensive and machine time limited (mass spectrometers tend to get used for measuring isotopes rather than concentrations), ID measurements are limited to cases where high precision is required, generally for geochronology.

The most routinely analysed elements by ID are the platinum group elements (PGE; Ru, Pd, Os, Ir, Pt, but not Rh as it is mono-isotopic and therefore cannot be spiked for) and elements associated with the PGE, such as Re and Ag (but not Au as it is mono-isotopic). Also, elements which are the parents and daughters of routinely used radiogenic isotope tracers are often analysed by ID on the same

dissolution as the isotope ratio measurement is performed to eliminate sample heterogeneity or 'nugget' effects. Therefore, Rb, Sr, Sm, Nd, U, Th, Pb, Re and Os can all be done routinely by ID if the radiogenic isotopes are also being done.

Prior to the rise of routine instrumental neutron activation analysis (INAA) and ICP-MS techniques, the REE were often measured by ID. All REE except Pr, Tb, Tm and Ho (which are mono-isotopic) can be done by ID, and quite often data obtained in this way are more robust than those obtained by ICP-MS. Hence 20-year-old REE ID data are likely to still be as good as much of the data obtained today.

4

Stable isotopes

When considering stable isotopes, it is worth bearing in mind that most naturally occurring nuclides are themselves actually stable. Only a small number, of the order of 34, are known to be radioactive with sufficiently long half lives that they are 'primordial' and hence still available on the Earth. Many of these have such long half lives (e.g. ^{209}Bi, 4.6×10^{19} yr; ^{180}W, 1.8×10^{18} yr – whereas the age of the universe is only ~13.7×10^{9} yr!) that they are for all intents and purposes stable. Hence, of all the natural nuclides we observe on the earth, we are left with only a small number which are effectively radioactive and of use in the geosciences (see Chapter 5). The result of this is that stable isotopes comprise the vast majority of systems we have available to interrogate.

As described in detail in Section 2.2, a range of processes are capable of fractionating isotopes from one another. Stable isotope fractionation effects can take place on isotopes of *any* element (except of course if an element is monotopic (or mono-isotopic), such as F, Na, P, Au, etc.); however, stable isotope fractionation effects are most clearly developed in the light elements. This is because the relative mass difference is greater between the isotopes of light elements than it is between heavy elements. Remember that both equilibrium and kinetic fractionation are controlled by *relative* masses between species displaying otherwise identical chemistry. Therefore the greater the relative difference in masses, the greater the fractionation. Hence there will be greater fractionation between ^{18}O and ^{16}O in reaction than between ^{17}O and ^{16}O. In contrast, although there is still a 2 amu difference between ^{142}Nd and ^{144}Nd, the relative mass difference is only ~0.5 per cent (compared with ~13 per cent between ^{18}O and ^{16}O), and hence the stable isotopic fractionation due to kinetic and equilibrium processes is correspondingly smaller.

Until relatively recently, it was generally assumed that mass fractionation for isotopes heavier than ~80 amu (i.e. isotopes of Sr) was effectively non-existent. This assumption still plays an important role in many systems

of radiogenic isotopic measurement, since the fractionations are indeed minuscule relative to the radiogenic isotopic effects. However, increasingly sophisticated chemical extraction and analytical techniques have allowed detection of stable isotopic variations in elements as heavy as $_{81}$Tl and indeed $_{92}$U, the heaviest naturally occurring element. At the risk of labouring the point, these shifts are very small and at present such measurements are undertaken in only a handful of laboratories worldwide. However, by understanding the basic nomenclature employed in stable isotope discussions, and the processes associated with their variation, the reader can apply the first principles observations to any stable isotopic system, regardless of whether they have come across it before. Therefore the nomenclature and insights gained from O and S isotopes can be directly translated to (say) Cu and Zn isotopes, even though their respective chemical behaviours are significantly different.

4.1 Nomenclature

Regardless of the isotope system in question, the combination of kinetic and equilibrium fractionations results in very small isotopic enrichments and depletions. For this reason, variations are expressed as the parts per thousand deviation (expressed 'per mil', or ‰) between that measured in the sample and the ratio of a standard material. Such a deviation is the delta (δ), or difference in isotopic signature:

$$\delta^{\mathrm{h}}X = \left[\frac{{}^{\mathrm{h}}X/{}^{\mathrm{l}}X_{(\mathrm{sample})} - {}^{\mathrm{h}}X/{}^{\mathrm{l}}X_{(\mathrm{standard})}}{{}^{\mathrm{h}}X/{}^{\mathrm{l}}X_{(\mathrm{standard})}}\right] \times 1000, \qquad \text{(Eq 4.1)}$$

or alternatively:

$$\delta^{\mathrm{h}}X = \left[\frac{{}^{\mathrm{h}}X/{}^{\mathrm{l}}X_{(\mathrm{sample})}}{{}^{\mathrm{h}}X/{}^{\mathrm{l}}X_{(\mathrm{standard})}} - 1\right] \times 1000, \qquad \text{(Eq 4.2)}$$

where ${}^{\mathrm{h}}X$ is the heavy isotope of element X and ${}^{\mathrm{l}}X$ is the light isotope.

For O isotopes, the variation in ^{18}O is most commonly investigated, and hence would have the following δ notation:

$$\delta^{18}\mathrm{O} = \left[\frac{{}^{18}\mathrm{O}/{}^{16}\mathrm{O}_{(\mathrm{sample})} - {}^{18}\mathrm{O}/{}^{16}\mathrm{O}_{(\mathrm{standard})}}{{}^{18}\mathrm{O}/{}^{16}\mathrm{O}_{(\mathrm{standard})}}\right] \times 1000. \qquad \text{(Eq 4.3)}$$

If one was interested in the variation of ^{17}O, then the form would read:

$$\delta^{17}\mathrm{O} = \left[\frac{^{17}\mathrm{O}/^{16}\mathrm{O}_{(\mathrm{sample})} - ^{17}\mathrm{O}/^{16}\mathrm{O}_{(\mathrm{standard})}}{^{17}\mathrm{O}/^{16}\mathrm{O}_{(\mathrm{standard})}}\right] \times 1000. \qquad \text{(Eq 4.4)}$$

By definition, therefore, the standard has a value of 0‰.

For even heavier elements, such as Tl and U, as alluded to previously, the differences may be even smaller, and so are expressed as epsilon (ε) units, which are the parts per 10 000 difference:

$$\varepsilon^{\mathrm{h}}X = \left[\frac{^{\mathrm{h}}X/^{\mathrm{l}}X_{(\mathrm{sample})} - ^{\mathrm{h}}X/^{\mathrm{l}}X_{(\mathrm{standard})}}{^{\mathrm{h}}X/^{\mathrm{l}}X_{(\mathrm{standard})}}\right] \times 10\,000, \qquad \text{(Eq 4.5)}$$

or:

$$\varepsilon^{\mathrm{h}}X = \left[\frac{^{\mathrm{h}}X/^{\mathrm{l}}X_{(\mathrm{sample})}}{^{\mathrm{h}}X/^{\mathrm{l}}X_{(\mathrm{standard})}} - 1\right] \times 10\,000, \qquad \text{(Eq 4.6)}$$

where $^{\mathrm{h}}X$ and $^{\mathrm{l}}X$ are again the heavy and light isotopes of element X, respectively.

Regardless of the notation used, the standard referred to must always be clearly specified. For O isotopes two have been used widely, and are distinguished by abbreviations as subscripts:

PDB refers to a belemnite from the PeeDee formation in South Carolina (which was also used as a standard for C isotopes). Unfortunately the original belemnite has now been completely consumed, and it is also a somewhat arbitrary geological choice as it does not correspond to a globally unique or significant event. More commonly ***SMOW***, or standard mean ocean water (present day) is used, with the standard light Antarctic precipitation (SLAP) being another that is sometimes used. Older literature will refer to just PDB or SMOW, though their absolute reference values were fixed by convention in Vienna, and so more recent publications will refer to VPDB and VSMOW.

Remember, δ values are expressed as per mil (‰), which is a variation from a standard ratio. The reason for this is in part analytical, but also quite practical – one only has to look at the *actual* values of the isotopic ratios as expressed in Table 4.1 to understand why dealing with numbers with so many decimal places is cumbersome, and a more intuitive (and ultimately meaningful) basis for comparison of measurements is adopted. Further, δ values are now routinely expressed as the ratio of the heavy isotope/light isotope. This also generally corresponds to the less abundant isotope/most abundant isotope (Table 4.2), which is far and away the most common situation. Historically there was much discussion in the literature regarding Li isotopes where the more abundant isotope is the heavier one ($^{7}\mathrm{Li} > ^{6}\mathrm{Li}$), so care needs to be exercised when using these data. The convention has

Table 4.1 *Standard ratios for commonly measured light element stable isotopic systems and the standards against which they are measured. Other standards can be found, but are less common.*

Element	δ	Measured ratio (R)	International standards	R of standard
H Hydrogen	δD_{VSMOW}	$^{2}H/^{1}H$	Vienna standard mean ocean water (VSMOW)	0.00015575
	δD_{SLAP}	$^{2}H/^{1}H$	Standard light Antarctic precipitation (SLAP)	0.000089089
C Carbon	$\delta^{13}C_{VPDB}$	$^{13}C/^{12}C$	Vienna PeeDee belemnite (VPBD)	0.0112372
N Nitrogen	$\delta^{15}N_{air}$	$^{15}N/^{14}N$	Air	0.003676
O Oxygen	$\delta^{18}O_{VSMOW}$	$^{18}O/^{16}O$	Vienna standard mean ocean water (VSMOW)	0.0020052
	$\delta^{18}O_{VPDB}$	$^{18}O/^{16}O$	Vienna PeeDee belemnite (VPBD)	0.0020672
	$\delta^{18}O_{SLAP}$	$^{18}O/^{16}O$	Standard light Antarctic precipitation (SLAP)	0.0018939
S Sulphur	$\delta^{34}S_{CDT}$	$^{34}S/^{32}S$	Canyon Diablo troilite (CDT)	0.045005

$\delta D = \delta^{2}H$; where D stands for deuterium. Deuterium, and the other (radioactive) isotope of hydrogen, tritium (^{3}H), are the only accepted cases where individual isotopes have their own names and symbols, although IUPAC stresses that such usage is 'non-preferred'.

Table 4.2 *Relative abundances of commonly used light element stable isotope systems.*

Element	Symbol	Isotope	%	Isotope	%	Isotope	%	Isotope	%
Hydrogen	H	^{1}H	99.9885	^{2}H	0.0115	^{3}H	(a)		
Carbon	C	^{12}C	98.9	^{13}C	1.10	^{14}C	(b)		
Oxygen	O	^{16}O	99.76	^{17}O	0.04	^{18}O	0.2		
Sulphur	S	^{32}S	95.0	^{33}S	0.75	^{34}S	4.21	^{36}S	0.02
Chlorine	Cl	^{35}Cl	75.76	^{37}Cl	24.24				
Lithium	Li	^{6}Li	7.5	^{7}Li	92.5				
Boron	B	^{10}B	19.9	^{11}B	80.1				

Li and B, while not major elements, are included as they are of the unusual case in which the heavier isotope is the most abundant and as such there is some variation in the older literature regarding the δ labelling convention. (a) radioactive, produced by human activity; (b) radioactive, produced by cosmic rays in the upper atmosphere.

now reverted to expressing them in terms of heavy/light, as this allows workers to immediately see what is being referred to from the sign of the measurement. That is, a positive (+ve) δ value will refer to isotopically heavy samples, and hence materials which have enriched the heavy isotope. These invariably relate to the lower energy state of the system in mind, such as residual seawater after evaporation, or the first minerals to crystallise out of a fluid or melt. Correspondingly, negative (–ve) δ values will refer to isotopically light material, such as water vapour in the air, or fluids and magmas that have fractionated or had the opportunity to previously precipitate solid phases.

4.2 Major element stable isotopes

Major elements in the geochemical sense are those that are highly abundant in the lithosphere. However, for our purposes, we need to extend this to the atmo- and hydrospheres as they form a series of interconnected reservoirs which are instrumental in determining the transport and precipitation of significant economic accumulations. Conventionally major elements in this sense are usually defined as those making up the common rock-forming minerals; however, these include a very limited range of predominantly metallic elements (commonly SiO_2, Al_2O_3, TiO_2, MgO, FeO, CaO, Na_2O, K_2O, MnO and $P_2O_5 \pm SO_3$; all expressed as wt% oxides), many of which are relatively minor constituents in ores or ore-forming processes. Therefore major elements in the ore-forming systems can be more usefully considered to include those that are critical in hydrothermal fluids (H_2O and CO_2) and ore-forming minerals (S, in various oxide forms as well as anionic forms bound with metals, usually S^- and S^{2-}), as well as those participating in key redox reactions (e.g. C in organic sediments and limestones).

Key major element isotopes commonly applied to ore deposit settings are summarised in Table 4.1. Nitrogen (N) is included only for comparison as it is the slightly unusual case of being the major constituent of the atmosphere, and hence is normalised to atmospheric values.

Whether an element is behaving as a major element in the system of interest becomes significant when quantifying its behaviour and calculating the fractionation effects. When an element is behaving as a major element, it is considered to be present in excess and therefore fully able to partake in the reactions controlling the fractionation of the isotopes. Such approximations greatly simplify calculations. In this sense, H behaves as a major element (H_2O) in hydrothermal fluid situations, whereas in mantle-melting situations it can simply be considered as an incompatible trace element with a compatibility comparable to, say, Ce, due to the anhydrous nature of much of the mantle.

It is clear that most of the commonly applied major trace element stable isotope systems are light, non-metallic elements. Historically these have been investigated because their relative abundance and volatile nature made them amenable to analysis by gas source mass spectrometry. Further, their low atomic masses resulted in larger relative shifts in isotopic signatures, allowing ready determination of anomalies.

4.3 Minor and trace element stable isotopes

Continued improvements in both TIMS and ICP-MS technology during the 1990s led to increased investigations into the isotopic characteristics of most elements in the periodic table. Combined with improved chemical purification and extraction techniques, high-precision stable isotopic investigations were undertaken and stable isotopic variations in virtually all trace elements have been observed. Of particular interest in ore-related processes have been those investigations into transition metal isotopes (particularly Cu and Fe). Such applications often followed on technical developments that were first applied in extraterrestrial and planetary formation studies. This was largely because extraterrestrial processes generally resulted in greater isotopic variations than terrestrial and hence were initially analytically easier than many terrestrial applications.

Summarised below are some of the more interesting stable isotopic systems.

Transition metals: Cr, Ni, Fe, Cu, Zn, ± Mo, Cd, Ag

Cu, Zn and Fe isotopes have been the focus of much effort, though in more recent times Mo, Ni and Cr have attracted much interest. Isotopic fractionation on these systems combines the interplay between lower temperature biogenic/hydrosphere processes and inorganic redox processes.

Other metals: Sr, Tl, U

Due to the high precision historically employed with Sr isotopes due to radiogenic studies, and their chemical affinities with Ca, Sr isotopes have enjoyed some applications in palaeo-environmental carbonate studies. Sr has four stable isotopes, of which one, ^{87}Sr, is formed by the ingrowth of ^{87}Rb. The remaining three (84, 86 and 88) exhibit fractionation, and due to its long history of radiogenic investigation, Sr was among the first 'non-traditional' stable isotopic systems to be thoroughly investigated. Applications associated with temperature-dependent fractionation during aragonite precipitation have allowed estimation of palaeo-seawater temperatures and preliminary investigations into hydrothermal fluids and carbonate precipitation are under way.

Fractionations in Tl (^{203}Tl and ^{205}Tl) and U (^{235}U and ^{238}U) have also been observed; however, usage has been limited. U, in particular, shows great potential

Table 4.3 *Relative abundances of commonly investigated transition metal stable isotopes.*

Element	Isotope	%	Isotope	%	Isotope	%	Isotope	%	Isotope	%
Iron	^{54}Fe	5.85	^{56}Fe	91.75	^{57}Fe	2.12	^{58}Fe	0.28	^{60}Fe	(2.6 My)
Chromium	^{50}Cr	4.34	^{52}Cr	83.79	^{53}Cr	9.50	^{54}Cr	2.37		
Nickel	^{58}Ni	68.08	^{60}Ni	26.22	^{61}Ni	1.14	^{62}Ni	3.63	^{64}Ni	0.93
Copper	^{63}Cu	69.15	^{65}Cu	30.85						
Zinc	^{64}Zn	48.27	^{66}Zn	27.98	^{67}Zn	4.10	^{68}Zn	19.02	^{70}Zn	0.63

as it exhibits both substantial redox variations in environmental applications and a potential range of MIF effects due to the differences in neutron capture cross-sections between ^{235}U and ^{238}U.

Non-metals: Si, Se, Cl

Despite being the main constituent of the rock-forming minerals, the analytical difficulties associated with Si isotopic analysis (^{28}Si, ^{29}Si, ^{30}Si) have to date limited their application. A number of pilot studies have been conducted, focusing largely on cataloguing the distribution of Si isotopes in the solid earth. Studies on cherts suggest that BIFs have lighter isotopic signatures (low $\delta^{30}Si$) than intertidal cherts, consistent with a hydrothermal origin for Si in BIFs. Several studies have also been applied to aqueous systems (both ground and river waters) where Si isotopes have been applied as a tracer in weathering studies, with continental detritus trending towards greater $\delta^{30}Si$ and chemical precipitates, including opals to lower values. So, too, S-type granites, which are themselves derived from sources that have experienced a weathering cycle, tend to lesser $\delta^{30}Si$ than I-types.

Se isotopes have been investigated for extraterrestrial materials and in biogenically mediated sedimentary systems, the latter due to their highly redox sensitive nature. Since Se has six stable isotopes (74, 76, 77, 78, 80 and 82), several combinations for measurement exist; however, generally $\delta^{82}Se$ is reported as the $^{82}Se/^{80}Se$ ratio due to higher precision on the analyses. The $^{82}Se/^{76}Se$ ratio is generally strongly correlated with $^{82}Se/^{80}Se$.

Given that Se is geochemically similar to S, attention has turned to characterising hydrothermal fluids and redox-sensitive processes, such as those associated with organic materials. Significant fractionations have been reported, particularly in low-temperature hydrothermal processes, of the order of approaching 1 per cent (i.e. 10‰).

Cl possesses two stable isotopes (35 and 37), and is the lightest of the halogens which is able to be measured (F is monotopic). Due to the highly hydrophilic nature of Cl, and its role in several biological pathways, Cl isotopes are of immense utility in hydrosphere studies, enjoying widespread applications in the environmental sciences as well as in tracing hydrothermal fluids. Hydro–lithosphere linkages have been investigated with the transfer of Cl through subduction zones and back arc basins, and numerous groundwater and acid mine drainage studies have also been explored.

5

Radioactivity, radioactive decay and isotope systems applied in the geosciences

As observed above, there are combinations of protons and neutrons which result in an unstable nucleus. Such nuclei subsequently fall apart, forming new daughter nuclei and emitting some form of radiation. If the daughter nuclei are themselves unstable, they, too, will disintegrate, until a stable isotope is reached. The four key kinds of radioactive decay relevant to geology are as follows.

α decay: this is the ejection of a ^{4}He nucleus (an 'α particle') from the nucleus. This results in a daughter nucleus which has A four fewer than the parent, and Z two fewer. For example (note that both A and Z balance on either side of the equation):

$$^{147}_{62}\mathrm{Sm} \rightarrow {}^{143}_{60}\mathrm{Nd} + {}^{4}_{2}\mathrm{He}.$$

β decay: this is an example of where a nucleus loses excess energy through the ejection of either an electron (β^{-}) or a *positron* (β^{+}) (a positively charged electron), depending on the scheme in question. Since electrons have charge, but vanishingly little mass (with respect to protons and neutrons), this results in a change of Z, but not of A. In essence, it is the conversion of a neutron to a proton plus an electron or of a proton to a neutron plus a positron. For example (note that Z does not balance in this case):

$$^{87}_{37}\mathrm{Rb} \rightarrow {}^{87}_{38}\mathrm{Sr} + \beta^{-} + \nu.$$

The symbol ν represents a neutrino, which is a chargeless, (possibly) massless particle which interacts only very weakly with matter, and is of no interest to geologists.

Electron capture: this is (for our purposes) essentially the reverse of β decay; a highly energetic electron interacts with a proton to produce a neutron. For example (note that Z does not balance in this case):

$$^{40}_{19}\mathrm{K} + \mathrm{e}^{-} \rightarrow {}^{40}_{18}\mathrm{Ar}.$$

γ decay: although it doesn't produce any change in atomic number or mass, γ decay is a common means by which a nucleus emits energy to move from an excited state to a more stable state. A γ particle is simply a high-energy form of light, and as such has neither mass nor charge. The general form for these reactions is (note that neither A, Z or E change in this case):

$$^{A}_{Z}E^{*} \rightarrow ^{A}_{Z}E + \gamma,$$

where E* merely indicates a nucleus in an excited state.

Since γ radiation does not produce a change in the mass or chemical properties of an element, it has limited applications in isotope geochronology. γ radiation does have applications in geophysics and in some forms of geochemistry and U-series geochronology, where it can be used to measure the relative abundances of particular isotopes through γ-ray spectrometry.

5.1 Half life and decay constant

The key aspect of radioactivity is that it occurs at the same rate regardless of pressure and temperature. Therefore, for a given number of atoms of a radioactive isotope, a given number of decays are likely to occur per unit of time. Thus each decay scheme has its own *decay constant* (λ). The decay constant is simply the probability that a single atom will disintegrate in a given unit of time, and is generally expressed in units of per year (yr^{-1}). From the values listed in Table 5.1, it is exceedingly improbable that a single atom will decay in a year.

Table 5.1 *Summary of commonly used naturally occurring radioactive decay schemes in high-temperature geosciences.*

Parent isotope	Daughter isotope	Decay mode	Decay constant (λ), yr^{-1}	Half life ($T_{1/2}$), yr	Normalising isotope
^{40}K	^{40}Ar	β^-, β^+, ec	0.581×10^{-10}	1.25×10^{9}	^{39}Ar
^{87}Rb	^{87}Sr	β^-	1.42×10^{-11}	48.8×10^{9}	^{86}Sr
^{147}Sm	^{143}Nd	α	6.54×10^{-12}	106×10^{9}	^{144}Nd
^{238}U	^{206}Pb	dom α	0.155×10^{-9}	4.468×10^{9}	^{204}Pb
^{235}U	^{207}Pb	dom α	0.985×10^{-9}	0.704×10^{9}	^{204}Pb
^{232}Th	^{208}Pb	dom α	0.049×10^{-9}	14.01×10^{9}	^{204}Pb
^{176}Lu	^{176}Hf	β^-	1.867×10^{-11}	37.1×10^{9}	^{177}Hf
^{187}Re	^{187}Os	β^-	1.666×10^{-11}	45.6×10^{9}	^{188}Os

Note that the decay of U and Th to Pb occurs via a series of short-lived (geologically speaking) intermediaries, whereas all other decay schemes are via a single step.
ec, electron capture; dom, dominantly

This is not surprising, given that atoms with higher probabilities of disintegrating (i.e. larger λ) are likely have decayed away over the lifetime of the earth.

What people are perhaps more familiar with is the concept of *half life*, which is simply the period of time that it will take for half of a mass of radioactive material to decay away. This term is mass independent, and hence it will take exactly the same amount of time to decay from 1 kg to 0.5 kg of radioactive material as it will from 0.5 kg to 0.25 kg. This is because radioactivity is an exponential process.

The half life ($T_{1/2}$) is linked to the decay constant by the following relationship:

$$T_{1/2} = \frac{\ln 2}{\lambda}. \qquad \text{(Eq 5.1)}$$

5.2 Equations

The basic decay equation is:

$$\frac{\mathrm{d}N}{\mathrm{d}t} = -\lambda N, \qquad \text{(Eq 5.2)}$$

where N is the number of atoms of a radioactive isotope, and t is the period of time elapsed.

Rearranging and integrating ultimately gives:

$$N_t = N_0 \mathrm{e}^{-\lambda t}, \qquad \text{(Eq 5.3)}$$

where N_t is the number of atoms remaining from an original number of atoms (N_0) after a period of time, t.

This process obviously produces some products, or daughter nuclides. These are *radiogenic*, as they have been produced by radioactivity.

The number of daughter nuclides (D) produced is simply $N_0 - N_t$ (assuming that each decay produces one daughter). Thus, rearranging and substituting into Equation 5.3, we can isolate N_0 and express the radioactive decay in terms of the number of daughter atoms and parent atoms after a given period of time has elapsed:

$$D_t = N_t(\mathrm{e}^{\lambda t} - 1). \qquad \text{(Eq 5.4)}$$

Since in geological situations there are usually some atoms of the daughter isotope around initially (i.e. at $t = 0$), then we need to account for those as well, giving:

$$D_t = D_0 + N_t(\mathrm{e}^{\lambda t} - 1). \qquad \text{(Eq 5.5)}$$

Equation 5.5 is referred to as the age equation, and is the form most generally used as a starting point for geochronology.

A note on the subscripts: always take care to think about what they are representing, as you will find that while in most cases the symbol t will refer to the amount of time that has elapsed, the subscript 0 can refer to either the **o**riginal number of atoms (i.e. the number that existed t years ago) *or* the number of atoms that exist at $t = 0$, i.e. the number of atoms that existed zero years ago, which is today.

5.3 Geologically useful decay schemes

Based on Table 5.1 we can write a form of Equation 5.5 for any of the above schemes by substituting in the relevant terms as follows:

$$^{87}\mathrm{Sr}_t = {}^{87}\mathrm{Sr}_0 + {}^{87}\mathrm{Rb}_t\left(\mathrm{e}^{(1.42\times10^{-11}t)} - 1\right), \qquad \text{(Eq 5.6)}$$

for Rb–Sr, or:

$$^{187}\mathrm{Os}_t = {}^{187}\mathrm{Os}_0 + {}^{187}\mathrm{Re}_t\left(\mathrm{e}^{(1.666\times10^{-11}t)} - 1\right), \qquad \text{(Eq 5.7)}$$

for Re–Os, and so on.

Note: it is critical that the correct decay constant is used for the relevant scheme!

Since the measurements are made at the present day, we generally omit the subscript t when referring to ratios at the present day.

5.3.1 Normalisation

For analytical and mathematical reasons, it turns out to be far more practical to measure ratios of isotopes, with the denominator being a stable isotope of the daughter element. Therefore, the expressions become of the type:

$$\left(\frac{^{187}\mathrm{Os}}{^{188}\mathrm{Os}}\right)_t = \left(\frac{^{187}\mathrm{Os}}{^{188}\mathrm{Os}}\right)_0 + \left(\frac{^{187}\mathrm{Re}}{^{188}\mathrm{Os}}\right)_t\left(\mathrm{e}^{(1.666\times10^{-11}t)} - 1\right). \qquad \text{(Eq 5.8)}$$

This is because we are able to cancel out errors associated with measuring the exact number of atoms of a given isotope by comparing how much of a given isotope is present with the amount of a stable isotope of the same element.

For example, Figure 5.1 is the same as Figure 1.1, except that over time a significant amount of $^{87}\mathrm{Sr}$ has accumulated due to the decay of $^{87}\mathrm{Rb}$ in the same rock. What is immediately apparent is that the ratio of $^{88}\mathrm{Sr}/^{86}\mathrm{Sr}$ is the same in both

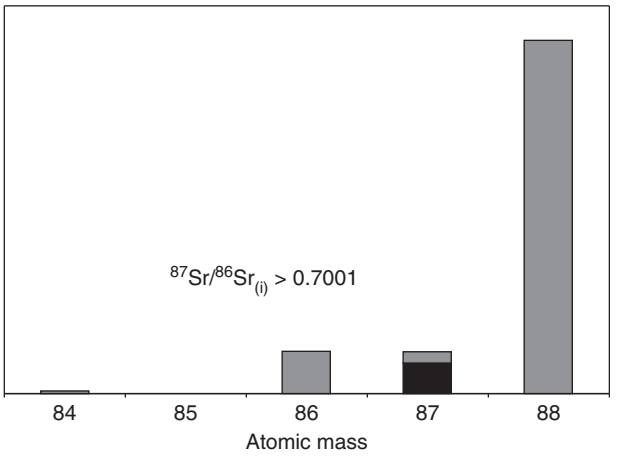

Figure 5.1 Relative abundances of Sr isotopes, highlighting how the initial amount of ^{87}Sr (black column) is less than ^{86}Sr, but over time the addition of radiogenic ^{87}Sr (grey portion of mass 87) is such that the total amount of ^{87}Sr is now greater than or equal to the abundance of the stable isotope ^{86}Sr. Despite the accumulation of ^{87}Sr, the ratios of the other three isotopes with respect to each other (^{88}Sr/^{86}Sr, ^{84}Sr/^{86}Sr and ^{88}Sr/^{84}Sr) remain constant.

cases, but the ^{87}Sr/^{86}Sr ratio is significantly different (^{87}Sr/^{86}Sr is <1 in Figure 1.1, and is >1 in Figure 5.1). Therefore the ratios of the stable isotopes of a given element should be constant (although we shall see that this doesn't always hold true for the light elements), and we can quickly compare the ratios of the radiogenic isotope to that of a stable one without having to go to the trouble of counting the total number of individual atoms of each isotope in a sample (which is what would be necessary to be able to use Equation 5.7). Instead we normalise all of our measurements to a stable isotope, and are able to use the decay equation in the form of Equation 5.8 in a simple manner.

Such normalisation is also a consequence of the analytical methods, whereby mass spectrometers simply measure the relative ratios of the isotopes, rather than counting all atoms (or, more precisely, ions) individually. This expedites the process, meaning that only a subset of the sample needs to be analysed as opposed to all material that is available.

5.3.2 A brief overview of the commonly applied decay schemes

In essence, both stable and radiogenic isotope geochemistry are versions of geochemistry in which the trace elements have labels on them. This enables us to track the passage of elements through earth systems. Radiogenic isotopes have the advantage of linking two (or more) chemical elements, sometimes with very different geochemical properties and affinities, as well as providing

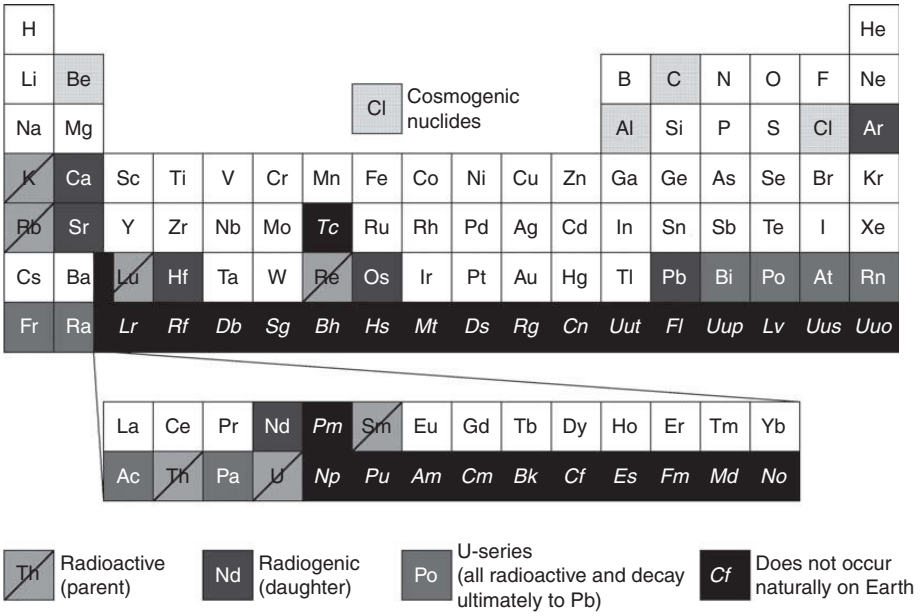

Figure 5.2 Periodic table highlighting the commonly applied radioactive decay schemes in geochemistry. Table 5.1 summarises the decay styles and time scales associated with each scheme.

some time information due to the radioactive decay of the parent isotope. Therefore it is useful to have a first-order appreciation of the geochemistry of commonly applied radioactive isotope systems, and indeed the nature of their half lives and decay paths (summarised in Table 5.1). The locations of the elements which comprise the schemes outlined in Table 5.1 on the periodic table can be found in Figure 5.2.

5.3.2.1 K–Ar and Ar–Ar

^{40}K decays to ^{40}Ar with a decay constant of 0.581×10^{-10} yr^{-1}; however, not every ^{40}K produces ^{40}Ar. Actually 89.1 per cent of the decays produce ^{40}Ca via typical beta decay, and only 10.9 per cent of the decays produce ^{40}Ar, via positron emission. Such branched decay schemes are not unusual in nuclear physics, but the K–Ar decay is the only example routinely used in the geosciences. Theoretically it would therefore be possible to apply a K–Ca chronometer (Figure 5.2) as well; however, not only is Ca very common in the earth, but also ^{40}Ca is the most abundant isotope, comprising 96.94 per cent of all Ca. Therefore a very large amount of ^{40}K is required to decay in order to produce a measurable shift in the ^{40}Ca abundance or ^{42}Ca/^{40}Ca ratio.

Both systems are widely applicable in situations that have relatively high K concentrations and in materials in which the Ar is retained once it has been produced. The presence of excess Ar and atmospheric contamination are an issue for K–Ar, but Ar–Ar methods enable this to be addressed (Chapter 9). This has resulted in applications focused largely on individual minerals, as Ar retention is generally better than on a whole-rock scale. Minerals such as hornblende, muscovite and biotite are all widely used, with K-feldspars often analysed as well, although there is a broader range of open system behaviour in the feldspars. These minerals allow not only extensive investigation of igneous and metamorphic rocks, but also interrogation of hydrothermal alteration and activity in fault systems. Some novel applications relevant to mineralised systems have included dating pyrite – more specifically muscovite inclusions in pyrite – however, irradiating Fe-rich phases induces a high residual background radiation in the sample and so this is not routinely employed.

5.3.2.2 Rb–Sr

^{87}Rb decays to ^{87}Sr via β^- decay, with a decay constant of 1.42×10^{-11} yr^{-1}. Rb is an alkali earth metal, and as such is highly incompatible in magmatic systems. Sr is also an incompatible element, belonging to the alkaline earth metals; however, due to its divalent nature it is able to substitute readily for Ca^{2+}, making it particularly compatible in plagioclase. This fractionation led to some of the earliest isochron applications of Rb–Sr in magmatic systems due to the range in Rb/Sr ratios, produced as a consequence of fractionation and crystallisation. Conversely, Rb can be relatively enriched in minerals such as phyllosilicates (e.g. biotite, muscovite and chlorite) with respect to Sr due to its large ionic radius and single 1+ charge. Rb can also substitute for K to a more limited extent in minerals such as K-feldspar.

The main applications for Rb–Sr have been through isochron approaches to geochronology (Chapter 7) in magmatic and metamorphic systems. While this is a very powerful system due to the relatively high abundances of both Rb and Sr, its one drawback is that both Rb and Sr are relatively mobile in hydrothermal fluids, most notably during alteration and metasomatism. This drawback, however, is also one of the system's greatest utilities, particularly when applied to potassic or calcic alteration systems (e.g. albitisation), as it can sometimes be applied to the altered mineralogy in an attempt to date the alteration itself. In such situations, the resulting dates do not record the age of the rock itself.

Sr isotope stratigraphy is a powerful tool which relates recognised $^{87}Sr/^{86}Sr$ variations in seawater through time with carbonate material of interest. Since Sr^{2+} can substitute for Ca^{2+} during carbonate precipitation, the Sr isotopes can record the prevailing isotopic composition of the seawater at the time. Correlation of

samples with the well-calibrated Sr seawater curve can allow relatively high-precision stratigraphic correlation; however, it is limited to those portions of geological time for which the seawater curve is well known. Due to the poorer state of preservation of ancient carbonates, the resolution of this record becomes poorer beyond the Mesozoic.

Sr isotopes are also very important in palaeontology, where the Sr isotopic ratios of skeletal material will record the Sr isotopic signature of the environment the organism was living in. This is particularly useful when investigating tooth material, made of apatite, as there is minimal inherited Rb which can interfere with the measurement of the Sr isotopes. Such signatures can be used to track migration patterns.

5.3.2.3 Sm–Nd

^{147}Sm decays to ^{143}Nd via an α decay with a decay constant of 6.54×10^{-12} yr^{-1}. Both Sm and Nd are rare earth elements (REE) and as such have very similar chemistry, resulting in relatively small fractionations between parent and daughter isotopes in the earth. Sm–Nd can be used in conventional isochrons, most commonly in magmatic systems, or, more importantly, in metamorphic systems involving the growth of the mineral garnet, since this is one of the few minerals that will fractionate Sm from Nd. Garnets therefore generally have a very high Sm/Nd ratio, and hence will comparatively rapidly produce radiogenic ^{143}Nd.

In contrast, due to the relatively small fractionations of Sm from Nd on the whole-rock scale, and the relative resistance of both elements to diffusional re-equilibration, Nd isotopes allow us to 'see through' younger metamorphic and magmatic events. They have therefore also widely been applied to investigate the source(s) of rocks with respect to whole-earth reservoirs, such as the depleted mantle through the application of model ages (see Sections 10.1.1 and 11.1.1).

Sm–Nd has also been critical for understanding the evolution of the solar system, with studies of meteorites used to define the nature of the bulk earth composition through the definition of the chondritic uniform reservoir (CHUR). This reservoir offers a basis for comparison of all terrestrial igneous rocks (see Part III).

Confusingly enough, there is also a second Sm–Nd decay scheme, that of the now extinct ^{146}Sm to produce ^{144}Nd with a half life of ~109 Myr. This decay scheme is extinct as all primordial ^{146}Sm has decayed away; however, this system has enjoyed significant success in applications investigating planetary formation and core segregation.

5.3.2.4 Re–Os and Pt–Os

^{187}Re decays to produce ^{187}Os with a decay constant of 1.666×10^{-11} yr^{-1}. Re and Os are both highly chalcophile and siderophile elements, and therefore have been

used extensively to investigate sulphide-bearing systems. Moreover, Re can be readily fractionated from Os and hence a wide range of potential applications were envisaged. To date, the main geochronological applications have been through whole-rock isochrons on mafic and ultramafic complexes, and molybdenite geochronology. Molybdenite is particularly suited to this application as Re is highly compatible in its lattice during crystallisation and Os incompatible, resulting in extraordinarily high Re/Os ratios (Section 8.5). Further applications of the Re–Os chronometer have been through the dating of the depositional age of organic-rich sediments, as both have been observed to behave in an 'organophile' manner.

The other main application of Re–Os has been through calculation of model ages regarding the stabilisation of the subcontinental lithospheric mantle, due to fractionation of Re from Os during mantle melting effectively locking the age of depletion events. Several model age calculations have been applied to this system, and they differ from 'conventional' model ages such as those of Nd and even Pb (see Section 10.1.3).

Finally, because of the highly siderophile nature of both elements, Re–Os has been extensively applied in meteorite studies, particularly in investigating the timing of metal formation. In this endeavour, a second Os chronometer, that of the decay of ^{190}Pt to ^{186}Os, has also been applied. This chronometer is of very limited application elsewhere as ^{190}Pt comprises only 0.014 per cent of the total Pt on earth, and has an extraordinarily long half life of 650 Gyr, or ~43 times the age of the universe! Indeed, early Re–Os isotopic studies normalised the ^{187}Os measurements to ^{186}Os since it was assumed that the contribution of radiogenic ingrowth to the amount of ^{186}Os would be trivial, and it could be considered stable; however, variations have been observed and ^{188}Os has been used subsequently. In terrestrial systems, the Pt–Os system has been applied where extreme variations in Pt/Os are observed, such as core–mantle interaction.

5.3.2.5 Lu–Hf

^{176}Lu decays to produce ^{176}Hf with a decay constant of 1.867×10^{-11} yr^{-1}; however, there is considerable uncertainty (~4 per cent) in this value. This has been determined by calibration of the Lu–Hf decay scheme with independently dated terrestrial rocks and is very similar to that obtained from direct counting measurements (1.86×10^{-11} yr^{-1}), but differs from the initial determinations obtained from calibration with independently dated meteorites (1.94×10^{-11} yr^{-1}). For all practical purposes in regional geology (e.g. zircons) and ore deposit systems, the value of 1.867×10^{-11} yr^{-1} is appropriate, but users must bear in mind that this issue is currently still being investigated.

Lu is the heaviest REE and Hf behaves as a high field strength element (HFSE) and can substitute for Ti and Zr in accessory phases such as Zr. The greatest

fractionations between the two can be observed in phases such as zircon (Hf can contain up to several wt% in the lattice, forming the mineral hafnon) and garnet, which contains very high Lu/Hf ratios. Geochronological applications are therefore best applied to the latter situation, where rapid ingrowth of radiogenic Hf in metamorphic garnet can take place, allowing highly precise metamorphic isochrons. Mineral separates within mafic lithologies also allow an isochron approach to magmatic ages due to a spread of Lu/Hf during crystallisation. Applications of model ages in the mineral zircon are widespread due to the very low Lu/Hf ratio at the time of zircon crystallisation making subsequent ingrowth of ^{176}Hf insignificant and preserving the initial $^{176}Hf/^{177}Hf$ of the environment at the time of crystallisation (see Section 11.1.3.1). Whole-rock Hf isotopes have also been used to investigate the evolution of whole-earth reservoirs through model ages in a manner analogous to Sm–Nd. Finally, Lu–Hf geochronology has also been widely applied to extraterrestrial studies, particularly in achondrites (magmatic meteorites) where significant fractionation of Lu from Hf has taken place; however, the concerns regarding the decay constant necessitate care when interpreting these data.

5.3.2.6 U–(Th)–Pb

Both common isotopes of U decay to form different isotopes of Pb. ^{235}U decays to ^{207}Pb and ^{238}U to ^{206}Pb with decay constants of 0.985×10^{-9} yr^{-1} and 0.155×10^{-9} yr^{-1}, respectively. ^{232}Th (the only long-lived naturally occurring isotope of Th) also decays to ^{208}Pb with $\lambda = 0.049 \times 10^{-9}$ yr^{-1}. Unlike all decay schemes described above, these decays do not take place in a single step, but occur via a series of short-lived intermediaries, such as Ra, Rn, Bi and other isotopes of Pb. Most of these intermediaries have short (less than a decade) to very short (less than a second) half lives and can be considered essentially instantaneous for most purposes in ore geology. However, a handful of these have longer half lives, such as ^{234}Th ($T_{1/2}$ = 248 000 years), ^{230}Th (75 000 years), ^{226}Ra (1600 years) and ^{231}Pa (34 000 years), all of which can be used in active magmatic systems and recent environmental studies ('U-series', see Section 8.2). However, for most practical purposes in ancient systems, once started the decay can be considered to take place effectively instantaneously and hence treated in terms of a single decay equation for each scheme.

The power of this system is that it contains within it an independent internal check. Since different isotopes of the same element (U) are decaying to produce different isotopes of Pb, any process which disturbs or resets one system will effectively disturb or reset the other. The high precision obtained from U–Pb geochronology, due to the combination of two decay schemes and relatively short half lives allowing precise direct determinations of decay

constants, has resulted in this system being the 'gold standard' for calibration of all other decay schemes. Such internal cross correlation of independent decay schemes with common parent and daughter elements allows application of U–Pb isotopes in ways that no other scheme can – most significantly through concordia diagrams, the common Pb–Pb method and the application of the geochron for model age studies (Chapter 8). Geochemically, U is highly lithophile and Pb moderately chalcophile, resulting in significant partitioning between the two in high-temperature processes and many ore systems. Most significantly, the relative compatibility of U and incompatibility of Pb in zircon has led to the development of the most broadly applied field of geochronology. U–Pb isotopes can also be applied to conventional isochron studies; however, U (in particular) is both redox sensitive and highly mobile under low-grade metamorphic conditions and weathering, resulting in open system behaviour.

Th is often overlooked in this context, but theoretically it can be used to derive conventional isochrons, particularly for high-Th phases. Generally, Th is far less mobile in the weathering environment and during low-grade metamorphism than U, and so is more applicable than U–Pb isochrons; however, generally U–Pb zircon (or other U-bearing accessories) in the same rock can be measured easily and so Th is rarely measured in its own right. Even the Th decay chain has no long-lived intermediaries (the longest is ^{228}Ra; $T_{1/2}$ = 6.7 years) and so has no applications except for lavas erupted in the last 30 years.

5.3.2.7 (U–Th)/He

Given that each ^{238}U atom produces daughters that emit α particles (^{4}He), by the time it has decayed to produce ^{206}Pb, if the sample retains all of the ^{4}He we have a direct measure of the number of decays that have taken place. Over time, more ^{4}He will accumulate, and if it is possible to measure the amount of U in the sample, then an age can be determined directly. In reality, any sample which contains appreciable U and retains He will also be accumulating He from the decay of ^{235}U (seven α particles to produce ^{207}Pb) and ^{232}Th (six α particles on its way to ^{208}Pb), and therefore not only the total He needs to be measured but also the U and Th concentrations. In some samples ^{147}Sm may also contribute ^{4}He as it decays to ^{143}Nd.

Such a chronometer was the basis of some of the very first isotopic dating efforts, such as that employed by Rutherford in 1905. However, because He has a very small atomic radius and is chemically inert, it very readily diffuses from crystal lattices and hence is readily reset at low temperatures (<90 °C). This makes it ideally suited to dating of upper crustal and low-temperature events.

5.3.2.8 Fission track analysis

Although not specifically an isotopic decay scheme, or even an isotopic geochronological tool, fission track analysis or fission track geochronology is a technique which can be used to date materials with very low closure temperatures (see Section 8.4). The approach is based on the numerical analysis of the trails left in a mineral lattice caused by the spontaneous radioactive decay of ^{238}U. The principle is quite simple; a small number of radioactive decays of ^{238}U are not those that ultimately produce ^{206}Pb, but rather spontaneous fission producing ^{143}Ba and ^{90}Kr. Approximately one decay in two million (~0.00005 per cent) is in this mode, with a half life of 8×10^{15} years. These massive daughter products are ejected with enough kinetic energy to damage the crystal lattice. Therefore, rather than measuring the daughter isotope via mass spectrometry, the fission tracks (or trails) are a direct proxy for the number of daughter atoms produced. Over time, more decays will have taken place and hence more fission tracks will be preserved in the mineral lattice. The fission tracks are generally large (up to 15–20 μm) and are visible optically in the microscope after chemical etching with nitric acid to enhance their visibility. Samples are assessed in terms of which surface (internal vs external) is being investigated and indeed whether the tracks are wholly contained within the crystal.

Therefore, by measuring the fission track density, and independently obtaining the U content of the grain, it is possible to calculate the amount of time that has elapsed since the grain formed. The U is generally measured either through LA-ICPMS, or historically through irradiation in a neutron flux to induce spontaneous fission of ^{235}U in the sample and produce fission tracks into a high-quality mica which is placed in firm contact with the sample. Since the ratio of $^{235}U/^{238}U$ is essentially invariant for the purposes of geochronology, from measuring the ^{235}U in the sample it is possible to calculate the ^{238}U.

Importantly, as the temperature of the mineral grain is increased, the radiation damage to the crystal lattice becomes repaired as the mineral re-organises itself. This process is termed annealing and results in progressive shortening of the fission tracks until they are completely obliterated at the annealing temperature for that particular mineral. Minerals typically used for fission track analysis include apatite and zircon, which undergo complete annealing at ~120 °C and <300 °C, respectively. Fission track analysis has also been applied to monazite (>50 °C) and titanite (<320 °C) in some cases.

Such relatively low closure temperatures, and the common abundance of resistate minerals such as apatite and zircon in detritus have led to widespread application in the oil industry, where burial histories in relation to oil maturation have been obtained. Other applications include uplift and denudation histories.

5.4 Closure temperature (T_c)

Closure temperature (T_c), sometimes referred to as blocking temperature, is a much-used and often misunderstood concept in geochronology. In its simplest sense, T_c can be considered to be the temperature at which a mineral (for example) began to accumulate the radiogenic daughter product, and hence the geochronological clock started ticking. Above this temperature, the daughter isotope is able to diffuse out of the mineral structure (i.e. the mineral is 'open'), and hence no age information is preserved.

More formally, this is equivalent to the temperature a given mineral had at the time of the date (or age) recorded by the mineral. Thus, as a rock cools down, different minerals can begin to lock-in the parent and daughter isotopes at different times. Another way of thinking of this is to consider that, below a certain temperature, the crystal structure of a given mineral becomes sufficiently well developed to prevent further diffusion (or exchange) of isotopes with surrounding minerals or the atmosphere. In cases where the parent and daughter have significantly different diffusion properties for a given mineral (e.g. K and Ar in amphibole), the closure temperature is entirely dependent on the diffusion behaviour of the less compatible species (in this case Ar).

Even when closure temperature is described physically as the temperature below which no significant diffusion of either parent or daughter isotopes can occur to the surrounding environment, it is immediately apparent that T_c is specific to rock types and individual minerals and isotopic systems. For rocks that cool very quickly, such as volcanic rocks, all minerals within them will close at essentially the same time, since they effectively crystallise simultaneously during eruption. Therefore the age of any mineral will be the age of the rock. Other rocks that have cooled very slowly may preserve a host of minerals that started accumulating daughter isotopes at different times, depending on how long it took the rocks to cool through the closure temperature for that particular mineral (Figure 5.3).

Therefore, often dating individual minerals may also provide information regarding the age of the whole rock itself, but there are assumptions in this approach. Because an individual mineral records only the last time they cooled below their specific closure temperature, this may not always be representative of all of the geological events that rock has experienced.

More mathematical considerations of this notion have been discussed at length in the literature, particularly with respect to the Ar–Ar system. The first mathematical formulation of T_c was that of Dodson (1973):

$$T_c = \frac{E}{R \ln(\mathrm{A}\ \tau D/\alpha^2)}, \qquad \text{(Eq 5.9)}$$

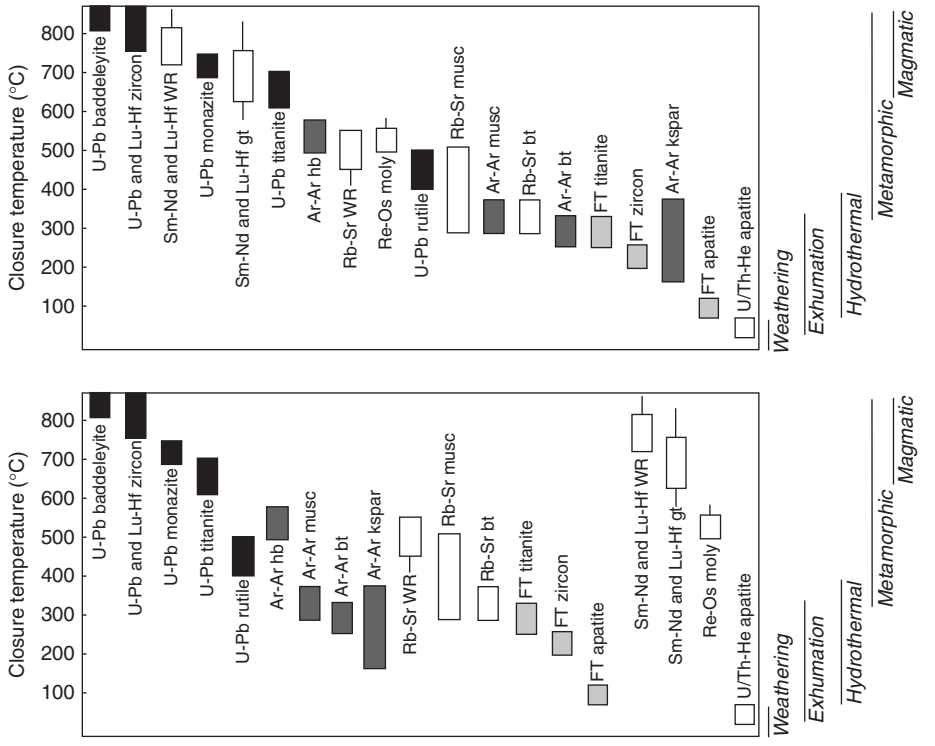

Figure 5.3 Approximate range in closure temperatures for commonly applied mineral chronometers relevant to mineralised systems, ordered by decreasing closure temperature (upper panel) and by isotopic system (lower panel). For reference indicative temperature ranges of processes that could cause systems to close or subsequently re-open are indicated on the right, although of course it must be borne in mind that ultimately weathering is capable of resetting even the highest of closure temperature systems. Note: gt, garnet; hb, hornblende; moly, molybdenite; musc, muscovite; bt, biotite; FT, fission track; WR, whole rock.

where R is the gas constant, E is the activation energy, τ is the the time coefficient with which the diffusion constant (D) diminishes, α is the diffusion size and A is a numerical constant which is a function of the geometry and the decay constant of the parent isotope. A can generally be considered to be 55 for diffusion from a sphere, 27 for a cylinder and 8.7 for a planar sheet. Most subsequent equations for closure temperature are in some way reworkings of this treatment, and the reader is referred to the specific literature for further discussion if they are interested.

Therefore, to a first order, it is useful to summarise the closure temperatures of some of the commonly applied isotopic systems and their contexts, as in Figure 5.3. It is critical for the geologist to bear in mind which part of the geological history

5.1 Plain language summary for T_c

Often different geochronometers, when applied to the same rock, will produce different ages. This is not surprising, as different elements behave differently in different minerals, so some will cease interacting with their environment at different times to others, i.e. they will 'close'.

Hence, once a rock passes through the closure temperature for a given isotope system, the clock will start ticking for that system. At some time later, it will cool sufficiently to close another chronometer, and hence will record a slightly younger age. And so on.

However, a later disturbance, such as low-grade metamorphism, may reheat the rock above the closure temperature for some of the geochronometers, but not all of them (Figure 5.4).

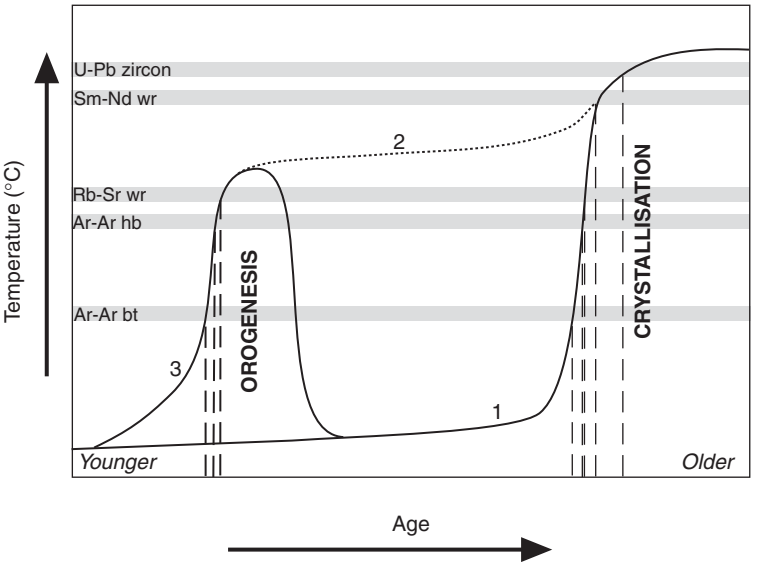

Figure 5.4 Temperature–time evolution for a hypothetical rock cooling through five different geochronometers. In theory a gradual cooling curve would produce a simple spread of ages, with the lower T_c systems proceeding sequentially from the higher, as in the case of a crystallising magma (curve 1). However, the observation that the Rb–Sr and Ar–Ar systems are clustered at distinctly younger ages than Sm–Nd and U–Pb suggests either that the rock was held at elevated temperatures for a long period of time (curve 2), or that it had cooled and been subsequently reheated above the closure temperature of these systems (curve 3). Isotopic data alone are unable to distinguish between these alternatives (although some clues may be gained from the initial ratios, see Chapter 7 and Part III) and so the data must always be evaluated in the geological and petrological context of the samples. Temperature–time trajectories allow inferences to made regarding the state of the palaeogeotherm (curve 1) or indeed the uplift and exhumation rate of rocks from beneath mountain belts (curve 3).

Thus the same rock can record a lot of information, including its initial formation, subsequent metamorphism and cooling history. The Ar system is particularly useful for cooling histories, since it has a low closure temperature. This is because Ar is very easily removed from minerals as it does not bond with them, so slight heating will liberate radiogenic Ar. Sm–Nd, on the other hand, are not very mobile on the whole-rock scale, and hence will not re-equilibrate readily. Thus they have a high closure temperature. Generally, mineral isochrons for a given system will have lower closure temperatures than whole-rock isochrons for the same isotopes (see Part II).

they are interested in interrogating when choosing their geochronological tool – if they wish to know about the nature of the protolith, then the high T_c chronometers are appropriate; if, however, one wishes to know about the uplift history of a region, then the lower-temperature fission track type chronometers are more applicable.

Significantly, most professionals in the minerals industry need to bear in mind that the importance of the closure temperature is that it simply relates to the *last time* a mineral or rock was at or above that temperature – it does not necessarily require that the age recorded be the primary age (Figure 5.4). Isotopic systems can be reset (or even more confusingly, partially reset when one is dealing with more than one chronometer within the same sample) due to subsequent, younger thermal perturbations. However, this feature can be particularly useful when trying to constrain different parts of the history of a region – especially if a mineralising event is associated with hydrothermal fluid flow which may post-date magmatism or orogenesis significantly. Therefore, when trying to ascertain the age of mineralisation, it may be far more important to select a chronometer with a closure temperature which corresponds to that of the fluid itself, rather than higher-temperature chronometers, such as magmatic zircon, which might be found in the host rock.

It is worth noting that closure temperature is not simply a term related to geochronology – it is a term that can be applied to any element capable of diffusion into or out of a given mineral during cooling, and hence simple diffusion itself offers another means of calculating the rate of cooling. Such an approach has been applied to calculate the residence time of phenocrysts in recently erupted magmas, but has comparatively limited applications in ancient systems. So, too, temperature is simply one of the more important ways of controlling when a mineral or rock may be open or closed to accumulation of a given element (and hence its isotopes which allow geochronology). Open system behaviour can

take place for a whole host of reasons after a rock has formed, resulting in either complete or partial isotopic resetting. Precise geochronology (Part II), and indeed isotopic tracing (Part III), requires closed system behaviour in order to allow the original isotopic compositions to be preserved. Common factors inducing open system behaviour in rocks (in addition to temperature) can be fluid flow and weathering.

Part Two

‘When’

Geological time, ages and rates of geological phenomena

6

Underpinnings of geochronology

Background and principles

Various definitions of geochronology can be found, including those which incorporate some aspects of relative time. However, for our purposes, it is useful to consider geochronology as the discipline of the geosciences which quantitatively measures the age of earth materials and provides the temporal framework in which other geological phenomena can be investigated. For industry geoscientists this is usually focused around determining the age of the mineralisation in a given system, or, if not the age of a specific ore body itself, the age of a mineralising system or event, in order to facilitate exploration for other, potentially mineralised portions of the same system.

That said, mineralised systems are themselves notoriously difficult to date. This is due to several reasons, the most common being the composition of the mineralised assemblages themselves. Often there can be a perception that an age determination is sacrosanct, and therefore it or its interpretation cannot be changed. More commonly, reported ages record something other than what the user thinks it is. Therefore it is critical to understand *how* various ages are obtained and hence gain an appreciation of the approaches and limitations of geochronology.

Some techniques are based around a single principle which can be applied to many different isotopic systems (e.g. isochrons, Chapter 7). Other techniques, such as U–Pb zircon (Chapter 8) and Ar–Ar (Chapter 9) geochronology and thermochronology (Section 8.4) are based upon individual technological approaches specific to a single decay system and select minerals. Still other approaches exploit unusual parent–daughter behaviour or chemical affinities (e.g. Re–Os in molybdenite and petroleum systems; Section 8.5) or use the measured isotopic ratios to calculate theoretical ages for materials based upon certain assumptions (e.g. Nd model ages, Chapter 10).

6.1 Accuracy and precision in geochronology

All of these approaches rely on inherent assumptions regarding closed system behaviour (see Section 5.4 for a summary of what this means) in order to produce accurate ages. Accompanying accurate determinations should be some estimate of the precision of the analysis. Accuracy and precision are two very different but equally important parameters. Precision is a measure of how well you can make a measurement, whereas accuracy is a measure of whether the answer you get is the 'right' answer. There is no point making highly precise measurements if they are not returning the right answer. Conversely, there is no point returning the same answer time and time again if it is not precise enough to discriminate between the events you want to measure (see Figure 6.1).

For example, a lava may have erupted at 1600 Ma. If we obtain a determination that is 1600 ± 1250 Ma, then this measurement, while highly accurate, is not much use as it is imprecise – the age could be as young as 350 Ma or as old as 2850 Ma, i.e. a span of over half the age of the earth! On the other hand,

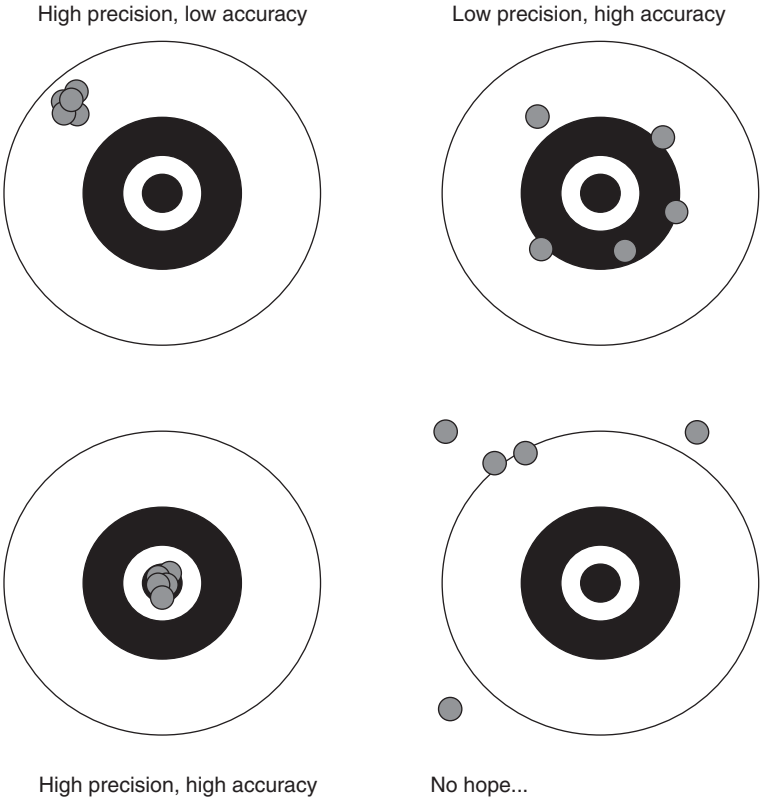

Figure 6.1 Accuracy and precision.

a determination of 1550 ± 0.5 Ma is just as unhelpful. It is highly precise, but is clearly not returning the appropriate age. We must therefore constantly strive to achieve the most accurate determination at the greatest precision possible. In this case it may mean returning an age of, say, 1598 ± 3 Ma. The challenge for geochronologists (and geochemists in general!) is to continually develop methods of returning the most precise analyses without compromising accuracy. Even for the same sample, each measurement made will tend to be very slightly different due to minor fluctuations in the efficiency of the machine. Therefore the data will not form a single sharp peak at the 'correct' value, but will instead form a distribution curve, typically a normal, or Gaussian distribution for repeat determinations. The mean (average) of this range of data is taken as the 'true' value, but some expression of the analytical precision – the range of data on which this mean is based – is needed. The measure used is the standard deviation, or some expression of the variance (see below). These form the basis of the error values we see quoted with a measurement.

6.2 Statistical treatment of geochronological data

Far and away most users are simply interested in when an event occurred in order to inform exploration and mineralisation models. Sometimes this can simply involve, say, targeting intrusives of a certain magmatic event, and hence age, in a terrain; or alternatively attempting to precisely date a specific mineralising event, either directly or by bracketing it in terms of other geological phenomena (e.g. cross-cutting relationships).

Intrinsic to obtaining these constraints is some appreciation of how the data are handled. Some techniques involve many repeated analyses of the same material in order to refine a single value, and so require statistical handling of large data sets. Alternatively, some systems, such as *in situ* analyses, may sometimes return a single value for a single data point, and hence the precision of this measurement may be reliant upon comparison with other samples of known value that were conducted in the same analytical session. The mathematical handling of each of these scenarios is different, and while many people are averse to statistics, on a conceptual level at least the statistical treatment of geochronological data is one of significance to all geologists.

6.2.1 Reproducibility: internal vs external

Reproducibility is subtly different from accuracy and precision in that it has nothing to do with the 'right' or 'wrong' answer, it is simply a reflection of how well a given machine or technique can produce the same answer over a period of time.

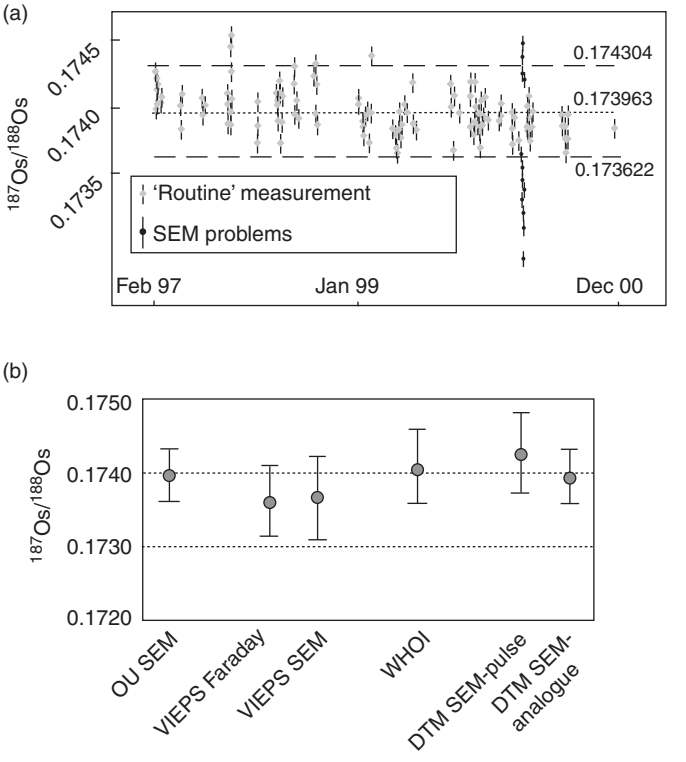

Figure 6.2 Examples of internal (a) and external (b) reproducibility. The internal case is for analysis of the same standard solution over a period of time on the same instrument in one lab, with a running average and error range labelled at 2σ. It highlights that by routinely monitoring standards such as this, problems such as component failure (in this case problems with the detector) can be quickly observed and rectified. Had this not been the case, routine analyses might have continued and generated data that were meaningless, along with the loss of valuable samples. The lower panel illustrates measurement of the same standard solution by laboratories in Australia, the UK and the United States, in some cases with subtly different detectors. The overall external reproducibility is a function of the range reported for all laboratories; however, the internal reproducibility varies slightly from lab to lab. Overall, all labs are producing the same result within the reported precision of the analyses (all errors 2σ).

Internal reproducibility is a measure of the range observed in the analysis of a standard (i.e. the same material of known value) over a period of time in the same laboratory on the same machine (e.g. Figure 6.2a). Monitoring this is very important for a laboratory as it is a direct measurement of whether the machine or the whole technique is returning the 'right' answer, and how well it is doing it. Monitoring internal standards allows laboratory managers to assess data quality and track whether parts of the equipment are deteriorating and affecting the quality

of the analysis. Hence one would not always expect an internal standard to necessarily return the 'right' answer; however, any data collected during an analytical campaign when such standards did not do so must be discarded and reanalysis undertaken.

External reproducibility is more directly related to accuracy, in the sense that if a number of different laboratories can get the same result for the same material (ideally using different techniques or equipment), then there is a greater level of confidence that the value obtained is the 'right' one.

However, graphs such as in Figure 6.2 immediately highlight the issues regarding the statistics within analysis. Each of the ~130 analyses in Figure 6.2a consists of a single run of at least 150 determinations of the ratio of interest (in this case $^{187}Os/^{188}Os$). Yet those have been somehow reduced to a single value with an error for that analytical session. Each of those analytical sessions was then plotted over time to monitor the internal reproducibility. This combined data set is then reduced further to produce the single value in Figure 6.2b for comparison with other laboratories. In essence, this comprises ~130 × 150 determinations, but obviously not all of them should be included in the final calculation, as some of them were obviously collected when the instrument was not performing optimally (remember that part of the point of monitoring internal reproducibility is to monitor machine performance). Therefore how does one handle these data? Data collected several years apart when the machine may have had different detectors (for example) may be expected to have different inherent precisions, and hence may be more or less significant. Handling these scenarios can be problematic, and the approaches are often specific to the isotope system and analytical equipment in question. Therefore it is important to have a general appreciation for what constitutes the error, or uncertainty of a measurement, and how it is handled.

6.2.1.1 Standards

We assess accuracy by analysing standards of known composition. There are two classes of standards:

(1) *External standards* are internationally available, and allow direct comparison of the data produced by different labs (as in the case in Figure 6.2).
(2) *Internal standards* are usually used only within individual labs. Their compositions are carefully determined, and calibrated against an external standard. Internal standards are used because they are cheaper, and may be selected to be closer in composition to the samples you are analysing than the external standard, allowing more accurate calibration of your results. This is a key point – there is no point calibrating or comparing your analyses with an international basalt standard if you are analysing granites!

Furthermore, standard rock powders or laser ablation standards need to be homogeneous in composition, so that repeated sampling will always extract material of the same concentration. This can be important for elements which fractionate strongly into specific phases. Highly siderophile elements, such as the platinum group elements (PGE) will inevitably be concentrated in sulphide grains or metal alloys (e.g. gold, osmiridium) in silicate rocks. Therefore it can be exceedingly difficult to obtain sample powders and laser glass standards in which these elements are homogeneously distributed. Many cases exist of a user taking an aliquot of an internal standard powder which happened to contain one or two grains of sulphide or metal alloy, and subsequently the standard returned PGE concentrations that were 2–3 orders of magnitude higher than the accepted value. It tends to get worse over time with sample powders as these alloys and sulphides are denser than silicates and will gradually work their way to the bottom of the jar the standard is kept in. This effect is referred to colloquially as the 'nugget effect', and has dogged highly siderophile element chemistry for some time.

The nugget effect is nowhere near as severe for lithophile elements, since they are distributed to varying degrees throughout all of the silicate phases in the rock. However, some accessory phases such as zircon and apatite can acts as sinks for the rare earth elements (REE). While not generally a problem in splitting and taking aliquots, zircon can be very resistant to chemical dissolution and will therefore hold on to its inventory of REE, resulting in analyses for these elements which are lower than they should be.

6.2.2 Errors and error propagation

Statistics can be very confusing. At the end of the day, all we want to know is whether two analyses are the same or not. In general, we will observe some estimate of the measurement error quoted after the value of an analysis. This error is a measure of the precision, and is usually derived in some way from the standard deviation (see below). We most commonly see errors quoted on radiometric ages; e.g. 1850 ± 2 Ma. There are many sources of error that need to be accounted for, but to start with we will simply deal with the errors introduced through the statistical collection of numbers on a machine (referred to as the 'counting statistics'). From this basis it is then necessary to subsequently include other sources of error, including geological scatter and uncertainty in constants, such as the decay constant for a radioactive decay system.

6.2.2.1 Population vs sample statistics

Statisticians make the distinction between *sample* statistics, where the statistics are calculated from a subset of a larger population 'out there', and *population*

Table 6.1 *Symbols for sample and population statistical parameters.*

Numerical summary	Sample statistic	Population parameter
Mean	$\overline{X}$	μ
Variance	$s_X{}^2$	$\sigma_X{}^2$
Standard deviation	s_X	σ_X
Number of measurements	n	N

statistics (Table 6.1), where every sample in the population is actually measured, or the analyst does not wish to generalise their results further than the actual population measured.

Population statistics are generally appropriate when there are only a small number of samples in the data set and they are all analysed or included in the statistical analysis. Sample statistics are used when the parameters of a population are unknown, since they are being extrapolated to a large number of cases that were not analysed based on the sample subset that is actually analysed. This is more commonly the case in the geosciences as we are generally only ever measuring a (small) proportion of the population (e.g. atoms) in the sample.

For most geochemical purposes the differences are trivial, and are often ignored; however, strictly speaking from a purely analytical perspective we generally should be using population statistics. This may seem contradictory, but the very act of measurement means that we are left with a complete population of data that we must account for, and hence the statistics we are reporting are those corresponding to the whole population that *actually was* analysed. The *extrapolation* of this population of data to the extent of the (geological) sample is when we need to consider their geological significance, and is generally done in a discussion manner or semi-quantitative way as we can never be completely certain how representative our sample is of the 'true' population. Hence statistics in geochemistry in general falls into the very rigid, quantitative handling of population data derived from analytical equipment (i.e. we must account for all the data we have produced) through semi-quantitative sample statistical handling (e.g. using the mean square of weighted deviates (MSWD) as an estimate as to whether there is excess geological scatter in a data/sample set beyond that accounted for by the analytical (population) statistics), through to the entirely qualitative assessment as to whether a given sample is representative of, say, a whole granite intrusion.

In the following discussion, statistical parameters will be presented in terms of sample statistics and their formulation, except where significant differences exist. These will be highlighted where appropriate to clarify any potential

confusions that may arise. However, for completeness it is useful to summarise what the parameters statisticians commonly use are and some of the relevant equations, should you ever need to use them.

6.2.2.2 Mean

This is probably the statistical concept most people are comfortable with; it is simply the average value within a set of data:

$$\overline{X} = \frac{\Sigma_i x_i}{n}; \quad \text{or for a population:} \quad \mu = \frac{\Sigma_i x_i}{N}. \qquad \text{(Eq 6.1)}$$

6.2.2.3 Standard deviation

We all know that the average of 0 and 100 is exactly the same as the average of 49 and 51. Therefore, in geochemical applications it is important to have a feel for how large the scatter defining the mean value of a data set is. Clearly the precision on the average value for the data set of 0 and 100 is far lower than that for 49 and 51 – despite them both returning the same mean. Therefore it is necessary to also report a parameter which describes how far the data defining that mean lie from the mean. This is the *standard deviation*.

The standard deviation is the measure of the amount of scatter in a data set, and is calculated according to the formula:

$$s_X = \sqrt{\frac{\Sigma_i (X_i - \overline{X})^2}{n-1}}, \qquad \text{(Eq 6.2)}$$

where X_i is a given individual value in the data set. Therefore, by subtracting the mean from it, we are measuring how far away from the mean it is, and hence the scatter within the data set. Significantly, this is one case where the difference between population and sample statistics can become important. Note that the population standard deviation is described in terms of Equation 6.3 and includes the total number of determinations on the denominator (compared with $n - 1$ in the sample standard deviation in Equation 6.2):

$$\sigma_X = \sqrt{\frac{\Sigma_i (X_i - \mu)^2}{N}}. \qquad \text{(Eq 6.3)}$$

Within a normal, or Gaussian, distribution ~68 per cent of the data lies within one standard deviation of the mean, and ~95 per cent lies between two standard deviations of the mean (Figure 6.3). A normal distribution is a very common

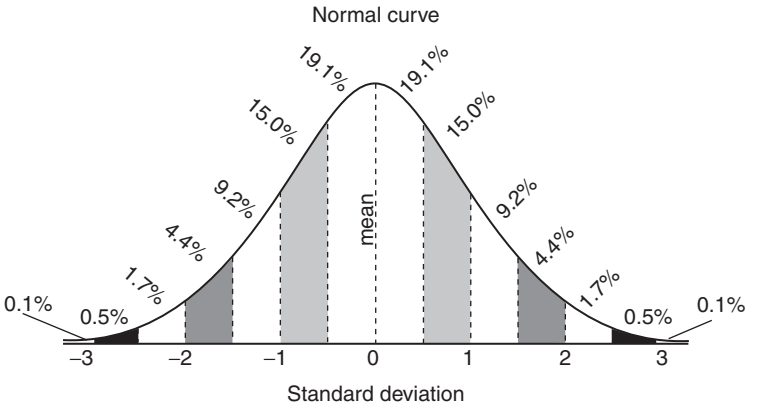

Figure 6.3 Illustration of the standard deviation, or amount of variation of data, about the mean. One standard deviation either side of the mean in a normal distribution includes 68 per cent of the measurements, $2\sigma_X$ contains 95 per cent and $3\sigma_X$ 99.87 per cent. The remaining 0.13 per cent of the measurements (in the case of $3\sigma_X$) comprises the outliers, which define the tails of the distribution curve.

distribution of data encountered in the geosciences, and is important when considering the standard error, as discussed below.

A hypothetical example may be when considering the difference in ages of various zircons all derived from a single sample. Consider a case where we have 17 zircon grains defining a mean age of 1850 Ma and an additional three zircons defining a subset with a mean of 2000 Ma. Ignoring analytical errors for the moment, from a purely statistical point of view the whole data set (n = 20) would have a mean of 1872.5 Ma. However, we know that geologically there is likely to be a valid reason, such as inheritance, for regarding the three older zircons as a different population. We generally tend to make such a-priori assumptions before any statistical analysis of such data sets.

In this scenario, the difference in population vs sample statistical analysis can be emphasised (exaggerated even) by the handling of the inherited population. If the ages of the older zircons were 1995, 2000 and 2005 Ma, then the standard deviation calculated using sample statistics would be 25 Myr, and using the population statistics 16.67 Myr, a difference of 33 per cent. Since the statistical error that is often quoted in such ages is usually derived in some way from the standard deviation, it is clear that when one is dealing with small populations such as this, the choice between sample and population statistics becomes important. We know that we are never actually going to measure every zircon in a rock, and inevitably we do discard some metamict grains etc., so in this scenario, and indeed almost every geological situation, we have to use sample statistics and the resultant greater estimates in the corresponding error. However, as the sample sets become larger

and larger, the difference between dividing by N and by $(n - 1)$ becomes smaller and smaller, and ultimately, for very large sample sets, the difference in standard deviations converges to be smaller than other sources of error in the analysis. Therefore one strategy to obtain robust statistics is to simply analyse a large number of samples. Hence one often reads of 'statistically significant' populations and sample sets.

Finally, it is common to quote two standard deviations about the mean as the 'error bars', e.g. Cu, 25 ± 2 ppm ($2\sigma_m$). So the higher the precision of an analysis, the smaller the quoted error bar. Therefore, in the case of our Cu = 25 ± 2 ppm, the value, 25, is the mean of a large number of determinations carried out during the analysis (depending on the technique, this is often of the order of several hundred determinations). The accompanying error is a reflection of the precision of the technique. For many techniques this is simply the 2σ value calculated from the variation within the counting statistics, and hence will be a population statistic. This is why it is expressed as 2σ and not $2s$. Other techniques (particularly isotopic techniques) include a component of error which is propagated from the uncertainty of the external calibration used, and hence the estimate of the error incorporates other uncertainties.

6.2.2.4 Variance

The *variance* of a sample set is simply the square of the standard deviation, and is another statistical measure of the amount of variation about the mean. This term is little used in geochemistry, but is frequently used in geostatistics and hypothesis testing. In essence variance is the most effective way to handle the probability theory associated with data handling. Probability theory is appropriate because, when we analyse a rock, we return a value, and the errors we calculate for that analysis are a statement regarding the probability, or likelihood, of returning the same result within the errors stated if we analysed it again.

Hence statistical analysis is inextricably linked to probability theory. The standard deviation, and hence variance, are simply two of several descriptors of probability distribution. In essence they describe either the *actual* probability distribution of a complete population in a data set, or the *theoretical* probability distribution of a sampled subset of a larger population. Since we are generally dealing with sample statistics in the geosciences due to the nature of our samples, we are generally dealing with theoretical probability distributions. However, often we are dealing with analytical techniques that produce a large but finite number of determinations of the same parameter (e.g. hundreds of isotopic ratios analysed during a single run of a sample); when we are dealing with analytical results we are invariably looking at the population statistics. This leads to the notion of the standard error.

6.2.2.5 Standard error

As we could see above, the standard deviation gives some measure of the range of values that incorporate some proportion (68 per cent, 95 per cent, etc.) of the data set. It is critical to remember that these are the range of values either side of the mean. If we are able to reproduce the experiment a very large number of times (i.e. n becomes very large, of the order of >100 in a single analytical run) then we are left with a situation in which the sampling distribution of the mean itself becomes normal. That is, we end up with a large number of mean values *which will themselves define a normal distribution, regardless of the shape of the frequency distribution that we are actually measuring the mean of!* Therefore, this mean of the means will begin to approximate the actual population mean even though we are still only measuring a sample of the population – i.e. the mean of the means approaches the population mean:

$$\overline{\overline{X}} \approx \mu. \qquad \text{(Eq 6.4)}$$

The standard deviation of this sampling distribution of means is referred to as the standard error (SE), and is in effect a measure of the standard deviation that we would observe from an infinitely large number of measurements of the mean. Algebraically, the SE can be defined as:

$$\mathrm{SE}_{\overline{X}} = \frac{s_X}{\sqrt{n}}, \qquad \text{(Eq 6.5)}$$

or simply the standard deviation divided by the square root of the number of measurements. The statistical rationale behind this approach is that it allows us to test whether our sample set is approaching the theoretical limits of distribution predicted by the Central Limit Theorem, though this will not be investigated any further here.

The thing about the SE is that it inevitably returns a smaller estimate of the error than the standard deviation, and hence it can be used to imply a level of precision in a measurement which is smaller than that which is applicable. On the other hand, many instrumental techniques, particularly the forms of mass spectrometry, produce data which are themselves the means of a large number of mean analyses. Therefore it is appropriate in some situations to quote errors in this form. Regardless of whether standard deviations or standard errors are used, it should always be clearly stated which is being cited.

The final use of SE is that algebraically it lends itself to more straightforward conversions to probabilities than standard deviations as the distribution associated with the variation about a large number of repeat analyses of a mean will always be

a normal (or Gaussian) distribution (as n becomes large), regardless of the shape of the distribution that the mean is itself measuring.

6.2.2.6 *Confidence limits/interval*

Geochemists commonly calculate a measure for the internal precision of a data set at the 95 per cent confidence limit. This is the range of values for which there is a 95 per cent probability of a repeat measurement falling in this range. Therefore it is intimately associated with two times the standard deviation, which is simply a measure of the range of values you need to span to cover 95 per cent of the data set.

However, this requires that we are dealing with a normal (Gaussian) distribution. The only time we *know* this is when we are dealing with a mean-of-means situation and hence are using SE as an estimate of the spread in the range of mean values returned from a series of measurements. Having said this, many other geological situations approximate a normal distribution adequately well to allow approximation via the standard deviation; however, the strict definition for any confidence interval for the population mean is given in terms of the SE. This is because the SE is an approximation of the error on the population mean and not the sample mean. Therefore a general formula for large sample confidence intervals can be expressed as:

$$\text{Sample mean} \pm z\ (\text{standard error of the sample mean}), \qquad \text{(Eq 6.6)}$$

where z is a value chosen from a table of standard normal distribution values to convey the desired degree of confidence (normally 95 per cent in geosciences). More specifically, this can be summarised as:

$$\overline{X} \pm z(\mathrm{SE}_{\overline{X}}) = \overline{X} \pm z\left(\frac{s_X}{\sqrt{n}}\right). \qquad \text{(Eq 6.7)}$$

Appropriate values for z can be found in Table 6.2.

For example, if we determine the age of biotite by Ar–Ar 155 times (i.e. multiple steps on multiple plateaus from multiple grains, or multiple single-spot analyses) and we get an age of 12.97 Ma and a standard deviation of 2.42 Myr, what is the error on the age at the 95 per cent confidence interval?

Using Equation 6.7:

$$\begin{aligned}\text{The age is } 12.97 \pm z \text{ multiplied by (standard deviation/square root of } n) \\ &= 12.97 \pm 1.96 \times (2.42/\sqrt{155}) \\ &= 12.97 \pm 0.38 \text{ Ma at 95 per cent CI.}\end{aligned}$$

Table 6.2 *Summary of critical parameter values for use in calculation of confidence intervals.*

Confidence interval $P(z \geq \|Z\|)$	Critical value z	Confidence interval $P(z \geq \|Z\|)$	Critical value z
0.1	0.126	**0.95**	**1.960**
0.2	0.253	0.98	2.326
0.3	0.385	0.99	2.576
0.4	0.524	0.995	2.807
0.5	0.674	0.999	3.290
0.6	0.842	0.9995	3.480
0.7	1.036	0.9999	3.890
0.8	1.282	0.99999	4.420
0.9	1.645	0.999999	4.900

The 95 per cent confidence interval is highlighted in bold and has a corresponding critical value of 1.960.

In other words, we are 95 per cent confident that the mean age of the biotite in this sample is between 12.59 and 13.35 Ma.

Therefore it is important to assess what is actually being reported before using an error. Sometimes $1\sigma_m$ errors are reported, since these most accurately reflect the precision of the technique employed; however, users who are not completely familiar with the technique may assume the more common 2σ situation. Other techniques will quote errors at the 95 per cent confidence interval. In essence, the message is that errors and their reporting are a very important part of the value of a geochronological (and geochemical) data set, but care must be taken with both their reporting and application in order to ensure clarity of meaning.

6.2.2.7 Error propagation

This is one area where geoscientists in general are a little inconsistent. Cases abound where errors magically disappear during mathematical modelling, and indeed, in some cases, such as the calculation of Nd model ages, say, where the aim is not to obtain a precise age *sensu stricto*, but rather to compare relative ages of extraction (see Chapter 11), then the actual errors may not be as important as the comparison itself. However, in general if somebody has gone to the effort of reporting a precision for an analysis that you are using, you should make the effort to propagate this uncertainty through any calculations you do with the measurement. Not only is this the rigorously appropriate approach to science, it can also

sometimes open your eyes as to whether you should be placing as much emphasis on the result of the calculation as you were before you propagated the errors! Statisticians possess a bewildering array of over-engineered (to the eyes of the field geologist!) approaches to this problem. However, in general a simple 'root of sum of squares' approach is adequate. For example:

$$
\begin{aligned}
&(A \pm a) + (B \pm b) = (A + B) \pm \sqrt{a^2 + b^2};\\
&\frac{(A \pm a)}{(B \pm b)} = \frac{A}{B} \pm \left(\frac{A}{B}\right) \times \sqrt{\frac{a^2}{A^2} + \frac{b^2}{B^2}};\\
&(A \pm a)^n = A^n + A^n \sqrt{\frac{(na)^2}{A^2}},
\end{aligned}
\qquad \text{(Eq 6.8)}
$$

where A and B are the measured values and a and b are the respective associated errors.

Some key points to note regarding Equation 6.8:

- The top example is also applicable for subtraction.
- The middle example is for multiplication too. Note that if you are multiplying or dividing a measurement by a constant (e.g. π or 2), then the error must also be multiplied or divided by the same factor.
- Propagating through exponents is seldom used in geochemistry, and it must be noted that there are several variants on the rule illustrated in the bottom example. In these situations it is best to refer to a more advanced statistical reference.

Some simple examples are included below in order to aid in the application of this approach:

Case 1, addition:

$$
\begin{aligned}
(100 \pm 5) + (30 \pm 1) &= (100 + 30) \pm \sqrt{5^2 + 1^2}\\
&= 130 \pm \sqrt{26}\\
&= 130 \pm 5.09\\
&= 130 \pm 5
\end{aligned}
$$

Note that the final error is quoted to the same number of significant figures as the original error – we don't magically gain some precision in the form of extra decimal places through addition or subtraction; you should quote the same number of significant figures in both the error and the precision (cf. Case 2).

Case 2, division:

$$\begin{aligned}\frac{(100 \pm 5)}{(30 \pm 1)} &= \left(\frac{100}{30}\right) \pm \left(\frac{100}{30}\right) \times \sqrt{\frac{5^2}{100^2} + \frac{1^2}{30^2}} \\ &= 3.3333 \pm 3.3333 \times \sqrt{\frac{25}{1000} + \frac{1}{900}} \\ &= 3.3333 \pm 3.3333 \times \sqrt{0.0025 + 0.0011} \\ &= 3.3333 \pm 0.2003 \\ &= 3.3 \pm 0.2\end{aligned}$$

Again, note how it is fine (even desirable) to carry the decimal points through the calculation – this can be quite important if this calculation is simply one step in a series to get to another, as you minimise further error introduced by rounding. However, note that the final error is still cited to one significant figure (the precision we started with), in which case it is appropriate to quote the value to the same number of decimal places. Another way to look at this is that we started with errors of 5 per cent and ~3 per cent for each of the measurements respectively, and have finished with an error estimate of ~6 per cent on the calculated value.

Refresher: significant figures and rounding The previous example made use of the rules for rounding based on an appreciation for significant figures. For those who have forgotten what these are, here's a quick and dirty summary.

Significant figures How many significant figures you report your results to is influenced by another type of error that creeps into experimental work: roundoff error. The number of significant digits (figures) that you report implies the level of precision you were able to accomplish. The numbers in Table 6.3 all have the same number of significant figures.

The rule operates in the following way:

- If there is no decimal point then the left-most, non-zero number, is the most significant digit and the right-most number is the least significant digit, provided it is not zero.

Table 6.3 *A table of numbers containing the same number of significant figures (four).*

1234	12 340	123.4	12.34
1001	10.10	0.0001010	100.0

- If there is a decimal point, then the most significant digit is found the same as above, but now the right-most number, even if it is zero, is the least significant number. *The least significant number implies the precision.*

Rounding Rounding off is usually done to the results to imply the precision and it is something we do deliberately. The rules for rounding are as follows:

- the digit to which you are rounding off is governed by the digit to its immediate right:
  - if that value is 5 or greater you round the least significant digit up one count;
  - if less than 5 you leave it the same (you simply truncate).

The special case of when there are multiple 5s immediately after the least significant figure, apply the following rule: round up if the least significant digit is odd, truncate if it is even. For example:

- 1.979 ± 0.082 becomes 1.98±0.08;
- 25.8350 becomes 25.84.

Computational roundoff is done by computers and is something we need to be aware of, particularly if you are conducting calculations near the limits of the number of figures the machine can handle. It can also introduce a systematic error in measurement during data collection routines on certain kinds of analytical equipment; however, in general the people who maintain these machines are aware of this and incorporate it in the estimates of precision.

6.2.3 Mean square of weighted deviates

When dealing with isochrons (see Chapter 7), the spread of parent–daughter ratios can sometimes be the limiting factor regarding the utility of an isochron. However, the confidence we can place in any calculated age which requires the fitting of a line or curve to a data set of measured values, all of which have associated uncertainties, can be expressed in terms of the mean square of weighted deviates (MSWD). At its simplest level, the MSWD is commonly used to simply assess whether an age is 'good' or not, but the MSWD is a critical quantitative piece of information when regarding geochronological data. The MSWD can be used to describe the 'goodness of fit' in isochrons and when fitting curves through clouds of data for concordia plots and (U–Th)/He analyses. In general it is worth having an understanding of what the MSWD is in order to fully interpret the veracity of a data set, and hence this concept is developed further below.

The MSWD is a statistical parameter used to describe the goodness of fit of a regression (such as an isochron) through an array of data. In essence it allows a comparison between expected analytical scatter due to measurement and the actual observed scatter on a suite of analyses. The MSWD provides a measure of whether the scatter in our measured data is equivalent to or less than the measured uncertainty in the analyses, or whether there is an external source of scatter (perhaps due to a geological event) which diminishes the significance of the age calculated. In general, the MSWD returns a numerical value, and corresponds to:

- MSWD < 1: the data fit a normal probability distribution, and the total uncertainty on the measured data is less than that predicted by the analytical uncertainties. Such data sets are often generally regarded as excellent isochrons; however, values significantly less than 1 suggest that some of the uncertainties are likely to have been over-estimated, suggesting that maybe the age is 'too good to be (analytically) true'.
- MSWD = 1: realistically the 'best' case for isochrons, whereby the scatter in the data set is what would be predicted by the estimates of the uncertainties in the analyses. Such isochrons (and those with MSWD < 1) are termed 'model 1' isochrons; however, a more general usage has model 1 isochrons being applied to data sets with MSWDs as high as 2.5 (see discussion below).
- MSWD = 1–10: model 2 isochrons. These are isochrons in which the scatter is greater than the analytical uncertainty, but is small enough for the data to retain some geological significance. The errors on the ages determined by such means should therefore, strictly speaking, be multiplied by the square root of the MSWD (e.g. if the MSWD is 9, then the error should be multiplied by 3) in order to reflect the additional uncertainty in the measurement. However, such an approach is a convenient work around, and in general one should be cautious of such regressions.
- MSWD > 10: model 3 isochrons, or 'errorchrons'. Such regressions may indeed preserve some geological significance, but the scatter is significantly beyond that expected from the analytical precision. Such data can be treated in a qualitative manner only (at best).

The mathematics behind calculation of an MSWD is based purely on statistical premises, involving the probability that the line fitted through the data (i.e. the regression) is the best fit based on each of the uncertainties associated with each individual measurement. In actual fact, all uncertainties reflect at some level *probabilities* that the correct age has been returned, not necessarily that the measurements have actually measured the correct age. For example, if the samples selected do not meet the initial criteria required for an isochron (see Chapter 7), then regardless of how low the MSWD is or how precise the measurements are, the age

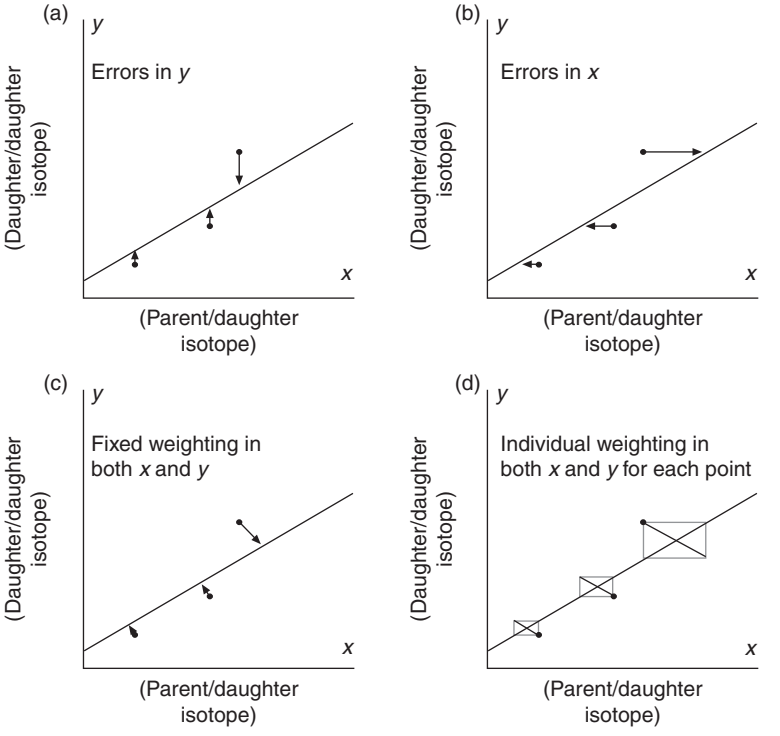

Figure 6.4 Schematic illustration of least squares regression analysis for isochrons. Different types of error weighting can be assigned depending on the confidence of the analyses in each of the variables. Generally the most appropriate weighting is that of individual weighting of errors for both x and y (i.e. parent–daughter and daughter–daughter ratios in the case of isochrons) for each individual sample.

returned will be meaningless. Therefore the mechanism by which uncertainties are assigned to the data points used to define the array can become important. Figure 6.4 schematically illustrates how this can be considered – for example the top two panels assume the (unrealistic) situation in which there is effectively no uncertainty associated with one of the variables. Panel c illustrates a situation which is sometimes employed, whereby a uniform error (say a fixed percentage of the measured value) is assigned to both of the variables, but in most cases this too is inappropriate as the uncertainties associated with measuring the parent–daughter isotope ratio will be different from that associated with measuring the daughter–daughter ratio. The most realistic scenario will be the case where individual errors for each of the variables for each individual sample will be measured, and these then need to be considered when calculating an error for the regression (in this case an isochron).

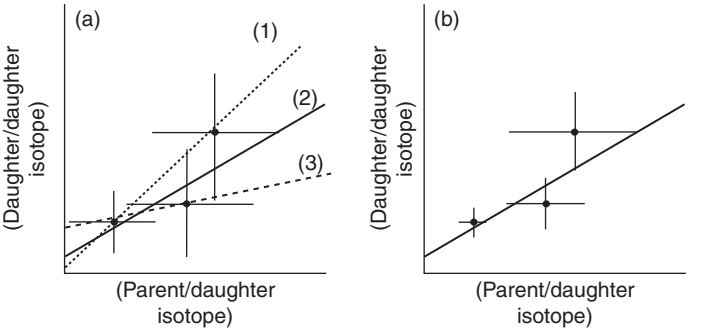

Figure 6.5 Illustration of fitting curves through a data set within the measured errors of the points defining it. (a) Permits a wide range of lines with significantly differing slopes to pass within the measured errors of all three data points. Improved precision on some of the data points (b) permits only a limited range of lines to pass through the reported errors of both the higher ratio samples simultaneously, thus producing a more precise regression.

As noted above, the MSWD in no way offers insights into whether you actually have the 'right' age for your analysis. *The MSWD simply describes whether the curve that you fit to the data is reasonable within the errors that have been assigned* to the data points. This can be best illustrated by schematically considering how a curve can be fitted to a set of data (Figure 6.5). A simple case of three data points (the simplest case required for an isochron, albeit one of dubious veracity) containing relatively large errors (Figure 6.5a) permits a number of straight lines to be fitted through the points and still remain 'within error' of all points. Since the age determined by the isochron is determined by the slope of the line (see Chapter 7), obviously there will be a big difference in ages as calculated from lines 1, 2 and 3. In all cases, however, the MSWD will be comparatively low, as all three lines plot within the assigned errors for each data point. Hence there is no excess scatter beyond that expected from the precision of the analyses, but the overall precision will still be low as there is a wide range of lines able to fit the data.

Figure 6.5b uses the same data points but now with smaller uncertainties in the data points. It is immediately clear that only a smaller range of lines can be fitted which will actually pass through the measured uncertainties of each of the data points. Hence the slope can be determined with a great(er) level of precision as there is in effect only one curve which satisfies the data within the analytical uncertainty of the measurement. In this case the MSWD will still be low, but the precision on the age will be high as there is effectively only one solution. Both examples in Figure 6.5 are in effect model 1 isochrons in that the data can be fitted by a curve within the errors reported.

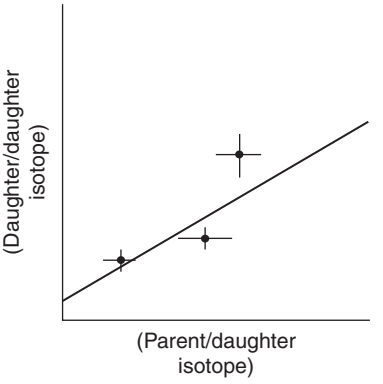

Figure 6.6 A data set that does not permit a single straight line to pass through the reported uncertainties for all data points simultaneously. This implies some other source of uncertainty in the regression beyond that obtained from the analytical procedure alone, which needs to be accounted for.

Model 2 and 3 isochrons are likely when the regression does not pass through the reported errors of all data points comprising the data set (Figure 6.6), hence implying there is a source of excess scatter beyond that which we can account for through the process of analysis itself. This excess scatter can arise from many sources – some could still be analytical, such as estimating the errors at a precision that is greater than is appropriate, therefore making the error bars on each data point smaller than they actually are, or geological, such as including samples on an isochron that should not be included as they were not part of the same magmatic event (for example) or the system has been open due to metamorphism (see Chapter 7). Often such data sets do retain some geological significance, but it is not always possible to ascertain the source of the uncertainty. Hence the rules for dealing with model 2 and 3 isochrons are simply a numerical device acknowledging that there is an extra level of uncertainty that we can account for statistically without (always) fully understanding its nature.

7

Isochron geochronology

7.1 Principles of isochrons

Consider the case of an intermediate magma fractionating to produce a series of subsequently more evolved liquids as it crystallises. This will have the effect of changing the parent–daughter ratios of various radioactive decay schemes due to differences in compatibility of the parent and the daughter in the crystallising minerals. For example, since Rb is likely to be enriched in more evolved magmas with respect to Sr, the parental andesite will have comparatively low Rb/Sr, whereas more evolved magmas from the same system (e.g. granites) will contain progressively more Rb with respect to Sr (Figure 7.1).

However, because the crystallisation takes place over a relatively short period of time with respect to the half life of ^{87}Rb, all minerals crystallised (and any remaining liquid) will have the same $^{87}Sr/^{86}Sr$. This is the key point – there is a spread in Rb/Sr between the different minerals in the rock, or between the different magmas in the fractionating series in Figure 7.1. Therefore, there is a spread in $^{87}Rb/^{86}Sr$ between these minerals or magmas. However, *when they crystallised, all of the minerals or comagmatic magmas would have incorporated Sr which had the same* $^{87}Sr/^{86}Sr$ *ratio*, since crystallisation is a chemical process, and will not significantly affect the isotopes of the elements.

So too, for a single rock, such as a granite composed of the minerals quartz, feldspar and biotite (for argument's sake), each mineral will have differing amounts of trace elements but the same daughter isotopic ratio when it crystallises. For example, feldspars have huge amounts of both Rb and Sr. In contrast, micas, such as biotite, typically do not have as much Rb and Sr; however, they have a lot of Rb compared with Sr, i.e. they have a high Rb/Sr ratio, whereas feldspars will have relatively lower Rb/Sr ratios. Quartz has virtually no Rb or Sr, but typically has very low Rb/Sr. However, if we ground a representative portion of the whole rock

Table 7.1 *Summary of Rb–Sr characteristics of minerals in a hypothetical granite at the time it crystallises.*

Mineral	$^{87}Rb/^{86}Sr$	$^{87}Sr/^{86}Sr$
Feldspar	Medium	Equal in all minerals
Biotite	Very high	
Quartz	Low	
Whole rock	Medium	

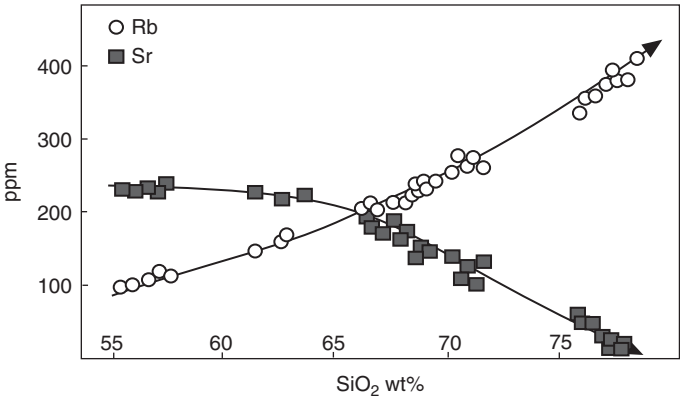

Figure 7.1 Variation of Rb and Sr (in ppm) as a liquid fractionates from a basaltic–andesite composition ($SiO_2 < 60$ wt%) through to granitic compositions ($SiO_2 > 65$ wt%). Note that the concentration of Rb is higher in the more siliceous magmas, whereas the Sr concentration is lower. This has the effect of changing the Rb/Sr ratio, from being <1 at $SiO_2 < 65$ per cent through to Rb/Sr ≫ 1 (i.e. closer to 8) at $SiO_2 > 75$ wt%. Therefore a very large range of Rb/Sr ratios can be produced by fractionation, resulting in large parent–daughter isotopic ratios. These will subsequently produce substantially different $^{87}Sr/^{86}Sr$ ratios over time.

up, we would have a mixture which is an average of both the feldspar and the biotite (and quartz), and so will have a Rb/Sr ratio somewhere in between.

So, at crystallisation, the feldspar, biotite, quartz and whole rock would have had the same $^{87}Sr/^{86}Sr$, but each would have had a different $^{87}Rb/^{86}Sr$ ratio. This is summarised in Table 7.1. Hence, at this time, t_0, a plot of $^{87}Sr/^{86}Sr$ vs $^{87}Rb/^{86}Sr$ will comprise a horizontal line with a range of parent/daughter ($^{87}Rb/^{86}Sr$) ratios (Figure 7.2a).

However, over time (i.e. millions of years after crystallisation), ^{87}Rb will decay to ^{87}Sr. Therefore, there will be new (radiogenic) ^{87}Sr added to that which already existed in the minerals (as in Figure 7.2a). It therefore follows that those minerals with the greatest amount of Rb relative to Sr (i.e. highest Rb/Sr ratios) will see the greatest increase in ^{87}Sr with respect to ^{86}Sr (Figure 7.2b).

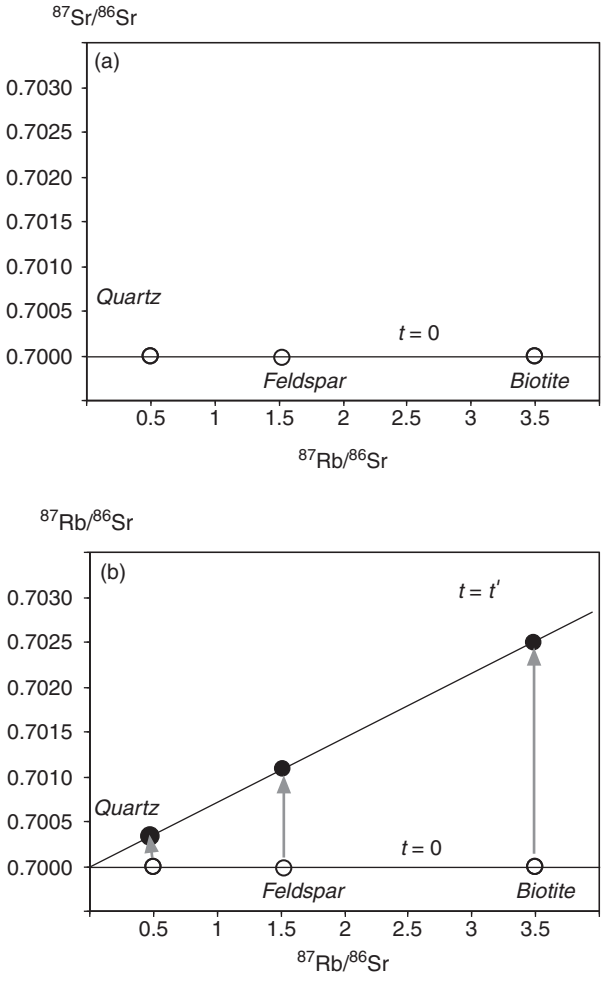

Figure 7.2 Schematic representation of an Rb–Sr isochron diagram. (a) At time t_0, all samples have the same daughter isotope ratio. Over time, those samples with higher amounts of parent isotope (i.e. higher parent/daughter isotope ratio) grow more of the daughter isotope than those with lower amounts of the parent isotope. (b) After a given period of time, the samples will define a linear array which passes through the *y*-axis at the *initial ratio* (D_0), i.e. the value of the daughter isotopic ratio at which all samples started. The slope of the line, *m*, is directly proportional to the amount of time elapsed, and can be used to calculate the age.

Hence, over time, those minerals with the highest $^{87}Rb/^{86}Sr$ will produce the highest $^{87}Sr/^{86}Sr$.

Indeed, this can be generalised further:

Those phases with the highest parent/daughter ratio will, over time, ingrow the highest daughter isotope ratio.

Thus, if we plot our samples from Table 7.1 on a graph of daughter vs parent isotopic ratio, we get something that looks like Figure 7.2. Initially, all minerals have the same daughter isotopic ratio, but a range of parent/daughter ratios, which gives them a spread along the *x*-axis. So, from the example above, our biotite, which has the highest Rb/Sr, would be the point on the right-hand side of Figure 7.2a, whereas our quartz, which had a low Rb/Sr, would plot on the left, closest to the *y*-axis. The feldspar (and whole rock) would plot somewhere in the middle.

However, over time, those minerals with high Rb/Sr will ingrow a lot more ^{87}Sr than those with low Rb/Sr. This will occur in a systematic manner, resulting in a line of slope *m* with the passage of time. Over time this line will become steeper and steeper due to the progressive accumulation of more and more ^{87}Sr, producing higher and higher daughter isotope ($^{87}Sr/^{86}Sr$) ratios. Hence we can see intuitively that the steeper the line, the more time has elapsed in order to allow the accumulation of the radiogenic ^{87}Sr. The line defined by such an array is termed an *isochron*. Therefore, we can see that, qualitatively, the age of crystallisation of the magma is directly proportional to the slope of the array, i.e. the steeper it is, the older the rock is. On its own this is not really much use to us as we want to know the age quantitatively, i.e. put a number on it.

Significantly, such an isochron diagram can be described mathematically in terms of Equation 5.8 from Section 5.3.1. In the case for Figure 7.2, note that Equation 7.1, and the derivative isotope ratio equations from it, has a general form of $y = c + xm$, which is the equation of a straight line, where *c* is the *y*-intercept and *m* is the slope of the line:

$$\left(\frac{^{87}Sr}{^{86}Sr}\right)_t = \left(\frac{^{87}Sr}{^{86}Sr}\right)_0 + \left(\frac{^{87}Rb}{^{86}Sr}\right)_t \left(e^{(1.42\times10^{-11}t)} - 1\right).$$

$$y \quad = \quad c \quad + \quad x \quad m \qquad \text{(Eq 7.1)}$$

Therefore, for a plot such as Figure 7.2b, this equation describes the form of the isochron. The only unknown in this equation is *t*, and following from Equation 7.1:

$$m = \left(e^{(1.42\times10^{-11}t)} - 1\right); \quad \text{or more generally: } m = (e^{\lambda t} - 1). \qquad \text{(Eq 7.2)}$$

Rearranging gives:

$$t = \frac{1}{\lambda}\ln(m + 1). \qquad \text{(Eq 7.3)}$$

We can measure the slope (*m*) from the isochron diagram, either by eye after drawing a line of best fit through it (which is not altogether accurate, but will give

an estimate), or by conducting a least squares regression on the data set (see discussion of MSWD in Section 6.2.1).

Remember that graphically the slope of a line is simply:

$$m = \left[\frac{\Delta y}{\Delta x}\right] = \left[\frac{y_2 - y_1}{x_2 - x_1}\right], \qquad \text{(Eq 7.4)}$$

where $y_2 > y_1$ and x_2 and x_1 are the corresponding x values for the appropriate y coordinate.

Given that we know λ for the isotope system of interest, we can plug both of these values into Equation 7.3 and calculate an age in years (since the only variable which has units is λ, which has units yr^{-1}, the inverse of which is yr).

This example has used the different minerals within a granite; however, isochrons can be generated for any magmatic system which preserves a spread in parent/daughter isotope ratios and crystallised rapidly with respect to the half life of the decay scheme being used (as in the more general example summarised below). Therefore, the example illustrated in Figure 7.2 can be applied on a whole-rock scale, simply by taking samples of different SiO_2 content, since the Rb/Sr ratio varies with fractionation (as in Figure 7.1). Since fractionation occurs quickly with respect to the decay of ^{87}Rb, we have satisfied the conditions for generating an isochron (Section 7.1.1). Figure 7.3 is a whole-rock isochron that would be appropriate for the fractionating magma series summarised in Figure 7.1.

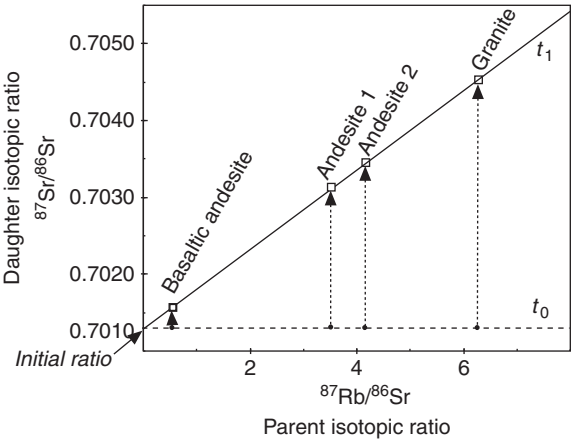

Figure 7.3 Whole-rock isochron diagram for a suite of fractionating magmas, such as those illustrated in Figure 7.1. Since the Rb/Sr ratio of the whole rock varies depending on how fractionated the sample is, a range of parent/daughter ratios are produced during fractionation. Those rocks, which have the highest Rb/Sr ratio, have the highest $^{87}Rb/^{86}Sr$ ratio, and hence will, over time, produce the highest $^{87}Sr/^{86}Sr$ ratios.

Such a whole-rock approach can be applied to any fractionating magmatic system, and indeed similar composition magmas derived from the same magma chamber. Basically, over time, those portions of a now-crystallised igneous complex with high Rb/Sr will ingrow a lot more ^{87}Sr than those with low Rb/Sr. This will occur in a systematic manner, resulting in a line of slope *m* with the passage of time. Over time this line will become steeper and steeper due to the progressive accumulation of more and more ^{87}Sr, producing higher and higher daughter isotope ($^{87}Sr/^{86}Sr$) ratios. Therefore, the age of crystallisation of the magma is directly proportional to the slope of the array.

7.1.1 Conditions necessary for an isochron

Such an approach can be applied to *any* radiogenic isotope system, and need not be limited to the Rb–Sr decay scheme (e.g. Figure 7.4). Indeed, the conditions necessary to form an isochron that records the age of a rock (or suite of rocks) are:

(1) all samples had the same initial daughter isotopic ratio at the time of closure (T_c);
(2) all samples have subsequently remained closed systems with respect to parent and daughter diffusion since formation; and
(3) the samples display a spread in parent/daughter (P/D) ratios.

Criterion 3 is not strictly essential for forming an isochron; however, the precision of the age determined is greatly increased if there is a range in P/D. Whole-rock samples of similar composition (for example) are likely to show only a limited range in P/D and so a number of lines of best fit can potentially be fitted for them, resulting in lower precision. Sm–Nd isochrons of minerals containing garnet, for example, often produce excellent ages because garnet has very high Sm/Nd ($^{147}Sm/^{144}Nd$) ratios compared with most other minerals in garnet-bearing rocks. However, sometimes such isochrons reflect only the age of garnet growth, and not that of the other metamorphic mineral phases in the rock, since the garnet is causing the sample to behave as a two-point isochron. Therefore it is critical to have a good understanding of the petrogenesis of your sample when attempting (particularly metamorphic) geochronology. In contrast, Sm–Nd isotopes are less commonly used to produce whole-rock isochrons since the silicate minerals that crystallise in most magmas often do not significantly fractionate Sm from Nd, resulting in a very low spread in P/D ($^{147}Sm/^{144}Nd$) and hence low precision.

The statistical underpinnings and significance of the ages produced were explored in Chapter 6 for the interested reader; however, most users of geochronological data require only a conceptual understanding of these notions in order to be able to interpret their data with confidence.

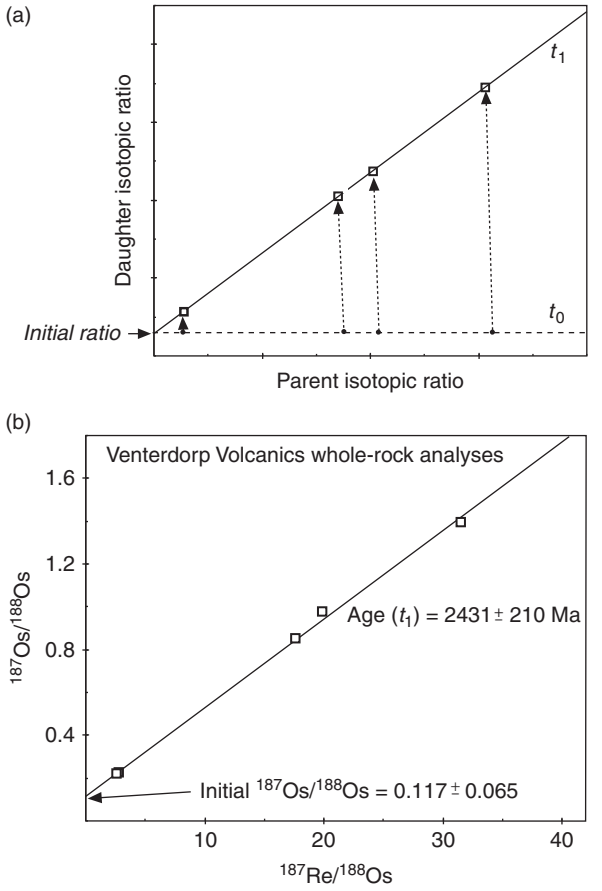

Figure 7.4 (a) General schematic representation of an isochron diagram. At time t_0, all samples have the same daughter isotope ratio. Over time, those samples with higher amounts of parent isotope (i.e. higher parent/daughter isotope ratio) grow more of the daughter isotope than those with lower amounts of the parent isotope. Thus, after a given period of time, the samples will define a linear array which passes through the *y*-axis at the *initial ratio* (D_0), i.e. the value of the daughter isotopic ratio at which all samples started. The slope of the line, *m*, is directly proportional to the amount of time elapsed, and can be used to calculate the age. (b) Example of a real isochron, using the $^{187}Re \rightarrow {}^{187}Os$ decay scheme. Five basalt samples from South Africa define a linear array which crosses the daughter isotopic ratio (i.e. *y*-axis, which in this case is $^{187}Os/^{188}Os$) to give an initial ratio (D_0), which is the $^{187}Os/^{188}Os$ value of the last time all the samples were in *isotopic equilibrium*. Often this is likely to be when the lavas were all in the same magma chamber. The slope of the line is directly proportional to the time elapsed since all of the samples had the same D_0.

7.2 Metamorphism and resetting of isochrons

During metamorphism, the destruction of existing minerals and growth of new ones results in the redistribution of isotopes among the newly grown minerals. As in the case of magmatic isochrons, since daughter isotopes are chemically identical to each other, the daughter isotopic ratio of new minerals will be the same for all minerals. However, the parent/daughter isotopic ratio will vary depending on the relative compatibility of the parent and daughter element in the mineral of interest, potentially resulting in a range of ratios on an isochron diagram. This process is summarised in Figure 7.5, whereby the ancient daughter isotopes that have ingrown through the evolution of the precursor are redistributed in the various phases of the new metamorphic rock. Significantly, the initial ratio of the metamorphic rock will, by definition, be more radiogenic than that of the protolith, since the daughter isotope has accumulated within the protolith since it first formed.

For example, a granite has an age of t' years (Figure 7.5a). At this time, it experiences a homogenisation or metamorphic event. This event effectively destroys the existing minerals (quartz, feldspar, mica) and grows new ones (plagioclase, garnet, biotite). In the process, all of the radiogenic Sr is released from the old assemblage and incorporated into the new minerals (Figure 7.5b). Because these minerals are growing in a rock that has already accumulated a large amount of ^{87}Sr due to ingrowth when it was a granite, the new (homogeneous) $^{87}Sr/^{86}Sr$ ratio is more radiogenic than when the granite first formed.

The new minerals then evolve to form a new isochron (Figure 7.5c), which reflects the amount of time that has passed since the growth of the metamorphic minerals. All record of the previous history of the rock is erased, *except* for the observation that the initial (metamorphic) $^{87}Sr/^{86}Sr$ ratio (i.e. the ratio that all of the minerals had when they were formed) is quite radiogenic, implying that these minerals formed in a rock that had previously had a significant amount of time to ingrow ^{87}Sr.

A similar case can also occur when minerals with low closure temperatures are not necessarily destroyed, but are open to diffusion of the isotopic system of interest for long enough to allow equilibration between them. In this case we experience open system behaviour of the isotopes, and ideally this can be considered identical to the destruction of old minerals and the growth of new ones. Unfortunately this is rarely the case, with some minerals of higher closure temperatures (e.g. zircon) holding on to their inventory of (for example) REE, while others may be open to diffusion. This may result in partial resetting of the rock during metamorphism and is often responsible for some of the excess scatter observed in some isochrons.

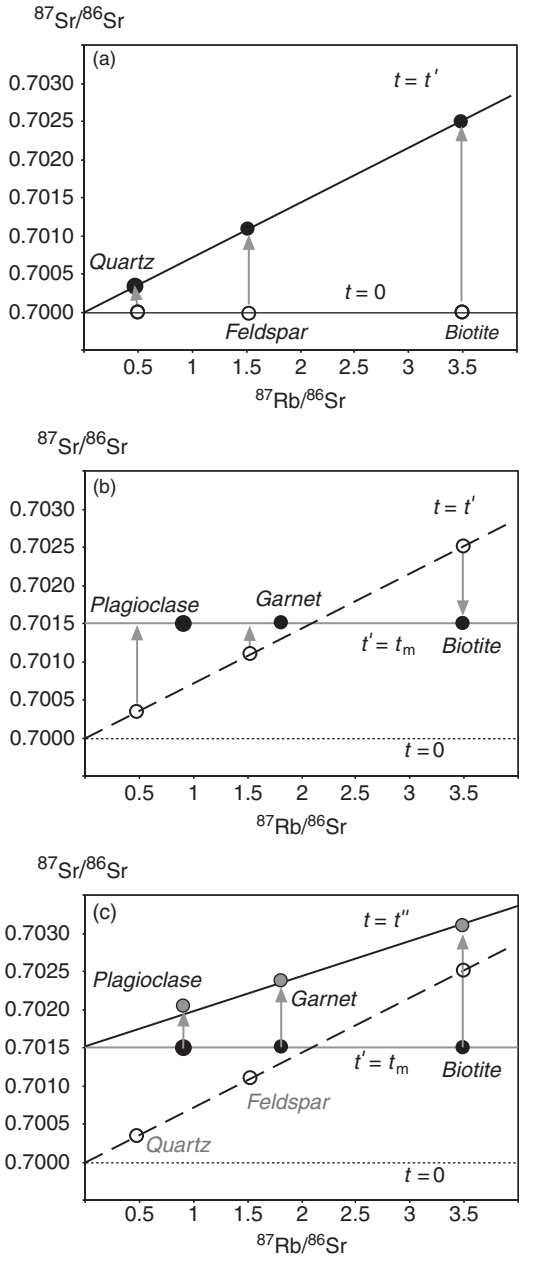

Figure 7.5 Resetting of an isochron. A quartz, feldspar and biotite granite crystallises and ingrows ^{87}Sr for t' years (a). At this time (t_m), it is metamorphosed to a plagioclase, garnet, and biotite gneiss, resulting in a uniform $^{87}Sr/^{86}Sr$ ratio across all of the newly grown phases, all of which contain their own $^{87}Rb/^{86}Sr$ (b). Over time a new isochron with a slope corresponding to the amount of time elapsed since the metamorphism grows, preserving an initial ratio equivalent to the $^{87}Sr/^{86}Sr$ ratio of the granite whole-rock precursor at t_m (c).

Significantly, this can become important when attempting to obtain isochrons on ancient igneous rocks, as phases such as some feldspars and micas may have been open to isotopic exchange during low-grade metamorphism, whereas other accessory phases and amphiboles may remain closed (e.g. see Figure 5.4).

Careful selection of individual phases known to contain extreme parent/daughter ratios can provide particularly powerful chronometers for unravelling the *P–T–t* evolution of a terrain. Garnet, for example, is one of the few minerals that significantly fractionates Sm from Nd and Lu from Hf when it grows, resulting in very high Sm/Nd and Lu/Hf ratios. These produce very rapid ingrowth of the daughter isotope (^{143}Nd and ^{176}Hf, respectively) and can allow determination of high-precision isochrons. Of particular power in these cases is the ability to often link the garnet composition with *P* and *T* calculations for the metamorphic conditions, and double check this with the two independent chronometers.

8

U–Pb, Pb–Pb and Re–Os sulphide geochronology

The U–Pb decay scheme is the most widely applied geologically robust geochronometer. Due to its unique attribute of containing two independent decay chains, starting from different parent isotopes and finishing with different daughter isotopes of the same elements, it is possible to cross-correlate the data obtained simultaneously to produce routine, high-precision (often ~0.1 per cent) geochronological data on ancient samples. In addition, U-series disequilibria can be employed to investigate very young processes; however, the principles behind these techniques are quite different and relevant to only a smaller number of mineralised settings, and hence are introduced separately below. Finally, the spontaneous fission products of ^{235}U produce radiation damage trails in crystalline materials, such as apatite and zircon, and form the basis of fission track analysis (Section 8.4)

The utility and precision of U–Pb stems from a number of significant factors:

- The half lives of both the key decay schemes (^{235}U to ^{207}Pb = ~704 Myr and ^{238}U to ^{206}Pb = ~4.47 Gyr) are short enough to have been calibrated to high precision by direct observation measurements.
- Although each scheme decays via a series of short-lived intermediaries (^{238}U undergoes eight α and six β decays, ^{235}U seven α and four β decays) to reach their respective daughter products, provided closed system behaviour is maintained, each decay from U to Pb can be considered to take place geologically instantly (Figure 8.1).
- The existence of the 'parallel' schemes allows coupled ages to be calculated using the concordia method (see below), with a resulting inherent measure of closed system behaviour and increased precision due to cancellation of errors due to simultaneous acquisition of ages.
- Due to the significantly different compatibility of U and Pb, there is a wide range of common rock-forming minerals which will incorporate U (and Th) in their lattice and exclude Pb – notably zircon, monazite, titanite and baddeleyite.

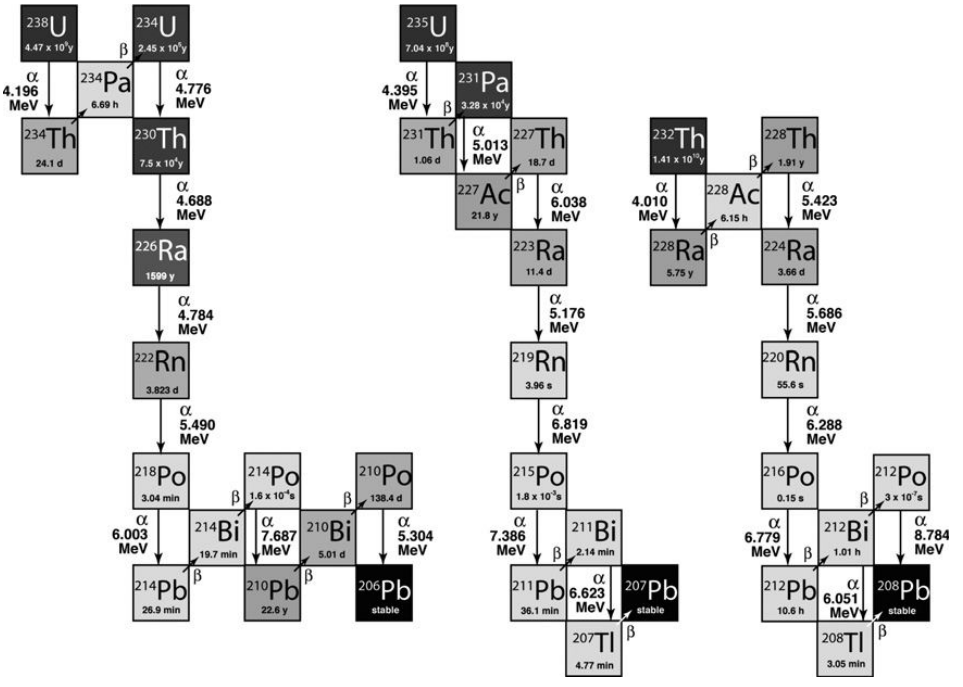

Figure 8.1 Decay chains for isotopes of Th and U to form Pb isotopes. Note the large number of intermediaries, many of which have geologically insignificant half lives (e.g. 0.15s for ^{216}Po) However, each of the different elements formed along the way can have significantly different chemical properties (e.g. Rn is an inert gas, cf. Ra which is a large ion lithophile element (LILE)), and hence a range of geological processes can act upon these on very short time scales. This forms the basis for U-series disequilibria geochemistry, a completely separate field of geochemistry. For ancient rocks (>2 Ma), each individual decay series can be simplified to comprise a single step as a parent–daughter pair as for Sm–Nd or Rb–Sr. This is a powerful tool in isotope geodynamics in addition to geochronology. The darker shading represents longer half lives of the intermediaries.

- Geological understanding of U–Pb systematics are quite mature, with over 100 years worth of investigations into the applicability for geochronology commencing with Rutherford and Holmes in the first quarter of the twentieth century.

U–Pb isotopes can be applied to obtain high-temperature, ancient (>0.5 Ma) ages via one of three techniques, depending on the material being analysed and the problem being investigated:

(1) Either decay scheme (generally ^{238}U to ^{206}Pb, but ^{235}U to ^{207}Pb and even ^{232}Th to ^{208}Pb) can be used to produce isochrons (see Chapter 7).

(2) Pb–Pb dating, based solely on the measured Pb isotopes and assuming a ratio for the $^{235}U/^{238}U = 1/137.88$ can be applied, generally on whole-rock sample suites that have maintained closed system behaviour (intrusive bodies such as granites, the whole Earth and some meteorite studies).
(3) 'U–Pb dating' using a concordia plot that derives ages using coupled geochronology.

Each of these will be dealt with in turn, and additional sections on U-series for very young samples (<500 ka, applicable mainly in environmental, groundwater and volcanological studies) and fission track analysis (low-temperature histories outlining denudation and uplift), are included below.

8.1 Principles of U–Pb geochronology

For the reader interested in manipulating data sets or recalculating ages, or even looking for a thorough understanding of how the U–Pb system works, a brief background of the mathematics and the principles of age determination is provided below. The applications of these principles, largely in the context of zircons, are provided subsequently in Section 8.1.4.

8.1.1 Isochrons

From the basic decay equation (Equation 5.8), we can normalise to ^{204}Pb, the only non-radiogenic isotope of Pb, and the decay of ^{238}U to ^{206}Pb can be simplified as occurring in a single step with a single decay constant, λ_1:

$$\left(\frac{^{206}Pb}{^{204}Pb}\right) = \left(\frac{^{206}Pb}{^{204}Pb}\right)_i + \frac{^{238}U}{^{204}Pb}\left(e^{\lambda_1 t} - 1\right). \qquad \text{(Eq 8.1)}$$

Correspondingly, the decay of ^{235}U to ^{207}Pb can be expressed in terms of its own decay constant, λ_2:

$$\left(\frac{^{207}Pb}{^{204}Pb}\right) = \left(\frac{^{207}Pb}{^{204}Pb}\right)_i + \frac{^{235}U}{^{204}Pb}\left(e^{\lambda_2 t} - 1\right). \qquad \text{(Eq 8.2)}$$

Either of these decay systems alone would form the basis of an isochron, in a manner analogous to Rb–Sr as outlined in Section 7.1. Indeed, theoretically a third isochron, based on the Th–Pb decay scheme, could also be considered, where λ_3 is the appropriate decay constant:

$$\left(\frac{^{208}Pb}{^{204}Pb}\right) = \left(\frac{^{208}Pb}{^{204}Pb}\right)_i + \frac{^{232}Th}{^{204}Pb}(e^{\lambda_3 t} - 1). \qquad \text{(Eq 8.3)}$$

Such isochrons are very rarely applied, since the very different geochemical behaviour of U and Pb, particularly in weathering, low-grade metamorphic conditions and those with changes in redox, will often negate the closed system criteria essential for isochrons (Section 7.1.1). So, too, the analytical challenges required in the analysis of Th have meant this isochron system is very rarely, if ever, applied. Further, as we shall see below, since both U and Pb are obtained in the same analysis for two decay systems, ages with a greater precision and their own inbuilt check for open system behaviour can be obtained using the concordia approach.

8.1.2 Pb–Pb dating

Since there are two U–Pb decay schemes, which involve decay from different parent isotopes to produce different daughter isotopes of the same element, it is possible to do some mathematical manipulation which is not available to us for other decay schemes. Since both Equations 8.1 and 8.2 are normalised to the same, non-radiogenic isotope of Pb (^{204}Pb), it is possible to combine these equations using the parameters in Table 8.1 and ultimately cancel for ^{204}Pb:

$$\frac{\left(\frac{^{207}Pb}{^{204}Pb}\right) - \left(\frac{^{207}Pb}{^{204}Pb}\right)_i}{\left(\frac{^{206}Pb}{^{204}Pb}\right) - \left(\frac{^{206}Pb}{^{204}Pb}\right)_i} = \left(\frac{^{207}Pb}{^{206}Pb}\right)^* = \frac{^{235}U}{^{238}U}\left[\frac{(e^{\lambda_2 t} - 1)}{(e^{\lambda_1 t} - 1)}\right], \qquad \text{(Eq 8.4)}$$

where ($^{207}Pb/^{206}Pb$)* is the Pb produced purely by the decay of U during the time t which has elapsed since the system closed.

Such an equation has several uses. For systems in which we can assume no initial Pb, such as can sometimes be the case for the mineral zircon, simply measuring the

Table 8.1 *Parameters for the U–Pb decay system.*

Parent isotope	Daughter isotope	Decay constant (λ), yr^{-1}	Half life ($T_{1/2}$), yr	Normalising isotope
^{238}U	^{206}Pb	0.155125×10^{-9}	4.468×10^{9}	^{204}Pb
^{235}U	^{207}Pb	0.98485×10^{-9}	0.704×10^{9}	^{204}Pb
^{232}Th	^{208}Pb	0.049475×10^{-9}	14.01×10^{9}	^{204}Pb

$^{207}Pb/^{206}Pb$ ratio and assuming that $^{235}U/^{238}U = 1/137.88$ enables us to solve Equation 8.4 iteratively for different values of t. Thus it is possible to calculate an age that corresponds to the measured $(^{207}Pb/^{206}Pb)^*$. Such an approach was employed by the zircon evaporation or 'Kober' technique, but the combination of assumption of no initial Pb and the time-consuming nature of the measurements has seen it largely superseded by *in situ* zircon techniques.

More significantly, however, rather than considering a situation where there was no initial Pb, we can consider Equation 8.4 in the context in which we have a number of samples that all had the same initial ratios some time (t_0) in the past (e.g. whole-rock samples of granite, or mineral separates within a granite that have fractionated U from Pb, such as feldspars). Each sample will develop a different Pb isotopic signature depending on their U/Pb ratio over time (Figure 8.2). If we therefore plot the present-day Pb isotope ratios against each other, providing our closed system criteria have been met, they should form a straight-line array, with a slope that depends solely on the amount of time t that has elapsed (Figure 8.2). Significantly, we do not need to know anything about the actual concentrations of either U or Pb, simply the Pb isotopic ratios.

Note that this diagram differs from a conventional isochron in that it does not plot the parent isotope, and therefore the initial ratios for both decay schemes plot as a single point in this space. Although there is no requirement to know the actual U or Pb concentrations of the samples analysed, we know that over time each sample will accumulate both ^{207}Pb and ^{206}Pb depending on the amount of U present in the sample. Since the half life for ^{238}U is very much longer than that of ^{235}U, young samples will accumulate ^{207}Pb relatively rapidly and hence have steeper slopes. Hence over time the slope of the isochron on a Pb–Pb diagram will decrease, in contrast to the conventional isochron diagram (Figure 8.2b).

Graphically, Equation 8.5 plots families of lines which have a slope m:

$$m = \frac{1}{137.88}\left[\frac{\{e^{\lambda_2 t} - 1\}}{\{e^{\lambda_1 t} - 1\}}\right]. \qquad \text{(Eq 8.5)}$$

These lines all pass through the point $(^{207}Pb/^{204}Pb)_0$, $(^{206}Pb/^{204}Pb)_0$ (Figure 8.2), which is the combination of initial ratios for these samples.

8.1.3 The geochron

The other situation in which the assumption of common initial ratios is valid is in the case of iron meteorites. While discussing the formation of meteorites and the age of the Earth may at first seem unrelated to direct application of Pb isotopes to ore deposits and economic geology, the approach *is* directly applicable to

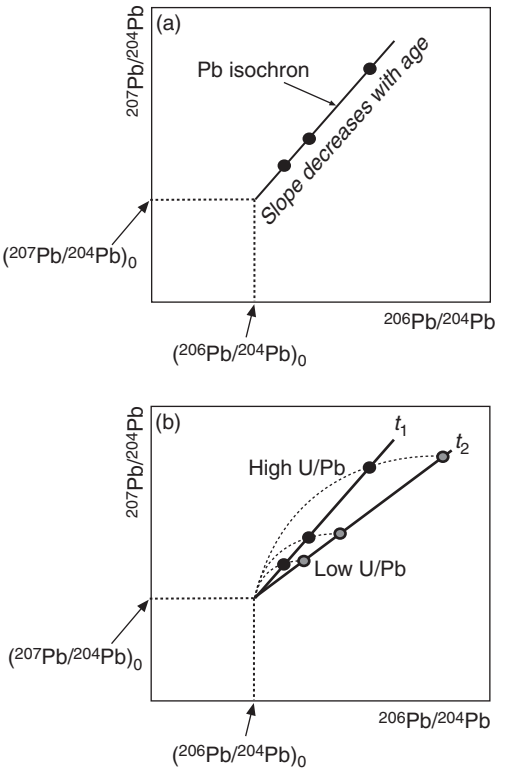

Figure 8.2 Pb–Pb isochron diagram. Note that in this case the initial ratio is a point (a), and that with time the slope of the isochron *decreases*. This is because the amounts of ^{206}Pb and ^{207}Pb are both increasing; however, they are increasing at different rates since ^{238}U (the parent of ^{206}Pb) is far more abundant than ^{235}U (the parent of ^{207}Pb) and they decay at different rates. Therefore, rather than defining straight-line trajectories over time, each sample will evolve via a curved path, with the most radiogenic samples evolving from those with the highest initial U/Pb ratios (b). Therefore, if t_1 and t_2 are considered in terms of time before the present, $t_1 < t_2$.

understanding both concordia diagrams and the calculation of Pb model ages, both of which have been applied to ore bodies and mineralised systems. It is therefore worthwhile understanding the geochron in the context of Pb–Pb dating before exploring the more complex issue of concordia plots.

During planetary formation and differentiation, U (and Th) are very efficiently segregated into the silicate (mantle) portion of the planetesimal, leaving the relatively siderophile Pb enriched in the metallic iron core – particularly in any troilite (FeS) within it. Certain types of iron meteorites represent the earliest cores formed in the solar system, and since they contain effectively no U or Th, they have experienced no ingrowth of Pb since the formation of

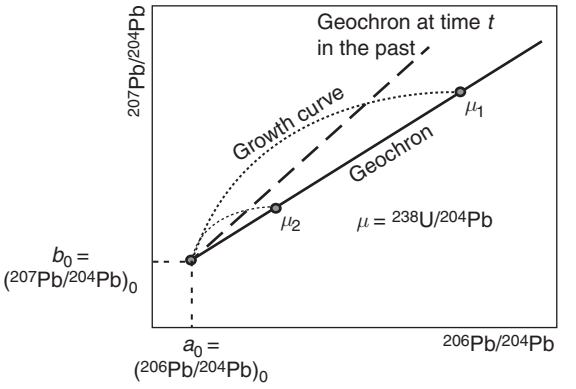

Figure 8.3 The geochron refers to the isochron defined by the whole Earth and solar system as a closed system. The solar system initial ratio is best defined by troilite from iron meteorites, with stony meteorites defining higher U/Pb (μ_1) components along the geochron. Terrigenous sediments (μ_2), a bulk estimate of the average upper silicate portion of the Earth, also plot on the geochron, confirming that the Earth has the same age and ultimate origin as the remainder of the solar system. This figure also highlights that the geochron is evolving through time, and it is possible to calculate the slope of the geochron for any time, *t*, in the past.

the solar system. Therefore they have preserved within them the primordial (or fossil) Pb isotopic composition of the solar nebula, and hence this is the $(^{207}Pb/^{206}Pb)_I$ ratio for the whole of the Earth. Such measurements were first conducted on troilite from the Canyon Diablo meteorite (the meteorite which formed Meteor Crater in Arizona). When plotted on a Pb–Pb isochron diagram, the Canyon Diablo troilite (CDT) and indeed other troilites from primitive iron meteorites preserve the lowest Pb isotopic ratios ever measured and define an initial ratio as in Figure 8.3.

So too, we can consider what happens when we take the amount of U into account as well. The U/Pb ratio, or perhaps more usefully the $^{238}U/^{204}Pb$ ratio, is one that is referred to regularly in Pb isotopes, and is denoted by the Greek letter μ (pronounced 'mu'). In essence, μ directly approximates the U/Pb ratio, since ^{238}U is the longest-lived U isotope and ^{204}Pb is not radiogenic, and hence invariant with time. Therefore samples with high μ (μ_1 on Figure 8.3), will rapidly ingrow radiogenic Pb (i.e. high $^{207}Pb/^{204}Pb$ and $^{206}Pb/^{204}Pb$ since high $^{238}U/^{204}Pb$ corresponds to high $^{235}U/^{204}Pb$ as well), whereas samples with lower μ (μ_2 on Figure 8.3) will ingrow relatively less.

Therefore, if we then measure the Pb isotopes for differentiated stony meteorites, these can be plotted on the same diagram. Since we can assume that these contain the U and Th that was left behind at the time of iron meteorite formation, such

samples will have high μ and correspond broadly μ_1 on Figure 8.3. They have therefore evolved to produce highly radiogenic Pb isotopes, and since they had the same initial Pb isotope ratios as the iron meteorites, they fulfil the criteria for an isochron. Therefore the age of planetesimal differentiation can be calculated from such a Pb–Pb diagram and is of the order of 4.55 Ga.

However, what is significant about Figure 8.3 is not that meteorites of different types lie on the same Pb–Pb isochron, but rather that pelagic sediments, which can be considered to approximate an average bulk Earth composition, also plot on the same isochron between the two families of meteorites. These materials have comparatively lower μ (e.g. μ_2). The implication is that the Earth has the same age as the meteorites and the material within it came from the same place. Indeed, the significance of this is that all material in the solar system shares a common source, and so this isochron has been termed the geochron.

As it turns out, average pelagic sediment is not actually a particularly good estimate for the bulk Earth, and in detail, due to substantial reprocessing within the Earth, the age of the Earth itself is actually slightly younger than the geochron. However, this approach was the first highly accurate determination of the age of the Earth – subsequent refinements in the age of the Earth are only just outside of the 4.55 ± 0.07 Ga determined by Patterson (1956) and today it is placed at 4.54 Ga.

8.1.4 The concordia (Wetherill) plot

As alluded to above, the U–Pb system is unique in that it contains two entirely independent chronometers from the same parent element that produce different isotopes of the same daughter element. Whereas previously we manipulated the decay equations to remove the need to normalise to ^{204}Pb (Equation 8.4), it is also possible to combine these equations to express them purely in terms of age and daughter/parent ratios. This allows us to consider the system, or more commonly an individual sample or mineral, in terms of its age, t. Hence it is possible to rearrange this equation such that we can calculate an age based on each decay scheme:

$$\frac{^{206}\mathrm{Pb}^*}{^{238}\mathrm{U}} = e^{\lambda_1 t} - 1, \qquad \text{(Eq 8.6)}$$

which rearranges to:

$$t = \frac{1}{\lambda_1}\left(\frac{^{206}\mathrm{Pb}^*}{^{238}\mathrm{U}} + 1\right), \qquad \text{(Eq 8.7)}$$

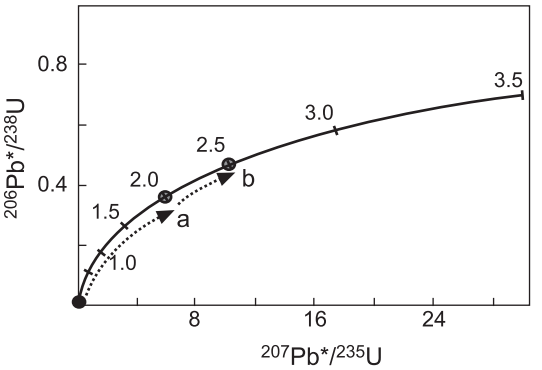

Figure 8.4 Concordia plot. The concordia is the curve defined by points of the same age determined independently from the decay of ^{235}U and ^{238}U through time for samples that have little or no initial Pb. Hence, at time 0, there is no radiogenic ^{206}Pb or ^{207}Pb, and the sample will plot at the origin. Over time it will ingrow both Pb isotopes, with the total amount of ingrowth depending solely on the amount of time elapsed. Hence after 2.0 Gyr the sample will have moved along the curve to point a. After an additional 500 Myr, the sample is now aged 2.5 Ga and hence will plot at point b. This example assumes closed system behaviour.

and for the decay of ^{235}U to ^{207}Pb:

$$\frac{^{207}Pb^*}{^{235}U} = e^{\lambda_2 t} - 1 \qquad \text{(Eq 8.8)}$$

and:

$$t = \frac{1}{\lambda_2}\left(\frac{^{207}Pb^*}{^{235}U} + 1\right) \qquad \text{(Eq 8.9)}$$

The utility of this approach is that Equations 8.7 and 8.9 are parametric equations which describe the locus of compatible sets of $^{206}Pb^*/^{238}U$ and $^{207}Pb^*/^{235}U$ ratios for values of t. This curve is called the concordia (Figure 8.4), and the curve reflects the relative rates of decay of ^{235}U and ^{238}U, and hence the rate of production of ^{206}Pb with respect to ^{207}Pb. Such plots are also sometimes referred to as Wetherill plots.

The example given in Figure 8.4 is a sample which starts out with no inherited Pb, and hence there is no initial $^{206}Pb^*$ or $^{207}Pb^*$. This may be the case for certain minerals, such as zircon, in which U and Th (and the REE) are highly compatible in the crystal structure, but Pb is not, effectively excluding it from incorporation in the crystal lattice. Over time the U decays to produce radiogenic Pb, and hence the sample will move along the concordia away from the origin, the distance travelled along the curve being due entirely to the amount of time elapsed. Provided the system remains closed to either Pb loss or U gain, an age can be determined for

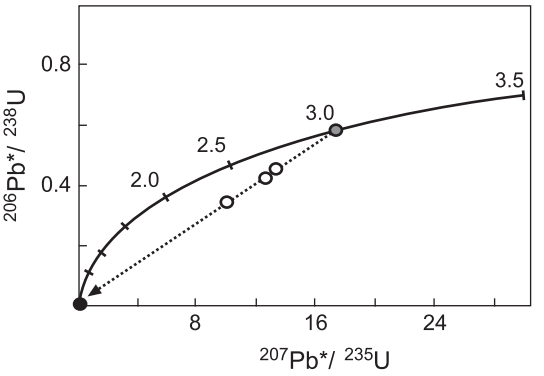

Figure 8.5 Concordia plot illustrating the effect of Pb loss on a sample 3.0 Ga in age. Complete resetting results in the sample plotting at the origin (black symbol), whereas partial Pb loss will result in a series of samples projecting back towards the origin, depending on the degree of Pb loss (open symbols). Such samples are said to be discordant.

a single sample with a single analysis, as it will plot directly on the concordia. Such analyses are said to be ***concordant*** and provide highly robust and precise ages as the very observation that they lie on the concordia is evidence that the system has remained undisturbed, and the age is determined simultaneously from two chronometers.

However, in the crust there are many processes which can lead to open system behaviour, most commonly those associated with Pb loss. Metamorphism, for example, can heat samples above the closure temperature for Pb in zircon, thus potentially resetting the system. In such a case, if all of the Pb is lost, the system is completely reset and the sample will no longer have any radiogenic Pb, and hence it will plot at the origin of the concordia again (Figure 8.5). In such a scenario, the sample will subsequently regrow radiogenic Pb and will move along the concordia as previously described. More commonly, however, the system is likely to be partially reset, with different individual samples (zircon grains, for example) experiencing relatively different amounts of Pb loss. In such a scenario, each sample will be displaced from the actual age of the sample (3.0 Ga in Figure 8.5) along a straight line (chord) towards the origin. The more Pb that has been lost from an individual grain, the closer to the origin it will plot. These partially reset samples are now said to be ***discordant***; however, the fact that they lie on a straight line at the time of the disturbance is immensely useful.

When a sample lies off the concordia curve we call it discordant. Discordia relations result from:

(1) radiogenic Pb loss or U gain between the age of the mineral and the present;
(2) U loss between mineral growth and the present day; or
(3) inheritance of components of mixed and older ages.

8.1.4.1 Radiogenic Pb loss

Consider the case of Figure 8.5, where the 3.0 Ga rock was partially reset. The samples are now dispersed along a chord which projects back to the origin (open circles in Figure 8.5). Now consider the case that the rock is allowed to sit, undisturbed, for another 500 Myr. After this time, any undisturbed portions of the original sample will lie on the concordia at 3.5 Ga, and the completely reset samples will have moved along the concordia from the origin to 500 Ma (Figure 8.6a). The partially reset samples will themselves also have evolved along curved trajectories representing 500 Myr ingrowth of Pb. Significantly, however, the partially reset samples still lie on a straight line between the original sample and the completely reset sample. Therefore, within this single sample we can preserve the age of the protolith (3.5 Ga) and the metamorphic event (0.5 Ga). In the case of Figure 8.6a such an interpretation is straightforward as we still have the concordant samples returning ages of 3.5 Ga and 0.5 Ga. What is far more common in situations involving Pb loss and metamorphic resetting is that none of the samples are completely reset, and also all of the samples have experienced some degree of Pb loss, meaning that none of the analyses are concordant (Figure 8.6b). In this case we are still able to conduct a linear regression through the discordant data points and calculate where the line crosses the concordia. Such extrapolation gives two ages, the upper intercept corresponding to the age of the protolith (t_0) and the lower intercept, the age of metamorphism (t*).

Such discordia are commonly associated with Pb loss, particularly from individual crystals, such as zircon. This is because not only is Pb incompatible in zircon, but when the radiogenic Pb is formed in the zircon due to the decay of U, the crystal lattice will have suffered some radiation damage. Therefore the Pb is only loosely bound to the site where U was previously tightly bound, and hence becomes comparatively readily mobile, particularly at the margins of the crystal and along fractures. Hence partial Pb loss is particularly common.

8.1.4.2 Reverse discordance

Reverse discordance, represented by data that plot above the concordia, also occurs, and is usually due to either Pb gain or U loss during metamorphism. Minerals such as monazite and allanite, which along with zircon are often used for geochronology, tend to be more susceptible to such alteration and mobility than zircon. Reverse discordance can also sometimes be induced by the SIMS analytical

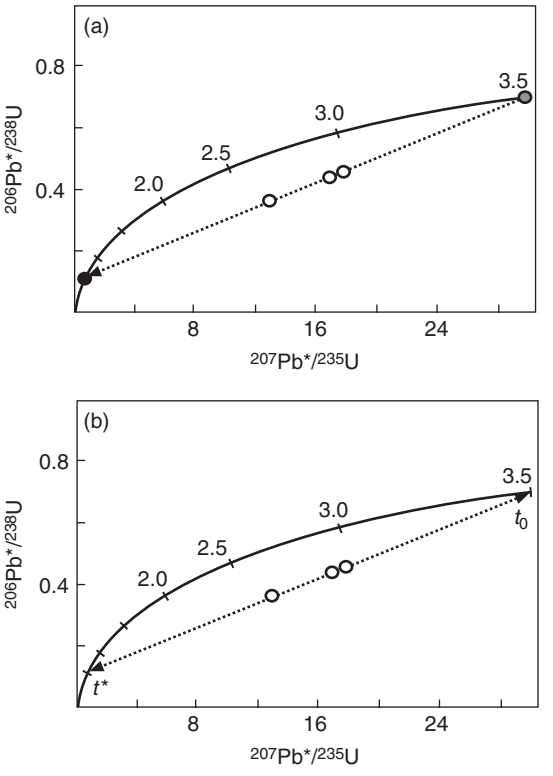

Figure 8.6 Age calculations involving concordia plots with samples that have experienced Pb loss. (a) After 500 Myr, samples which were completely reset will have moved along the concordia to record an age of 500 Ma. The 3.0 Ga protolith will have aged an additional 500 Myr, and so will now plot on the concordia at 3.5 Ga. Samples which have experienced partial Pb loss will also have ingrown further radiogenic Pb, but will still lie on a chord connecting the protolith and the reset samples. (b) More commonly in geology, neither the protolith nor completely reset samples are preserved, and hence we are left with an array of discordant samples. Projection of this array to the concordia results in two ages associated with where it intersects – the upper intercept records the age of the protolith (t_0) and the lower the age of Pb loss (t*). For illustrative purposes these intercepts correspond to the protolith and metamorphic ages illustrated in (a).

technique in particularly U-rich zircons where the rate of U sputtering is different from that of the reference material analysed. However, natural reverse discordia in such grains can generally be dealt with in a similar manner to 'normal' discordance, whereby projection of the chord through the data cloud can preserve both the age of the protolith and the Pb gain event. Significantly, in such cases there will often also be normally discordant grains within the same sample, suggesting that the Pb redistribution is often on a relatively local scale (Figure 8.7). Other materials which will often be reversely discordant may be various feldspars, which not only

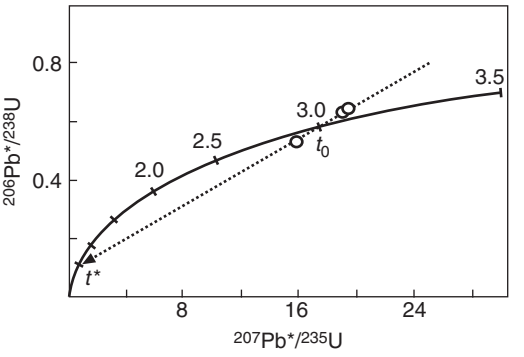

Figure 8.7 Reverse discordance on a concordia plot. Some samples may sometimes plot about and above the upper intercept, corresponding to the age of the protolith (t_0). If the spread in the data is great enough, particularly if some samples preserve regular discordance, it is theoretically possible to project to a lower intercept (t*) which would correspond to the age of Pb gain or U loss.

will incorporate significant amounts of Pb during growth, but are more susceptible to U (and Th) loss during metamorphism.

8.1.4.3 Inheritance of mixed components

In complex polydeformed terrains, high-grade metamorphism may liberate Pb from different minerals of different ages. Therefore, new minerals grown during this event may contain Pb from a variety of sources, and, particularly in migmatite terrains, may not wholly isotopically equilibrate between new partial melts being generated in different portions of the terrain. Therefore possibilities for complex mixing behaviour incorporating common Pb, ancient radiogenic Pb and different proportions of components can occur, resulting in non-systematic Pb isotopic signatures, particularly on the whole-rock scale. In order to address such issues, careful and rigorous analysis on chemically robust minerals, such as zircon, may enable resolution of multiple populations of zircons of different ages within a single magmatic rock. However, the absence of inherited zircons in a granite does not mean it did not receive ancient Pb from them – peralkaline magmas, which have very high Zr saturation levels, are able to effectively dissolve zircons, thus obliterating the direct evidence of zircon inheritance. However, in all of these cases zircons, which are crystallised directly from the magma itself, will preserve the age of the magma, regardless of the amount of inheritance, as long as care is taken in the analyses to measure the common Pb contribution. Such mixing does, however, greatly complicate the petrogenetic interpretation of such magmas, and will be explored further in Part III.

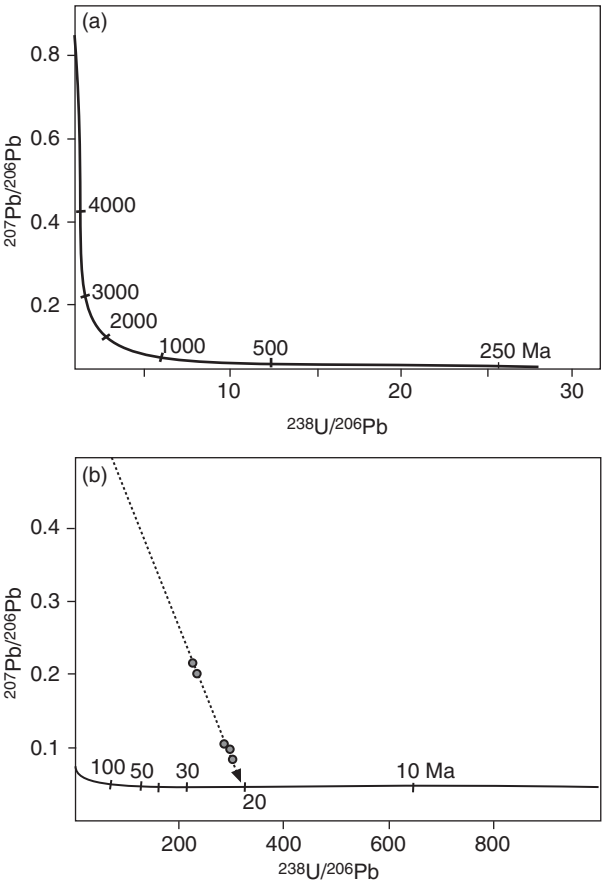

Figure 8.8 Tera–Wasserburg concordia plots. Such concordia plots can be more powerful for samples with younger ages, but more importantly for potentially distinguishing between, and obtaining ages for, materials which have inherited Pb isotopes. Discordia plots (b) can be constructed in a manner analogous to conventional isochron diagrams.

8.1.5 Tera–Wasserburg concordia

Another method of representing the U–Pb isotope data for geochronology is on the so-called 'Tera–Wasserburg' concordia plot (Figure 8.8). On a conventional concordia diagram, the errors in both axes are highly correlated because of the manner in which each is measured – in reality the $^{207}Pb/^{235}U$ is actually calculated from the measured $^{238}U/^{206}Pb$ and $^{207}Pb/^{206}Pb$ ratios on the basis of assuming a constant $^{235}U/^{238}U$ ratio in all terrestrial samples. Further, this approach assumes no common Pb contribution, and hence on the plot all ^{206}Pb and ^{207}Pb are considered to be radiogenic and are represented as $^{206}Pb^*$ and $^{207}Pb^*$. Partly to

minimise the problems associated with error propagation, and also partly to ease the plotting of young samples, the Tera–Wasserburg approach plots $^{207}Pb/^{206}Pb$ and $^{238}U/^{206}Pb$ (Figure 8.8a,b). There are two approaches to plotting the data. One can conduct a common Pb correction prior to plotting, based on the measured ^{204}Pb, in which case the plot resolves to one of $(^{207}Pb/^{206}Pb)^*$ vs $^{238}U/^{206}Pb^*$, and it can be treated and interpreted in a manner directly analogous to the conventional concordia. In this approach one has assumed that any common Pb conforms to a typical two-stage terrestrial Pb evolution curve.

However, if the raw data are plotted directly as measured ratios, then, provided there is only one source of common Pb, precise Pb ages can be obtained via the discordia approach without assuming a priori what the isotopic composition of the common Pb is (Figure 8.8b). In reality, this approach is a simplification of a three-dimensional isochron approach that has the measured $^{204}Pb/^{206}Pb$ ratio as a third axis, hence allowing for calculation of partly open whole-rock U–Pb systems and more robust handling of large common Pb contributions to the samples. In this terminology, the 3D U–Pb isochron is sometimes referred to as a 'total-Pb/U isochron' and the Tera–Wasserburg discordia as the 'semi-total-3D isochron'.

For all practical purposes, such distinctions are generally significant more for the specialist geochronologists rather than the geologists who are interested in using the geochronological data; however, it is important to be aware that there are subtle differences between the types of Tera–Wasserburg diagrams that can be plotted and hence how the ages can be interpreted.

8.1.6 A comment on regression of discordant analyses

Just as in the case of fitting lines through data points to produce isochrons, there is a huge amount of statistical rigour that goes into fitting chords through clouds of discordant data. As discussed in Section 6.2.1, an MSWD can be calculated for any linear regression, and is an excellent measure of the dispersion of the data points and their associated errors about the regression used in the calculation for the interception with the concordia. In general, with U–Pb geochronology it is best to obtain as large a data set as practical in order to be able to test for inheritance and mixing – hence fitting a chord through three data points is often very dangerous. Additionally, the size of the errors and how they relate to each other becomes very important in these matters. As alluded to in the case of the conventional concordia plot, the errors in the parameters that are plotted are very strongly correlated since one variable is calculated in part from the other, using a constant. Such error correlation needs to be considered when calculating the final age, with most modern software packages

available doing so in an almost seamless manner. Hence, knowing this may influence the choice of regression that is performed – the same data set, when regressed on a concordia diagram, can sometimes produce subtly different ages and errors than when regressed on a Tera–Wasserburg plot due to differences in the way the errors in the isotope ratios used in the age calculations are handled. In all cases, however, it is critical that you report the number of samples used in the regression (n), how many were rejected (!) and the MSWD of the corresponding regression, in addition to the age, its error and the confidence (1σ or 2σ, with or without the confidence interval). Such considerations have become increasingly important with increased access to both SIMS and laser zircon U–Pb analytical techniques which are able to analyse large amounts of data relatively quickly.

8.2 U-series isotopes

In general, U-series isotopes are directly applicable for systems which are <1 Ma in age, and hence are of limited use in ore deposit exploration as such occurrences are invariably older than this. However, U-series isotopes are an immensely powerful tool in investigating the rates of geological processes, particularly in magmatic (and by extension, hydrothermal) systems and in environmental studies which include dating the ages of speleothem formation and groundwater transport and erosion rates. Therefore this section aims to describe very briefly the basic underpinnings of the principles involved in U-series disequilibria without exploring the detailed mathematics and limitations. For this sort of level there are any number of specialist publications that the reader can refer to, including volume 52 of the *Reviews in Mineralogy and Geochemistry* series from the Mineral Society of America and the Geochemical Society.

From Figure 8.1 we can see that ^{238}U, ^{235}U and ^{232}Th all have very long half lives (~4.47 Gyr, 704 Myr and 14.01 Gyr, respectively). Significantly, after this initial decay each has a long subsequent series of intermediate decay products with short half lives which ultimately lead to a stable daughter isotope of Pb (^{206}Pb, ^{207}Pb and ^{208}Pb, respectively). Under normal circumstances, and indeed the assumption we use in conventional U–Pb geochronology, the rate of production of the short-lived daughter product is controlled by the rate of decay of the parent isotope. That is, the rate of production of the daughter isotope is what is controlling how abundant it is, rather than the rate at which it is decaying. Hence the amount of a short-lived radioactive isotope can be expressed in terms of its *activity*, which is simply a function of the number of atoms of the isotope present in the sample of interest and its decay constant.

Hence, when the decay of the daughter product is controlled by the rate of decay of the parent, the ratio of parent activity to daughter activity is (by definition) 1, i.e. the amount of decay of the daughter isotope is the same as the amount of its production, therefore both parent and daughter have the same activity ratio. This case is referred to as secular equilibrium. Since the daughter isotope has its own unique half life, during secular equilibrium there will always be a store or reservoir of daughter isotope in the system which is continually being added to by decay from the parent and diminished by decay.

However, if we are able to somehow fractionate the parent isotope from the daughter isotope, the system becomes disturbed and is therefore in disequilibrium. Such a case might happen if we were to introduce more of the parent to the system (parent excess) or, alternatively, introduce more of the daughter isotope to the system (daughter excess). Obviously the converse will also have the same effect – removal of the daughter isotope will leave the system with the parent isotope in excess, and removal of the parent isotope will leave the daughter in excess.

In cases of disequilibrium, the system will subsequently (if left undisturbed) move towards equilibrium. For example, in the case of parent excess, since there are now relatively more atoms of parent decaying than there are atoms of daughter decaying, the activity of the parent has effectively increased. This in turn produces more atoms of the daughter (i.e. ingrowth of the daughter) and hence the activity of the daughter will increase until such time as the activities of the parent and daughter approach equality and return to secular equilibrium. In the opposite situation, where the parent isotope may have been removed and the activity of the daughter isotope has increased with respect to the parent, then the activity of the daughter is greater than that of the parent isotope and hence we have more daughter decaying than is being produced through decay of the parent. Thus the excess ('unsupported') daughter isotope is able to decay away until its activity is in equilibrium again with the rate of production due to decay from the parent. Such behaviour has been observed since the early days of the discovery of radioactivity, and indeed was one of the key processes for distinguishing between different isotopes and even new chemical elements in the early twentieth century.

Of central importance in short-lived isotope systematics is that the time taken for a perturbed system (i.e. one in disequilibria) to return to secular equilibrium is approximately five half lives of the *daughter* isotope. It is this characteristic that has allowed U-series isotopes to be applied to rapid geological processes because, depending on which parent–daughter isotopic pair is selected, time scales from <30 years (^{228}Ra–^{232}Th) to <1.5 Myr (^{234}U–^{238}U) can be investigated. Note that U-series isotopes are often expressed in terms of the daughter isotope

first as this is the isotope which controls the rate of isotopic ingrowth towards equilibrium. This contrasts with other isotopic systems, such as Sm–Nd, where the parent is normally expressed first as it is the decay of the parent which is governing the behaviour of the system.

In magmatic systems, ^{230}Th–^{238}U (itself a multiple decay system incorporating three other intermediaries) is useful for processes operating up to ~350 kyr, and ^{226}Ra–^{230}Th for time scales <8 kyr have enjoyed widespread usage. These are both part of the ^{238}U decay chain, with ^{231}Pa–^{235}U (~165 kyr) from the ^{235}U decay scheme also applied to silicate magmatic systems.

In general, these tools have been applied in high-temperature settings to explore melting, segregation, ascent and emplacement rates in volcanic systems, and hence an understanding of the rates and time scales can be applied to investigating magmatic and hydrothermal processes associated with mineralisation.

One other direct application, which has met with limited success, has been to attempt to date the formation of roll-front U deposits through U-series isotopes. Such mineralised systems are somewhat unique in that they are in 'steady state disequilibrium'. That is, they are constantly precipitating and redissolving in an active groundwater regime, but as climatic conditions and groundwater flow (and theoretically chemistry) change it is possible to constrain when the ore deposit was last in equilibrium with the groundwater. Such situations are further complicated in areas of particularly high-grade mineralisation where there may be a greater neutron flux than normal, leading to increased neutron capture in some U isotopes, and, more significantly, the potential to fractionate ^{235}U from^{238}U due to neutron field shift effects due to the different neutron capture cross-sections of the two isotopes. This is in a large part driven also be the redox conditions of the ore deposit and the high throughput of radioactive material. Hence, even in what should be 'ideal' circumstances (i.e. very young ore deposits with large amounts of U and Th), U-series isotopes are non-trivial in their application.

Finally, U-series geochronology has enjoyed widespread application in environmental studies, both for dating (particularly carbonate) mineralisation and also in weathering and erosion studies due to the different geochemical behaviours of the intermediaries during the time scales of material transport. From a mineral exploration industry perspective, these applications are of limited interest; however, applications in environmental monitoring are possible.

8.3 EPMA and CHIME dating

If one is able to assume there was no common Pb incorporated into a mineral lattice at the time of growth, then theoretically it is possible to calculate an age purely on the basis of the amount of Pb that has accumulated in that crystal

since it grew, as a function of the amount of U and Th within it. Hence, if the abundances of U, Th and Pb can be measured precisely using an electron microprobe, it is not necessary to measure the individual isotopes. This approach, and variations on it based upon using the chemical abundance of these elements using electron probe microanalysis (EPMA), is also sometimes referred to as CHIME (chemical Th–U–total Pb isochron method). Typically this method has been employed on monazite as it generally incorporates no Pb on growth, and on ancient samples (>100 Ma) the contribution of ^{204}Pb to total Pb is negligible due to the ingrowth of the radiogenic isotopes.

Such an approach makes two major assumptions, namely that no common Pb was present in the mineral at the time of growth, and that the system has remained closed. Other analytical considerations are important, including that of interference of La and Ce on the Pb peak being analysed on the microprobe, but, assuming that these can be detected and corrected for, the theory behind chemical monazite EPMA dating is as follows:

$$\mathrm{Pb_{Total}} = \mathrm{Pb_{initial}} + {}^{206}\mathrm{Pb} + {}^{207}\mathrm{Pb} + {}^{208}\mathrm{Pb}$$

$$\therefore \mathrm{Pb_{Total}} = \mathrm{Pb_{initial}} + {}^{238}\mathrm{U}(e^{\lambda_1 t} - 1) + {}^{235}\mathrm{U}(e^{\lambda_2 t} - 1) + {}^{232}\mathrm{Th}(e^{\lambda_3 t} - 1). \quad \text{(Eq 8.10)}$$

Assuming that all Pb measured is due to the radioactive decay of U and Th, then:

$$\mathrm{Pb_{measured}} = {}^{238}\mathrm{U}(e^{\lambda_1 t} - 1) + {}^{235}\mathrm{U}(e^{\lambda_2 t} - 1) + {}^{232}\mathrm{Th}(e^{\lambda_3 t} - 1). \quad \text{(Eq 8.11)}$$

Since ^{238}U/^{235}U is generally considered equal to 137.88 and invariant,

$$\mathrm{Pb_{measured}} = \mathrm{U_{measured}}\left[\frac{(137.88e^{\lambda_1 t} + e^{\lambda_2 t})}{137.88} - 1\right] + \mathrm{Th_{measured}}(e^{\lambda_3 t} - 1). \quad \text{(Eq 8.12)}$$

Since U and Th have been measured quantitatively using EMPA, it is possible to iteratively input values of t (the age) in order to calculate an expected Pb concentration until the calculated value matches the measured Pb concentration.

Such an approach is attractive as the electron microprobe is a far more widespread and readily available tool, making the analyses far more cost effective and accessible. Precision is limited, however, by the inability to test for initial Pb and the closed system behaviour, although it can approach that of isotopic analysis (0.5 per cent) in some situations. Precision can be improved by increasing the number of spots analysed, and by careful screening and cathodoluminescence (CL) imaging prior to analysis to ensure data are collected from grain domains of the

same generation. However, such additional analysis begins to offset some of the speed and cost-effective advantages of this technique.

Open system behaviour is generally limited by our understanding of U and Th diffusion from monazite, and the chemical reactivity of monazite during orogenesis or thermal events. Being a phosphate, monazite is generally more reactive than zircon.

Notwithstanding, monazite chemical dating is a useful tool, particularly for reconnaissance studies and in testing whether monazites might be suitable targets for more precise *in situ* analytical techniques.

8.4 Thermochronology: fission tracks and (U + Th)/He

Thermochronology in its broadest sense refers to the systematic investigation of the thermal evolution of a portion of crust. For our purposes we will restrict ourselves predominantly to the continental crust, but thermochronology can also refer to oceanic crust and indeed that of other planets. In general, thermochronology can be applied to any number of chronometers of different T_c which enable the reconstruction of the temperature–time (T–t) evolution of a terrain. Often implicit in this is a sense of the P–T–t evolution of a terrain during orogenesis.

The term thermochronology has also become synonymous with the application of fission track analysis and (U + Th)/He geochronology, often in conjunction with Ar–Ar geochronology, to track the final stages or low-temperature evolution of a terrain, commonly including the denudation and exhumation history. As such it has enjoyed widespread application in the petroleum industry for monitoring and tracking thermal maturation of reservoirs and the timing of their uplift. Of more significance to the minerals industry are the applications of thermochronology in hydrothermal systems, basin formation, fluid flow and basinal thermal evolution.

8.4.1 Fission track analysis

Although not specifically an isotopic decay scheme, or even an isotopic geochronological tool, fission track analysis or fission track geochronology is a technique which can be used to date materials with very low closure temperatures (T_c).

Approximately one in two million decays of ^{238}U results in spontaneous nuclear fission, rather than commencing the decay chain to ultimately produce ^{206}Pb:

$$^{238}U \rightarrow {}^{143}Ba + {}^{90}Kr + 5n; \text{ or } {}^{238}U \rightarrow {}^{145}La + {}^{90}Kr + 3n; \; T_{1/2} = 8 \times 10^{15}\,\text{yr}.$$

Regardless of the exact products (there are a number of possibilities, but most importantly spontaneous fission produces two daughter isotopes of masses

in the ratio ~⅔:1) this fission yields massive energetic particles in comparison with the more common α, β and γ radiation emitted during radioactive decay. The two particles produced move very rapidly 180° away from each other, damaging the surrounding crystal lattice as they move. This is because the amount of energy released during fission is quite large, and the velocity of the products and hence their kinetic energy is very high. Thus these massive, high-energy products produce a trail of damage through the crystal, the combined path length of which can often be ~20 μm long. Over time, more spontaneous fissions take place and the total number of fission tracks will increase in direct proportion to the amount of U in the crystal and amount of time elapsed. Therefore, rather than measuring the daughter isotope via mass spectrometry, the fission tracks (or trails) are a direct proxy for the number of daughter atoms produced.

Direct observation of the actual fission tracks themselves (so called latent tracks) is very difficult, since, although they are very long, their diameter is still only <10 nm, which is not visible with standard optical methods. Routine fission track analysis requires a chemical etching process involving diluted nitric acid. By cutting a grain open and polishing it, then treating the surface with acid, the latent tracks which are exposed on the surface are enlarged where the acid can attack them and become visible under a conventional optical microscope. Thus it is possible to count the numbers of tracks visible on the polished surface. In this situation, each track represents an actual ^{238}U atom which has undergone decay. Care must be taken to avoid spurious features such as cracks and crystal dislocations. One of the key criteria is that fission tracks are always randomly oriented.

Counting is then conducted under the microscope using a calibrated grid in order to obtain a figure for the track density per unit area of the polished surface. Because the tracks contain a 3D geometry in a transparent medium (e.g. usually apatite or zircon), each track is counted in terms of where it intersects the surface of the slide. This density per unit area is directly proportional to the volume density of tracks, and hence fission events. The calculated volume density is also dependent on the track length – obviously longer tracks will result in more intersections across an arbitrary planar surface than the same number of shorter tracks, and this becomes important when considering annealing (see below). However, to a first order, the volume density of fission tracks gives a direct measure of the number of spontaneous fission decay events, and the greater the number of tracks, the longer the period of time that has elapsed in order to allow them to accumulate.

However, in order to quantitatively calculate an age, it is necessary to know the concentration of U in the sample. Obviously samples with high

U concentrations will undergo more spontaneous fission per unit time than those with low U contents. Historically, it was this portion of the procedure that was a little more time and resource intensive, as one of the most precise ways to measure U concentration was to obtain the ^{235}U concentration through inducing fission in the sample via neutron irradiation. The amount of ^{235}U is measured by measuring the fission track density produced in a high-purity grain of mica which is clamped onto the surface of the sample. Therefore, as each atom of ^{235}U undergoes induced fission, a certain proportion of them will produce tracks which will cross into the grain of mica, where they can be counted in a manner analogous to that of the sample. Some straightforward mathematical transformation, including calibration of the neutron dose, is then required to extract the ^{235}U concentration of the grain of interest.

Increasingly, however, the U concentration is measured by laser ablation ICP-MS on the surface after the grains have been counted. While this greatly speeds up the process and simplifies the mathematics involved (Equation 8.13), it does have the drawback of destroying the surface upon which the counting has been conducted.

Since the ratio of ^{235}U/^{238}U is essentially invariant for the purposes of geochronology, from measuring the ^{235}U in the sample it is possible to calculate the ^{238}U. From the decay equation, assuming that each fission track corresponds to a single ^{238}U decay, and that all of the fission tracks intersecting the two-dimensional surface are measured, the age of the grain is calculated (Equation 8.13):

$$t = \frac{1}{\lambda_{238}} \ln\left(1 + \xi \frac{\rho_s}{C_U}\right),$$

where:

$$\xi = \frac{\lambda_{238} A}{\lambda_f N_0 D R \alpha}, \qquad \text{(Eq 8.13)}$$

where λ_{238} is the total decay constant for ^{238}U (0.155125×10^{-9} yr^{-1}), ρ_s is the internal surface fission track density and C_U is total U concentration in the grain. ξ is a combined set of constants that can be obtained empirically via calibration against a standard of 'known' age, or can be calculated on a case by case basis. The constants in ξ are A, atomic mass of ^{238}U (238.050788), λ_f, the spontaneous fission decay constant for ^{238}U (8.46×10^{-17} yr^{-1}), N_0, Avogadro's number (6.02214×10^{23}), D, density of the mineral, R, etchable range of one fission fragment (= half confined track length) and α, counting/etching efficiency for the etched surface.

This equation has the slightly confusing notation of requiring two values of λ for the same isotope, since we are dealing with two distinct decay modes, and it is important to remember that the total amount of U in the sample has decreased over time by both spontaneous fission (a minor contributor) as well as conventional decay to Pb (a major contributor, especially in very old samples).

In summary, by measuring the fission track density, and independently obtaining the U content of the grain, it is possible to calculate the amount of time that has elapsed since the grain formed. The U is generally measured either through LA-ICPMS or historically through irradiation in a neutron flux to induce spontaneous fission of ^{235}U in the sample and producing fission tracks into a high-quality mica which is placed in firm contact with the sample. Since the ratio of $^{235}U/^{238}U$ is essentially invariant for the purposes of geochronology, from measuring the ^{235}U in the sample it is possible to calculate the ^{238}U.

Importantly, however, as the temperature of the mineral grain is increased, the radiation damage to the crystal lattice becomes repaired as the mineral re-organises itself. This process is termed annealing, and results in progressive shortening of the fission tracks until they are completely obliterated at the annealing temperature for that particular mineral. Minerals typically used for fission track analysis include apatite and zircon, which undergo complete annealing at ~120 °C and <300 °C, respectively. Fission track analysis has also been applied to monazite (>50 °C) and titanite (<320 °C) in some cases.

Such relatively low closure temperatures, and the common abundance of resistate minerals such as apatite and zircon in detritus, have led to widespread application in the oil industry, where burial histories in relation to oil maturation have been obtained. Other applications include uplift and denudation histories of sediments.

8.5 Re–Os geochronology of molybdenite and LLHR (low-level highly radiogenic) sulphides

Molybdenite (MoS_2) is an unusual case among sulphide minerals in that it very strongly partitions Re into its lattice during growth, with virtually no Os. Hence typical molybdenites will contain ppm level Re and sub-ppb level Os, resulting in rapid and dramatic ingrowth of radiogenic ^{187}Os. Such extreme parent–daughter fractionation is essentially analogous to the situation in zircon, whereby it was initially assumed that all Pb in a zircon crystal was due to radiogenic ingrowth and hence directly proportional to the age of the sample. Hence it can be considered that for samples in which no common Os was incorporated, the age (t) is recorded by:

$$t = \frac{1}{\lambda} \ln\left(\frac{^{187}\mathrm{Os}}{^{187}\mathrm{Re}} + 1\right). \qquad \text{(Eq 8.14)}$$

Early studies assumed that all Os measured in molybdenites was due to such ingrowth and that the contribution from analytical blank was negligible. In many situations these assumptions are valid, but it is now routine to measure and apply both a laboratory blank and common Os correction to the measured data. However, because of the highly unusual isotopic composition of the Os in the samples (this is because almost all of the Os being measured is ^{187}Os, which is more abundant in these materials than ^{192}Os, which normally constitutes ~41 per cent of natural Os), it has become more common to apply an Os 'double spike' technique, in which a precisely weighed amount of artificially enriched (by ^{188}Os and ^{190}Os) spike is added to the sample prior to extraction of the Os by wet chemistry. Such a refinement, although laborious and time consuming to set up, provides two major improvements in precision and reproducibility of data generated: (1) the within-run fractionation correction is dramatically improved, particularly for low-abundance samples in which the measurements are done by ion counting; and (2) the common Os composition as well as concentration is determined to a far greater precision, allowing a more robust common Os calculation. These two refinements allow analysis of not just molybdenite but also other low-level, highly radiogenic Os samples (generally other sulphides) due to the ability to remove the non-radiogenic contribution to the Os isotopic signal with high precision.

Such treatment of LLHR phases (including some pyrites) also potentially allows the dating of very young systems due to the anomalously high Re/Os resulting in very rapid ingrowth of measurable ^{187}Os despite the very long half life of ^{187}Re. Indeed, double spike analysis improves precision through only analysing for the isotopes of Os that are truly necessary for correct fractionation and to calculate an age, rather than all of the Os isotopes, which is done in conventional analysis. Hence data may sometimes be measured and reported in terms of ^{187}Os (i.e. that ingrown by radioactive decay and hence the basis for the age correction), ^{188}Os and ^{190}Os, the two spikes, and ^{192}Os, the most abundant common Os isotope. In fact, for many molybdenites a double spike is not necessary, and only ^{187}Os (age), ^{190}Os (spike) and ^{192}Os (common/blank) are measured. In this case, normalising to ^{192}Os (instead of the conventional ^{188}Os, which is in very low abundance in these samples) allows samples to be plotted on a pseudo-isochron plot of ^{187}Os/^{192}Os vs ^{187}Re/^{192}Os, whereby through plotting blank corrected Re the *y*-intercept gives the isotopic ratio of the combined laboratory blanks and common Os (Figure 8.9). The slope on such a diagram has age significance and the precision is improved as it removes

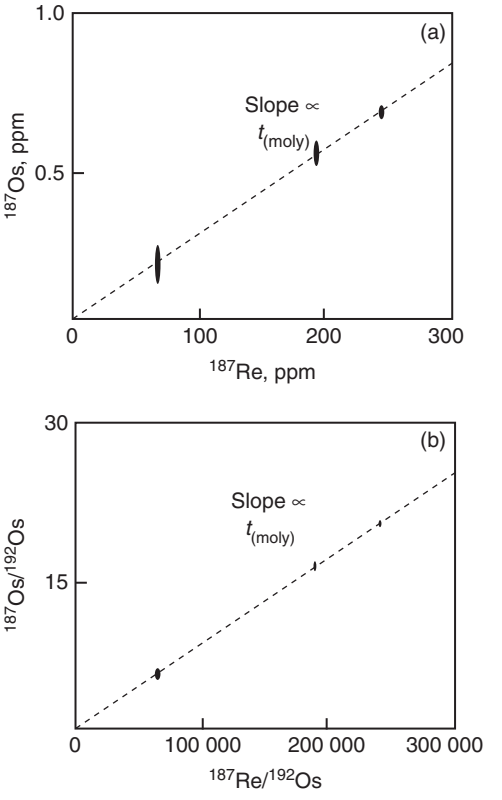

Figure 8.9 Illustrative Re–Os isochron plots for molybdenites. (a) Plot of concentration of ^{187}Os vs ^{187}Re. Closed system behaviour will produce an isochron which passes through the origin and a slope directly proportional to the age. (b) Schematic representation of the improvement in precision for the same three analyses when using a double spike technique and normalising to ^{192}Os instead of the conventional ^{188}Os. In these diagrams the isochron should still pass through the origin; any 'common' Os component will result in a *y*-intercept above the origin.

potential analytically induced error correlations which can be obtained when ion counting on low beam intensities for ^{188}Os in single spike samples.

Finally, although not LLHR, some magnetites can contain elevated Re/Os, and hence may provide a useful point on an isochron for mineralised systems when magnetite is clearly part of the mineralising assemblage.

There are several caveats to bear in mind when applying the Re–Os chronometer to sulphide-bearing systems.

First, such techniques are time consuming and can be expensive. Many laboratories that undertake Os analysis are not equipped for sulphide or LLHR double spike techniques as they have specialised in other applications of the technique.

Next, any age information obtained is always only going to be as good as the context of the sample and the external constraints regarding the evolution of the mineralising system. Molybdenite can have a relatively high closure temperature (of the order of 500 °C in some situations), but it can also allow open system behaviour and diffusive loss of Os from grain margins due to the mineral structure of MoS_2. Therefore, when selecting molybdenites for analysis, preference can be given where possible to those in a clear petrographic context and ideally large enough to allow physical removal of grain margins. Furthermore, some mineralised systems may not grow molybdenite, or can occasionally contain inherited molybdenite (more rare).

When attempting to analyse other sulphides in order to apply an LLHR approach, sulphides such as pyrite, arsenopyrite and tennantite (in conjunction with an isochron approach to minimise the common Os contribution) have been applied. A major issue to bear in mind here is that the initial samples *must* have high Re abundances – simply having a pyrite does *not* mean it is amenable to Os geochronology. This is particularly significant in systems in which the mineralising fluids may have contained comparatively low amounts of Re anyway, and precipitated vast volumes of sulphides. In this scenario, a comparatively small Re budget will be spread relatively thinly between the very large amount of sulphide available, resulting in very low Re/Os ratios and a concomitant high common Os. Hence analyses of such materials are unlikely to yield high-precision ages.

9

Argon geochronology

9.1 K–Ar

Naturally occurring K has three isotopes, ^{39}K (93.2581 per cent), ^{40}K (0.0117 per cent) and ^{41}K (6.7302 per cent), of which ^{40}K is radioactive with a half life of 1.248×10^9 years ($\lambda = 0.581 \times 10^{-10}$ yr^{-1}). Unlike most other decay schemes in geochemistry, however, the decay of ^{40}K is via a branched decay scheme, in which 89.1 per cent of the decay events produce ^{40}Ca via beta decay and the remaining 10.9 per cent produce ^{40}Ar through electron capture. Both of these decay products are the most abundant isotopes of the daughter element in question. Therefore, particularly in the case of ^{40}Ca, the radiogenic contribution is very hard to detect as Ca is a highly abundant element, and >96 per cent of all Ca is ^{40}Ca. In contrast, although >99 per cent of all Ar is ^{40}Ar, because there is so little Ar present on earth, the contribution to the total Ar budget through the radioactive decay of K is significant and can be measured readily enough – despite a half life of 1.248 Gyr and only ~10 per cent of those decays producing Ar.

Ar is of particular interest for geochronology, as it is a noble gas and hence does not form any molecular bonds in minerals or bind with the crystal lattice in any way. Hence, when minerals grow, they do not incorporate Ar as a fundamental part of the crystal itself, and hence Ar (and indeed all noble gases) are the most incompatible of elements in geochemistry. However, when K within a crystal decays to form Ar, the Ar remains trapped within the crystal lattice as it has a larger ionic radius than the parent ^{40}K atom, and hence is typically larger than other gaps in mineral lattices as well. Therefore, to a first order it can often be considered that all ^{40}Ar measured within a mineral is the result of radioactive decay since the mineral will not contain any when it grows.

However, changes in pressure and/or temperature may warp the lattice of the mineral sufficiently to allow the accumulated Ar to diffuse and escape, thus

effectively resetting the system. Because Ar does not chemically bind with the lattice of the minerals, the closure temperature of Ar is relatively low in most silicate minerals.

Hence, in a principle, K–Ar dating is comparatively simple. Assuming that all of the Ar measured in a sample (either mineral or whole rock) is due to the *in situ* decay of K, simply by measuring the ^{40}Ar concentration and the total K concentration, the age can be expressed as:

$$t = \frac{1}{\lambda} \ln\left[\frac{^{40}Ar^{*}}{^{40}K}\left(\frac{\lambda}{\lambda_e}\right) + 1\right], \qquad \text{(Eq 9.1)}$$

where λ is the total decay constant for ^{40}K (i.e. taking into account both branches of the decay scheme; 5.549×10^{-10} yr^{-1}) and λ_e is the decay constant specific to the production of ^{40}Ar (0.575×10^{-10} yr^{-1}).

Historically, the measurement of ^{40}K was conducted by measuring the total K in the sample (through X-ray fluorescence (XRF), flame photometry, isotope dilution (ID), atomic absorption or even gravimetric chemistry) and assuming ^{40}K constitutes 0.0117 per cent of the total K. Alternatively, if these measurements were conducted by mass spectrometry, then ^{39}K (the most abundant K isotope) was measured, and ^{40}K calculated assuming $^{40}K/^{39}K = 0.0001255$ (= 0.0117 per cent/93.2581 per cent).

Such an approach requires some critical assumptions regarding the nature and history of the sample, as alluded to above, and, critically, these are rarely met. The key assumptions specific to K–Ar are:

(1) All ^{40}Ar in the sample is due to *in situ* radiogenic production. This assumption is probably the most commonly violated, owing to contamination of the sample from either incorporation of additional ^{40}Ar from xenolithic material entrained during magmatism, or atmospheric contamination and/or incomplete degassing of magmas. One of the main drivers for the development of the Ar–Ar technique (see Section 9.2) was to circumvent these issues.
(2) The sample has remained a closed system, thus preventing loss or gain of either ^{40}Ar or ^{40}K. This is another commonly violated assumption, particularly in polydeformed metamorphic terrains, since Ar is readily lost from the crystal lattice. Chemical weathering may also result in the loss of unspecified amounts of Ar, as can laboratory preparation methods including grinding during sample preparation.

Due to the very different geochemical behaviour of K and Ar, and hence the very different analytical methods employed to analyse the parent and daughter elements,

the utility of K–Ar has become much diminished in recent years in preference to Ar–Ar dating. However, K–Ar still enjoys some applications in clay mineral geochronology, and was the fundamental tool used in first establishing the geomagnetic polarity time scale based on magnetic reversals in the ocean basins, following observations of the similarity in closure temperature of the system in rapidly quenched basalts and the Curie point of iron in geological materials.

9.2 Ar–Ar

Ar–Ar ($^{40}Ar/^{39}Ar$) is a geochronological technique whereby an isotope of the parent element, ^{39}K, is converted to an isotope of the daughter element that does not occur in nature (^{39}Ar) by subjecting the sample to an intense neutron flux in a nuclear reactor:

$$^{39}K + n \rightarrow {}^{39}Ar + p.$$

Such a conversion enables the measurement of both parent (albeit by proxy) and daughter isotope simultaneously during Ar analysis, thus greatly reducing analysis time and dramatically increasing precision. More significantly, it also allows analysis of all three Ar isotopes, hence providing independent tests for atmospheric contamination, partial resetting and excess Ar incorporation.

In practice the technique involves irradiating the sample (either K-rich minerals such as K-feldspars or micas or potassic whole rocks) with a standard of known age. Measurement takes place either through a resistance furnace or via a laser (see below), and the standard allows precise calculation of a $^{40}K/^{40}Ar^*$ for a given irradiation batch. In such analysis, any ^{36}Ar which is measured is assumed to be either atmospheric contamination or inherited from the sample. Since the $^{40}Ar/^{36}Ar$ ratio of atmospheric contaminants is considered to be constant (= 295.5), it is possible to subtract the contribution of this contamination from the total ^{40}Ar to give only the radiogenic component ($^{40}Ar^*$).

Hence the age of a sample can be calculated directly from a single analysis by:

$$t = \frac{1}{\lambda} \ln \left[\frac{^{40}Ar^*}{^{39}Ar} J + 1 \right], \qquad \text{(Eq 9.2)}$$

where J is the neutron fluence of the irradiation, and is calculated from the standards irradiated at the same time, λ is the decay constant for the combined decay schemes (= 5.549×10^{-10} yr^{-1}).

Ultimately this approach is only as good as the standard that is measured along with the samples, as the age is calculated relative to the 'known' age of the

standard, specifically via calculation of the *J* factor. Since the actual age of the standard cannot (by definition) itself be measured by $^{40}Ar/^{39}Ar$, it must be determined by another method. Originally this was via K–Ar, as described in Section 9.1; however, improvements in analytical techniques, and cross calibration with U–Pb isotopes, which offer the combined benefit of an internal check for closed system behaviour through the two decay schemes, have allowed a greater refinement in both precision and accuracy in Ar–Ar geochronology, particularly in ancient samples.

These refinements have come about as improvements in the stated decay constant, and hence care needs to be exercised when using Ar–Ar data from before ~2008 as to exactly which values are being used. Such differences are generally of the order of ~0.65 per cent in the age.

9.2.1 Step heating

Critical to this process is the manner in which the Ar is liberated from the sample of interest. By incrementally heating a sample (say, an individual mineral grain), additional information can be obtained. By placing the sample in a furnace, and slowly increasing the temperature, it is possible to sequentially measure the Ar–Ar ratio, and hence age, for each individual temperature step. In the simplest case, a grain will contain uniform $^{40}Ar/^{39}Ar$ ratios throughout, and hence will return a uniform age irrespective of the temperature at which the Ar was released. Such a step heating profile will yield a 'plateau age', which is constant throughout liberation of Ar from the sample (Figure 9.1a).

However, if the mineral had suffered Ar loss from the grain boundaries due to heating and diffusion at some time in the geological past, then the $^{40}Ar/^{39}Ar$ ratios of the first (lowest temperature) Ar liberated will be spurious, and quite probably not have geological significance. At higher temperatures, as the centre of the grain which did not experience Ar loss during metamorphism is being decrepitated, the $^{40}Ar/^{39}Ar$ ratio will become more consistent with successive heating steps and hence a plateau age for that portion of the grain can be determined (Figure 9.1b). In some cases, with careful analysis, it can even be determined how long ago the Ar loss took place, as the first Ar released may record a small plateau indicating closed system behaviour and subsequent re-accumulation of Ar after the diffusive loss, and the core of the grain may record the 'original' Ar–Ar age (Figure 9.1c). Such multistage histories must be interpreted with caution, but the utility of step heating is that it is able to (semi-)quantify the multistage history of a sample.

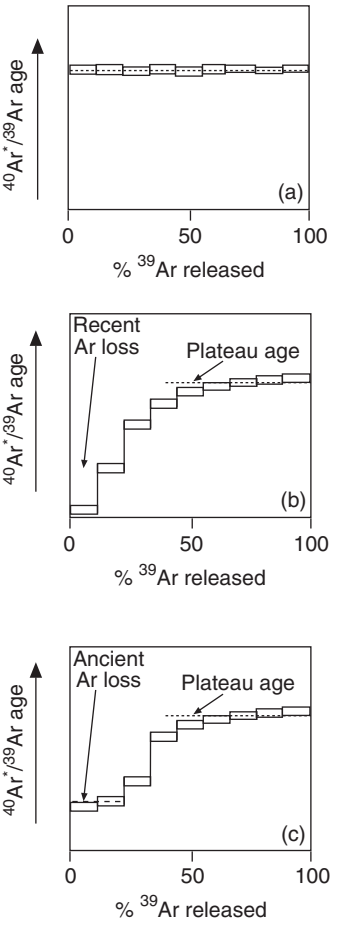

Figure 9.1 Ar–Ar step heating profiles. (a) A 'good' profile is one in which the same age is returned for every heating step, indicating the age of the sample and that it has remained closed throughout its history. (b) Ar loss in recent times, often due to sample preparation, will appear as a stepped profile of 'young' ages in lower-temperature heating steps before preserving a plateau age of crystallisation. (c) Geological argon loss events, such as partial Ar loss through thermal perturbation, will be preserved as a stepped heating profile, with the lower age steps recording the age of resetting.

9.2.2 Laser ablation

Lasers can be used in two ways in Ar–Ar analysis: (1) as a heat source for step heating experiments on single or multiple grains; and (2) for ablation of small areas of single grains for high spatial resolution analysis.

Generally long-wavelength infrared (IR) lasers (1064 μm) are used for incrementally heating bulk multi-grain samples or single spots of glassy

materials, such as pseudotachylites and volcanic glass. The extracted gases liberated from the laser for a single heating step are aggregated and then introduced to the mass spectrometer as a single aliquot to produce a single age, as in the case of step heating.

Shorter wavelength lasers (e.g. 266 μm) can be focused on single spots within individual grains, often still *in situ* in a 'thick section' for context, to produce an age for that individual site. Such applications are particularly powerful for texturally complex samples, and applications can include K-feldspar cements in sandstones or potassic metamorphic minerals.

9.2.3 Applications

The applications of Ar–Ar are generally upon igneous and metamorphic minerals, although care needs to be exercised in applying the data. For example, Ar–Ar will seldom record the emplacement age of intrusive rocks such as granites, as they have a protracted cooling history. Thus individual minerals within the granite will preserve different ages depending on their individual closure temperatures. For example biotite will often close at ~300 °C, muscovite at 400 °C and hornblende at ~550 °C (see Figure 5.3), and hence Ar–Ar will preserve information regarding the thermal regime of the crust within which the granite was cooling.

Such information can be very important for reconstructing the thermal evolution of a terrain, particularly when applied to metamorphic minerals. However, the critical caveat is to remember that due to the highly incompatible nature of Ar, these minerals are simply recording the last time they passed through the closure temperature, and not necessarily the actual age of growth of the mineral itself. Thus the mineral will not preserve a record of all of the events the rock has actually been through and, as always, a thorough understanding of the geological context of the sample is critical to accurately interpret the data.

Volcanic materials are also widely subjected to Ar–Ar studies since the rapid quenching will produce glasses which are amenable to laser analysis, with many magmas being relatively potassium-rich. Indeed, Ar–Ar is the tool of choice for geochronology of submarine volcanism due to the rapid quenching and excellent retention of Ar.

Ar–Ar has also been applied in a limited number of provenance studies, focused largely on detrital micas and feldspars. Such studies necessarily require juvenile sediments to preserve such readily weathered minerals, but also depositional basins that have experienced only low-grade metamorphism or diagenesis. Such detrital studies can be of use in reconstructing potential source regions for sediment, but more useful to the petroleum industry is linking such studies with an understanding of the closure temperature of the minerals in question in order to track the burial

history and hence thermal maturity of a basin. Hence, when detrital micas (in particular) start to show significant Ar loss, the implication is that temperatures within that portion of the basin have exceeded ~350 °C. Coupled with fission track analysis, it is therefore possible to extend the thermal evolution of non-hydrocarbon-bearing depositional systems to higher temperatures and allow predictions to be made regarding the prospectivity of various regions.

Finally, Ar–Ar can also be applied directly to date the age of deposition of sediments and fault activation in favourable circumstances where K-rich authigenic minerals, particularly illite, are precipitated.

9.2.4 Excess Ar

Finally, as alluded to above, Ar–Ar can be subject to contamination from extraneous Ar, either from the atmosphere or through incorporation of radiogenic Ar from other materials during the growth of the minerals or ascent of the magma. Such Ar is termed excess Ar, and can commonly be derived from one of two sources.

First, it can be incorporated in a mineral when it crystallises in an environment that has appreciable amounts of Ar in it. Some mantle-derived basalts can have excess Ar which has been derived from the decay of K in the mantle, resulting in ^{40}Ar being trapped in the mantle and incorporated in the magma at the time of melting. Hence, crystallising phases will incorporate this additional component of ^{40}Ar, resulting in anomalously old ages. Such Ar is referred to as inherited Ar, and can sometimes be accounted for through inverse isochron diagrams (see below). The second source of excess Ar can be due to diffusion out of a crystal lattice into an adjacent grain during a metamorphic or thermal event. In this case, the Ar diffuses directly into an adjacent grain, or from country rocks into an intrusion during cooling. In almost all cases, since the Ar is diffusing into the grain that is being analysed, its concentration will be greatest at the margins of the grain and hence it will tend to be the first Ar released at the lowest temperatures during step heating (e.g. Figure 9.2).

Inherited Ar can be more problematic to deal with, as it is intrinsically within and distributed throughout the sample at the time it cools through its closure temperature. However, since each heating step is essentially an independent measurement of the Ar isotopic composition, it is possible to consider the data in a manner analogous to a conventional isochron. However, since the parent isotope is being measured by proxy via ^{39}Ar, due to irradiation the *x*-axis of an isochron diagram plots ^{39}Ar/^{36}Ar instead of ^{39}K/^{36}Ar. Because of incomplete irradiation efficiency, the isochron equation is modified subtly, but will take the form:

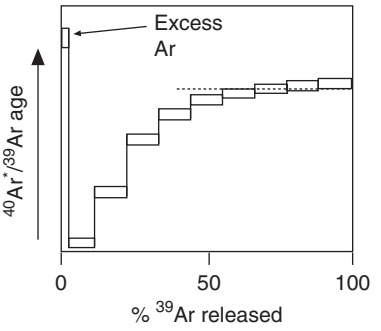

Figure 9.2 Ar–Ar step heating profile with excess Ar in the first heating step due to the incorporation of ancient Ar from surrounding minerals during crystallisation.

$$\frac{^{40}\mathrm{Ar}}{^{36}\mathrm{Ar}} = \left(\frac{^{40}\mathrm{Ar}}{^{36}\mathrm{Ar}}\right)_0 + J(e^{\lambda t} - 1), \qquad \text{(Eq 9.3)}$$

where J is an irradiation constant which varies from batch to batch.

Thus, a series of step release fractions from a single sample, or spots from a single grain which are ablated with a laser, will plot on a line, the slope of which is directly proportional to the age. Most importantly, however, the *y*-intercept (initial ratio) will be that of the excess Ar (Figure 9.2). The actual ratio also gives some indication as to the origin of the inherited Ar – atmospheric Ar always has $^{40}Ar/^{36}Ar = 295.5$, whereas an ancient source (such as the mantle) will have ingrown more ^{40}Ar and hence will have higher ratios, up to 20 000 in some cases.

However, because ^{36}Ar is present on both axes of such plots and, critically, it is present in vanishingly small amounts in many samples (remember it comprises only 0.3336 per cent of natural Ar), errors in its measurement can introduce correlations that mimic isochrons. A more robust alternative is to use a so-called 'inverse' isochron plot, one of $^{36}Ar/^{40}Ar$ against $^{39}Ar/^{40}Ar$ (Figure 9.3).

Since all ^{36}Ar is non-radiogenic, the age of the sample can be calculated from the intercept with the $^{39}Ar/^{40}Ar$ axis, since this is the point at which $^{36}Ar = 0$ and hence all the Ar being measured is due to ingrowth and therefore recording the age. By contrast, the *y*-intercept corresponds to the point at which there is no radiogenic Ar from ingrowth within the sample, and hence all of the Ar measured was therefore present when the sample cooled through its closure temperature, and hence this ratio is that of inherited or trapped Ar.

In geochronology, this Ar can be either atmospheric or excess (inherited). Since the atmosphere has a constant $^{39}Ar/^{40}Ar$ ratio of 295.5, if the intercept plots at 1/295.5 then we can identify the source of this contaminant and interpret the age with some confidence. In the case of excess Ar, the data will lie along a straight line with

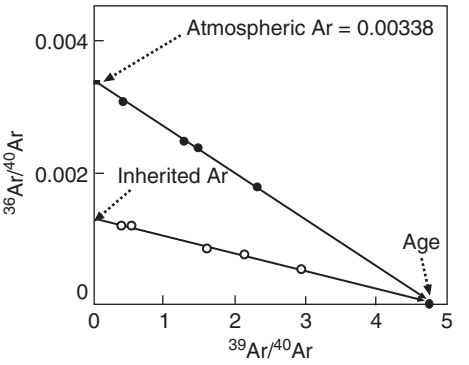

Figure 9.3 Inverse isochron diagram for Ar isotopes. By definition the Ar isotopic ratio used to calculate the age of the sample will be when $^{39}Ar = 0$, and hence the $^{40}Ar/^{39}Ar$ ratio also is 0; i.e. the *x*-intercept of the plot. Atmospheric Ar projects towards $^{40}Ar/^{39}Ar = 1/295.5$, whereas mixing with inherited (excess) Ar from another terrestrial source will project on an array with a lower slope (open symbols).

a *y*-intercept which is lower than that of the atmosphere, as the sample has incorporated some ^{40}Ar from another source within the earth (e.g. from other minerals due to diffusion during cooling, or from Ar which has accumulated over time in the mantle).

This is the power of the inverse isochron approach over plateau ages, since the age determined by an inverse isochron does not change with additional excess Ar. This is because it depends solely on the $^{39}Ar/^{40}Ar$ when $^{36}Ar/^{40}Ar = 0$, and is independent of the slope of the inverse isochron. Plateau ages, in contrast, are determined from all of the measured $^{40}Ar/^{39}Ar$ in a single step, and hence will record older ages due to excess ^{40}Ar.

Inverse isochrons can therefore potentially preserve several components of excess Ar, depending on where the Ar was coming from when the sample cooled through its closure temperature, and in some cases these distinct components can be identified within a single sample (e.g. Figure 9.3).

A final point regarding inverse isochron diagrams is that they can themselves be perturbed by Ar loss. This is because Ar loss will not change the $^{36}Ar/^{40}Ar$ ratio, but because the ^{39}Ar on the plot is actually ^{39}K (remember that we simply covert it to Ar in a nuclear reactor for ease of measurement) then the $^{39}Ar/^{40}Ar$ will *increase* during resetting due to Ar loss (i.e. we are removing Ar and holding K constant). If complete resetting occurs, then the new $^{39}Ar/^{40}Ar$ age will record the age of resetting. However, if only partial resetting takes place (i.e. Ar loss is not complete), then the inverse isochron will record a meaningless age somewhere between the initial cooling event and the subsequent cooling of the resetting event through the closure temperature.

Part Three

‘Where’

Tracking the course of material through the earth

10

Isotopes as tracers

General principles

In addition to their utility in geochronology, radiogenic isotope systems can preserve information regarding the isotopic signature of the source region of a magma or detritus at the time of formation. If the system has remained closed since this time, it is possible to age-correct, or back calculate, the measured present-day isotopic ratio of the sample (sedimentary, igneous or even metamorphic) to the time of formation of the rock. It is then possible to compare this age-corrected ratio with that of potential source regions in order to constrain whether the sample in question was derived from one region of the lithosphere or mantle rather than another. Such isotopic tracing is potentially a very powerful tool, and is commonly used in igneous petrogenesis and detrital sedimentary studies. However, as with all tools, such approaches are severely limited by our understanding of the nature of the source region with which we are comparing our sample – often we are forced to make assumptions regarding (for example) the nature of the mantle a particular sample might have been derived from, or the source terrane for detritus may have been entirely eroded away, leaving no other record of its existence. Therefore radiogenic (and indeed stable) isotopic tracing requires a full understanding of the geological context of the samples in question, and cannot be applied blindly to 'solve' questions of source for samples. There is no magic bullet in understanding whether a particular magma or fluid was derived from the crust or mantle (say), but a weight-of-evidence approach through multiple chemical and isotopic studies can lead to a high degree of confidence in such interpretations when applied in an integrated manner.

The following section attempts to set out the commonly applied tools applied to tracing the when and where of mass transfer within and across the (dominantly) solid earth. The principles are directly transferable to, and indeed often are intimately linked with, the hydro- and atmospheres. They can also be scaled down from a whole-earth geochemical reservoir approach to that of piecing together the evolution of individual cratons and terranes (and terrains!), to the local scale when

testing for contamination and assimilation. This chapter outlines the general tools that are used and their mathematical underpinnings. The notions of model ages, mixing and AFC (assimilation–fractionation–crystallisation) are described in their broadest possible senses from an isotopic perspective. This is done in the hope that even the most reluctant mathematician will be able to work their way through the general equations to apply the relevant parameters to their situation and isotopic system. Chapter 11 offers more specific applications in terms of whole-earth differentiation, mass transfer and recycling. This is done through exploring crustal growth using Nd model ages and two-stage Pb evolution, before developing the aspects of intracrustal recycling and differentiation through detrital zircons and combined Pb–Hf isotopes. The isotopic characteristics of the mantle and the reservoirs contained within it are briefly touched upon in order to offer context for industry professionals to assess the relevance of mantle–crust interaction and potentially decipher the existing literature and perform their own assessment. Chapter 11 concludes with an introduction to tracing petroleum migration and generation through the Re–Os system, a relatively new endeavour that has applications in the oil industry and also in mineral systems in which hydrocarbons have played a role. Chapter 12 finishes with a very brief look forward at emergent systems and technologies which may potentially play an increasing role in the coming decades.

10.1 Generic model ages

One useful concept is to calculate when a sample was last in isotopic equilibrium with a hypothetical isotopic reservoir, such as the chondritic uniform reservoir (CHUR), or perhaps more usefully, a reservoir that still exists on the earth, such as the depleted MORB mantle (DMM), which we can measure directly from mid ocean ridge basalt (MORB). The amount of time elapsed since a sample was last in equilibrium with one of these reservoirs is termed the *model age*. The applications of this approach are twofold; in some cases, when the sample is one that has come directly from the mantle, then the model age may approximate (sometimes quite accurately) the age of the sample. The second application is far more widespread, and is used for tracing or estimating when the sample was last in isotopic equilibrium with the mantle. When compared with the actual age of the sample, this provides a control on whether the sample has been formed from recycling ancient crustal material, or if indeed the mantle has contributed significantly in the genesis of the sample. Such a concept is developed further below, and may become important when exploring for ore deposits which require a mantle input in their genesis. First, however, it is instructive to explore what constitutes a model age, and which systems are generally used. The most straightforward example, and one

of the more common whole-rock model ages, is the Sm–Nd system. However, model ages are also widely calculated for Hf isotopes in zircon (see Section 11.1.3.1) and the parameterisation is the same in all cases.

10.1.1 Sm–Nd model ages

Figure 10.1 illustrates schematically what is meant by the term model age. Provided we know the modern-day $^{143}Nd/^{144}Nd$ isotopic ratio and its $^{147}Sm/^{144}Nd$, we can calculate what the $^{143}Nd/^{144}Nd$ ratio of any sample was at any time (t) in the past. More importantly, large geochemical reservoirs on the earth can also be considered to have evolved through geological time – particularly those that are able to convect (e.g. the DMM) and thus homogenise any isotopic heterogeneities within them. Therefore we are also able to calculate what the $^{143}Nd/^{144}Nd$ isotopic ratio of the DMM (or indeed any other reservoir, such as CHUR) was at any time in the past as well.

Such a process is illustrated in Figure 10.1a, whereby we can imagine the CHUR melting at the formation of the earth to produce a fractionated melt with a low Sm/Nd ratio, and leaving behind a melt-depleted reservoir which has a high Sm/Nd ratio. Correspondingly the depleted reservoir will ingrow more ^{143}Nd over time than the extracted melt as it has a higher $^{147}Sm/^{144}Nd$ ratio. For comparison, unmelted CHUR (by definition the undifferentiated reservoir) will evolve in its own manner somewhere between the two. Such a situation can be considered crudely analogous to the formation of the (first) crust of the earth and the corresponding depleted reservoir to be the DMM. Most importantly for the geologist, if

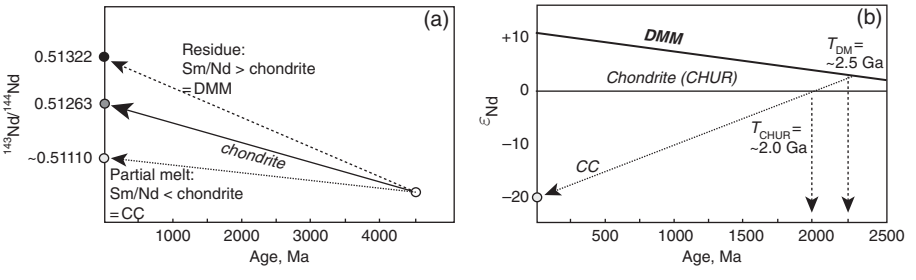

Figure 10.1 Schematic representation of a model age. (a) Reservoirs evolve to their own unique $^{143}Nd/^{144}Nd$ values over time, depending on their $^{147}Sm/^{144}Nd$ ratios. (b) The evolution of the DMM through time in terms of ε_{Nd} instead of $^{143}Nd/^{144}Nd$. Samples with Sm/Nd less than chondritic will have positive slopes on this diagram, and so will produce a T_{CHUR} that is younger than T_{DM} (as illustrated). Samples with Sm/Nd > chondrite (e.g. depleted basalts, such as MORB) will have negative slopes, and will only intersect the DMM, and hence will only have a T_{DM}.

we subsequently remelt the DMM to produce some new continental crust, then that new crust will initially have the $^{143}Nd/^{144}Nd$ ratio of the DMM at the time (t) it formed. However, the new crust will have a far lower Sm/Nd ratio than the DMM, and hence, over time, will not produce as much ^{143}Nd as the residual mantle. Therefore, if we analyse that 'new' crust today, even if we do not know its age, we are able to calculate the last time it was in isotopic equilibrium with the DMM, and therefore estimate when it was extracted from it.

Such a calculation is illustrated in Figure 10.1b, where a sample of continental crust (CC) is analysed at the present day. Note that this panel is now in ε notation, and hence samples with Sm/Nd ratios lower than CHUR will appear to have positive slopes (i.e. they do not produce ^{143}Nd as rapidly as CHUR), whereas samples with Sm/Nd > CHUR will have negative slopes since they are producing ^{143}Nd more rapidly than CHUR, resulting in higher $^{143}Nd/^{144}Nd$ ratios and hence higher ε_{Nd} values. Therefore we can calculate algebraically the last time any given sample was in isotopic equilibrium with any reservoir of our choosing (Equations 10.1 and 10.2). Note that Figure 10.1b illustrates two of these model ages for the same sample – one with respect to CHUR and a second, older value with respect to the DMM. In reality, since we do not consider the CHUR to actually still exist within the earth, this is not a particularly useful model age to calculate. Another way to think about T_{CHUR} is that it is the last time the sample had an ε value of 0:

$$T_{CHUR} = \frac{1}{\lambda}\ln\left(\frac{(^{143}Nd/^{144}Nd)_{sample} - (^{143}Nd/^{144}Nd)_{CHUR}}{(^{147}Sm/^{144}Nd)_{sample} - (^{147}Sm/^{144}Nd)_{CHUR}} + 1\right), \quad \text{(Eq 10.1)}$$

$$T_{DM} = \frac{1}{\lambda}\ln\left(\frac{(^{143}Nd/^{144}Nd)_{sample} - (^{143}Nd/^{144}Nd)_{DMM}}{(^{147}Sm/^{144}Nd)_{sample} - (^{147}Sm/^{144}Nd)_{DMM}} + 1\right), \quad \text{(Eq 10.2)}$$

where $^{143}Nd/^{144}Nd_{DMM\ today} = 0.51315$ and $^{147}Sm/^{144}Nd_{DMM} = 0.2137$.

A range of different reservoirs are appropriate, depending on the isotope system of interest – for example, Nd isotopes usually use T_{DM}, i.e. the time which has elapsed since the sample was extracted from the depleted (MORB) mantle; however, the CHUR is also often used (see Figure 10.1b).

In effect, the choice of reservoir makes no difference to the mathematics – as long as we know what the critical parameters for a given reservoir are (i.e. its parent/daughter ratio and daughter/daughter ratio), then we can calculate when a given sample was last in isotopic equilibrium with it (i.e. the sample's model age). In general, however, irrespective of choice of reservoir, the general form for model age calculation is the same for all isotopic systems. In general Nd whole-rock and Hf zircon model ages are the most commonly applied; however, some Sr model

ages have also been considered. Os model ages can be used in a slightly different manner due to their differing chemical behaviour, and are considered separately in Section 10.1.3.

10.1.2 Pb model ages

One of the more widespread applications of the model age concept has been in relation to Pb isotopes. This is particularly the case for Pb ores which have formed in environments that have the Pb directly extracted from the mantle. In this scenario, one can assume that the earth's mantle had an initial Pb isotopic ratio, which has subsequently evolved as a function of the primordial U/Pb ratio. Since there are two decay chains in the U–Pb system, and they decay at different rates, then the resulting Pb isotopic evolution of the mantle is not a simple linear evolution, as in the case of the DMM for Nd as described above, but rather is a curve, whereby there was rapid initial ingrowth of ^{207}Pb due to the shorter half life of ^{235}U, with ^{206}Pb ingrowth dominating later in earth history. Therefore, a galena formed directly from the mantle-derived Pb will lock in the Pb isotopic composition of the mantle at the time of its formation, since galena contains no U or Th and hence will not change its Pb isotopic signature after formation.

Figure 10.2 plots galenas from Pb deposits of different ages globally from a wide range of continental and oceanic environments. At best, such a curve approximates the terrestrial Pb growth curve. However, some galenas even plot to the right of the geochron and hence record 'future' ages. Therefore such an approach is clearly not

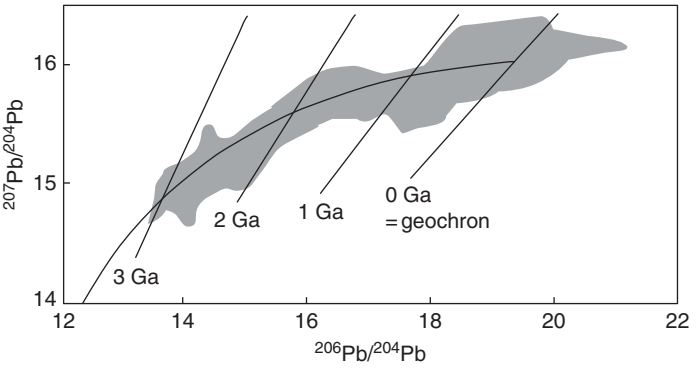

Figure 10.2 Pb isotope signatures of galenas from ore deposits of different ages (grey field). The distribution of Pb isotopes broadly approximates the terrestrial growth curve (curved line); however, significant scatter is observed. Isochrons of various ages are also illustrated, culminating in the modern-day isochron, also referred to as the geochron. Note that all isochrons project back to the same initial Pb isotopic ratio, that of the primeval solar system, which is approximated by the Canyon Diablo troilite (CDT).

universal and applicable for all terrestrial Pb. If these data are filtered to remove those galenas which have formed in continental settings (and hence have experienced additional Pb ingrowth due to the higher U/Pb and Th/Pb ratios preserved in the continental crust), and one focuses on oceanic deposits, the fit improves but there is still substantial excess scatter. Hence it would seem that such a single-stage Pb model age is appropriate for only a small number of very specific ore deposits whereby the Pb is directly extracted from the mantle and has experienced no subsequent ingrowth of Pb or contamination/incorporation during formation. Such single-stage Pb models can be approximated by the following equations whereby we are assuming that the Pb is extracted from a single, very large, homogeneous Pb reservoir at time t containing an initial Pb isotope ratio at time T (in this case the age of the earth):

$$\left(\frac{^{207}\mathrm{Pb}}{^{204}\mathrm{Pb}}\right)_t = \left(\frac{^{207}\mathrm{Pb}}{^{204}\mathrm{Pb}}\right)_T + \left(\frac{^{235}\mathrm{U}}{^{204}\mathrm{Pb}}\right)(e^{\lambda_{235}t} - 1). \qquad \text{(Eq 10.3)}$$

A directly comparable equation could be written for $^{206}\mathrm{Pb}/^{204}\mathrm{Pb}$ and the parent isotope, $^{238}\mathrm{U}$. Then if we assume that the initial Pb isotope ratio of the earth is that of the Canyon Diablo troilite (CDT), we can approximate the single-stage Pb isotope evolution of the earth by combining the two equations and cancelling out the parent/daughter isotopic ratios to leave the modern-day U ratio:

$$\frac{\left(\frac{^{207}\mathrm{Pb}}{^{204}\mathrm{Pb}}\right)_t - \left(\frac{^{207}\mathrm{Pb}}{^{204}\mathrm{Pb}}\right)_{\mathrm{CDT}}}{\left(\frac{^{206}\mathrm{Pb}}{^{204}\mathrm{Pb}}\right)_t - \left(\frac{^{206}\mathrm{Pb}}{^{204}\mathrm{Pb}}\right)_{\mathrm{CDT}}} = \frac{1}{137.88}\left(\frac{e^{\lambda_{235}t} - 1}{e^{\lambda_{238}t} - 1}\right). \qquad \text{(Eq 10.4)}$$

However, such a single-stage Pb model is really only applicable for a small number of Pb deposits, those of 'conformable' sediments and volcanics in greenstone belts and island arcs.

10.1.2.1 Two-stage model ages

Instead, during the mid 1970s Stacey and Kramers (1975) took an empirical approach to Pb model ages, and plotted in detail a large number of global galenas and feldspars. They observed that they could approximate the global model age distribution by somewhat arbitrarily breaking the Pb evolution of the earth into two stages. The early phase evolved from the primordial solar system Pb isotopic signature (i.e. CDT) until about 3.7 Ga, after which the earth differentiated into reservoirs of distinctly different $^{238}\mathrm{U}/^{204}\mathrm{Pb}$ (= 'μ'). One was 'high μ' (or 'HIMU'), comprising the upper crust and the upper mantle which had been

contaminated by recycled/subducted upper crust (see Section 11.2); the other reservoirs were comparatively low μ and comprised the lower mantle, outer core and to some degree the lower crust. Therefore they modelled the Pb evolution of the earth as initially comprising a uniform U/Pb (μ_1) = 7.2, and after 3.7 Ga containing a Pb reservoir available to form ore deposits which had a higher U/Pb (μ_2) = 9.7. Such a model was attractive as this age broadly corresponded to the then oldest known crust of the earth, the Amitsoq Gneiss in Greenland. It is important to note that no-one was suggesting that all of the continental crust formed simultaneously at this time, simply that this age represented the peak of stabilisation of the crust and early differentiation of the earth.

The advantage of such a model was that it accounted for the so-called future ages of some of the galenas plotted in Figure 10.2; because the second stage of earth evolution had a higher U/Pb ratio, it was possible to ingrow more Pb and hence produce Pb/Pb isotope signatures which were substantially more radiogenic than those predicted by a single-stage model. This difference is summarised in Figure 10.3.

What does all this mean for using model ages to understand a mineralised system? It means that for any given deposit which contains galena, it is possible to theoretically derive a Pb model age for it which will reflect the source of the metals within it. Ore deposits which contain a single-stage Pb evolution model age which is close to the stratigraphic age of the deposit can be conceptually thought

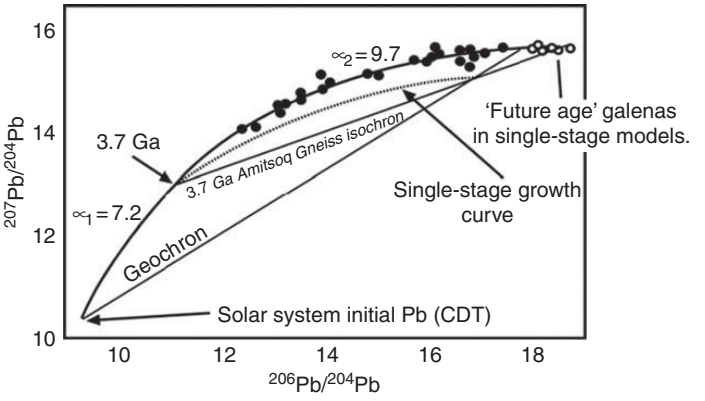

Figure 10.3 Two-stage Pb evolution for the earth and Pb ore deposits. After 3.7 Ga galenas in ore deposits were derived dominantly from a source that had significantly higher $^{238}U/^{204}Pb$ (μ) than the primordial solar system. Such a model produces a better fit for younger galenas and also accounted for the production of radiogenic Pb isotopic signatures in young ore deposits which produced 'future ages' in a single-stage evolution (open symbols). Modified from Stacey and Kramers, *EPSL*, 1975, reproduced with permission.

about in terms of having been formed by extraction directly from the mantle at the time of ore deposit formation. Those whose ages correspond more closely to a two-stage model age could therefore have been sourced from the lower crust or modified upper mantle.

10.1.3 Unusual model ages: Re–Os

Another case is the unusual behaviour of Re with respect to Os in mantle melting situations. Because $D_{Re} \ll D_{Os}$, at high degrees of partial melting ($F > 15$–20 per cent) it is possible to produce a residue which has incredibly low Re/Os ratios. So low that in fact it is possible to assume that there is *no* Re left, meaning that the mantle residue does not ingrow any more radiogenic Os (^{187}Os) over time.

Therefore, when we sample these highly depleted residues, such as portions of the subcontinental lithospheric mantle (SCLM; e.g. xenoliths), ophiolites and massif peridotites, we can assume that there has not been any increase in $^{187}Os/^{188}Os$ since the melt extraction event. Therefore we can calculate a model age which reflects the amount of time that has elapsed since the Re was removed from the source. This is termed a 'rhenium depletion' model age (T_{RD}):

$$T_{RD} = \frac{1}{\lambda} \ln\left(\frac{(^{187}Os/^{188}Os)_{sample} - (^{187}Os/^{188}Os)_{chondrite}}{0 - (^{187}Re/^{188}Os)_{chondrite}} + 1\right). \quad \text{(Eq 10.5)}$$

Note that Equation 10.5 is simply a restatement of Equation 10.1 with the simple assumption that there is no ^{187}Re and hence the material has not ingrown any ^{187}Os since the time of Re removal. It must be noted that this approach is applicable only for a small number of samples which have very, very low Re/Os ratios (i.e. $^{187}Re/^{188}Os$ can be considered to be 0). Obviously this can only work for samples which have subchondritic $^{187}Os/^{188}Os$, because if they have radiogenic ratios then extrapolation back in time will not intersect the chondritic evolution line and hence will not produce a T_{RD} (Figure 10.4). In this scenario, it is possible to calculate a conventional model age using Re–Os, which is referred to as a T_{MA}. This model age is directly analogous to the calculation of the Nd model age (Equation 10.2), and differs only in the choice of reservoir (in this case chondrite instead of depleted mantle) that is used. The chondritic evolution is used as a reference model reservoir as Re and Os have not behaved in the same manner as Nd and Sm during the evolution of the earth, and it would appear that even the convecting mantle is quite heterogeneous for these elements. Therefore calculating an Os model age that is analogous to a T_{DM} for Nd is not appropriate.

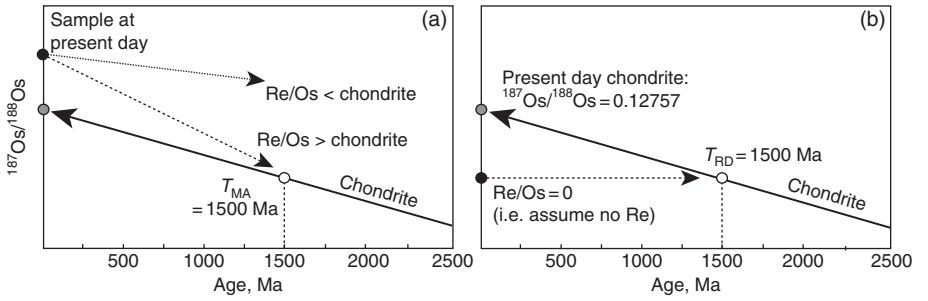

Figure 10.4 Comparison of calculation of conventional model ages (a) for the Re–Os system, whereby the parent/daughter ratio is used to extrapolate back in time, with the calculation of T_{RD} ages (b) whereby it is assumed that there is no parent isotope (i.e. Re) in the sample, and hence the $^{187}Os/^{188}Os$ has not changed since it was extracted from the mantle reservoir.

10.2 Mixing

One process that occurs in many geological situations is *mixing*. Mixing refers to a range of processes in which several mineral phases or chemical components are brought together in either multiphase (e.g. sediments) or multicomponent (e.g. magmas, fluids or seawater) systems to form an array of hybrid samples (mixtures). Thus we can have physical and chemical mixing, or some combination of both. *Bulk mixing* is used to refer to those systems in which there is no preliminary sorting of phases or preferential extraction of chemical components, and hence is the simplest case to consider. In this context, ***phases*** have homogeneous chemical properties which remain physically distinct in a mixture (i.e. individual grains in a sediment, crystals in a magma chamber). In contrast, ***components*** lose their physical identity upon mixing, and so are commonly applied with respect to fluids (e.g. the dissolution of salt in water, or the contamination of a well-mixed magma by ingesting the crust). Both terms can be referred to using the mixing-specific term ***end member.***

10.2.1 Two-component mixing

The simplest case considers the mixing of two components, A and B, together in differing proportions, as specified by the parameter f:

$$f = \frac{A}{A + B}, \qquad \text{(Eq 10.6)}$$

where A and B are the weights of the end member components in any given mixture.

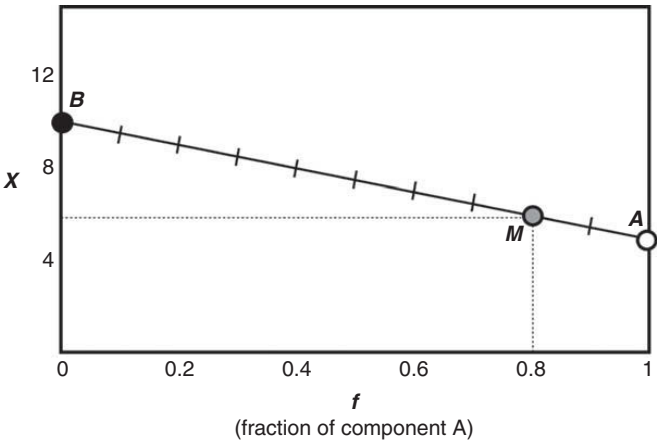

Figure 10.5 Simple mixing between two end members of different concentration (X_A = 5 and X_B = 10; units are arbitrary, but must be weight units such as wt%). A mixture containing 80 per cent component *A* (f = 0.8) will have a concentration of 6.

Therefore the concentration (in weight units) of a given element in a mixture (X_{M}) can be expressed in terms of the concentrations of the end members (X_A and X_B) and the proportions in which they are mixed (f):

$$X_{\mathrm{M}} = f(X_A - X_B) + X_B. \qquad \text{(Eq 10.7)}$$

The effect of this is that if the concentration of a given element is the same in each end member, then the mixture will have the same concentration as the end members, regardless of how much each end member is contributing. In contrast, if the concentrations are different, then the mixture will have a concentration directly proportional to the relative contributions of each end member, and will lie on a straight line between them as a function of *f*.

More importantly, since we can measure the composition of the mixture (X_{M}), and we can determine (through measurement, calculation or, in the worst case, approximation by using comparable end members from other tectonic settings) the composition of the end members, we can calculate the relative contributions of each member to the final mixture (i.e. calculate f). This can become very important in contamination studies, and is also vital for mineralisation and petrogenesis of magmatic systems as magmas and fluids invariably interact with their surroundings as they evolve.

Hence, understanding mixing becomes central to understanding a whole range of geological phenomena – particularly fluid evolution in metallogenesis. Significantly, however, since fluids often themselves have multistage histories, an understanding of mixing can also allow us to place constraints on potential sources

of fluids in a mineralised system – i.e. are we seeing interaction between a basinal brine and a magmatic fluid, and if so, how much has either contributed to the resulting fluid composition? Such understanding may be the deciding factor for distinguishing between mineralised and barren systems, for example.

The preceding discussion was based purely on the concentration of an element during simple mixing. However, for many elements, fluids of quite different origins may have very similar concentrations of particular trace elements, often making it impossible to determine the origins of the mixture from an understanding of the concentration alone. Isotopes can greatly simplify identifying mixing relationships as they can be distinct 'fingerprints' of the components that are mixing. That is, even if different end members have the same concentration of an element, they are likely to have different isotopic compositions. Therefore the isotopes will still record a signal of the mixing, even for situations in which the concentration does not change during the mixing process.

More commonly, though, most end members will have both different isotopic compositions and different elemental concentrations. Therefore the measured isotopic ratio of the mixture depends on the isotopic compositions of the end members, and the concentration of the element in each end member. Generally, mixtures of such materials will plot as hyperbolic arrays on isotopic ratio vs concentration diagrams (Figure 10.6a). Plotting against the inverse of concentration converts these arrays to straight lines (e.g. Figure 10.6b) and hence this is an excellent test in real data

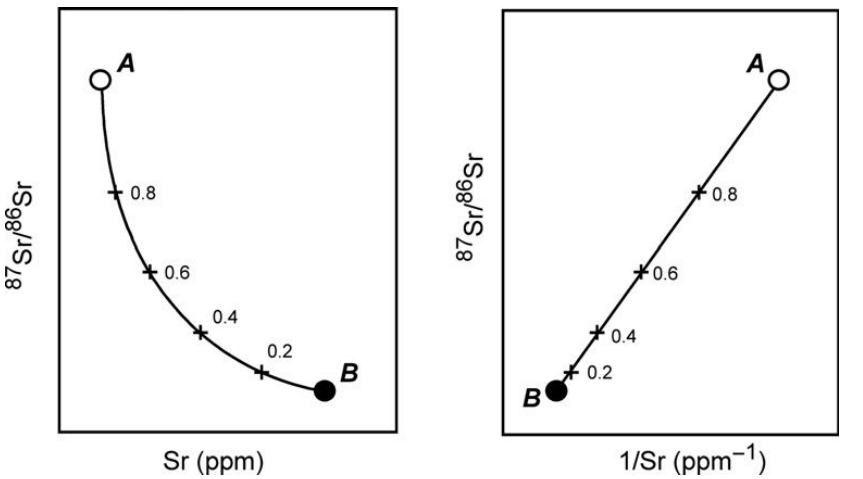

Figure 10.6 Mixing between two components, *A* and *B*, in isotope–concentration space (a). Different values of *f* will result in non-linear shifts in the isotopic ratio. (b) Converting the plot to the inverse of the concentration produces a linear mixing array between the two, where each additional increment of a given component results in a different shift in isotopic ratio from the preceding increment.

sets for mixing. If a straight line is not observed when isotope ratios are plotted against the inverse of the concentration of the element, then mixing cannot be the source of variation within the data set.

Mathematically, these relationships can be summarised as:

$$R^X_{\mathrm{M}} = \frac{R^X_A X_A f + R^X_B X_B (1-f)}{X_A f + X_B (1-f)}, \tag{10.8}$$

where R^X = the isotopic ratio of element X in components A (R_A) and B (R_B), and X_A and X_B are the concentrations of element X in end members A and B, respectively.

Such an approach to mixing is applicable in a very large number of systems, including magma mixing, contamination of groundwaters, hydrothermal fluids and even to the mixing between different geochemical reservoirs on the scale of the whole earth, such as the DMM and crust. However, an additional complexity is introduced when considering mixing at some time in the past if one is using radiogenic isotopes as their tracer. This is because the mixing process will produce a mixture that not only has a different isotopic ratio from either of the end member components that are being mixed, but also the mixture itself will have a different parent/daughter isotopic ratio than the parents and hence will evolve to an isotopic signature that may not be obviously apparent from the actual ratios of the end members. Hence such calculations need to be conducted for the age at which mixing took place.

For example, we might suspect that a series of basaltic andesites erupted as the result of mixing between a rhyolitic magma chamber and the injection of a more mafic magma during a recharge event. In an ideal situation the andesite may even contain fragments (autoliths) of both the mafic and the felsic magmas, which we can measure directly. In this scenario we can directly test whether the andesite is indeed a direct mixture between these two magmas, or whether another process, such as AFC, is involved. In the first instance consider the example that the eruption took place in historic times, and so is essentially of zero age.

For a zero-age scenario, testing for mixing is straightforward – simply plotting the samples on an isotopic ratio vs inverse concentration plot illustrates whether the samples plot on a straight line (Figure 10.7a,b). Revealingly, the basaltic andesites in Figure 10.7 not only define a straight line in panels a and b, but also appear to project (roughly) towards the hypothesised end member components (i.e. the rhyolite and the basalt). Note that there is usually some scatter in such data sets, as illustrated in this example, due to both geological effects (i.e. not 'pure' mixing) and potential analytical artefacts. Note that in terms of Figure 10.7a the samples plot closer to the basaltic end member, and in Figure 10.7b they plot closer towards

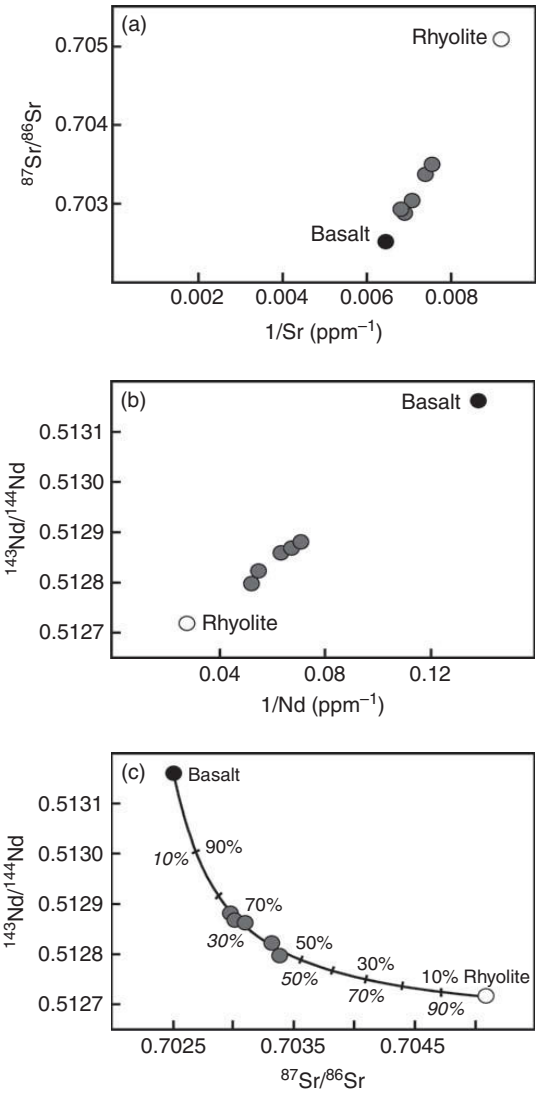

Figure 10.7 Example of hypothetical magma mixing in a magmatic system. A rhyolitic magma chamber (open circle) is recharged by a basaltic magma (solid circle), triggering an eruption of basaltic andesites (grey circles). This is illustrated in plots of isotopic ratios against the inverse of the concentration of the daughter isotope (a and b). (c) Isotope–isotope diagram with a calculated mixing curve (Equation 10.8); tick marks at 10 per cent intervals. Non-italic figures represent proportions of basalt in the mixture; italicised figures correspond to the proportion of rhyolite.

the rhyolitic. This is because each of the end members themselves have different concentrations of both Sr and Nd, as well as different isotopic signatures, and hence the same amount of mixing will produce different apparent shifts in concentration and isotopic composition for each system.

Given that our inverse concentration plots show encouraging evidence that mixing has occurred, it is worth undertaking a more robust analysis, and plotting an isotope–isotope diagram with a calculated mixing curve (Equation 10.8) superimposed (Figure 10.7c). This can then provide an estimate of the proportions of each of the end members. Note that in this space, the mixing model is a curve, and the data plots at between ~30–45 per cent basaltic magma mixed in with the corresponding proportions (70–55 per cent) rhyolite. This is a significant amount of basalt to have added to a rhyolitic magma chamber, so it is no surprise that the sudden influx of both heat and volume resulted in an eruption!

In the case of ancient samples, it is of course necessary to first age-correct the isotopic ratios of all samples and end members before testing for mixing. It is also important to bear in mind that mixing is not necessarily confined to two magmas, with contamination of magmas by the crust often defining mixing trends.

10.3 AFC (assimilation–fractionation–crystallisation)

Of critical interest in many ore deposit studies, and virtually every magmatic system, is the role of AFC. While the theoretical background and petrographic details of this process (or rather competing processes) are best understood through a thorough grounding in igneous petrology, because it is a common and critical process by which the chemistry and isotopic composition of magmas can be changed (and often drives mineralisation), it is important to understand how it operates in terms of isotopes.

Basically the process was first quantified by DePaolo (1981), and mathematically describes the change in concentration of a given trace element within a magma in terms of the magma's interaction with the surrounding country rock, and the minerals phases that it is crystallising. Such an interaction depends critically upon the mass of magma, the rate of crystallisation and the rate at which it is assimilating the country rock, three variables that will themselves vary dramatically over the life of the magmatic system.

In terms of trace elements alone, AFC can be described as the changing composition of a given trace element X as:

$$\frac{C_l}{C_l^0} = F^{-z} + \left(\frac{r}{r-1}\right)\frac{C_a}{zC_l^0}(1 - F^{-z}), \tag{10.9}$$

where C_l is the concentration of element X in the liquid (C_l^0 is the initial concentration); C_a is the concentration of element X in the assimilated solid/wallrock (e.g. crust); F is the portion of melt remaining (F is the 1 at the start); and $r = M_a/M_c$, where M_a is the mass assimilation rate and M_c is the fractional crystallisation rate, with:

$$z = \frac{r + D_X - 1}{r - 1},$$

where D_X is the bulk distribution coefficient of element X.

Fundamentally, AFC is described in terms of r. If $r = 0$, pure fractional crystallisation is occurring (i.e. no assimilation is taking place). If $r = 1$, the mass of the magma remains constant as assimilation and crystallisation are occurring at the same rate, and a *zone refining* process is occurring in which the concentration of element X is changing in the magma. For cases when $r < 1$ the AFC process is a combination of fractional crystallisation and zone refining, whereas for $r > 1$ and as $r \to \infty$ the process becomes dominated by binary mixing and is dominated by assimilation.

AFC becomes a little more complex when dealing with isotopic ratios. Again, as in the case of simple mixing, it is critical to use initial (age-corrected) isotopic ratios, and the following AFC modelling assumes no isotopic fractionation between the solid and the liquid phase – clearly not the case for light stable isotopes such as O. As such, this approach is generally confined to isotopic systems heavier than mass ~80, or the element Sr.

The general equation for AFC dealing with an isotope ratio R is:

$$R_\mathrm{l} = \frac{\left(\frac{r}{r-1}\right)\frac{C_\mathrm{a}}{z}(1 - F^{-z})R_\mathrm{a} + C_\mathrm{l}^0 F^{-z} R_\mathrm{l}^0}{\left(\frac{r}{r-1}\right)\frac{C_\mathrm{a}}{z}(1 - F^{-z}) + C_\mathrm{l}^0 F^{-z}}, \tag{10.10}$$

where R_l is the isotope ratio in the liquid (melt/magma); R_a is the isotope ratio in the assimilant (wallrock); R_l^0 is the initial isotope ratio in the liquid (melt/magma) prior to commencement of the AFC process. All other symbols are as for Equation 10.9.

One advantage of this formulation is that normalised isotope ratios, such as ε_Nd can be used, greatly simplifying the calculations and chances of error.

This relationship can be illustrated by exploring the variations in Sr isotopes and concentration of a basaltic magma ascending through the crust and interacting with a wallrock. Since Sr in basaltic systems is largely controlled by the interplay between plagioclase and ferromagnesian phase crystallisation (e.g. olivine, pyroxene, amphibole), a magma body will crystallise significantly differing portions of these minerals during ascent through the crust. The possible evolutionary paths plotted in Figure 10.8 emphasise the effects of decreasing r and increasing D_Sr (i.e. greater plagioclase crystallisation) during evolution. In Figure 10.8a the evolving magma assimilates comparatively little of the contaminant and so shows little isotopic variation but significant variation in [Sr] due to fractional crystallisation. Figure 10.8b, in contrast, highlights that the greater rate and total mass of

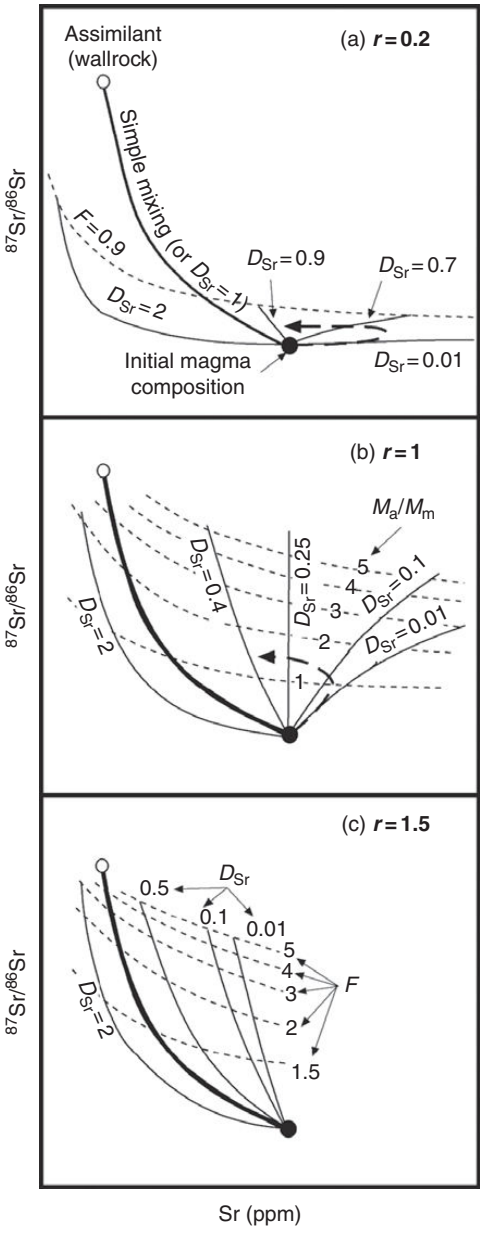

Figure 10.8 Illustration of the relative effects on $^{87}Sr/^{86}Sr$ and [Sr] through AFC processes for differing values of *r*. (a) and (b) plot possible evolutionary paths for a basaltic magma ascending through the crust (dashed arrow). (a) $r = 0.2$, (b) $r = 1$, (c) $r = 1.5$. (b) is contoured for the ratio of the mass of assimilant to the mass of initial magma (M_a/M_m; note this is distinct from M_a/M_c, which is the ratio of the *rate* of mass assimilation to the *rate* of crystallisation). Since $r > 1$ in (c), *F*, by definition, must initially be greater than 1. Reproduced with permission from DePaolo 1981, *EPSL* **53**: 189–202.

assimilant pulls the magma towards more radiogenic isotopic signatures comparatively quickly, and indeed that the final volume of the magma contains a far greater proportion of assimilated material.

In essence, since we virtually never know the *actual* masses of magma and assimilant (i.e. M_a and M_m), we can model systems in which AFC is suspected to have taken place by varying values of r (and D) for a given element. Since D and r are ratios and hence dimensionless they readily lend themselves to modelling (e.g. Figure 10.8), but one thing that is possibly counter-intuitive is that F, the proportion of magma remaining, can sometimes be greater than 1 since the total mass of magma has increased through assimilation. Critically this can only occur when $r > 1$ since it is assimilating country rock at a rate greater than it is crystallising and hence the net mass is increasing (remember $r = M_a/M_c$; this is illustrated in Figure 10.8c).

It is worth remembering that assimilation takes place in many forms. Ascent of a hot, positively buoyant ultramafic magma may induce partial melting in the surrounding country rock, and these partial melts are far more readily assimilated than bulk fusion (digestion and xenolithic entrainment) of wallrocks. Energetically the efficiency of assimilation and hence the total volumes of assimilant involved will vary dramatically depending on which process is active; however, the compositions and concentrations of partial melt assimilants can themselves be readily modelled from a basic understanding of the composition and mineralogy of the country rock lithologies.

Finally, AFC modelling can be applied readily enough to (light) stable isotope systems, particularly those in which the element in question is a major element, such as O. On the one hand, there is the additional complexity that the crystallising phases will themselves be displaced from that of the crystallising magma by the factor α (Equation 2.1) during Rayleigh fractionation as per kinetic fractionation processes (e.g. Equation 2.4). In fact, this is true also of radiogenic isotopes, but the combination of very small shifts with, more critically, the normalisation procedures employed during measurement obviates the need for such considerations.

Since stable isotopes are generally reported as normalised deviations from a standard (e.g. δ notation) we can consider that the difference in isotopic signature between the crystals and the liquid they are crystallising from, Δ, can be expressed as:

$$\Delta = \delta_{\text{crystals}} - \delta_{\text{magma}} \sim 1000 \ln \alpha. \tag{10.11}$$

Therefore AFC can be considered in terms of:

$$\delta_m - \delta_m^0 = \left(\delta_a - \delta_m^0 - \frac{\Delta}{r}\right)(1 - F^{-z}). \tag{10.12}$$

In this case $z = r/(r - 1)$ since the assumption is that $D = 1$ as the element of interest (generally O in the case of silicates, or more rarely S in the case of sulphides) is a major element in the phases of interest and hence present in excess.

This equation breaks down for trace element stable isotopes, or in situations in which $\delta_a - \delta_m^0 > \sim 20$.

The role of AFC can be absolutely critical in driving mineralisation, particularly in magmatic sulphide systems where assimilation and/or contamination can be responsible for providing the S necessary for sulphide saturation, or fractionation driven by assimilation can lead to sulphide saturation. Critically, if the *r* factors are too low, even interaction with a high-S assimilant may still result in either no sulphide precipitation or low-tenor mineralisation.

11

Applications of radiogenic tracers

The earth can be simply divided into several broad geochemical reservoirs. At the first order, the earth is composed of a metallic core, the convecting silicate earth (including the asthenosphere), and the lithosphere. The lithosphere comprises a crust and corresponding lithospheric mantle, which does not convect. Continental crust and subcontinental lithospheric mantle (SCLM) are quite heterogeneous and compositionally distinct compared with the oceanic crust and oceanic lithospheric mantle.

Since each reservoir is chemically distinct, they will evolve to correspondingly distinct isotopic ratios, potentially allowing the tracking of magmas and fluids from and between them. The relevance of this in the minerals industry can be varied, from requiring/desiring magmas sourced from the mantle for exploration models, or needing crustal contamination to drive sulphide saturation, through to monitoring the effects of fluids of differing compositions in a hydrothermal system.

11.1 Differentiation within the crust and crustal growth

11.1.1 Nd model ages (T_{DM}) and crustal evolution

Nd isotopes offer an effective way of placing first-order constraints on processes pertaining to the formation and subsequent stabilisation and recycling of continental crustal material. In principle, when new continental crust is formed (e.g. on the modern earth at plate margins), the crustal material will start out with an isotopic signature in equilibrium with the depleted mantle (DMM) from which it was derived (Figure 11.1a). However, because continental crustal material contains relatively low Sm/Nd ratios with respect to the mantle, this new material will only ingrow new (additional) ^{143}Nd relatively slowly. Hence it will evolve to negative ε_{Nd} values (Figure 11.1a), and if unmodified will

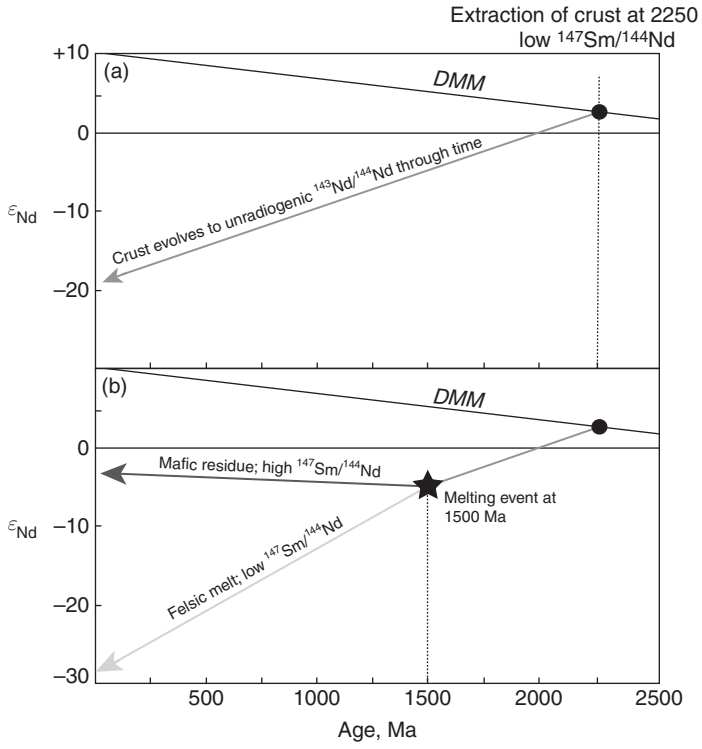

Figure 11.1 Schematic representation of the Nd isotopic evolution of a portion of continental crust that is extracted from the convecting mantle at 2.25 Ga. (a) If the crust remains unmodified, it will subsequently evolve to unradiogenic $^{143}Nd/^{144}Nd$ through time with respect to the DMM as it has a lower $^{147}Sm/^{144}Nd$ and hence less ingrowth of ^{143}Nd. (b) If this crust undergoes a subsequent differentiation (melting) event at 1.5 Ga, this could result in the production of a felsic (granitic) differentiate with low Sm/Nd and a residue comprising higher Sm/Nd. Each product then evolves to distinctive Nd isotopic signatures through time.

preserve a T_{DM} which is the same as its magmatic age. Hence we would be able to measure its Nd isotopic signature today and calculate a T_{DM} which would reflect precisely the age of formation of that portion of the continental crust, and hence constrain the time of that particular episode of crustal addition.

However, more generally, the continental crust undergoes processes of continued internal differentiation. For example, remelting of this crust during orogenesis or granite formation will segregate crustal material into a more differentiated granitic component, with even lower Sm/Nd ($\propto$ $^{147}Sm/^{144}Nd$) ratios, and a (relatively) more mafic residue with higher Sm/Nd ratios than the protolith. Over time these two products will evolve to distinctly different measured values today (Figure 11.1b).

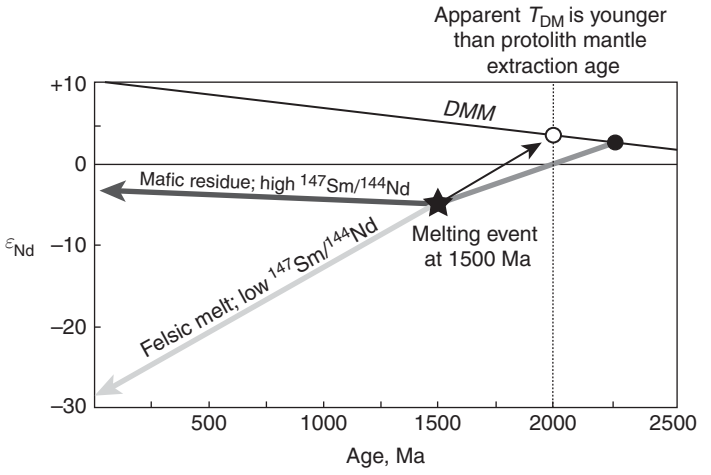

Figure 11.2 Measurement of granitic material at the present day could result in extrapolation back to the depleted mantle, implying a time of granite protolith extraction from the mantle more recent than it actually was. Thus T_{DM} can be considered to place *minimum* constraints on the timing of crustal growth when applied to rocks which have been through a cycle of internal crustal differentiation. Intersection of the evolutionary curve of a suspected source lithology for the granite, such as granulite, with the evolution of the melt product, the granite, at 1.6 Ga might imply that since the two were in isotopic equilibrium at the time, one was derived from the other.

A consequence of this is that simply measuring the Nd isotopic signature of a granite in isolation would result in model ages which would appear to be younger than the time at which the Nd which is in the granite actually was extracted from the mantle (Figure 11.2). One net result is that measurement of the differentiated granitic product will result in an underestimate of the antiquity of the protolith responsible for its generation. This is not surprising really, since most granites are themselves the products of melting of crustal material of some description.

Correspondingly, simply measuring the Nd isotopes of the mafic residue illustrated in Figures 11.1b and 11.2 would result in trajectories back in time which would never intercept the DMM and hence would not produce a model age. However, the intersection of the evolution curves of the more mafic or migmatitic lithologies with the granite at 1.6 Ga may infer a cogentic relationship. This interpretation would need to be undertaken in geological context, suggesting that the migmatites may have been the source region for the granites.

However, another common method of crustal formation (and, indeed, differentiation) is direct extraction of new material from the upper mantle (e.g. the DMM), which then interacts extensively with existing crust (contamination, mixing and/or AFC) to produce a hybrid melt which contains both primitive and recycled

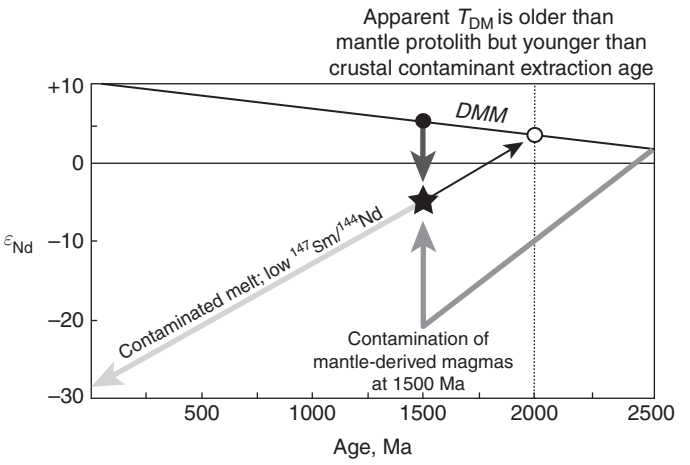

Figure 11.3 Production of a granitic rock with an Nd isotopic signature identical to that in Figure 11.2 through mixing of a juvenile mantle source with older continental crust. Such a combination of new crustal addition and recycling of older material is likely to dominate the record of crustal growth during the latter portions of the geological record.

components (Figure 11.3). Such a mixture could result in a granite with identical Nd isotope characteristics to the example in Figure 11.2; however, in this instance the T_{DM} would record an age older than the crustal addition, but younger than the contaminant. Hence such mixtures would effectively average the time of formation and stabilisation of the continental crust throughout earth history.

The power and utility of whole-rock Nd model ages in this context comes when we have an independent age constraint on the lithology that is being analysed. Granites, for example, are generally readily dated by U–Pb zircon geochronology, which allows comparison of their magmatic crystallisation age with their mantle derivation, or model, age. Hence, for lithologies which contain significant amounts of new crustal addition, or so-called juvenile components, their 'stratigraphic' age (i.e. that of magmatic crystallisation, or deposition age of sediments) will be close to that of the T_{DM}. Granites which are produced from crustal recycling (e.g. melting of sediments which may themselves have been recycled a number of times) will have stratigraphic ages which are very much younger than their model ages.

The whole-rock model age approach is applicable only for isotopic systems in which the parent and daughter are relatively immobile and robust with respect to each other, and hence preserve only events which are of very large scale. Hence, most commonly Nd and Hf isotopes are applied, as Rb is generally readily fractionated from Sr during magmatism and is subject to alteration and hydrothermal processes. Given that analysing whole-rock Hf is more

time consuming than analysing whole-rock Nd, which has become routine, Hf models and model ages are more generally applied to *in situ* zircon analyses (Section 11.1.3.1), which lend themselves to rapid acquisition of precise data.

Therefore, when considering whole-rock model ages, as discussed above, a combination of factors will result in a spread of T_{DM} ages which themselves average the combination of processes and contributions to crustal growth. Hence, to a first order, it may be appropriate to use the distribution of model ages for rocks throughout the geological record to identify periods of major crustal growth as opposed to periods typified by crustal recycling. In this context, although a specific model age is of itself not necessarily tied to a discrete geological event in the same way that a magmatic crystallisation age (say) is, model ages do record periods of heightened crustal growth and/or differentiation. Such distinctions become important in exploration as many ore-forming systems require a significant mantle input (either directly to supply metals or indirectly to supply heat), and often magmas with significant juvenile components may be considered desirable targets. Other ore deposits, notably Sn greisens, require reduced magma crystallisation settings which are favoured by S-type magmatism and hence crustal recycling. Therefore magmas with very old model ages with respect to their emplacement age will be of interest.

11.1.2 Two-stage Pb models

As discussed in Chapter 10, the two-stage Pb model for the earth (Figure 10.3), which was derived from galenas, offers a direct insight into the nature of the metal contained within a Pb deposit. Ore deposits containing a single-stage Pb evolution model age which is close to the stratigraphic age of the deposit can be conceptually regarded as having been formed by near-direct extraction from the mantle at the time of ore deposit formation. Those whose ages correspond more closely to a two-stage model age could therefore have been sourced from the lower crust or modified upper mantle, whereas galenas which plot significantly away from either of the model curves would reflect significant recycling and remobilisation. Such source and process observations are often intimately linked to the size and grade of ore-forming systems, and hence can be used as a first-order tool in prospectivity analysis.

11.1.3 Detrital zircon populations

One major utility of the development of *in situ* U–Pb zircon techniques was the potential application in measuring the ages of detrital zircons. Such data provide an immense amount of information regarding the depositional system

that was receiving sediment and also the nature of the crust that was exposed to supplying detritus. Hence detrital zircons allow us to (a) place a maximum age of deposition on the sediment itself; (b) determine the age characteristics of the provenance of the sediment; (c) through comparison of the provenance regions for different packages of sediments test palaeogeographic reconstructions; and (d) apply the chemistry and other isotopic systems (generally O and Hf) of the zircons to constrain the nature of the crust that was eroding (i.e. juvenile vs recycled).

All such approaches make some inherent assumptions regarding the zircon sample being analysed. First and foremost, it is critical to assess whether the sample collected in the field is truly representative of the facies/unit being studied, and, for provenance studies, whether the stratigraphic horizon being analysed is typical of the broader package. For example, conglomeratic horizons are likely to represent more locally derived detritus than shales; however, shales will contain far fewer zircon grains and those that are present will be of smaller size. Indeed, simply selecting zircons from a sample on the basis of size may well be biasing the subsequent age data by over-representing one particular source of detritus with respect to another, possibly more distal source of smaller grains. So, too, preferentially avoiding fractured or metamict grains may result in bias as such grains may be the only record of a particular lithology or province which is supplying sediment to the system. Therefore one approach is to simply analyse representative grains of every population separated, acknowledging that there will be significant resultant scatter in the data set with some poor-quality data due to the analytical challenges involved. More commonly, however, due to constraints on time and cost, grains are selected from specific populations which are thought to be most representative (i.e. often equated with the most abundant in the sample!) and also most likely to yield analytically robust data (i.e. not metamict or fractured, and with simple morphologies or clear core–rim relationships). Such approaches acknowledge the concomitant biases, but these can be overcome to some extent by simply analysing more grains, thus catching examples of the smaller populations which fulfil the criteria for ‘good’ analysis.

In contrast with igneous or metamorphic geochronology, in which the aim is to date a single event (i.e. the age of magmatism or metamorphism), detrital zircon geochronology aims to characterise the complete detrital age population through (ideally) a large number of single-grain analyses. Data obtained are often first displayed on a concordia or Tera–Wasserberg diagram to illustrate the spread in ages obtained, and how concordant the data are. Generally a filter is applied to exclude highly discordant analyses – for detrital studies this might be those with >10 per cent discordance.

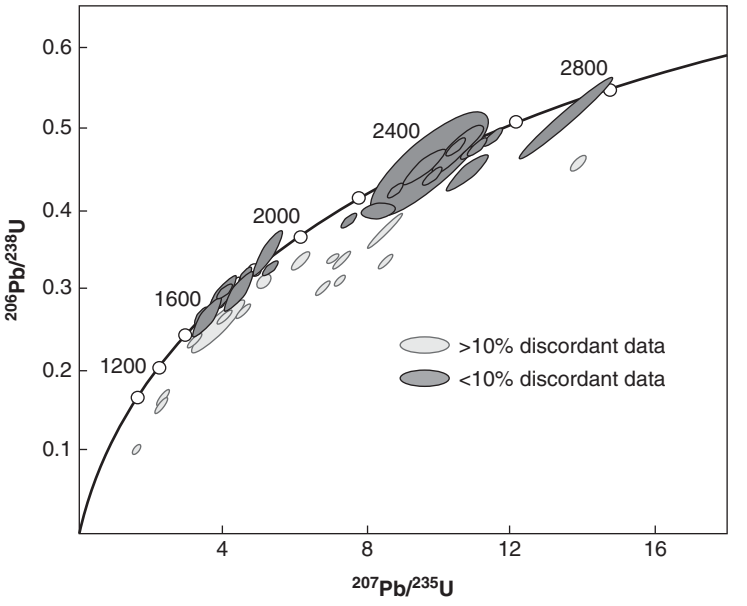

Figure 11.4 Concordia plot displaying detrital zircon data for a metasedimentary rock from the Proterozoic of Australia (author's unpublished data).

Because *in situ* techniques such as SHRIMP or LA-ICPMS generate large volumes of data, and due to the large number of different populations present in a typical sediment, such figures are very busy and difficult to see clearly for interpretation. Figure 11.4 is one such example, highlighting the issues of discordance and the possibility of multiple populations being obscured by the scale of such plots.

A more effective way was to present the data as frequency histograms, whereby the number of analyses falling within a particular age range (termed 'bins') can be plotted against the age, thus providing both a visual representation of the actual range and the relative proportions of the populations present. Statistically, the goal of such an approach is to attempt to move beyond simple visual characterisation of such spectra, where a single age population may be disproportionately large in that particular sample, or the bin size (the 'bandwidth') of the age populations is arbitrarily assigned (e.g. 250 Myr in Figure 11.5). Instead, it is necessary to statistically estimate a probability distribution function (PDF), which is an estimate of the relative likelihood of the different ages within the population being statistically significant.

Hence, a statistically robust PDF will give the probability for a randomly selected grain from the population falling within a given age range. This probability is expressed as the integral of PDF over the specified age range:

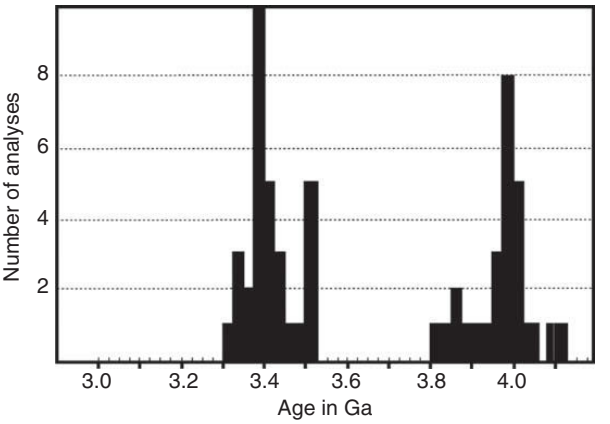

Figure 11.5 Cumulative frequency histogram for a detrital zircon population. Each age is placed into an arbitrarily assigned 'bin' (or age range, in this case 250 Myr) and the total number of zircons analysed in each bin is considered to constitute an increasingly significant source of detritus to the sediment.

$$P(t_1 \leq t \leq t_2) = \int_{t_1}^{t_2} \mathrm{PDF}(t)\mathrm{d}t. \qquad \text{(Eq 11.1)}$$

Without delving deeper into the statistical underpinnings of this approach, in geosciences the method used to estimate the PDF is based upon a function that cumulatively stacks a Gaussian bell curve on top of each age measurement whose standard deviation is determined by the analytical precision of that individual measurement. This is in contrast to simply counting the frequency of ages that are returned in each bin interval, as per Figure 11.5. This is because poor data can end up looking very significant on a plot such as Figure 11.5 – for example, the population of five analyses at 3.5 Ga might look very important, but it may be that analytically each of those zircons returned ages of ±100 Myr, whereas the five zircons at 3.4 Ga might have a precision of the order of ~10 Myr. Hence, if we had selected a bin size that was smaller, our 3.5 Ga population might have ended up being distributed into small groups of one grain each, whereas the 3.4 Ga population, along with the 3.375 Ga population might still be tightly clustered, pointing to a true population at about this time.

There are several ways to circumvent this issue. Conventional statistics applies a smoothing algorithm to convert from the discontinuous histogram (e.g. Figure 11.5) to a smooth and continuous alternative via a kernel density estimator (KDE). Avoiding the statistical background, this can be conceptually considered as sequentially stacking the measurements along a line (in geology corresponding to the age returned by the analysis) and stacking a kernel of a certain bandwidth on top of them. Generally a Gaussian curve of equal

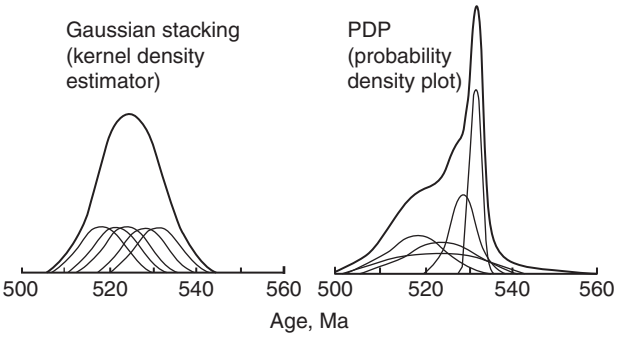

Figure 11.6 An example of a kernel density estimator (KDE) and probability density plot (PDP) for a detrital zircon population whereby individual zircon analyses and their associated error are illustrated by the thin lines. In the KDE (left), individual ages are effectively assigned a uniform error via the selected bandwidth; in the PDP (right) they are weighted as a function of their analytical precision. A cumulative curve is calculated at each given age as a function of the sum of the signals contributing to the age, effectively 'stacking' the curves at a given time.

bandwidth (conventional KDE) is applied to each measurement (Figure 11.6). If locally very large numbers of analyses are present then the bandwidth may vary according to the density of measurements within a particular age range (adaptive kernel density estimation), reflecting the increased number of measurements contributing to the final frequency plot. Effectively, such kernel estimators apply the same precision in age to each measurement (locally at least in the case of adaptive estimators) and generally have the assumption that geological data sets are unimodal and smooth. Given that geological data sets in general, and detrital zircon data sets in particular, are neither smooth nor unimodal, such a statistical approximation is inappropriate and only a minor step forward over a histogram.

A probability density plot (PDP) attempts to circumvent this issue by weighting the significance of each age as a function of its precision, and then summing the total probabilities at each given age. Obviously this approach gets around the issue of arbitrary bin selection and assigning a uniform precision as per KDEs, and gives a more realistic approximation of the relative proportions of zircons of differing ages in a given population. However, it does also introduce its own biases. Importantly, it implies that simply by virtue of more precise age, a given zircon is considered to be more geologically significant than others in the same sample. This is clearly not the case, and certain zircons within the population which are sourced from different rock types may be analytically more challenging than others due to their provenance

(e.g. higher U and Th contents leading to more metamict zircons and hence more Pb loss in one population with respect to another). Therefore the PDP is an excellent visualisation tool which is extensively used in the earth sciences for visual comparison of data sets, but just as in the case of an isochron, a high degree of analytical precision does not always imply a geologically meaningful answer.

11.1.3.1 Data interpretation

Maximum depositional ages First, a sediment cannot be older than the (detrital) grains it contains. Therefore it is possible to place a maximum age for the deposition of the sediment ('max dep' age) based on the age of the youngest zircon grains analysed in a sediment. Obviously the youngest grains need not be synchronous with the age of deposition, as they could be recycled from older sediments or very ancient source rocks in the hinterland. A useful way to conceptualise this might be to consider a modern beach sand, which will be made up of an abundance of quartz grains. More significantly it will contain detrital grains of various heavy minerals (rutile, ilmenite, garnet, zircon), depending on what is available to be eroded and supply detritus to the beach. Beaches on the margins of ancient cratonic nuclei with no active tectonism will therefore contain zircons which are very much older than the depositional age of the beach itself. In contrast, beaches forming in active tectonic regions where zircons are actively forming and eroding (e.g. continental arcs such as the Andes, or rapidly exhuming terranes such as the Himalaya) can potentially receive zircons which are of an age very close to the age of deposition of the sediment. Therefore detrital zircons can be used to place broad constraints on the age of deposition itself.

Sediment provenance Given the above discussion regarding maximum deposition ages, is it possible to extract more information regarding the nature of the crust that was eroding at the time of deposition? In many cases the answer is yes, and often this can be quite straightforward for cases in which the sediments are juvenile with a short transport distance from the material that was eroding – often in such circumstances (unless there has been very significant tectonic dismembering of the terrain) the source of detritus may be preserved nearby, along with unconformities due to the short transport distance. Hence a detrital population may contain zircons with ages that correspond to the intrusive ages of granites in surrounding basement terrains (say), and often it would appear reasonable to suggest that these granites were exposed at the surface in order to be eroded into the sedimentary sequence being analysed. In reality, conglomerates are the best test, even in these circumstances, as it is possible to

compare directly the zircon populations of clasts in the conglomerates with comparable lithologies in the hinterland. Often, however, in such well-preserved scenarios the sedimentological evidence for the source of the detritus is more powerful, and hence more compelling for reconstructing past depositional environments. The utility of a detrital zircon approach is where there may be several potential source regions, on either a local or a continental scale, and distinguishing between them can be critical for plate-scale reconstructions.

This can be critical when considering source regions containing multiple numbers of similar lithologies. Since many granites (for example) appear similar, many studies have returned results in which the detritus does not contain the same populations as the adjacent basement lithologies, much to the surprise of the investigators. This situation could imply the presence of other source regions which are no longer exposed, tectonically removed or, even more problematically (and often likely, particularly in the case of ancient sediments), eroded completely and hence no longer in existence. Therefore simple reconstruction of provenance on the basis of pattern matching the ages of detrital populations requires systematic elimination of possibilities in order to be able to confidently predict links between source and sediment. Indeed, the manner of interpretation of detrital populations depends largely on the nature of the problem to be solved (i.e. is one trying to reconstruct the relative movement of continental blocks with respect to each other through time, or correlate two packages of now far removed sediment with each other?).

11.1.3.2 Hf–Pb in zircons

Since Pb isotopes potentially provide a precise *in situ* chronometer within zircons, the ability to couple these analyses with *in situ* Hf isotopes provides an extremely powerful tool for exploring crustal evolution. Such analyses can be conducted either by SIMS, such as the SHRIMP, or using laser ablation coupled with MC-ICPMS.

Whereas Nd and other lithophile isotope systems are either present in low abundances in zircon, or they possess masses with significant interferences during *in situ* analysis (e.g. ^{87}Rb on ^{87}Sr), Hf is an excellent target for isotopic analysis. This is largely because Hf is able to substitute for Zr in the lattice and thus it is highly resistant to mobility and contamination. Indeed, very high abundances can produce the mineral hafnon (cf. zircon) instead. The very high Hf concentrations produce very low Lu/Hf ratios and thus minimise the affects of age corrections. Most importantly, Pb and Hf isotopes can be obtained from the same spot or domain within the zircon crystal, allowing multiple crustal histories to be derived from complex grains with a high degree of confidence.

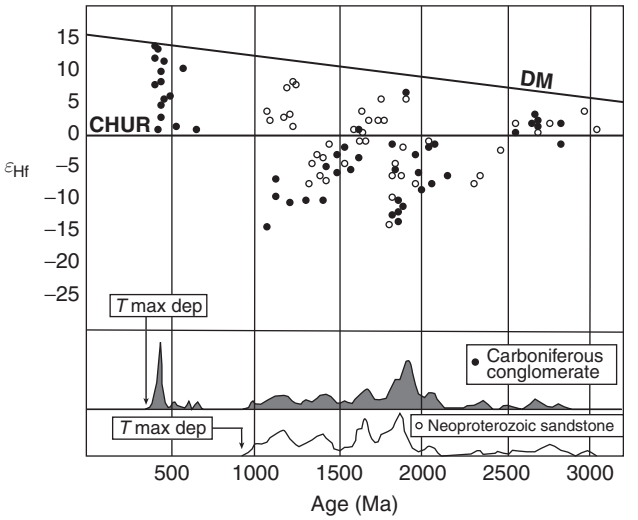

Figure 11.7 Detrital zircon U–Pb and Hf *in situ* isotopic data from two hypothetical sedimentary packages of different ages in the same terrain. The lower panel summarises the U–Pb ages as a probability density curve for each unit. Hf isotopic data are plotted as epsilon Hf (ε_{Hf}) at the U–Pb age determined for the same analytical spot. CHUR, chondritic uniform reservoir and DM, depleted mantle.

Figure 11.7 presents some hypothetical data from two sedimentary packages in the same terrain (and potentially the same terrane – see the glossary for the distinction between these terms). The U–Pb crystallisation ages are presented in the lower-most two panels as a probability distribution curve. This example has an identical number of analyses from both sedimentary packages, and hence the proportions of age populations represented by the relative heights of the two curves are directly comparable (i.e. the total area under each of the two curves is the same). When comparing age distributions in a quantitative sense for packages that may have significantly different numbers of analyses (e.g. 40 analyses from one sediment and 300 from the other), it may be necessary to normalise the curves in order to allow meaningful comparison. Commonly, however, this additional normalisation step is omitted and a visual, qualitative comparison undertaken.

The example in Figure 11.7 is immediately quite striking. Both packages contain peaks of detrital zircons at ~1.85–1.9 Ga and a subordinate peak at ~1.6, 1.4 and 1.1–1.2 Ga. The Carboniferous conglomerate also contains a large population at ~330 Ma, which obviously will not be observed in the Neoproterozoic sandstone since these zircons grew well after the Neoproterozoic. Indeed, this forms the basis of the maximum age of deposition (*T* max dep in Figure 11.7, colloquially referred to as ‘max dep age’), whereby we know that the sediment cannot be older than any

of the detrital grains contained within it. Hence, on this basis the Carboniferous conglomerate must have been deposited after ~330 Ma and the Neoproterozoic sandstone after ~950 Ma. Remember that these ages are simply maximum values – they could have been deposited substantially afterwards, so the ages of detrital grains alone are not generally a robust guide to the actual age of deposition of the sediment.

However, based on the U–Pb alone, it would seem reasonable to conclude that the Devonian conglomerate was simply sourced from the sandstone with an additional component of younger zircons from a region that formed after the sandstone was deposited. This is because of the striking similarity in not just the ages of the zircons in the two packages, but also the relative proportions of zircons in the populations. Alternatively, the conglomerate could have been sourced from the same terrane as that which supplied detritus to the sandstone, but given the difference in age between the two sediments (~400–500 Myr between the Neoproterozoic and Carboniferous) it would be highly unlikely that the same source region would be available to erode in the same proportions during the Carboniferous as it did during the Neoproterozoic. Although it is impossible to rule this latter possibility out completely from the U–Pb data, geologically the preferred interpretation would be recycling of the sandstone and hence the zircons within it.

However, when the Hf isotopes for the same zircons are considered, it seems that the story is more complex than first thought. While all of the zircons from the 1.85–1.9, 1.6 and 1.4 Ga populations in both packages of sediments have the same ε_{Hf} values at the relevant time, it is quite clear that the Hf isotopes for the 1.1–1.2 Ga populations are very different for the two sedimentary packages (Figure 11.8).

The Neoproterozoic sandstone contains 1.1–1.2 Ga zircons which have quite juvenile Hf isotopes – i.e. they contain ε_{Hf} values which are all greater than zero, whereas zircons of the same age in the Carboniferous conglomerate all contain $\varepsilon_{Hf} < 0$ (i.e. negative values) which correspond to older, recycled continental crust. Therefore the Carboniferous conglomerate cannot simply be deriving detritus from eroding the Neoproterozoic sandstone – it instead has to be obtaining zircons from a completely different source than those preserved within the sandstone. Therefore these two sedimentary packages are seeing detritus from two distinct terranes.

This notion of how isotopically juvenile or ancient a given zircon is can be a very powerful tool not only in distinguishing between detrital source regions but also in studies of crustal growth. In a manner analogous to Nd whole-rock model ages described in Section 11.1.1, multiple analyses of many individual zircons can be used to monitor whether the zircons were growing during

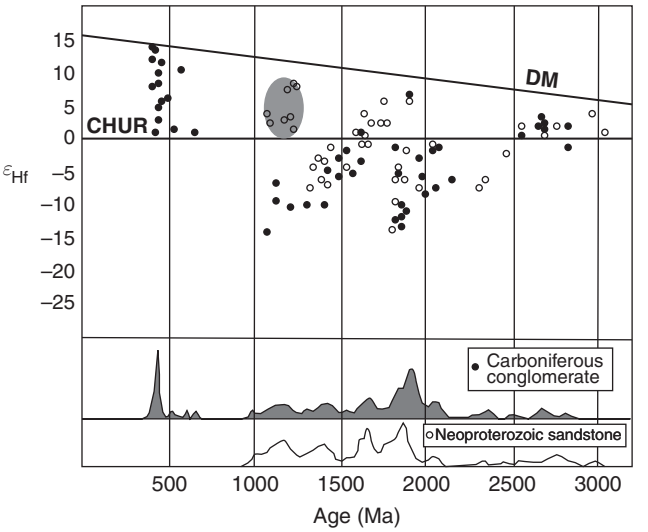

Figure 11.8 As for Figure 11.7, but with the population of isotopically juvenile zircons at ~1.1–1.2 Ga from the Neoproterozoic sandstone highlighted.

periods of addition of material from the mantle, or simply melting and recycling existing continental crust.

Ancient crust will naturally evolve with time towards lower (more negative) ε_{Hf} values due to the ingrowth of ^{176}Hf due to decay of ^{176}Lu. Growth of new zircons within this crust through melting or metamorphism will preserve the ε_{Hf} value of the crust at the time of growth. Such crustal recycling and subsequent erosion will result in detrital zircons preserving positive arrays on Figure 11.9, with a range of ages and increasingly negative ε_{Hf} through time. If, however, new magmatic material comes from the mantle at a given time and mixes with existing crustal material, then vertical mixing arrays are produced.

In some cases the crustal growth may be dominated by the mantle input with relatively little mixing with existing crust (such as the ~330 Ma event in Figure 11.9), whereas others may be dominated by mixing (e.g. the 1.85–1.9 Ga event in Figure 11.9) with very little preservation of the juvenile component (see also Figures 11.1–11.3 for an illustration of these contents using Nd isotopes). Indeed, the ~330 Ma event in the illustration here does not preserve any zircons which are themselves highly evolved, suggesting that the ancient crustal terrane that these mantle-derived magmas must have mixed with was not itself exposed at the surface of the earth at the time of deposition of the sediment. However, we can infer its existence from the quite distinct linear array in Figure 11.9.

On a global scale such a distinct time-evolved sawtooth pattern of intracrustal recycling punctuated by periodic (some would argue episodic) crustal growth

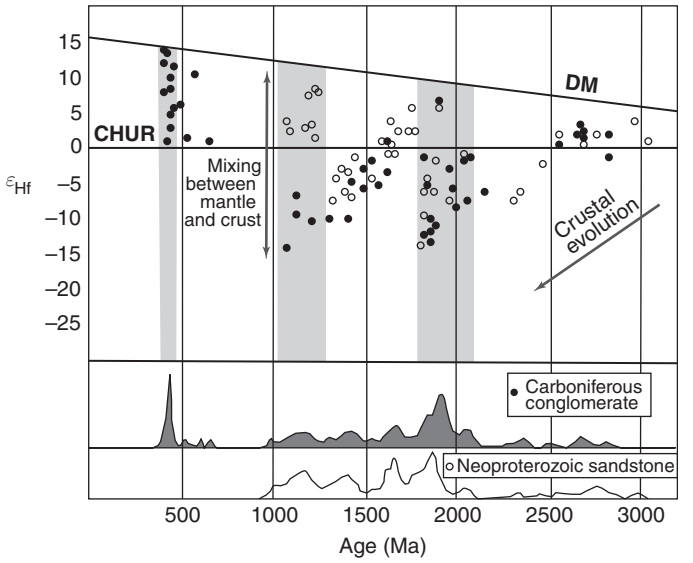

Figure 11.9 Hypothetical detrital zircon populations from Figure 11.7 in terms of distinguishing between addition of new material to the mantle, constituting crustal growth, and recycling of materials already within the crust. Recycling will form arrays with positive slope over a range of ages corresponding to the bulk crustal evolution. Input of new material from the mantle will produce vertical arrays between new, juvenile material and existing crust. Time intervals of crustal growth are shaded in grey.

events is observed for all Precambrian terranes. Hence the U–Pb Hf zircon approach is powerful not just at regional scales but can be scaled up to a cratonic and ultimately global assessment of the growth and stabilisation of the crust.

One of the most sophisticated approaches to this understanding from a metallogenic point of view has been the TerraneChron® approach whereby zircons are collected from modern drainage systems. This approach eliminates some of the potential biases inherent in the sampling of zircons from individual lithologies on a regional scale (and often can access lithologies that are currently buried by regolith), and large numbers of zircons are randomly analysed in order to provide appropriate weighting of the populations observed. Data are then interpreted on a modified version of Figures 11.7–11.9 whereby rather than plotting ε_{Hf} on the *y*-axis, the difference between the *actual* zircon crystallisation age and the Hf depleted mantle model age (T_{DM}) is plotted (Figure 11.10).

The utility of such event signature diagrams is that they can effectively summarise very large data sets on a regional scale. Significantly, world-class mineralisation is often associated with significant juvenile addition to the crust – in some cases this might be through addition of an inventory of metals,

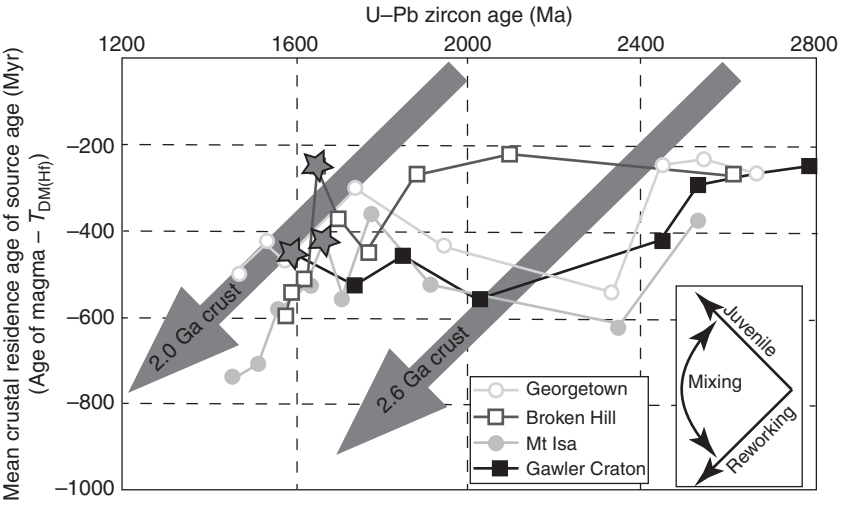

Figure 11.10 Event signature diagram for four Australian Precambrian terranes. Periods of juvenile addition to the crust are recorded by upward inflections in the crustal evolution trajectories for each terrain, whereas intracrustal reworking produces vectors which parallel the bulk crustal evolution vectors (grey arrows). Periods of mineralisation (stars) often accompany significant juvenile input within a given terrain, whereas the dominant long-term pattern for terranes is one of mixing between juvenile and reworked components to produce a broadly horizontal array. Reproduced with permission from Belousova *et al*. 2009, *Lithos*, pp. 570–582.

or in others simply providing a large source of heat to drive mineralising systems. Such relationships can be of great importance in area and even terrain selection.

Finally, the advent of increasingly sophisticated sampling and streamlining of analytical techniques by both SIMS and LA-ICPMS has resulted in a proliferation of high-quality data. Significantly, identification of potential source terranes can be done in a more sophisticated manner than simply comparing peaks in detrital zircon ages and then looking at the Hf isotopic signatures of these peaks on a unit-by-unit basis, such as in Figures 11.7–11.9. Access to regional-scale 'meta' data sets allows potential tracking of whole terranes with respect to the evolution of individual basins, thus providing a basis for tectonic reconstructions. Potential source terranes may have thousands of U–Pb and Hf *in situ* analyses, resulting in very confusing and hard-to-interpret diagrams (e.g. Figure 11.11a). Application of statistical contouring algorithms to the large baseline data sets (e.g. Figure 11.11b) can therefore allow a rapid visual comparison for large numbers of detrital zircons at a glance. Such an approach can aid in very rapid elimination of potential sources

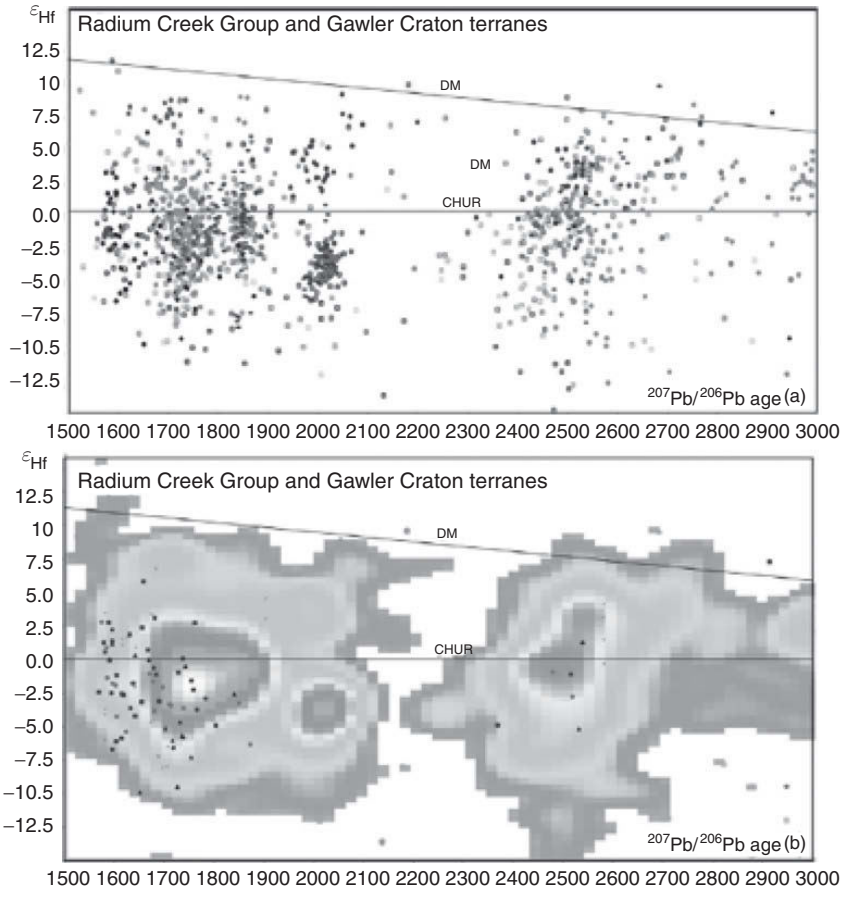

Figure 11.11 Use of U–Pb Hf plots for terrain comparison. (a) Data points from several studies from the terrane of interest (Radium Creek Group in the Mt Painter Inlier) are plotted with respect to many different lithologies from a potential source terrane, the neighbouring Gawler Craton. (b) In order to clarify the comparison, the Gawler Craton data are contoured in order to highlight the relative data density and visually compare the degree of similarity between the two. In this example data are gridded in 20 Myr bins and 0.5 ε_{Hf} units. Please see the original publication for a complete list of data sources for the more than 1000 analyses summarised in this figure. Reproduced with permission from Armit *et al.*, 2014, *Precambrian Research* 243, pp. 63–87.

of detritus, and on a more fundamental level determines whether two adjacent terranes have experienced the same tectonic evolution and hence first-order potential mineral prospectivity. Such data can be preserved through cycles of even quite high-grade metamorphism (amphibolite and in some circumstances granulite), and thus also offer a tool for investigating crustal evolution and interaction with the mantle.

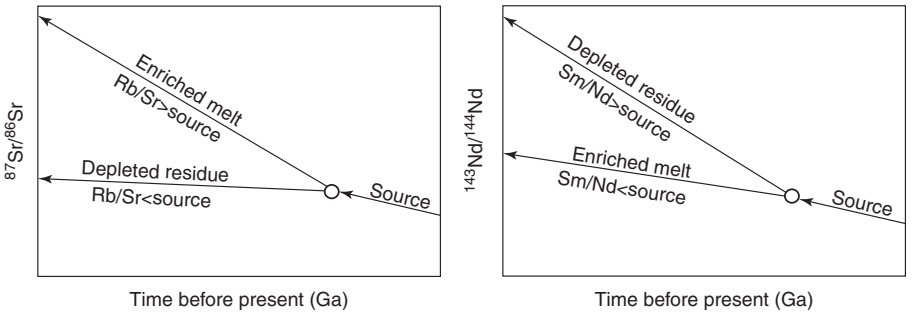

Figure 11.12 Schematic Rb/Sr and Sm/Nd isotopic evolution of a source region that experiences melting. The melting event produces a melt which is enriched in incompatible elements and a residue that is depleted in incompatible elements. Because Rb is more compatible than Sr in mantle melting situations, the melt will have a higher Rb/Sr than both the source and residue, and hence over time will evolve to radiogenic $^{87}Sr/^{86}Sr$. In contrast, Nd is more incompatible than Sm, and hence the melt will have a low Sm/Nd ratio and hence it will ingrow ^{143}Nd comparatively slowly compared with the source and the melt depleted residue.

11.2 Isotopic characteristics of the mantle

As alluded to above, many of the isotopic records of crustal evolution rely heavily on some assumptions regarding the nature of the mantle and the interaction of the crust with the mantle. However, from a geodynamic perspective, the mantle itself is not a single discrete entity, both in a physical (e.g. convecting vs lithospheric) and in a chemical (e.g. oceanic vs continental vs asthenospheric) sense. The manner in which the earth has differentiated and the resultant mantle evolution have resulted in a range of different mantle compositions which are able to interact with the crust in a variety of ways, each having different isotopic consequences.

To a first order, the crust and mantle can be considered in terms of partial melting of a chondritic source. This will produce a melt which is enriched in incompatible elements (i.e. those with $D < 1$ which ultimately form the crust) and a residue which is depleted in these elements (a mantle). Correspondingly, this process is able to fractionate the parent and daughter trace element ratios in both reservoirs, resulting in distinctive subsequent isotopic evolution. For example, the Sm/Nd ratios will be higher in the residue (mantle) and lower in the melt (crust, see Section 11.1.1). Hence the residue will develop radiogenic Sm–Nd isotope signatures (positive ε_{Nd}) with time (e.g. Figure 11.12). To a first order approximation, such a situation can be considered analogous to the formation of two terrestrial reservoirs, namely the continental crust and a complementary portion of the mantle, the so-called ‘depleted’ mantle.

11.2.1 The depleted MORB mantle (DMM)

This is depleted mantle which is sampled by mid ocean ridge basalts (MORB) during decompressive melting at mid ocean ridges. Even though MORB are themselves melts, they possess incompatible element depleted signatures which are consistent with melting of a source which has previously had melt extracted. Further, they have high $^{143}Nd/^{144}Nd$, confirming that the source of these magmas has experienced long-term enrichment in Sm with respect to Nd. This depleted mantle reservoir (or DMM for depleted MORB mantle) is thought to comprise the upper portion of the asthenosphere, and corresponds (very broadly) to the residue illustrated in Figure 11.12. Hence the DMM is characterised by high $^{143}Nd/^{144}Nd$, subchondritic $^{87}Sr/^{86}Sr$ and chemically depleted LREE and incompatible element patterns due to prior melt extraction events (Table 11.1).

Interestingly, if we view the continental crust as the complementary reservoir to DMM, and assume that continental crust, once it is formed, is not efficiently (or no significant volume is) recycled into the mantle, then an estimate for the volume of DMM required to extract the continents from can be made. Since continental crust approximates a 10 per cent partial melt of a chondritic starting composition, we calculate that the DMM should be an order of magnitude larger than the continental crust. Significantly, since the DMM comprises the upper convecting portion of the mantle, it is able, over long time scales, to effectively homogenise chemical and isotopic heterogeneities to produce a reservoir that is broadly quite homogeneous. This reservoir directly underlies all lithosphere in the planet, and is potentially available to be sampled by or mixed in with ascending plumes, to be metasomatised by subducting slabs, to interact with lithospheric mantle and to be directly accessed by rifting. In this sense the DMM can be considered to be the most accessible portion of the convecting Earth, and as such it is considered to be the starting point for addition of material to the continental crust during crustal growth. The actual mechanism, whether by a two-stage process in subduction zones in modern plate tectonics or through vertical accretion, partial melting and internal differentiation in Archaean tectonics, depends on one's perspective of the tectonic and geodynamic drivers during this time.

11.2.2 Ocean island basalts and continental flood basalts

While the DMM is sampled by MORB and provides a relatively uniform signature, other sources of basaltic magmatism in the ocean basins preserve distinctly different isotopic signatures. Ocean island basalts (OIB) associated with hotspot (e.g. Hawaii) or possible wetspot melting, or some combination

Table 11.1 *Compilation of present-day isotopic parameters for some terrestrial mantle reservoirs, for illustrative purposes.*

	Chondrite	Primitive mantle	Depleted MORB mantle (DMM)
Rb	2.32	0.635	0.0408
Sr	7.8	21.1	12.935
$^{87}Rb/^{86}Sr$	0.86031	0.08703	0.022
$^{87}Sr/^{86}Sr$	0.7047	0.7033	0.7025
Sm	0.1471	0.444	0.3045
Nd	0.4524	1.366	0.7375
$^{147}Sm/^{144}Nd$	0.1960	0.1969	0.2137
$^{143}Nd/^{144}Nd$	0.512630	0.512638	0.513215
Lu	0.0251	0.074	0.058
Hf	0.0106	0.309	0.157
$^{176}Lu/^{177}Hf$	0.0336	0.0245	0.0384
$^{176}Hf/^{177}Hf$	0.282785	0.28276	0.28326
Re (ppb)	36.5	0.272	0.270
Os (ppb)	486	3.4	3.43
$^{187}Re/^{188}Os$	0.3972	0.385	0.379
$^{187}Os/^{188}Os$	0.12757	0.1296	0.1280
U	0.0081	0.021	0.0022
Pb	2.47	0.084	0.018
Th	0.0294	0.071	0.0059
$^{206}Pb/^{204}Pb$	18.4	18.35	18.0
$^{207}Pb/^{204}Pb$	15.58	15.51	15.43
$^{208}Pb/^{204}Pb$	38.9	38.1	37.7

Abundances in ppm except where stated. Many of these parameters can be used for ε, γ and model age calculations. Care must be taken when comparing across isotope systems as terms such as 'primitive mantle' vary subtly in their meaning between Re–Os (primitive upper mantle, or PUM), U–(Th)–Pb (cf. PREMA, PHEM, FOZO and C) and Sr, Nd and Hf. Data compiled largely from the Geochemical Earth Reference Model (GERM) database and references therein, or calculated by the author. Care should be taken when using such parameters to ensure an internally consistent data set that is appropriate for the problem at hand.

of the two, preserve a variety of isotopic signatures that reflect heterogeneities within their sources. Commonly the source of such magmatism is also the convecting mantle; however, due to the nature of the isotopic differences with MORB there is clear evidence for ancient, chemically and isotopically discrete reservoirs within the earth.

The relationship between OIB sources and the large-scale development of the crust–mantle system has been the subject of much investigation. This has led to the recognition of several geochemically and isotopically distinct reservoirs, or end

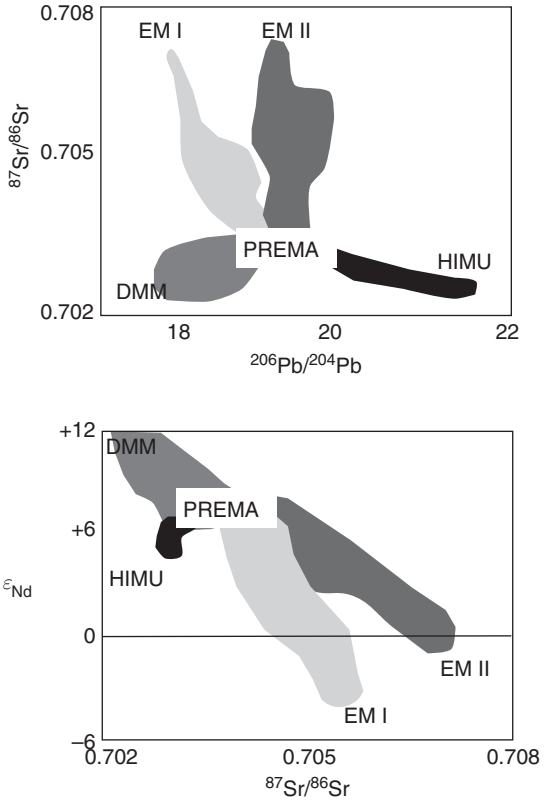

Figure 11.13 Isotopic variation diagrams for ocean island basalts (OIB) and MORB. The arrays on such diagrams appear to consist of a common component (PREMA, or 'prevalent mantle') which is then variably mixed or incorporated with isotopically distinct reservoirs within the mantle, as represented by the shaded fields. Plumes which show significant interaction with the upper mantle will mix towards the DMM, which is the source of MORB. The other components sampled reflect different types of recycled material within the mantle.

member components within the deep mantle. A first-order significant observation is summarised in Figure 11.13, whereby OIBs appear to diverge from a single common component (prevalent mantle, or PREMA) towards several other isotopically distinct end members. One end member is clearly due to mixing with the DMM, but there are also highly radiogenic Sr and Pb isotopic end members. The definition and description of these (EMI, EMII, HIMU, FOZO, etc.) has given rise to the 'mantle zoo' concept. While many of the nuances associated with the significance of these reservoirs are beyond the interest of many industry professionals, it is worth exploring the terminology and potential significance of such designations as they ultimately place first-order constraints on the nature of crust–mantle interaction and hence material and heat transfer to the continents.

Mantle plume activity (and hence the vast majority of OIB generation) is best characterised and most thoroughly studied in the ocean basins. Plume activity undoubtedly also takes place beneath the continents (most dramatically in the generation of continental flood basalts (CFB), arguably attendant upon the impingement of a mantle plume head at the base of the lithosphere); however, the potential for contamination and interaction of magmas with continental lithosphere adds an element of ambiguity to interpretation of plume mantle source characteristics. Therefore, the sample of OIB available to directly investigate on the modern earth is restricted to <200 Ma in age, this corresponding to the oldest surviving oceanic crust. OIB on the modern earth range from large buoyancy flux systems which are likely to be sourced from deep within the mantle (potentially even the core–mantle boundary) such as Hawaii and Iceland, and volumetrically smaller hotspot (wetspot?) volcanic systems such as the Azores, Samoa and Kerguelen.

Three end member compositions are generally invoked to describe the lithophile isotopic heterogeneity present within OIB. Termed EMI, EMII (enriched mantle sources) and HIMU (high-μ components; $\mu = {}^{238}U/{}^{204}Pb$), these are present in varying proportions in most OIB. Several workers have ascribed subtly different common components to all plumes (PREMA as above, FOZO or 'focal zone', C or common component), which are subsequently modified by mixing or interaction with portions of other distinct mantle sources. The differences between C, FOZO, PHEM and PREMA are incredibly subtle and of little significance here; they can all be considered to be a ubiquitous component present in the mantle source of plume magmas. Indeed, precisely where (or indeed whether) PREMA and equivalents are located has been the source of debate – whether these represent portions of the lower mantle or variably (un)depleted portions of the lower upper mantle is still open to research.

Of more interest is the nature of the end members that the OIBs are mixing towards. In broad terms, HIMU can be thought of as dehydrated subducted oceanic crust, EMI as subcontinental lithosphere mantle and EMII as terrigenous sediment. The rationale behind these assignations will be touched upon briefly below, but when describing these end members it is important to remember that when discussing EMI as subcontinental lithospheric mantle (SCLM) it is considered to be SCLM that has become detached from its attendant continent and is now a discrete entity within the convecting earth. So, too, terrigenous sediment refers to sediments that have been recycled into the deep earth, most probably by subduction. Further, it must be stressed that in no currently active hotspots are pure samples of any one of the three end members observed, but rather combinations of them.

From an isotopic perspective, both EMI and EMII contain radiogenic Sr isotopic ratios and unradiogenic εNd. Both features are typical of continental lithosphere due to the relative enrichment of Rb and Nd in the contents as a consequence of melting of the mantle during continental formation (see Figure 11.12). However, EMI possesses less radiogenic $^{87}Sr/^{86}Sr$ and $^{206}Pb/^{204}Pb$ than EMII, implying a source that has lower Rb/Sr and U/Pb. The SCLM contains such features, whereas the continental crust, and terrigenous sediments in particular, have very high Rb/Sr and U/Pb, resulting in significant ingrowth of radiogenic Sr and Pb, respectively. Hence, EMII appears to be a good match for average continental crust, and the most efficient mechanism for getting continental crust into the convecting mantle is via subduction of eroded continental material; i.e. terrigenous sediments.

In contrast, HIMU lavas contain exceptionally radiogenic Pb isotopes with virtually no radiogenic Sr and more radiogenic Nd than the EM sources. The Nd isotopes of HIMU basalts are not as enriched as modern-day DMM, but the positive εNd values do suggest a source that has been depleted (i.e. containing a high Sm/Nd) in the past. One mechanism that is quite effective at producing this combination of features is the subduction of oceanic crust. When oceanic crust is formed, it will have the Sr and Nd isotopic signatures of the DMM at the time – hence it will have positive εNd and unradiogenic Sr. However, a significant feature of subduction zones is the ability to fractionate U from Th and both U and Th from Pb due to redox-sensitive reactions which occur in the aqueous fluids fluxing from the downgoing slab. The relative solubilities of U and Th in aqueous fluids derived from slab dehydration are low when compared with that of Pb. Hence Pb will be depleted and Th and U comparatively enriched in the slab residue which may ultimately source OIB. It is this chemical fractionation which is able to produce the time-integrated high U/Pb ratios in the residual slab, and are thought to be the ultimate source of the HIMU component in OIBs. One caveat to these observations is that U mobility in aqueous fluids is strongly redox dependent. U^{6+} is able to form fluid mobile complexes, but if a significant proportion of the U is present as U^{4+}, then it is still possible to generate enrichment of U with respect to Pb during slab dehydration. Since it is this enrichment which is responsible for time-integrated ingrowth of radiogenic Pb (^{206}Pb and ^{207}Pb from U and ^{208}Pb from Th), which is characteristic of the HIMU source, the very observation that this component exists in the mantle requires that subduction zones, at least for a very significant portion of earth history, must have been sites of dominantly reducing fluids. A final test of the fractionation of Pb from U in subduction can be observed in modern-day island arcs, where erupted magmas have relatively low U/Pb

(μ),implying effective stripping of Pb from the slab and transfer into arc magmas and ultimately the continental crust.

Continental flood basalts are often considered to represent the impingement of plume heads upon the lithosphere, resulting in widespread (over thousands of kilometres) voluminous magmatism of comparatively short (5–10 Myr) duration. Generally CFBs show variable degrees of interaction with the overlying continental lithosphere, resulting in potential obscuring of the original features of the plume. However, plumes, and plume heads in particular, are of critical interest in metallogeny as they represent mechanisms of transporting both significant amounts of heat and potentially large volumes of metals, both of which are critical for driving mineralisation. Ultimately the isotopic reservoirs identified in OIBs can often also be identified in CFBs; however, there is not necessarily a link between primary mantle plume reservoirs and metallogenesis. Of more significance is the initial potential temperature of the plume (on the modern earth often a function of plume size) and manner of interaction of the plume with the crust and lithosphere. Phanerozoic plumes typically contain CFBs with tholeiitic basalts and picrites dominating, whereas Precambrian examples can also contain komatiites, which become more common the further back in the geological record one goes. The Bushveld Complex in South Africa, along with other layered mafic igneous complexes, are also arguably the result of plume head magmatism. All are of primary interest in mineralisation for magmatic Ni and platinum group elements (PGE), with many komatiite-hosted deposits in Australia and Canada, and the terminal Permian Siberian traps CFB producing the Noril'sk–Talnakh PGE deposits. In all cases, radiogenic isotopes can play a role in potentially tracking the source of metals and/or sulphur responsible for sulphide precipitation.

Critically, this can take place in several ways. First, all radiogenic isotopic data need to be age-corrected to the appropriate eruptive age, and if comparing with isotopic reservoirs in the mantle or the crust, these too need to be calculated for the appropriate time. The mixing and/or crustal contamination can be tested for through isotope ratio vs inverse concentration diagrams (Figure 10.6) or isotope–isotope diagrams containing likely components (Figure 10.7). Depending on the isotopic systems available, and the potential reservoirs available to interact with (i.e. assimilation, contamination, magma mixing, fractionation, etc.) it is possible to step-by-step strip off the various contributors to the final, crystallised product. Hence this could involve determining the relative contributions from the mantle (asthenospheric vs lithospheric), and indeed in some cases which type of mantle (DMM, EM, metasomatised or depleted SCLM), and then relevant crustal components. The latter are invariably determined by local geology – for example, are the flood

basalts flowing over highly reducing and reactive crustal lithologies such as coal measures as may be the case in West Greenland and the Siberian Traps? Or rather was the local crust very much older and hence highly radiogenic with respect to the plume-related magmatism?

Thus there is no single recipe for investigating a given magmatic system and the relative contribution of crustal and/or metasomatised components – the amount of information able to be derived will be controlled by a combination of petrography, major and trace element geochemistry and then finally by the isotopes. These must always be interpreted in the context of the appropriate local geology, and also from an appreciation of other critical factors pertaining to mineralisation – for example, depending on the source of a picrite, it may have varying concentrations of Ni. There are many ways to induce sulphide saturation and hence precipitation of Ni sulphides from these liquids; however, if this magma is not driven to sulphide saturation, then it will not form a magmatic Ni sulphide ore deposit, regardless of its initial Ni concentration. In contrast, a parental liquid with very low initial Ni values may, in the right conditions (e.g. encountering an external source of sulphur during eruption or emplacement) produce mineralisation. Therefore radiogenic isotopes can be applied either to investigate a system of known mineralisation in order to consider quantitatively the amount of assimilation (see Chapter 10 for the numerical formulation of this), or alternatively, in prospectivity analysis when considering whether a potential parental magma may have experienced interaction with crustally derived reductants elsewhere in the magmatic system.

Note that even all of the preceding discussion is very model-driven – there are assumptions regarding the need for the crust in driving mineralisation; some large igneous provinces may require minimal or even no crustal interaction in order to precipitate magmatic sulphides, depending on their depth of crystallisation and the S concentration of the primary magma. Therefore the radiogenic isotopes are simply an additional tool that can aid in the interpretation of individual systems.

11.2.3 Subduction zones

Subduction zones are the modern-day manifestation of the transfer of material from the DMM to the continents. They represent sites of net continental growth and are the combination of a number of complex geochemical interactions.

To a first order, they are sites where the DMM undergoes melting due to the introduction of water to the mantle wedge in the over-riding plate. The mantle wedge is isotopically a portion of the DMM; however, significant

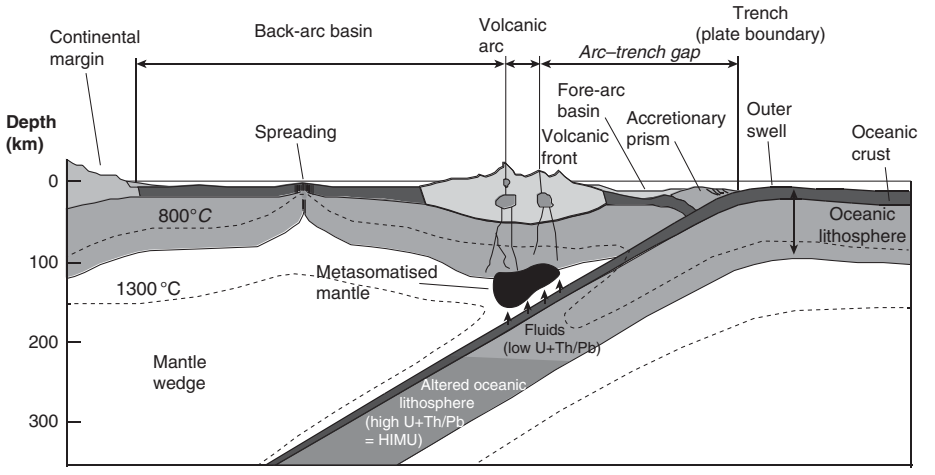

Figure 11.14 Schematic representation of a subduction zone with key geochemical reservoirs. The mantle wedge comprises DMM, which is sampled in back arc magmatism. Dehydration reactions in the down-going slab produce metasomatic fluids with low (U + Th)/Pb which modify both the DMM in the wedge and the over-riding lithospheric mantle. The 'flushed' oceanic lithosphere returns to the deep mantle with elevated (U + Th)/Pb leading to a HIMU component over time. Subduction of sediments (volumetrically minor at this scale) produces the EMII component in the convecting earth. Amalgamation and further differentiation of volcanic arcs ultimately give rise to modern composition continental crust.

metasomatism can take place due to fluxing of volatiles and potentially sediment and oceanic crust into the wedge and melting zone (Figure 11.14). Therefore, arc lavas will combine isotopic signatures of a number of reservoirs; however, the general trend will be to generate melts which are enriched in incompatible elements. Ultimately, arc lavas and hence new continental crust will be enriched in Rb/Sr, Re/Os and depleted in Sm/Nd and (U + Th/Pb). Significantly, it is the impact of subduction on the mantle that is most apparent in isotopic space. Metasomatic fluids derived from the down-going slab (dominated by the oceanic crust and accompanying sediment, but with varying contributions from the oceanic lithospheric mantle) not only drive melting of subduction-modified DMM, but are also able to metasomatise the lithospheric mantle (either oceanic or continental) in the over-riding plate. This metasomatism contributes to the active arc magmatism, but may also persist long after subduction has ceased, potentially providing a fertile source for intraplate magmatism after cratonisation.

Perhaps the most significant impact on mantle geochemistry by subduction is the return of material to the deep earth for potential later sampling. Subduction of

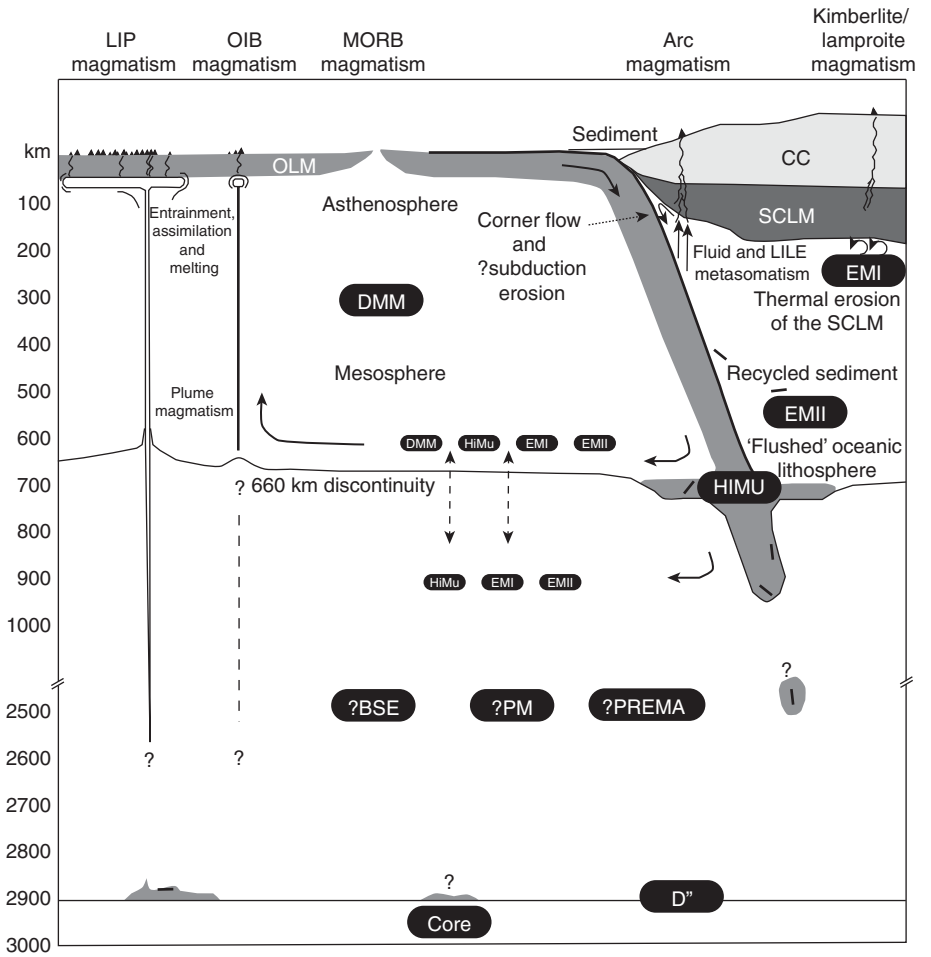

Figure 11.15 Schematic representation of mantle reservoirs and processes responsible for producing mantle heterogeneities. Subduction drives the return of sediment and subduction-modified oceanic lithospheric mantle (OLM) which can either be stored in the upper mantle or potentially pierce the 660 km discontinuity and be stored in D′ at the core–mantle boundary. Long-term evolution of the subducted OLM produces the HIMU reservoir and recycled sediment can be sampled in plumes and OIBs as EMII. Thermal and subduction erosion of the subcontinental lithospheric mantle (SCLM) can transport SCLM into the convecting earth to be resampled as the EMI reservoir. Depleted MORB mantle (DMM) is the chemically depleted residue left after extraction of the continental crust (CC). Note that the asthenosphere applies only to the upper portion of the convecting mantle. PM, primitive mantle; BSE, bulk silicate earth; PREMA, prevalent mantle and related reservoirs (FOZO, C). See text for further discussion regarding the significance of these reservoirs.

sediments can ultimately produce EMII sources, and the fractionation of U and Th from Pb during dehydration reactions in the slab ultimately results in an oceanic lithosphere that has high U + Th/Pb, leading over time to the HIMU (μ = U/Pb) component described above.

Overall the isotopic nature of the mantle can be considered in terms of a relatively small number (although confusingly named) of reservoirs in both the convecting and the lithospheric mantle (Figure 11.15). Their isotopic signatures represent the time-integrated enrichment or depletion of these reservoirs and include a record of arguably pristine mantle, continental crust extraction and recycling of oceanic lithosphere, sediments and continental lithospheric mantle. The manner of sampling of these reservoirs varies, with mantle plumes (in both plume heads and plume conduits as per OIBs), MORB and small-degree partial melts such as kimberlites and lamproites directly sampling portions of the mantle. Arc magmas sample variably metasomatised convecting mantle and hence often mantle signals can be obscured.

11.3 Tracing petroleum migration and sources

Both Re and Os can be considered organophile elements in reducing environments in the presence of organic matter. To a first order the Os isotopic signature of organic matter can be considered to be in equilibrium with the water column it is derived from. However, different portions of a depositional system will contain varying Re/Os while preserving the same $^{187}Os/^{188}Os$ during source rock deposition, thus fulfilling the first basic criteria for an isochron. Often such systems are associated with marine hydrocarbon systems, and hence the initial ratio of this isochron can be applied as a proxy for the seawater composition at the time of deposition. Since Os has a relatively short residence time in modern seawater (~30–10 kyr) that is of an order comparable to the mixing time of the oceans, this system is potentially able to record rapid changes in marine chemistry, particularly glacial–interglacial cycles.

Of more interest in recent times has been the ability to potentially trace hydrocarbon sources and hydrocarbon migration. Conventionally, biomarkers are routinely used in oil-to-source fingerprinting, but many processes, particularly biodegradation, preferentially remove these tracers. However, Re–Os isotope studies of the asphaltene fraction, which is more resistant to biodegradation, can provide both the timing of hydrocarbon generation and Os isotopic fingerprinting of the source rock. With some knowledge of the depositional system, source rock initial ratios ($^{187}Os/^{188}Os_{(i)}$) can be used to independently constrain from where within the basin the hydrocarbons ($^{187}Os/^{188}Os_{(og),}$ where og is oil generation) in question have been derived.

Such relationships are summarised on Figure 11.16. Panel (a) describes the synchronous deposition of a suite of organic-rich sediments in a marine setting. Note that not all samples in this system necessarily have TOC (total organic carbon) sufficient to subsequently generate hydrocarbons. However, they may have TOC levels high enough to effectively partition sufficient Re and Os that the budget of these elements in the sediment is overwhelmingly dominated by a hydrogenous component. Over time, these will ingrow ^{187}Os and define an isochron, as per Chapter 7. The initial ratio of this isochron will be the isotopic ratio of the seawater that was in equilibrium with the organic-rich matter at the time of deposition. Subsequently, at some later time, two of these source rocks undergo hydrocarbon generation, producing various hydrocarbon fractions, all of which are in isotopic equilibrium with their individual source rock (Figure 11.16b). Over time, these hydrocarbon fractions will evolve depending on their individual $^{187}Re/^{188}Os$, and, provided they maintain closed system behaviour, define an isochron with a slope that is directly proportional to the time that has elapsed since oil generation ($t_{(og)}$; Figure 11.16c).

Obviously such an approach contains a huge amount of potential information, but there are also a number of caveats – not least the analytical difficulty of obtaining such analyses and the role of detritus in contributing to the Os isotopic signature. This latter factor has been circumvented to a large degree through improved sample dissolution techniques which preferentially attack only the organic portion of the lithologies. However, at every step it is also critically important to carefully consider what information is actually being recorded in this system with respect to the samples. For example, Figure 11.16b illustrates fractionation of Re from Os during hydrocarbon generation. However, if the oil has migrated, then obviously there will be no whole-rock fraction to plot on the isochron in Figure 11.16c. Further, even though the two samples illustrated in Figure 11.6 generated hydrocarbons from source rocks deposited at the same time in the same depositional setting, each fraction will have its own initial isotopes depending on which source rock within that system they were derived from. If, however, these two oils mixed during trapping, then ultimately the age produced will be on a single isochron from a mixture and hence an age which will be broadly correct (although not as precise) and an initial ratio intermediate between those of the two source rocks (e.g. Figure 11.17).

Such mixing arrays can provide information regarding the time of hydrocarbon migration and final trapping, which can sometimes be different from the actual age of generation. The age of petroleum migration may be very important, but the initial Os ratio of mixtures ($^{187}Os/^{188}Os_{(mix)}$) does not necessarily directly reflect the $^{187}Os/^{188}Os_{(og)}$, in which case extrapolation back to a single source rock is obviously not possible. Testing for mixing

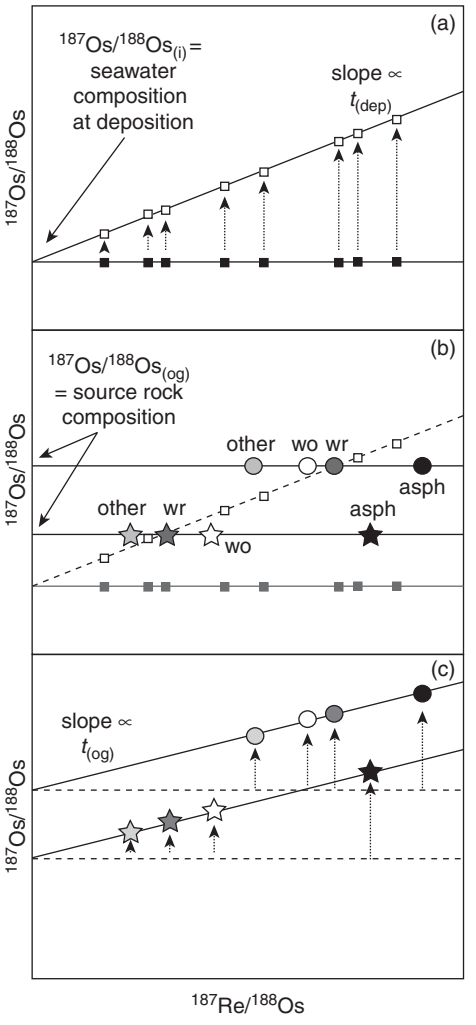

Figure 11.16 Os isochron diagram summary evolution of a simple hydrocarbon system. (a) Deposition of a number of facies of organic-rich sediments in a marine setting produces samples with $^{187}Os/^{188}Os_{(i)}$ in equilibrium with seawater and a range of Re/Os ratios. These subsequently evolve over time to produce an isochronous array with a slope directly proportional to the amount of time elapsed since deposition ($t_{(dep)}$) and an initial ratio equal to that of the seawater they were deposited from. (b) At some time subsequently, the basin is subjected to thermal maturation. Two of the whole rocks undergo hydrocarbon generation of various fractions (for convenience here considered to be asphaltene (asph), whole oil (wo), whole rock (wr, not a hydrocarbon fraction, but the source of the Os in the hydrocarbons) and an 'other' fraction, possibly of lighter hydrocarbons). Each fraction will contain its own $^{187}Re/^{188}Os$ but all will be in Os isotopic equilibrium with the whole rock that is their source. (c) These fractions may migrate to a reservoir together, or even remain trapped in the source; however, as long as they remain isotopically closed, they will, over time, evolve to produce isochrons with slopes proportional to the period of time that has elapsed since oil generation ($t_{(og)}$) and initial ratios ($^{187}Os/^{188}Os_{(og)}$) equal to the isotopic ratio of the source rock. $^{187}Os/^{188}Os_{(i)}$ = initial $^{187}Os/^{188}Os$ of seawater during deposition; $^{187}Os/^{188}Os_{(og)}$ = $^{187}Os/^{188}Os$ of the source at time of oil generation.

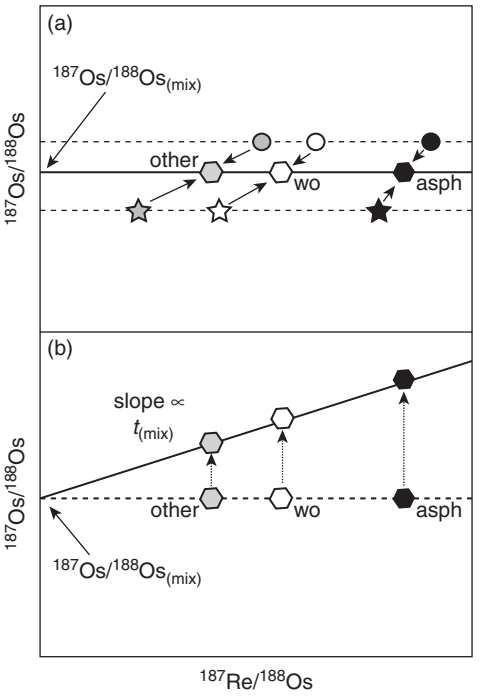

Figure 11.17 Effect of hydrocarbon mixing on an Os isochron diagram. This example uses mixing from two different source rocks during the same generation event; however, the result is the same when mixing hydrocarbons generated from events of different age. (a) The mixing event equilibrates the $^{187}Os/^{188}Os$ between various hydrocarbon fractions to produce a homogeneous mixed $^{187}Os/^{188}Os$ ($^{187}Os/^{188}Os_{(mix)}$ is Os isotopic ratio at the time of hydrocarbon mixing and is not necessarily equal to $^{187}Os/^{188}Os_{(og)}$) and a range of Re/Os. (b) Over time these mixed fractions evolve to produce an isochron with slope directly proportional to the time elapsed since the mixing event ($t_{(mix)}$).

should, however, be relatively straightforward, as such arrays will produce straight lines on an isotope vs inverse concentration plot, as per Section 10.2 (Figures 10.6 and 10.7). With this in mind, even mixing arrays can provide important information when attempting to distinguish between petroleum systems of significantly different ages. For example, a mixture of oils derived from Cambrian source rocks will generally be far more radiogenic than a mixture of oils derived solely from Eocene source rocks, thus providing a first-order constraint on sources in basins containing nested depocentres or protracted histories. More problematic is distinguishing between fractions that have separated from each other during the journey from generation to trap. In all cases, data generated need to be interpreted in the context of the understanding of the thermal evolution of the petroleum system in question, and can provide powerful insights that amplify the holistic understanding of basin evolution.

In conclusion, the Re–Os isotopic systems offer a powerful tool for investigating source rock deposition, hydrocarbon generation, subsequent migration, mixing and reservoir formation. However, each step in the process is exceedingly complex, and potential exists to either completely or partially obscure the earlier steps. Hence care needs to be taken when investigating oils and hydrocarbon fractions within a single system and the resultant data need to be interpreted in the context of characterised potential source rocks and other contaminants, including non-hydrocarbon detrital material.

12

New developments in radiogenic isotopes

12.1 Looking forward: the next generation of tools and techniques

As we have seen in the preceding chapters, although there is only a relatively small number of radioactive decay schemes with half lives appropriate to interrogate the terrestrial geological record, various developments and refinements in both techniques and materials being analysed have driven major conceptual understandings. In part, these advances have come through improvements in instrumentation, but also through recognition of a problem that needed to be solved. Hence it is possible to foresee both a technical progression which is technology and technique based, and an application-driven progression where existing techniques are applied in new and novel ways.

Although not covered to any degree in this book, increasingly the integration of radiogenic and stable isotope studies will yield a combined approach to understanding systems in ways that have not previously been possible. This can be combined with underutilised radioactive decay schemes, depending on the problem to be solved. For example, the ^{190}Pt–^{186}Os decay scheme has not been discussed here as the parent, ^{190}Pt, is present in only very low levels (~0.0014 per cent of all natural Pt) and has an incredibly long half life (~430 Gyr, or 30 times the age of the universe). Hence to date it has really only been investigated in a small number of extraterrestrial and core–mantle interaction settings, yet it may have a small number of niche applications in mineralisation situations where integration of Re–Pt–Os and even stable Os isotopes may offer insights that were previously unobtainable. This example, while technically feasible in the medium term, may well not bloom unless there is a real need for such sophistication in understanding mineralisation processes. Therefore the future will require a constant recognition of both what the important problems are and which tools are able to address them.

A list of potential developments would therefore have to include:

Incremental advances

- Improved precision of existing techniques allowing resolution of signals that were otherwise obscured

  Developments in this area will largely be seen in improved geochronology in all forms, allowing detailed petrogenesis histories to be developed, detailing the rates and time scales of mineralising processes. Coupled with these improvements will be improved resolution of initial isotopic ratios resulting in finer distinctions between source regions and contaminants, e.g. Pb and Os isotopes.

- Sampling of other materials with existing technologies

  The explosion of U–Pb geochronology on zircons, and the subsequent integration of Hf isotopes on the same material, changed the way we were able to consider the evolution of the crust–mantle system. Improved laser sampling with femtosecond lasers and the next generation of ion microprobes will allow improved resolution and precision on materials with lower levels of these elements and indeed extend to other isotopic systems as polybaric interferences can be filtered, removed or resolved with instrumentation. Hence common gangue minerals such as sulphides, calcite, fluorite and even iron oxides, in addition to monazite and zircon, could be interrogated routinely.

- Refinement and application of existing isotopic systems in novel ways

  The crossover of Os isotopes into the petroleum industry is an excellent example of the recognition of how the maturing of a tool in one discipline can be applied with effect in another. The potential exists for other such novel crossovers between fields, particularly as some of the more time-intensive techniques such as Re–Os or high-precision Pb and Sr are applied to more well-constrained portions of mineralised systems.

- Broader application of metallic stable isotopes in mineralised systems

  Led in part by applications to extraterrestrial materials, techniques for stable isotope analysis of elements such as Cu, Zn, Sn, Sb, Cd, Cr and particularly Fe are increasingly being applied to terrestrial situations in mineralised systems and also in oceanography. The procedures for analysis of these isotopes are derivatives from the radiogenic techniques described in this book, and increasingly the integration of these isotopes as tracers of processes will be seen. Also the stable isotopes of radiogenic isotope systems will grow in importance as the precision of their measurement becomes more routine (e.g. $^{86}Sr/^{88}Sr$, $^{189}Os/^{188}Os$), particularly those that are redox sensitive. There is even the possibility of clumped transition metal stable isotope analysis.

- Large data set and metadata isotopic analysis

  Acquisition of huge detrital zircon data sets has changed the way we are able to gauge the significance of individual populations in the context of crustal growth and recycling. Increasingly powerful computers and standardised sample analysis protocols have already enabled a greater sample throughput, which represents opportunities in re-evaluating existing data sets in the context of new, targeted analytical campaigns designed to address specific problems. Quantitatively interrogating the emergent structure within large data sets will allow recognition of events or processes that may have been either obscured or over-represented in smaller data sets.

Step-change advances

These changes will require significant breakthroughs in analytical techniques and procedures, or truly new thinking about how to solve a particular problem. Many of these advances are already being worked on, but are either non-routine or impractical for widespread application.

- Time of flight (ToF) mass spectrometry

  ToF has long been applied in analytical chemistry for simultaneous measurement of the atomic masses of a whole range of molecular species – effectively measuring the isotopic abundances of a whole range of molecules simultaneously. The precision of such measurements is at present not adequate to measure radiogenic isotopic ratio variations; however, if this could be improved, theoretically a single sample could be measured for multiple isotopic systems simultaneously. Such an ability would therefore allow measurement of all isotopes on the same aliquot of sample, eliminating errors associated with sample heterogeneity.

- Improved spatial resolution of sampling

  Current laser and SIMS systems routinely operate on spot sizes of ~20 μm, although both systems can be readily focused to beams that are far smaller, thus allowing for greater resolution between different stages of growth in minerals such as zircon. The inherent limitation is not so much how small a volume these beams can sample, but rather whether we are able to efficiently extract and precisely measure the isotopic ratios of these increasingly smaller amounts of sample. Several approaches to these issues are being adopted, including the application of femtosecond lasers which deliver a smoother energy spectrum to the sample, effectively resulting in greater ion transmission to the mass spectrometer, or using different ion beams (such as improving the Cs^+ gun in SIMS). Such approaches sit in the incremental advances listed above. However, a more radical approach has been to use lasers to cut out nanometre-sized samples which

can then be analysed on the atom probe – hence obtaining isotopic data on samples containing as little as several million atoms. At present, applications have largely been confined to materials engineering, but there is potential with significant investment for far-ranging geological applications.

- Mobile high-precision analytical apparatus

  Long a dream for even chemical analysis through the development of portable X-ray fluorescence (XRF) technologies to allow the measurement of the rock compositions in the field, the potential now exists for development of (admittedly quite low precision) isotopic analysis using transportable laser sample introduction methods. This very long-term goal is being led by developments in miniaturisation for planetary exploration, and may allow coarse-scale geochronology in the field or isotopic tracking of fluid pathways.

Appendix 1

Conversion between wt% oxide and ppm

Major elements are typically expressed as weight per cent (wt%) oxide. This is because they are the major rock-forming constituents, and it is assumed that oxygen is present in sufficient abundance to stoichiometrically balance the cation abundances measured. Therefore the sum of the major element oxides should always be close to 100 per cent. This analysis total is a good guide to the reliability of an analysis.

The problem is that trace elements are usually measured as simply the concentration of the cation (or anion) of interest, so often it may become necessary to convert between wt% oxide and ppm element.

From Table A.1, it is clear that 15.23 wt% MgO can be considered to be equivalent to 0.1523 g/g. However, this is 0.1523 g/g of MgO, *not* Mg. For many purposes having this extra O hanging around can be a nuisance, so it's useful to know how to convert from a wt% oxide to a concentration per unit mass. This is particularly so for elements such as Ti, P and K, which are typically measured as TiO_2, P_2O_5 and K_2O, respectively. These elements are often plotted on 'spidergrams', where they're compared with elements that are expressed in ppm, hence for consistency they need to be converted from wt% oxide to ppm.

To do this, it is necessary to first remove from the wt% measurement the proportion of the molecule that is oxygen. This will then leave a wt% which is purely the cation of interest, and this wt% can be converted to a ppm by multiplying by 10 000 (Table 3.1).

An example of such a calculation might involve TiO_2:

If we have 1.5 wt% TiO_2, then what is the concentration of Ti in ppm?

This molecule is composed of one atom of Ti for every two atoms of O. TiO_2 has a molecular weight of 79.90 (see Table A.1), and O has an atomic weight of 16.

Since $O = 16, O_2 = 32$,

$\therefore$ the proportion of the total molecule which is Ti is:

$$\text{wt\% Ti} = \frac{TiO_2 - O_2}{TiO_2} = \frac{79.90 - 32}{79.90};$$

$$\therefore \quad 1.50 \text{ wt\% } TiO_2 = 1.5 \times \frac{79.90 - 32}{79.90} \qquad \text{(Eq A1.1)}$$

$$= 0.899 \text{ wt\% Ti.}$$

To convert from wt% to ppm, we simply multiply by 10 000:

$\therefore$ 1.50 wt% TiO_2 = 8 990 ppm Ti.

Table A.1 *Molecular weights of common rock-forming elemental oxides.*

SiO_2	60.09	FeO	71.85	K_2O	94.20
TiO_2	79.90	Fe_2O_3	159.70	Na_2O	61.98
Al_2O_3	101.94	MgO	40.32	P_2O_5	141.95
Cr_2O_3	152.02	MnO	70.94	CO_2	44.01
CaO	56.08	NiO	74.71	O	16

So, too, it is possible to convert from any major element oxide to the corresponding elemental concentration by substituting the appropriate molecular weight and number of O atoms into the above formula.

There is no difference when dealing with molecules which have more than one atom of the cation, such as P_2O_5. Say we have 0.9 wt% P_2O_5, then, following the logic above:

Since $O = 16, O_5 = 80$,

$\therefore$ the proportion of the total molecule which is P is:

$$\text{wt\% P} = \frac{P_2O_5 - O_5}{P_2O_5} = \frac{141.95 - 80}{141.95};$$

$$\therefore \quad 0.9 \text{ wt\% } P_2O_5 = 0.9 \times \frac{141.95 - 80}{141.95} \qquad \text{(Eq A1.2)}$$

$$= 0.393 \text{ wt\% P.}$$

To convert from wt% to ppm, we simply multiply by 10 000:

$$\therefore \quad 0.9 \text{ wt\% } P_2O_5 = 3930 \text{ ppm P}$$

$$= 3900 \text{ ppm P (rounding down).}$$

Note that we structured the equation such that we calculated the total *proportion* of P in the molecule, regardless of whether it is present as P_2 or 2P. *How* it is distributed is irrelevant for the total concentration of P in the rock. If, however, we were going to continue with stoichiometry from this analysis we would need to take into account the fact that we have two P atoms for every five O atoms and this is the starting point for recalculating mineral formulae from chemical analysis.

Appendix 2

Isotopic abundances

Table A.2 *Isotopic abundances of the commonly used decay schemes in the geological sciences. Isotopes in italics are radiogenic products.* (λ, decay constant; T_c, closure temperature; *wr*, whole rock)

K–Ar

Parent	Daughter	λ (yr^{-1})	T_c (wr) °C	T_c (minerals) °C
^{40}K	^{40}Ar	0.575×10^{-10}	~400	–

Isotopic abundances (%)

^{39}K	$^{40}K*$[a]	^{41}K			
93.2581	0.0117	6.7302			
^{40}Ca	^{42}Ca	^{43}Ca	^{44}Ca	^{46}Ca	^{48}Ca[b]
96.941	0.647	0.135	2.086	0.004	0.187
^{36}Ar	^{38}Ar	*^{40}Ar*			
0.3336	0.0629	99.6035			

[a] ^{40}K decays via a branched scheme, producing both ^{40}Ca (89.1 per cent) and ^{40}Ar (10.9 per cent).
[b] ^{48}Ca is also radioactive, decaying to ^{48}Ti with a half life of 43×10^{18} yr^{-1}, meaning it is effectively a stable isotope for geological purposes.

Rb–Sr

Parent	Daughter	λ (yr^{-1})	T_c (wr) °C	T_c (minerals) °C
^{87}Rb	^{87}Sr	1.42×10^{-11}	~650	–

Isotopic abundances (%)

^{85}Rb	^{87}Rb*		
72.2	27.8		
^{84}Sr	^{86}Sr	*^{87}Sr*	^{88}Sr
0.56	9.86	7.00	82.58

Sm–Nd

Parent	Daughter	λ (yr^{-1})	T_c (wr) °C	T_c (minerals) °C
^{147}Sm	^{143}Nd	6.54×10^{-12}	>800	–

Isotopic abundances (%)

^{144}Sm	^{147}Sm*	^{148}Sm	^{149}Sm	^{150}Sm	^{152}Sm	^{154}Sm
3.07	14.99	11.24	13.82	7.38	26.75	22.75
^{142}Nd[a]	*^{143}Nd*	^{144}Nd	^{145}Nd	^{146}Nd	^{148}Nd	^{150}Nd
27.2	12.2	23.8	8.3	17.2	5.7	5.6

[a] ^{142}Nd was also formed by the decay of now extinct ^{146}Sm in the early solar system.

Lu–Hf

Parent	Daughter	λ (yr^{-1})	T_c (wr) °C	T_c (minerals) °C
^{176}Lu	^{176}Hf	1.867×10^{-11}	>800	–

Isotopic abundances (%)

^{175}Lu	^{176}Lu*				
97.41	2.59				
^{174}Hf[a]	*^{176}Hf*	^{177}Hf	^{178}Hf	^{179}Hf	^{180}Hf
0.16	5.26	18.6	27.28	13.62	35.08

[a] ^{174}Hf decays to ^{170}Yb with a half life of 2×10^{15} yr^{-1}.

Re–Os

Parent	Daughter	λ (yr^{-1})	T_c (wr) °C	T_c (minerals) °C
^{187}Re	^{187}Os	1.666×10^{-11}	~550	–

Isotopic abundances (%)

^{185}Re	^{187}Re*					
37.40	62.60					
^{184}Os	*^{186}Os*[a]	*^{187}Os*	^{188}Os	^{189}Os	^{190}Os	^{192}Os
0.02	1.59	1.96	13.24	16.15	26.26	40.78

[a] ^{186}Os is also formed by the decay of the very low abundance ^{190}Pt with a half life of ~430 Gyr.

U–Th–Pb

Parent	Daughter	λ (yr^{-1})	T_c (wr) °C	T_c (minerals) °C
^{232}Th	^{208}Pb	0.049×10^{-9}	~650	750
^{235}U	^{207}Pb	0.985×10^{-9}	~650	850
^{238}U	^{206}Pb	0.155×10^{-9}	~650	850

Isotopic abundances (%)

^{232}Th*	^{235}U*	^{238}U*	
100	0.716	99.284	
^{204}Pb	*^{206}Pb*	*^{207}Pb*	*^{208}Pb*
1.4	24.1	22.1	52.4

Glossary

Anion: Negatively charged ion.

Atom: Chemically neutral basic unit of matter comprising a nucleus and electrons.

Atomic mass: The mass of an individual atom, usually expressed in atomic mass units (amu), such that it very closely approximates the sum of the protons and neutrons in the atom.

Atomic number: The number of protons in a nucleus.

Atomic weight: The weighted mean of the masses of all of the naturally occurring isotopes of an element. Hence a monotopic element will have an atomic weight equal to its atomic mass number, since all of that element is made up of a single isotope.

Cation: A positively charged ion.

Element: A pure chemical substance consisting of only one type of atom as defined in terms of its number of protons (atomic number).

Equilibrium fractionation: Isotopic fractionation which takes place when the forward and backward reaction rates are the same. Since the forward and backward reaction rates are the same, isotopic fractionation can be described solely in terms of the ratio of the isotopes between the reactant and the product.

Fractionation: The process by which a mixture is separated into smaller quantities of differing compositions. Isotopic fractionation refers to the specific case where the mixture is separating into products with differing isotopic compositions relative to the starting materials, even though the chemical composition of the reactants and product may be the same.

Instrumental neutron activation analysis: Geochemical analytical technique whereby a sample is irradiated with neutrons in a nuclear reactor and the abundance of an element is directly proportional to the intensity of the emitted gamma radiation.

Ion: Electrically charged atom or molecule.

Isochron: A line joining points of equal age. In geochronology, an isochron is a straight line on a daughter/daughter vs parent/daughter plot, the slope of which is directly proportional to the age.

Isotope: An atom of a chemical element containing a given number of protons and neutrons. A different isotope of the same element will contain a different number of neutrons, thus changing the isotopic mass, but not its chemical characteristics. Some elements may have only one stable isotope, and hence are monotopic (Au, Rh, F); others may have none (Tc, Pm, Am, etc.) and hence can only be created artificially, whereas most elements have several isotopes.

Isotopic fractionation: Splitting of a mixture into smaller quantities where the products have differing isotopic compositions relative to the starting materials, even though the chemical composition of the reactants and product may be the same.

Kernel (statistics): A weighting function used to estimate the density function of a variable (such as an age). Kernels are used in the generation of probability density histograms, and can be weighted according to the error associated with the age measurement.

Kinetic fractionation: Isotopic fractionation associated with reactions in which the isotopes participate in the reaction at different rates; however, the ratio between the relative reaction rates is constant. Kinetic fractionation applies when the forward and backward reaction rates are not the same.

Magnetic sector: Isotope discrimination on the basis of mass due to deflection in a magnetic field.

Mass fractionation: Isotopic fractionation whereby the degree of separation of masses is proportional to the differences in isotopic mass. The vast majority of isotopic fractionation during chemical processes is of this type.

Mass-independent fractionation: Isotopic fractionation whereby the degree of isotopic dissociation does not scale as a proportion of the mass difference between the isotopes.

Mass spectrometry: The science of measuring the distribution and abundances of isotopes through analysis of charged elemental or molecular species as a function of their mass to charge ratio, hence allowing measurement of isotopic abundances.

Model age: A theoretical age calculated from a measured sample by extrapolating its measured isotopic ratio back in time to when it was last in equilibrium with a reservoir of interest (e.g. DMM, CHUR).

Molecule: The smallest portion of a substance that retains the chemical properties of that substance.

Mono-isotopic: *See* Monotopic

Monotopic: An element comprising only one isotope. Au, Rh and F are all examples.

Neutron activation analysis: *See* Instrumental neutron activation analysis.

Nucleon: Atomic particles which occur in the nucleus, i.e. protons and neutrons.

Photo-dissociation: The chemical breakdown of a molecule due to the interaction with light (photons). This phenomena is not limited to visible light, with many important reactions occurring due to the influence of (for example) UV radiation.

Population statistics: Statistics associated with collection of a data set in which all individuals are measured.

Quadrupole: Mass discrimination device (technique) which operates on the principle of oscillating radio frequencies and electrical fields.

Radioactive decay: The process by which an unstable nucleus loses energy through the emission of ionising radiation. Ultimately nuclei decay to a stable ground state, either through a single step of energy emission, or any number of unstable, intermediate decays. Substances which emit energy of this type are said to be radioactive.

Radiogenic: A nuclide or isotope produced by radioactive decay. Such radiogenic daughter products may themselves be either radioactive or stable.

Rayleigh fractionation: The most common formalisation of kinetic isotopic fractionation. This description applies for isotopic exchange between two reservoirs as one reservoir changes in size during the reaction at the expense of the other, and is valid for scenarios in which material is continuously removed from the site of reaction and the degree of fractionation can be approximated by a single, unchanging fractionation factor.

Reservoir (geochemistry): A geochemical body of large size that is able to be sampled and replenished by geological mass transfer processes. Geochemical reservoirs each have specific trace element abundances and hence will evolve to distinctive isotopic signatures through time.

Sample statistics: A set of data collected from a larger statistical population by a defined procedure and representative of the larger population.

Stable isotope: A naturally occurring isotope which is not susceptible to nuclear decay. Some radioactive isotopes with exceptionally long half lives ($>10^{18}$ yr) can be considered stable.

Standard deviation: See Section 6.2.2. The numerical quantification of the scatter of individual measurements about the mean of a data set.

Standard error: See Section 6.2.2. The standard deviation of a theoretical distribution for a large population of measurements.

Tenor: The metal content of a sulphide calculated on the basis of 100 per cent sulphide. Note that this is different from the actual ore grade of a rock, which may be comparatively low due to the presence of gangue. Sulphides with high metal tenors can ultimately produce high-grade ore concentrates from low-grade ores.

Terrain: A region of land or more specifically the geological features associated with it.

Terrane: A tectonostratigraphic terrane, which constitutes a distinct crustal assemblage or fragment of crustal material which has been accreted or sutured onto a tectonic plate other than the one upon which it formed.

Transient kinetic isotopic fractionation: Isotopic fractionations which take place during a chemical reaction, and the effects do not follow first-order kinetic or equilibrium effects. Although most chemical reactions are of this type, their isotope fractionations can be simplified and approximated in terms of either kinetic or equilibrium processes without significant loss of precision.

Variance: The square of the standard deviation.

Further reading

Listed below are some useful resources and more in-depth summaries of many of the topics discussed in this book. They are ordered by chapter to allow the reader to find them in context. When selecting journal articles, I have been guided by personal preference in terms of the ones I find myself using – this does not necessarily make them the best or most authoritative, and the reader is encouraged to search beyond these for greater coverage of current understanding and controversies. I have also often tried to include the 'first' reference or use of a key concept (such as model ages), as this will often explain a concept which has subsequently evolved to be reasonably complex in a straightforward manner.

Textbooks pertaining to the whole field

Albarede, F. 2009. *Geochemistry: An Introduction*. Cambridge University Press, pp. 355.
Dickin, A.P. 2008. *Radiogenic Isotope Geochemistry.* Cambridge University Press, pp. 492.
Faure, G. and Mensing, T.M. 2005 *Isotopes: Principles and Applications*. Wiley, pp. 896.
Hoefs, J. 2015. *Stable Isotope Geochemistry.* Springer, pp. 389.
White, W.M. 2015, *Isotope Geochemistry.* Wiley, pp. 426.

Chapter 1

Radzig, A.A. and Smirnov, B.M. 2012 *Reference Data on Atoms, Molecules and Ions*. Springer, pp. 466.

Chapter 2

Epov, V.N., Malinovskiy, D., Vanhaecke, F., Begue, D. and Donard, O.F.X. 2011. Modern mass spectrometry for studying mass-independent fractionation of heavy stable isotopes in environmental and biological sciences. *Journal of Analytical Atomic Spectrometry* **26**: 1142–1156.

Halevy, I., Johnston, D. and Schrag, D. 2010. Explaining the structure of the Archean mass-independent sulfur isotope record. *Science* **329**(5988): 204–207.

Maggi F. and Riley, W.J. 2010. Mathematical treatment of isotopologue and isotopomer speciation and fractionation in biochemical kinetics. *Geochimica et Cosmochimica Acta*, **74**(6): 1823–1835.

Thiemens M.H., Chakraborty, S. and Dominguez, G. 2012. The physical chemistry of mass-independent isotope effects and their observation in nature. *Annual Review of Physical Chemistry* **63**: 155–177.

Chapter 3

Gross, J.H. 2012. *Mass Spectrometry: A Text Book*. Springer, pp. 753.

Potts, P.J. 1987. *A Handbook of Silicate Rock Analysis*. Springer, pp. 622.

Chapter 4

Epov, V.N., Malinovskiy, D., Vanhaecke, F., Begue, D. and Donard, O.F.X. 2011. Modern mass spectrometry for studying mass-independent fractionation of heavy stable isotopes in environmental and biological sciences. *Journal of Analytical Atomic Spectrometry* **26**: 1142–1156

Hoefs, J. 2015. *Stable Isotope Geochemistry.* Springer, pp. 389.

Potts, P.J. 1987. *A Handbook of Silicate Rock Analysis*. Springer, pp. 622.

Chapter 5

Braun, J., van der Beek, P. and Batt, G. 2006. *Quantitative Thermochronology: Numerical Methods for the Interpretation of Thermochronological Data*. Cambridge University Press, pp. 270.

Chiaradia, M., Schaltegger, U., Spikings, R., Wotzlaw, J.-F. and Ovtcharova, M. 2013. How accurately can we date the duration of magmatic-hydrothermal events in porphyry systems? *Economic Geology* **108**(4): 565–584.

Dickin, A.P. 2008. *Radiogenic Isotope Geochemistry.* Cambridge University Press, pp. 492.

Dodson, M.H. 1973. Closure temperature in cooling geochronological and petrological systems. *Contributions to Mineralogy and Petrology* **40**: 259–274.

Faure, G. and Mensing, T.M. 2005 *Isotopes: Principles and Applications*. Wiley, pp. 896.

White, W.M. 2015. *Isotope Geochemistry.* Wiley, pp. 426.

Chapter 6

Ludwig, K.R. 1980. Calculation of uncertainties of U–Pb isotope data. *Earth and Planetary Science Letters* **46**: 212–220.

Sircombe, K.N. and Hazelton, M.L. 2004. Comparison of detrital age data by kernel functional estimation. *Sedimentary Geology* **171**(1–4): 91–111.

Vermeesch, P. 2004. How many grains are needed for a provenance study? *Earth and Planetary Science Letters* **224**(3–4): 441–451.

Vermeesch, P. 2012. On the visualisation of detrital age distributions. *Chemical Geology.* **312**–**313**: 190–194.

York, D. 1969. Least squares fitting of a straight line with correlated errors. *Earth and Planetary Science Letters* **5**: 320–324.

Chapter 7

Mahon, K.I. 1996. The new 'York' regression: application of an improved statistical method to geochemistry. *International Geology Review* **38**(4): 293–303.

Powell, R., Hergt, J. and Woodhead, J. 2002. Improving isochron calculations with robust statistics and the bootstrap. *Chemical Geology* **3**–4: 191–204.

York, D. 1969. Least squares fitting of a straight line with correlated errors. *Earth and Planetary Science Letters* **5**: 320–324.

Chapter 8

Bourdon, B., Turner, S., Henderson, G.M. and Lundstrom, C.C. 2003. Introduction to U-series geochemistry. *Reviews in Mineralogy and Geochemistry* **52**(1): 1–21.

Corfu, F. 2012. A century of U–Pb geochronology: the long quest towards concordance. *Geological Society of America Bulletin* **125**(1–2): 33–47.

Fitzgerald, P.G. and Gleadow, A.J.W. 1988. Fission track geochronology, tectonics and structure of the transantarctic mountains in Northern Victoria Land, Antarctica. *Chemical Geology* **73**(2): 169–198.

Gleadow, A.J.W. 1983. Fission track analysis: a new tool for the evaluation of thermal histories and hydrocarbon potential. *APEA Journal* **23**(1): 93–102.

Ludwig, K.R. 1998. On the treatment of concordant uranium–lead ages. *Geochimica et Cosmochimica Acta* **62**(4): 665–676.

Ludwig, K.R. 2000. Decay constant errors in U–Pb concordia-intercept ages. *Chemical Geology* **166**(3–4): 315–318.

Patterson, C. 1956. Age of meteorites and the earth. *Geochimica et Cosmochimica Acta* **10**(4): 230–237.

Stein, H.J., Markey, R.J., Morgan, J.W., Hannah, J.L. and Schersten, A. 2001. The remarkable Re–Os chronometer in molybdenite: how and why it works. *Terra Nova* **13**: 479–486.

Suzuki, K. and Kato, T., 2008. CHIME dating of monazite, xenotime, zircon and polycrase: protocol, pitfalls and chemical criterion of possibly discordant age data. *Gondwana Research*, **14**: 569–586.

Tera, F. and Wasserburg, G.J. 1972. U–Th–Pb systematics in three *Apollo 14* basalts and the problem of initial Pb in lunar rocks. *Earth and Planetary Science Letters* **14**: 281–304.

Wetherill, G.W. 1956. Discordant uranium–lead ages. *Transactions of the American Geophysical Union* **37**: 320–326.

Chapter 9

Kelley, S. 2002. Excess argon in K–Ar and Ar–Ar geochronology. *Chemical Geology* **188**(1–2): 1–22.

Kuiper, Y.D. 2002. The interpretation of inverse isochron diagrams in $^{40}Ar/^{39}Ar$ geochronology. *Earth and Planetary Science Letters* **203**(1): 499–506.

Lee, J.K.W., Onsott, T.C., Casman, K.V., Cumbest, R.J. and Johnson, D. 1991. Incremental heating of hornblende in vacuo: implications for $^{40}Ar/^{39}Ar$ geochronology and the interpretation of thermal histories. *Geology* **19**(9): 872–876.

Chapter 10

DePaolo, D.J. 1981. Trace element and isotopic effects of combined wallrock assimilation and fractional crystallisation. *Earth and Planetary Science Letters* **53**(2): 189–202.

DePaolo, D.J. 1983. The mean life of continents: estimates of continent recycling rates from Nd and Hf isotopic data and implications for mantle structure. *Geophysical Research Letters* **90**: 263–271.

DePaolo, D.J., Linn, A.M. and Schubert, G. 1991. The continental crustal age distribution: methods of determining mantle separation ages from Sm–Nd isotopic data and application to the southwestern United States. *Journal of Geophysical Research* **96**(B2): 2071–2088.

Luck, J.-M., Bircke, J.L. and Allegre, C.J. 1980. ^{187}Re–^{188}Os systematics in meteorites: early chronology of the solar system and the age of the galaxy. *Nature* **283**: 256–259.

Stacey, J.D. and Kramers, J.D. 1975. Approximation of terrestrial lead isotope evolution by a two stage model. *Earth and Planetary Science Letters* **26**(2): 207–221.

Walker, R.J., Carlson, R.W., Shirey, S.B. and Boyd, F.R. 1989. Os, Sr, Nd and Pb isotope systematics of South African peridotite xenoliths: implications for the evolution of the subcontinental mantle. *Geochimica et Cosmochimica Acta* **53**: 1583–1595.

Chapter 11

Armit, R.J., Betts, P.G., Schaefer, B.F., Pankhurst, M.J. and Giles, D. 2014. Provenance of the Early Mesoproterozoic Radium Creek Group in the northern Mount Painter Inlier: correlating isotopic signatures to inform tectonic reconstructions. *Precambrian Research* **243**: 63–87.

Belousouva, E.A., Reid, A.J., Griffin, W.L. and O'Reilly, S.Y. 2009. Rejuvenation vs. recycling of Archean crust in the Gawler Craton, South Australia: evidence from U–Pb and Hf isotopes in detrital zircon. *Lithos*, **113**(3–4): 570–582.

Cummin, V.M., Selby, D., Lillis, P.G. and Lewan, M.D. 2014. Re–Os geochronology and Os isotope fingerprinting of petroleum sourced from a Type I lacustrine kerogen: insights from the natural Green River petroleum system in the Uinta Basin and hydrous pyrolysis experiments. *Geochimica et Cosmochimica Acta* **138**: 32–56.

DePaolo, D.J. 1983. The mean life of continents: estimates of continent recycling rates from Nd and Hf isotopic data and implications for mantle structure. *Geophysical Research Letters* **90**: 263–271.

Hart, S.R. 1984. A large-scale isotopic anomaly in the Southern Hemisphere mantle. *Nature* **309**: 753–757.

Hofmann, A.W. 1997. Mantle geochemistry: the message from oceanic volcanism. *Nature* **385**: 219–229.

Jackson, S.E., Pearson, N.J., Griffin, W.L. and Belousova, E.A. 2004. The application of laser ablation-inductively coupled plasma-mass spectrometry to *in situ* U–Pb zircon geochronology. *Chemical Geology* **211**(1): 47–69.

Ravizza, G. and Turekian, K.K. 1989. Application of the ^{187}Re–^{187}Os system to black shale geochronometry. *Geochimica et Cosmochimica Acta* **53**(12): 3257–3262.

Selby, D. and Creaser, R.A. 2003. Re–Os geochronology of organic rich sediments: an evaluation of organic matter analysis methods. *Chemical Geology* **200**(3–4): 225–240.

Selby, D., Creaser, R.A. and Fowler, M.G. 2007. Re–Os elemental and isotopic systematics in crude oils. *Geochimica et Cosmochimica Acta* **71**(2): 378–386.

Sircombe, K.N. and Hazelton, M.L. 2004. Comparison of detrital age data by kernel functional estimation. *Sedimentary Geology* **171**(1–4): 91–111.

Stracke, A., Hofmann, A.W. and Hart, S.R. 2005. FOZO, HIMU, and the rest of the mantle zoo. *Geochemistry, Geophysics, Geosystems* **6**(5): 1–20.

Sun, S.S. and McDonough, W.F. 1989. Chemical and isotopic systematics of oceanic basalts: implications for mantle composition and processes. *Geological Society of London, Special Publications* **42**: 313–345.

Vermeesch, P. 2004. How many grains are needed for a provenance study? *Earth and Planetary Science Letters* **224**(3–4): 441–451.

Vermeesch, P. 2012. On the visualisation of detrital age distributions. *Chemical Geology* **312**–**313**: 190–194.

Woodhead, J., Hergt, J., Shelley, M., Eggins, S. and Kemp, R. 2004. Zircon Hf-isotope analysis with an excimer laser, depth profiling, ablation of complex geometries, and concomitant age estimation. *Chemical Geology* **209**(1–2): 121–135.

Zindler, A. and Hart, S. 1986. Chemical geodynamics. *Annual Reviews in Earth and Planetary Sciences* **14**: 493–571

Index